Royal Holloway University of London

Doctoral Thesis

Numerical Modelling of Basin Margin Stratal Geometries: Implications for Sequence Stratigraphy

Author:

Guy Prince

Supervisor:

Prof. Peter Burgess

A thesis submitted in fulfilment of the requirements

for the degree of Doctor of Philosophy

in the

Earth Sciences Department

February 2015

Declaration of Authorship

I, Guy Prince, declare that this thesis titled, 'Numerical Modelling of Basin Margin Stratal Geometries: Implications for Sequence Stratigraphy' and the work presented in it are my own. I confirm that:

- This work was done wholly while in candidature for a research degree at this University.
- Where I have consulted the published work of others, this is always clearly attributed.
- Where I have quoted from the work of others, the source is always given. With the exception of such quotations, this thesis is entirely my own work.
- I have acknowledged all main sources of help.

Signed:

_____

Date:

_____

Abstract

Numerical Modelling of Basin Margin Stratal Geometries: Implications for Sequence Stratigraphy

Sequence stratigraphy is an established methodology for the study of stratal relationships within a chronostratigraphic framework. The method is based on a number of simplifying assumptions, including that changes in relative sea-level (RSL) are the major control on stratal geometry formation. However, because stratal geometries are now understood to be controlled by a number of processes, not simply RSL variations, the application of sequence stratigraphic models and methods for various theoretical and stratigraphic problems is unlikely to be as simple as proposed.

This thesis uses numerical stratigraphic forward models to investigate how different combinations of parameter values for multiple processes can control formation of basin margin stratal geometries. To achieve this, many hundreds of stratal geometries are generated in two- and three-dimensional model runs covering a wide range of parameter values for different controlling processes. Stratal geometries are then characterised or examined to elucidate the likely controls on formation of various stratal architectures. How the numerically modelled stratal geometries in this work, including stacking patterns, stratigraphic surfaces and shoreline trajectories, can impact sequence stratigraphic interpretation is discussed and illustrated.

Stratal geometries generated from 1264 numerical simulations on a simple ramp topography and on a topography with a shoreline break of slope demonstrate that topset aggradation during RSL fall occurs across a wide range of values of terrestrial diffusion coefficients (representing sediment transport in the model), and of amplitudes and

durations of RSL fall. Topset aggradation during falling RSL is particularly prevalent in models with sediment transport rates at the low end of what is observed in modern delta systems. These results suggest that falling-stage topset aggradation is likely to be common in ancient strata, and consequently distinguishing between forced and unforced regressions in the ancient record could be difficult.

Sediment transport rates are also shown to be an important control on shoreline trajectories generated in the numerical model. With constant supply and duration of RSL fall, model runs with relatively high sediment transport rates lead to erosion at the shoreline and increased progradation, whereas model runs with low sediment transport rates lead to aggradation at the shoreline and reduced progradation. Other numerically modelled shoreline trajectories in this thesis also suggest that different shoreline trajectories can result from different sediment transport rates when all other controlling factors are constant. Reliably distinguishing between horizontal, ascending and descending shoreline trajectory classes requires knowledge of the paleo-horizontal surface. This surface can be difficult to identify when tectonic tilting or differential compaction has occurred. Modelled stratal geometries presented show how differential compaction can alter shoreline trajectory geometries to the extent that it is not possible to distinguish between the different trajectory classes. This suggests that it would be difficult to reliably distinguish between strata generated during rising or falling RSL using shoreline trajectories without very detailed two- and three-dimensional backstripping.

Since stratal geometries on basin margins a consequence of multiple different controls, correct sequence stratigraphic interpretation requires an understanding of how multiple controls can generate similar stratal geometries. Numerical model runs are executed in this thesis to explore the impact of time-variable sediment supply and different sediment transport rates on stratal geometries. Four common types of stratal geometry are shown

to form by more than one set of parameter values and are thus likely to be non-unique. A maximum transgressive surface can occur in the model due to an increase in rate of RSL rise during constant sediment supply, and due to a reduction in rate of sediment supply during a constant rate of RSL rise. Similarly, sequence boundaries, topset aggradation and shoreline trajectories are also examples of non-unique stratal geometries. If these model results are realistic and non-unique stratal geometries occur in the ancient record, this suggests that the sequence stratigraphic method requires a shift towards an approach that is capable of considering and evaluating multiple hypotheses and scenarios.

Shoreline trajectories interpreted directly from stratal geometries generated in three-dimensional numerical model runs in this work demonstrate that shoreline trajectories interpreted from two-dimensional outcrop or subsurface data may be limited in respect to describing three-dimensional clinoform development. The limitation exists because stratal architectures on basin margins contain significant variability along strike and are thus likely to exhibit different shoreline trajectories along various dip sections. A three-dimensional model run of a basin margin with time variable sediment supply from three sources illustrates how two-dimensional shoreline trajectories interpreted from different dip sections along a basin margin can look different. In order for shoreline trajectory analysis to account for this variability, multiple two-dimensional dip sections should be interpreted and compared.

Results presented in this thesis highlight the limitation of sequence stratigraphic models and methods for extracting reliable information from the ancient record. Stratigraphic correlation using particular stratal geometries, making predictions regarding volume and style of sediment bypass, and reconstructing RSL histories based on observed stratal geometries are probably more complex than sequence stratigraphic methods and models

suggest. The results highlight the requirement for a sequence statigraphic method based on constructing and evaluating multiple hypotheses and scenarios.

Acknowledgements

First and foremost I acknowledge my supervisor, Peter Burgess, for his first-class teaching and patience, as well as for his natural unselfishness with scientific discourse.

The support from other staff members during my time at Royal Holloway University of London is greatly appreciated: Dave Waltham, Gary Nichols, Margaret Collinson and Dan Le Heron for unparalleled training, useful discussions and motivation; Nicola Scarselli for seismic workstation expertise; Frank Lehane and Mark Longbottom for tremendous IT support, usually at the drop of a hat; Kevin D'Souza for printing and other departmental practicalities.

From the Institut Français du Pétrole, I wish to thank Didier Granjeon for his technical help with the understanding and running of Dionisos. Cedric Griffiths and Chris Dyt at the Commonwealth Scientific and Industrial Research Organisation are also thanked for help running the model Sedsim.

The National Environment Research Council are gratefully acknowledged for financially supporting my PhD Studentship at Royal Holloway University of London.

Finally, I wish to thank my family for their loving support throughout my studies, particularly Hanna for her endless patience and encouragement when it was most required.

Contents

List of Figures

List of Tables

Abbreviations

RSL	Relative sea-level
MTS	Maximum Transgressive Surface
SB	Sequence Boundary
$\boldsymbol{k}$	Diffusion coefficient
NCB	Northern Carnarvon Basin
SFM	Stratigraphic forward model
TWT	Two way travel time
s	Seconds
m	Metres
2D	Two-dimensional
3D	Three-dimensional
EMT	Elapsed model time

Chapter 1

Thesis Aims & Objectives

1.1 Thesis aim & rationale

The aim of this thesis is to investigate with numerical stratigraphic forward models the formation of basin-margin stratal geometries that can result from different parameter combinations of controlling processes and illustrate the consequences of this for sequence stratigraphic interpretation.

Basin-margin stratal geometries are understood to form as a result of multiple controlling processes including variations in sediment supply, accommodation and sediment transport rates. Therefore, correct sequence stratigraphic interpretation requires an understanding of how these different controls contribute to form various observed stratal geometries.

Sequence stratigraphic models and methods regularly applied to deal with theoretical and practical stratigraphic problems contain explicit and implicit simplifying assumptions and avoid consideration of multiple controls and consequent complexity in stratigraphic architectures.

Numerical modelling of basin-margin stratal geometries generated with different combinations of parameter values for different controlling processes can be used to investigate the likely consequences of time-variable sediment supply, accommodation variations and variable sediment transport rates on stratal geometries commonly observed and interpreted in subsurface and outcrop data from the ancient record.

1.2 Thesis objectives

The following five thesis objectives were established to meet the thesis aim:

1. Determine if aggradational topset strata occurs in the numerical model during falling RSL given a wide range of sediment transport rates and RSL fall amplitudes and durations.
2. Investigate if shoreline trajectories are a reliable indicator of RSL histories after formation with different sediment transport rates and modification by differential compaction during burial.
3. Investigate if similar sequence stratigraphic surfaces, stacking patterns and shoreline trajectories can be generated in a diffusional SFM using different parameter values for various controlling processes.
4. Interpret siliciclastic basin-margin stratal geometries from seismic data and apply the concepts and methods of shoreline trajectory analysis on dip-orientated 2D seismic lines.
5. Numerically reconstruct interpreted seismic geometries with a stratigraphic forward model interpreted stratal geometries and investigate if 2D shoreline trajectories interpreted from 2D seismic lines are suitable for describing 3D clinoform development.

1.3 Thesis layout

An introduction to some of the main methods and concepts in classic sequence stratigraphy relevant to this thesis, along side some important alternative findings from numerical and analogue modelling studies, is given in Chapter 2. Following this, Chapter 3 is devoted to describing the models and methods used in this thesis.

Analytical chapters 4, 5, 6 and 8 address stratigraphic problems through numerical modelling, and because these pieces of work are either published (Chapter 4), in press (Chapter 6) or in preparation for publication (Chapters 5 and 8 combined) there is a certain amount of overlap in the presentation of relevant introductory and background material.

Chapter 2

Introduction: Sequence Stratigraphy & Modelling of Basin Margin Stratal Architectures

This chapter is split into four sections. First, a short review of the fundamental methods and definitions within siliciclastic sequence stratigraphy is provided. The elements of sequence stratigraphy covered are of relevance to later chapters in this thesis. Second, some of the major developments in physical and numerical modelling work which are at odds with various aspects of the sequence stratigraphic methodology are reviewed. Third, future developments of the subject are covered. Finally there is a discussion of the motivation for this thesis, outlining the problems to be addressed.

2.1 Sequence stratigraphic methods

Sequence stratigraphy is a relatively recent methodology in the field of sedimentary geology, and it has been defined in a number of different ways since its inception, including:

- "the study of rock relationships within a time-stratigraphic framework of repetitive, genetically related strata bounded by surfaces of erosion or nondeposition, or their correlative conformities" (*Posamentier and Vail*, 1988)
- "the analysis of repetitive genetically related depositional units bounded in part by surfaces of nondeposition or erosion" (*Galloway*, 1989)
- "the analysis of cyclic sedimentation patterns that are present in stratigraphic successions, as they develop in response to variations in sediment supply and space available for sediment to accumulate" (*Posamentier and Allen*, 1999)
- "Sequence stratigraphy emphasizes changes in stratal stacking patterns in response to varying accommodation and sediment supply through time" (*Catuneanu et al.*, 2010)

Early definitions placed an emphasis on sequence bounding surfaces, a sequence being firstly described by *Sloss et al.* (1949) as a stratigraphic unit bounded by subaerial unconformities, and later being defined as a relatively conformable succession of genetically related strata (*Vail et al.*, 1977). Later definitions of sequence stratigraphy mention, albeit non-specifically, the role of sediment supply as well as accommodation variations. In each case the definitions of sequence stratigraphy contain differing and sometime rather impenetrable terminology.

2.1.1 A brief history of sequence stratigraphy

Sequence stratigraphy is generally acknowledged to have developed from seismic stratigraphy (*Vail et al.*, 1977), but some important understanding emerged prior to this. For example, *Sloss et al.* (1949) defined the term 'sequence' to identify a stratigraphic unit bounded by subaerial unconformities, whilst also recognising the role of tectonism in the generation of sequences and bounding unconformities. A number of other early studies also recognised the importance of unconformities, sedimentation variations and changes in base-level (*Barrell*, 1917, *Grabau*, 1913, *Wheeler*, 1959, 1964, *Wheeler and Murray*, 1957).

The concepts of seismic stratigraphy (*Vail*, 1975), and a description of the sequence stratigraphic methodology and definitions, were published alongside a global sea-level

cycle chart (*Vail et al.*, 1977). This method for analysing seismic reflection data was based on the assumption that eustacy is the main driving force behind sequence formation across the different levels of stratigraphic cyclicity.

Seismic stratigraphy soon evolved into sequence stratigraphy, incorporating outcrop and well data (*Posamentier and Vail*, 1988, *Posamentier et al.*, 1988, *Van Wagoner et al.*, 1990). Sequence stratigraphy took a new turn when the original idea of eustatic control was replaced with relative sea-level (RSL), combining eustacy with tectonics (e.g., *Hunt and Tucker*, 1992, *Jervey*, 1988, *Posamentier and Allen*, 1999).

Recent efforts have attempted to standardise sequence stratigraphy into a stratigraphic code or guide (*Catuneanu*, 2006, *Catuneanu et al.*, 2009, 2010, 2011), but despite wide use of the method (e.g., *Hubscher and Spieß*, 2005) this is yet to be realised and is a topic of disagreement (e.g., *Helland-Hansen*, 2009). The lack of standardisation alongside the wide use of the methodology is a reflection of the competing approaches and models advocated amongst sequence stratigraphic practitioners. The following section provides a review of the main methods and definitions within the sequence stratigraphic framework.

2.1.2 Sequence models

A number of depositional sequence models have been published since the original methods and definitions proposed by *Vail et al.* (1977) (Figures 2.1 & 2.2). Each model contains different terminology, and assigns different weight on the importance of stratigraphic surfaces (e.g., position of the sequence boundary, shown in Figure 2.2).

Although the different sequence models contain conflicting nomenclature (Figure 2.2), they also share a common set of principles and concepts. *Catuneanu et al.* (2009) referred to these shared principles and concepts across the sequence models as 'model-independent' methodologies. This is slightly misleading because the principles and concepts are not independent of sequence models, they are simply common to all the different sequence models. These principles and concepts used in sequence models are reviewed below.

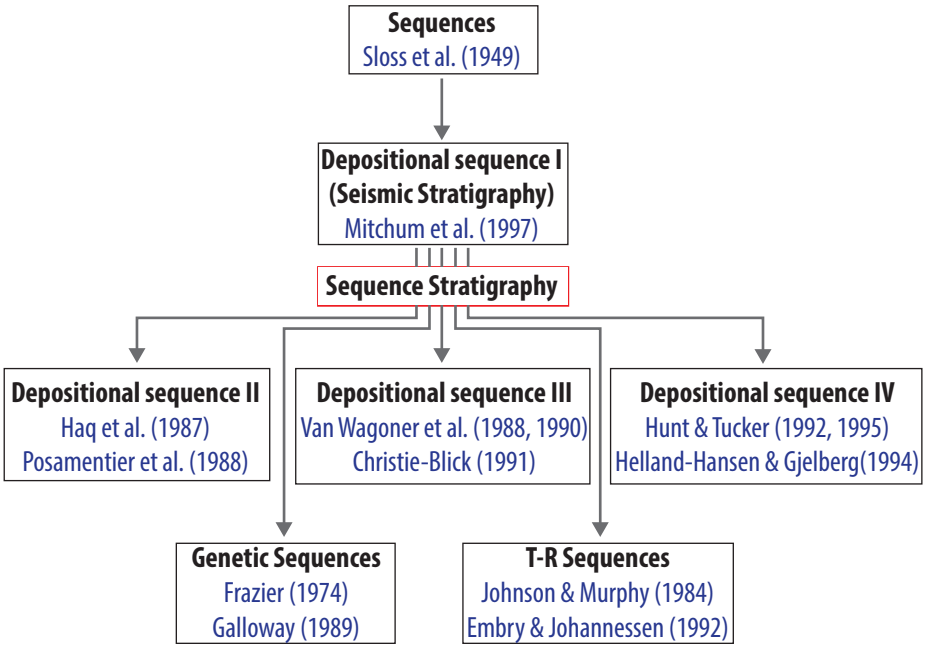

FIGURE 2.1: Evolution of the depositional sequence models (modified from *Catuneanu et al.*, 2009).

2.1.3 Methods & definitions of conventional sequence stratigraphy

Facies type and strike variability, conformable or unconformable contacts, depositional trends and stratal terminations are all features that can be observed in strata independent of any sequence model. Sequence model elements are used to determine the significance of these different observations, particularly in terms of what controlling factors may have led to their formation (e.g., accommodation variations).

Accommodation is defined as "the space available for sedimentation" (*Jervey*, 1988), and it is assumed in sequence stratigraphy that accommodation variations are the main controlling factor behind the development of various stratal geometries. In the marine environment, accommodation is equivalent to the space between base level (approximately sea level) and the sea floor. During filling of available accommodation by sedimentation the remaining space available is represented by the depth of water from the sea surface to the sea floor. Accommodation increases when the basin floor subsides or sea-level rises faster than sedimentation fills the available space (*Barrell*, 1917).

Base level is an imaginary 3D surface representing an equilibrium between deposition and erosion. It is often coincident with the shoreline and extended from sea-level beneath landscapes to represent the lowest level of continental denudation. It is generally agreed

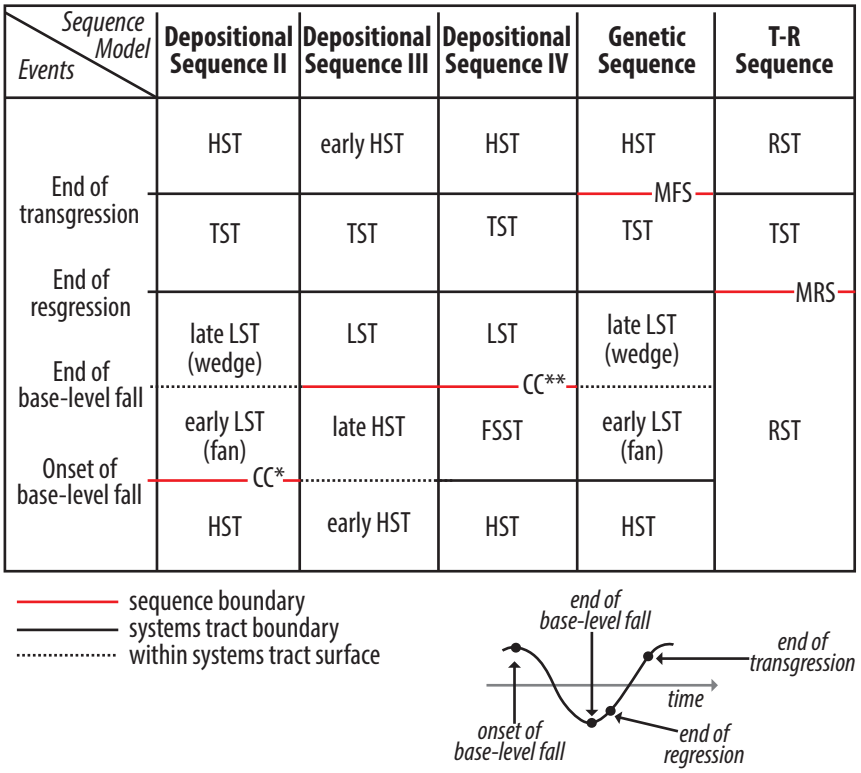

FIGURE 2.2: Nomenclature of systems tracts and timing of sequence boundaries for the existing sequence stratigraphic models (modified from *Catuneanu et al.*, 2009). Abbreviations: LST lowstand systems tract; TST transgressive systems tract; HST highstand systems tract; FSST falling-stage systems tract; RST regressive systems tract; TR transgressiveregressive; CC*correlative conformity *sensu Posamentier and Allen* (1999); CC** correlative conformity *sensu Hunt and Tucker* (1992); MFS maximum flooding surface; MRS maximum regressive surface. See Figure 2.1 for sequence model references.

that accommodation can be made available in both fluvial and marine environments by allogenic (external) controls (climate, tectonism, sea-level change), but if and how some change in base level controls upstream fluvial architecture has been an area of significant debate (*Blum and Törnqvist*, 2000). In the marine environment, quantifying accommodation is difficult given the dynamic nature of base level due to fluctuations in erosion rates and sediment supply (i.e. amount of sediment and grain size). Sea level is often a proxy for base level (*Schumm et al.*, 1987) so that accommodation is measured between sea level and sea floor. Amount of accommodation fluctuates through time due to independent and time-variable positions of sea level and sea floor relative to the Earth's centre.

Sea level is assumed to be a primary allogenic (i.e., external to the system) control on sedimentation, and is controlled by other allogenic factors climate and tectonism

(*Catuneanu*, 2006). Given this, and that variations in sea floor position relative to the Earth's centre are controlled by subsidence or uplift and sedimentation, the amount of accommodation available at any time and location equals some balance between how much space is created or destroyed by tectonism and sea-level change, and also how much of the space is consumed by sedimentation at the same time. The amount of accommodation created or destructed versus the amount consumed is a key aspect of sequence stratigraphy and is the basis for definition of systems tracts and sequence stratigraphic surfaces (*Catuneanu*, 2006).

Other important concepts and definitions involved in understanding accommodation include eustasy (sea level relative to the centre of the earth) and RSL (sea level relative to a datum that is independent of sedimentation, for example top basement), the latter being a proxy for an increase or decrease in available accommodation independent of sedimentation. Using RSL to express variations in accommodation during a period of time is different to simply water depth, since the latter accounts for the effect of sedimentation (*Catuneanu*, 2006).

Depositional trends

Depositional trends are defined on the basis of observed vertical facies relationships and classified as progradational, retrogradational and aggradational (*Van Wagoner et al.*, 1990; Figure 2.3A). The rate of change of accommodation (A) and rate of sediment supply (S) are the primary controls on shoreline migration and resulting stratal stacking patterns (*Barrell*, 1917, *Curray*, 1964, *Curtis*, 1970, *Frazier*, 1974, *Sloss*, 1962, *Vail et al.*, 1977) (Figure 2.3).

The influence these controls have on stacking patterns due to shoreline regression versus transgression can be expressed as a ratio. For example, where supply > accommodation, progradation results. Where supply < accommodation, retrogradation results. This relationship between accommodation and supply and the resulting contrasting scenarios were recognise prior to sequence stratigraphy. For example, *Curray* (1964) associated shoreline retreat with rising RSL and low sediment supply, and progradation during falling RSL and high sediment supply. The relationship between accommodation (via subsidence) and sediment supply was suggested by *Curtis* (1970) as a control on deltaic stacking patterns, before *Frazier* (1974) subdivided the Mississippi deltaic succession into progradational, aggradational and retrogradational phases. The use of regional

facies concepts to define depositional systems and systems tracts was later introduced by *Brown and Fisher* (1977).

The simple A/S relationship was later defined as the *A/S ratio concept* (*Muto and Steel*, 1992, 1997). It states that aggradation occurs when A/S is equal to 1, transgression occurs when $A/S > 1$, and progradation occurs when $A/S < 1$. Essentially, the A/S *ratio concept* forms the basis of all sequence models (Figure 2.2) in the sense that it is used to understand the origin of regression and transgression. However, despite this understanding, sequence stratigraphic models generally assume that accommodation variations are the dominant control on stacking patterns and other observed stratal architectures in basin margin settings (*Catuneanu*, 2006, *Catuneanu et al.*, 2009).

Stratal terminations

Mitchum et al. (1977) defined stratal terminations for interpreting reflection seismic profiles. Onlap and downlap terminations above and truncation and toplap below can be used to identify stratigraphic surfaces (Figure 2.4). Offlap was later recognised as an important stratal stacking pattern indicative of forced regressions, and subaerial unconformities and their correlative conformities (*Hunt and Tucker*, 1992).

Stratigraphic surfaces

Surfaces that can serve as boundaries between different genetic types of deposit (i.e. time related strata, such as forced regressive, reviewed below (Figure 2.5)) are regarded as sequence stratigraphic surfaces. Whether the surface observed is assigned as a sequence boundary, a systems tract boundary, or of some other significance, depends on the choice of depositional sequence model (Figure 2.2). For each type of surface, criteria available for identification includes the conformable versus unconformable nature of the contact, the depositional systems and depositional trends below and above the contact (Figure 2.3), and associated stratal terminations (Figure 2.4). There are seven sequence stratigraphic surfaces in total and some have more importance to sequence models than others. Three of these surfaces, which are of relevance to later chapters in this thesis, are briefly described below.

Subaerial unconformity

Unconformities that develop as a result of subaerial exposure in coastal and non-marine settings are integral to the definition of sequences. Subaerial unconformities can result from fluvial erosion and bypass, pedogensis and wind degradation (*Catuneanu et al.*,

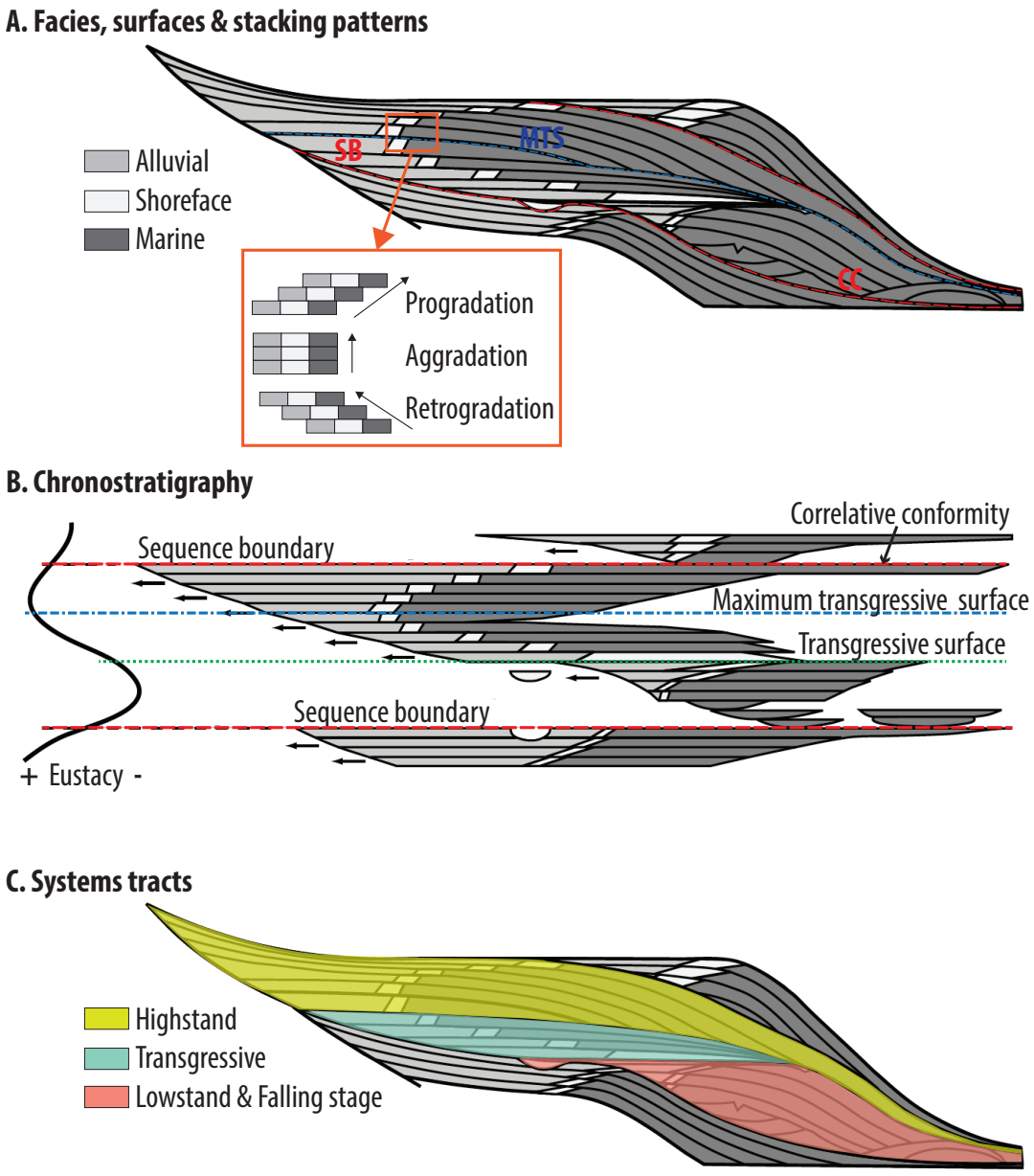

FIGURE 2.3: Elements of the sequence stratigraphic model, showing the predicted stratigraphic response to changing sea-level: A) Shelf-margin wedge schematic illustrating facies distribution, key sequence bounding surfaces (labelled in B) and depositional stacking patterns (*Van Wagoner et al.*, 1990). B) Chronostratigraphic diagram highlighting timing of key surfaces and stacking patterns in response to eustatic sea-level change. Red subaerial unconformities are commonly sequence boundaries and are correlated offshore to a marine correlative conformity. C) Representation of the three (*Posamentier et al.*, 1988, *Vail*, 1987) and four (*Hunt and Tucker*, 1995) stage systems tract models, the former not including a falling-stage systems tract, the latter including a falling-stage and separate lowstand systems tract. SB - sequence boundary, MTS - maximum transgressive surface, CC - correlative conformityAfter *Haq et al.* (1987) and *Posamentier et al.* (1988). Modified from *Swenson* (2005).

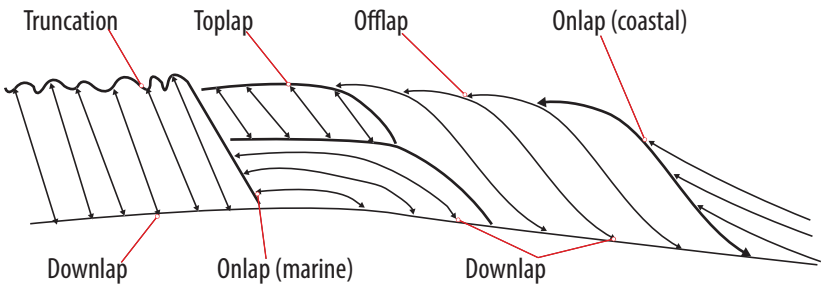

FIGURE 2.4: Types of stratal terminations for interpreting reflection seismic profiles, originally defined by *Mitchum et al.* (1977). See text for description (modified from *Emery and Myers*, 1996 and *Catuneanu*, 2006).

2009), and are assumed to form through all or part of a base level fall (Figure 2.3B), during periods of transgression provided there is coastal erosion, and during climate-driven fluvial discharge increase (e.g., *Blum*, 1994) (Figure 2.3B). *Plint and Nummedal* (2000) referred to the sequence bounding subaerial unconformity as the regressive surface of fluvial erosion, placing more weight on the assumption that rivers always incise during falling RSL. Unconformities can also develop by submarine erosion below sea level but are not used for sequence definition. Extending the correlation of a subaerial unconformity from the coastal setting to the marine setting (as illustrated in the schematic basin margin sediment wedge in Figure 2.3A) by recognising a correlative conformity is not straight forward, and this has been an area of debate in the mainstream sequence stratigraphic literature (e.g., *Hunt and Tucker*, 1992, *Posamentier et al.*, 1988).

Maximum transgressive surface

The maximum transgressive surface (MTS) records the maximum extent of marine flooding, separating transgressive units below from regressive units above (*Helland-Hansen*, 2009, *Miall*, 2010) (Figure 2.3A,B). The MTS is a downlap surface (Figure 2.4) in shallow water settings, where progradational clinoform toesets terminate as downlap onto a surface formed by sediment starvation during transgression. Along a depositional dip line the MTS corresponds to the end-of-transgression (Figure 2.3B). Along strike, the surface may record a higher degree of diachroneity, depending on subsidence rates and sediment supply variations (*Catuneanu et al.*, 2009). Some workers describe this surface as a maximum flooding surface (*Catuneanu*, 2006, *Catuneanu et al.*, 2009) since it represents a time of maximum flooding, whereas others refer to the surface as maximum

transgression because it is more consistent with other terminology in sequence stratigraphy (e.g., regression versus transgression) (*Helland-Hansen*, 2009, *Helland-Hansen and Martinsen*, 1996).

Correlative conformity

Two different correlative conformities have been proposed. *Posamentier et al.* (1988) describe the correlative conformity as a surface that marks the onset of RSL fall. The surface is placed at the base of the basin-floor submarine fan complex in deep-water settings. It is the oldest marine clinoform associated with offlap, representing the sea-floor at the onset of base level fall. In cases where offlap is not preserved this correlative conformity surface marks the change from an increase in the elevation of coastal facies. This correlative conformity is assumed to be marked by an increase in average grain size during continued progradation, due to the change in fluvial accommodation from the positive to negative at the onset of forced regression. A downside to this model assumption is that it could lead to circular reasoning. Circular reasoning would occur in this case because the correlative conformity is assumed to show an increase in grain size, therefore when an increase in grain size is observed it may be interpreted as evidence for the for the occurrence of a correlative conformity. This is then taken as evidence in support of the model validity. However, this could be an example of circular logic, because application of the model is not evidence that it is correct. *Hunt and Tucker* (1992) referred to this correlative conformity as basal surface of forced regression.

The second correlative unconformity advocated by *Hunt and Tucker* (1992) contrast to previous correlative conformity by marking the end of RSL fall. The surface is placed at the top of the coarsest sediment within the submarine fan complex in deep-water settings because it is assumed that this position marks the end of RSL fall. It is the youngest marine clinoform associated with offlap, representing the sea floor at the end of base-level fall at the shoreline. In cases where no offlap is preserved, this surface marks the change from a decrease to an increase in the elevation of coastal facies. Due to the change in fluvial accommodation from negative to positive at the end of forced regression, this type of correlative conformity may be marked by a decrease in average grain size during continued progradation.

Genetic types of deposits

Identifying stratal stacking patterns and stratigraphic surfaces is closely linked to interpreting the 'genetic' types of deposits shown in Figure 2.5. In sequence stratigraphy the genetically related deposits define strata deposited during different periods of an inferred sea-level cycle, including strata deposited during falling, steady and rising RSL. Unforced regressive strata are formed by supply driven progradation during steady or rising RSL, and recognised by aggradational topsets and a steady to rising shoreline trajectory. Forced regressive strata are formed during falling RSL and are distinguished by lack of topset strata and development of a subaerial unconformity. Transgressive strata formed by retrogradation during RSL rise are distinguished by a transgressive ravinement surface (*Catuneanu*, 2006), retrogradational stacking (Figure 2.3) and an ascending transgressive shoreline trajectory (shoreline trajectories are reviewed below).

These genetic types of deposit are often described as independent of the sequence stratigraphic model (*Catuneanu*, 2006, *Catuneanu et al.*, 2009). However, this is a potentially misleading description because the types of deposits shown in Figure 2.5 (e.g., forced regressive) are assigned specific stratal stacking patterns and stratigraphic surfaces which are assumed to result from particular RSL histories. This strict definition suggests that the genetic types of deposits in Figure 2.5 are highly model dependent, and their allocation in terms of RSL history is pre-determined and not open to interpretation. The definition of the strata shown in Figure 2.5 with respect to RSL history has been shown to be an oversimplification in a number of field, numerical and analogue modelling studies (e.g., *Blum and Törnqvist*, 2000, *Muto and Swenson*, 2005, *Petter and Muto*, 2008, *Swenson and Muto*, 2007, *Swenson et al.*, 2005).

Systems tracts

Systems tracts correspond to genetic stratigraphic units that incorporate strata deposited within a synchronous sediment dispersal system (*Galloway*, 2004), hence the systems tract concept is used to define a linkage between contemporaneous depositional systems. The different systems tracts are interpreted based on stratal stacking pattern and types of bounding surface, and each tract is assigned a position along an inferred curve of base-level changes at the shoreline (*Catuneanu*, 2006). From their initial definition (*Posamentier and Vail*, 1988, *Vail*, 1987, *Van Wagoner et al.*, 1988) systems tracts have received ongoing revisions (e.g., *Plint and Nummedal*, 2000, *Posamentier and Allen*, 1999). For example, early models defined four systems tracts, including the lowstand, transgressive, highstand and shelf-margin systems tract, relative to a curve of

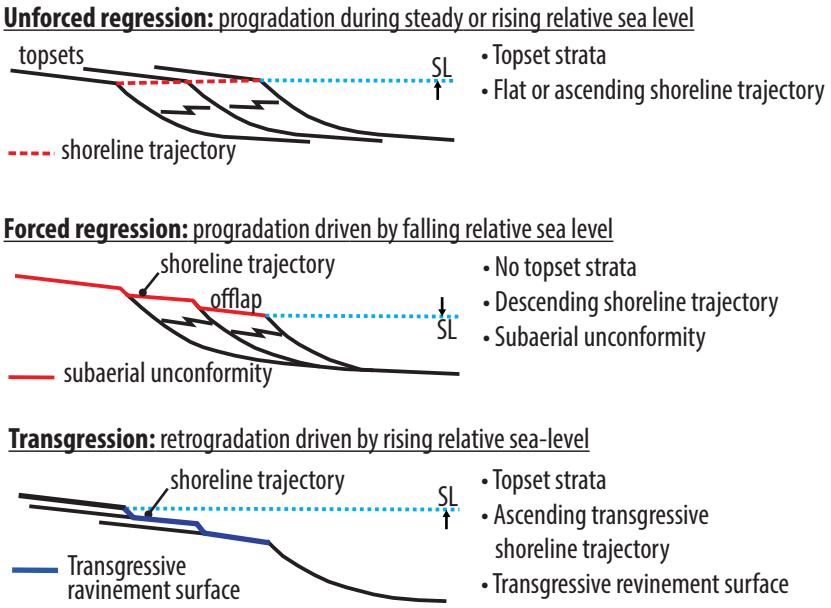

FIGURE 2.5: Genetic types of deposits: normal regressive, forced regressive and transgressive (modified from *Catuneanu et al.*, 2009).

eustatic fluctuations. This was replaced with a curve of RSL changes and a lowstand, transgressive, highstand and falling-stage systems tract (*Hunt and Tucker*, 1992) (Figure 2.3C).

2.1.4 The trajectory concept

Trajectory analysis is a relatively recent addition to the siliciclastic sequence stratigraphic methodology (*Helland-Hansen and Gjelberg*, 1994). The concepts and methods of trajectory analysis encompass both shoreline and shelf-edge trajectories (Figure 2.6) (note trajectories can be analysed on smaller scales, for example ripple migration), which can be defined as describing "the migration through time of sedimentary systems, using geomorphological breaks-in-slope that are associated with key changes in depositional processes and products" (*Helland-Hansen and Hampson*, 2009).

The basic principle of interpreting shoreline or shelf-edge trajectories, as illustrated in Figure 2.6, relies on identifying shoreline or shelf-slope-basin clinoforms and their maximum break-in-slope (known as a topset-foreset rollover) (*Helland-Hansen and Hampson*, 2009). In the case with shoreline clinoforms, the maximum break-in-slope represents a position of paleo sea-level. Shoreline clinoforms are observed with heights of tens of metres and the topset-foreset rollover is located close to the shoreline (Figure 2.6a) or, in some high energy deltaic settings (e.g., *Driscoll and Karner*, 1999), laterally separated from the shoreline (Figure 2.6b). In contrast to shoreline clinoforms, shelf-slope-basin

clinoforms generally have heights of hundreds of metres and record the advance of the shelf-margin (*Helland-Hansen and Hampson*, 2009) (Figure 2.6).

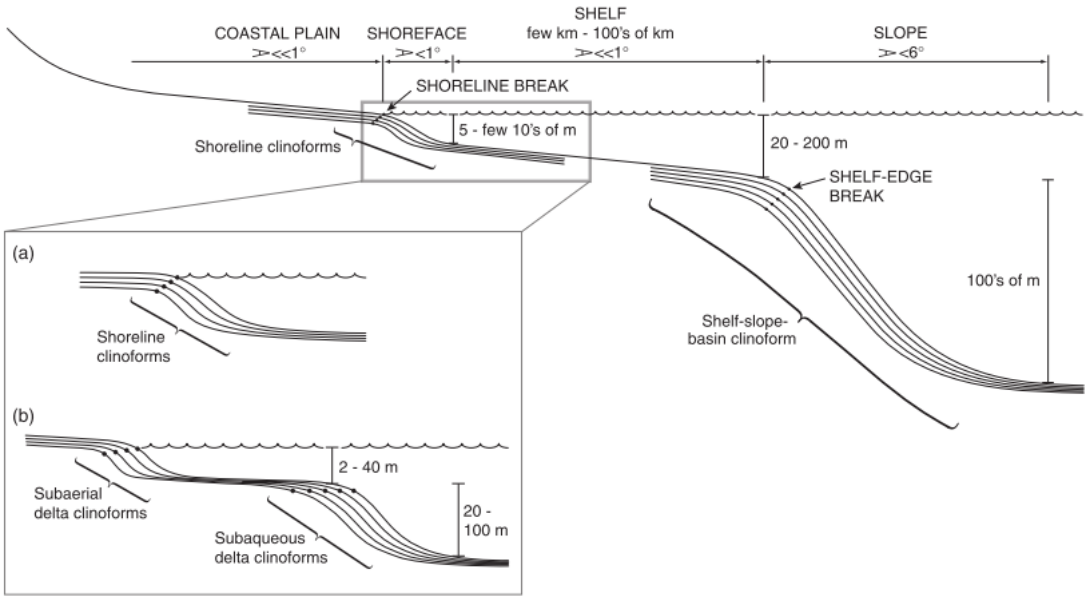

FIGURE 2.6: Shoreline and shelf edge trajectories illustrated on a simplified depositional-dip topographic profile (from *Helland-Hansen and Hampson*, 2009).

Trajectory classes

Trajectories can be interpreted from shoreline and shelf-slope-basin clinoforms observed in seismic sections which are orientated along the main depositional-dip axis. The trajectory of both the shoreline and shelf edge is function of bathymetry, sediment supply and RSL.

Shoreline trajectory classes, summarised in Figure 2.7, can be characterised on a descriptive bases. Ascending and descending classes emphasise the sense of verticle migration, whereas regressive and transgressive emphasise the basin or landward migration direction. In addition to these simple observational classes, *Helland-Hansen and Gjelberg* (1994) added an accretionary trajectory class to describe shoreline transits with sediment supply and a non-accretionary class to describe transits with no sediment supply. A final, recent addition to the trajectory classes is a stationary shoreline class, which occurs if a shoreline is stabilised in one position for a long period of time (*Helland-Hansen and Hampson*, 2009).

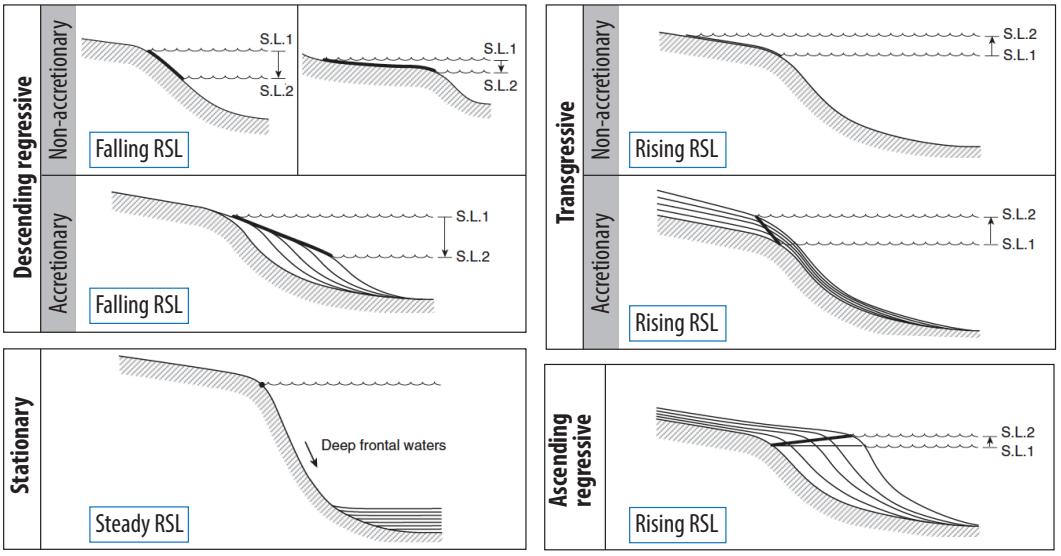

FIGURE 2.7: Shoreline trajectory classes of descending regressive (accretionary and non-accretionary), ascending regressive, transgressive (accretionary and non-accretionary) and stationary. Shoreline trajectory paths are indicated by bold lines (modified from *Helland-Hansen and Hampson*, 2009).

The shelf-edge trajectory is normally fixed or basinward-accreting, unlike the shoreline trajectory which can have complex trajectory paths due to both landward and basinward migration directions. Before considering preservation issues, one potential limitation of the method is the 2D nature of the interpretation (*Martinsen and Helland-Hansen*, 1995). Can 2D shoreline trajectories interpreted from seismic data successfully describe 3D clinoform development?

Reliability of shoreline trajectories

Classing shoreline trajectory transits or quantifying shoreline trajectory angles (e.g., *Hampson et al.*, 2009) realistically is dependent on knowledge of the original geometry during deposition. To determine this geometry a datum surface is required. Datum surfaces should be laterally extensive, have a palaeodip close to horizontal and be within a close stratigraphic proximity to the shoreline trajectory in question. Candidate datum surfaces include maximum transgressive surfaces, offshore and deep marine shale or carbonate markers and coal seams (*Helland-Hansen and Hampson*, 2009).

Quanitification of shoreline trajectories

Shoreline trajectories can be calculated from successive positions of the topset-foreset clinoform rollover, shoreline deposits, or facies-belt and erosional surface proxies for shoreline position (Figure 2.6; *Helland-Hansen and Hampson*, 2009). In each of these

cases, the trajectory angles are highly sensitive to the palaeo depositional-dip angle assigned to the datum surfaces. Post depositional compaction and data quality are also important factors that can influence accuracy of trajectory calculation. *Helland-Hansen and Hampson* (2009) provide a detailed methodology for shoreline trajectory calculation.

2.2 Modelling of basin-margin stratal geometries

2.2.1 Introduction

One of the first stratigraphic models by *Sloss* (1962) applied a simple numerical formulation to investigate basin-filling. This work suggested that stratal geometries are controlled by multiple variables including sediment supply, accommodation (a 'receptor value' of subsidence relative to base-level), sediment transport ('dispersal', measure of combined total effect of sediment transport), and sediment composition (*Sloss*, 1962). However, despite this early acknowledgement of multiple controls on sequence development, the subsequent sequence stratigraphic methodology went on to emphasise a eustatic control with strong predictive power in as-yet unexplored basins (*Vail et al.*, 1977).

This early model by *Sloss* (1962) of sequence development resulting from multiple controls set a scene for later numerical and physical modelling of basin filling. While conventional sequence stratigraphy focussed on a dominant control of sequence development by changes in accommodation (firstly by a global eustatic control (*Vail et al.*, 1977), and later by a RSL or base-level control (*Hunt and Tucker*, 1992, *Posamentier and Allen*, 1999), numerical and physical experiments exploring various aspects of the sequence stratigraphic model were providing evidence for multiple controls on sequence development.

In the following subsections, some results from physical and numerical stratigraphic modelling studies that impact sequence stratigraphy are reviewed chronologically.

2.2.2 Physical models of stratigraphic systems

There has been significant growth in the field of physical experimental stratigraphy and geomorphology over the last 20 years, with experiments now encompassing landscape

elements from channel reaches, from denudational hinterlands to depositional basins. The major advantage of physical stratigraphic modelling is that, despite the differences in spatial scale, time scale and material properties, the processes operating (e.g., erosional and transportation) are similar to those operating in natural systems (*Paola*, 2000).

Shelf gradients and lag times

Assumptions regarding reaction of coastal-plain, shelf and slope systems to changes in base-level made by sequence stratigraphic models were tested in physical modelling work by *Wood et al.* (1993,) and *Koss et al.* (1994). The flume tank experiments expanded on the simplistic sequence models in the sense that, during base-level fall, the shelf angle was shown to be an important control on sediment volumes derived from incision, and also that lags exist in delivery of fluvial sediment to deeper water systems as a consequence of time required for incision to propagate upstream.

Topset aggradation versus degradation & fluvial grade

In contrast to the sequence stratigraphic model (*Catuneanu et al.*, 2009; Figure 2.5) *Muto and Steel* (2004) demonstrated deltas aggrade during constant RSL fall using a series of flume-tank experiments. The authors suggested fluvial deltaic responses to steady RSL fall involves a switch from aggradational to a degradational regime, however, if this switch is not reached, deltas can aggrade throughout the duration of a RSL fall.

Sequence stratigraphic model predictions of sediment bypass versus topset aggradation are closely linked to the concept of graded fluvial profiles. "A graded river is one in which, over a period of years, slope is delicately adjusted to provide, with available discharge and with prevailing channel characteristics, just the velocity required for transportation of the load supplied from the drainage basin" (*Mackin*, 1948). Conventional sequence stratigraphic models predict that rivers aggrade during RSL rise and degrade during RSL fall, and that fluvial grade is an equilibrium response attained during steady RSL. In contrast to this view, *Muto and Swenson* (2005) showed with flume tank experiments that fluvial grade is more likely to be a non-equilibrium state. This is because with constant sediment supply and water discharge rate, rivers were incapable of attaining grade in the authors experiments with steady RSL. RSL fall was required for fluvial grade to be reached. A key point from their study is that their alluvial river system remained aggradational for a wide range of RSL amplitudes and durations.

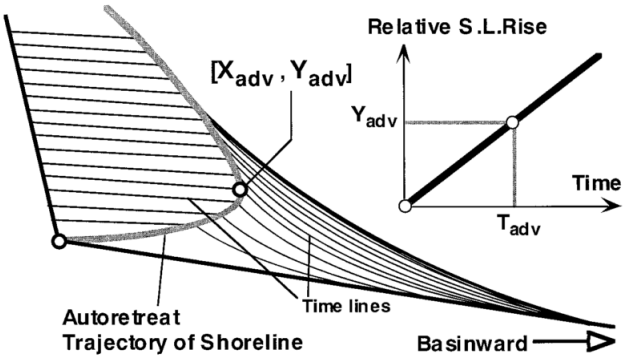

FIGURE 2.8: The theory of autoretreat demonstrated by *Muto and Steel* (1992). Autoretreat explains the inevitable landward retreat of a shoreline which occurs under conditions of constant rate of RSL rise and without change in any other parameters. Figure from *Muto and Steel* (1997).

2.2.3 Numerical modelling

Delta autoretreat

The theory of delta autoretreat (*Muto and Steel*, 1992) challenged the conventional viewpoint of sequence stratigraphy, that for a given constant sediment supply rate, increasing or decreasing rate of the horizontal component of the shoreline could only be caused by a decelerated or accelerated RSL change, respectively (*Posamentier et al.*, 1988). Autoretreat describes the autogenic response of the delta-front shoreline. If RSL is rising at a constant rate and all other parameters are constant, the shoreline will inevitably switch from regression to transgression during early progradation, and the rate of the movement of the delta front will change with time (*Muto and Steel*, 1992) (Figure 2.8). The retreat of the shoreline is inevitable because of the progressive increase in the surface area of the delta (both delta plain and delta front), hence constant supply of sediment cannot maintain progradation (*Muto and Steel*, 1997).

The A/S ratio concept

Closely related to the delta autoretreat theory is the principles of the accommodation (A) and sediment supply (S) ratio (A/S ratio). For example, autoretreat occurs when $A/S = const > 0$. The A/S ratio has been accepted for some time in the sense that migration of the shoreline (regression and transgression) is understood to result from some imbalance between accommodation and sediment supply (e.g., *Sloss*, 1962). However, (*Muto and Steel*, 1997) advocated the use of the A/S ratio concept in combination with autoretreat theory because neither of these two principles alone can account for regressive and transgressive shoreline transits (Figure 2.9).

Non-uniqueness

Non-uniqueness challenges sequence stratigraphy because it means that similar products

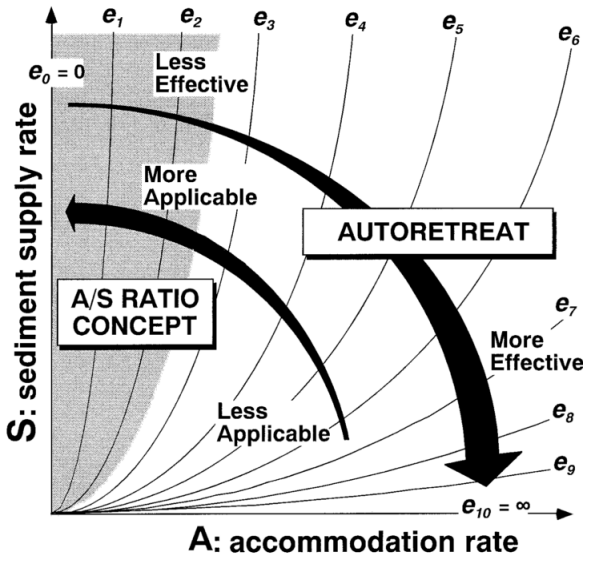

FIGURE 2.9: Conceptual diagram illustrating the 'effectiveness' of both the a/s ratio concept and delta autoretreat. Figure from *Muto and Steel* (1997).

can occur for different reasons. Sequence stratigraphic models are built on the assumption that various stratal geometries are unique in the sense they only form from one (non-specific) set of controlling processes. For example, sequence stratigraphy assumes topset aggradation is a unique product of steady and rising RSL, and therefore absence of topset aggradation indicates RSL fall (Figure 2.5). This is probably an oversimplification, and if so it complicates application of the sequence model. Maximum flooding surfaces (MFS) were demonstrated by *Flemings and Grotzinger* (1996) to be an example of a non-unique stratal geometry because they were generated by either an increase in the rate of accommodation creation during steady sediment supply, or by a steady increase in accommodation and a reduction in sediment supply through time. Such non-uniqueness has important implications for correlation using MFSs and is discussed later in the thesis.

Basin response time

The physical experiments demonstrating lag time in delivery of sediment (*Wood et al.*, 1993,) described above leads on to numerical studies investigating basin response time (*Marr et al.*, 2000, *Paola et al.*, 1992). The key reason for these studies is the importance of understanding the relationship between a basin's external conditions and its stratigraphic response when attempting to interpret stratigraphic architectures. The nature of a basin's response to external forcing can be highly dependent on the timescales of the forcing. This was demonstrated in terms of timescale forcing relative to a basin systems intrinsic timescale, or 'equilibrium time'. Systems with different intrinsic time scales (defined by the square of the basin length divided by the diffusivity, controlled

mainly by water flux) respond differently to identical forcing (*Marr et al.*, 2000, *Paola et al.*, 1992, *Rivenæ s*, 1997, *Steckler et al.*, 1993). Variable basin response time to external forcing is an important factor for sequence stratigraphy which attempts to subdivide stratigraphic architectures into time units. Similar but not necessarily contemporaneous stratigraphic response to external forcing could develop across a large area.

Alternative solutions to sequence stratigraphy

Although many studies have raised issues with the sequence stratigraphic methodology, few have provided any ways to enhance interpretation or prediction of siliciclastic sedimentary systems, for example timing of sand bypass to deep marine systems. An exception to this is a multiple-scenario numerical modelling method presented by *Burgess et al.* (2006) which accounts for a wide range of possible controls including sediment supply, sediment-transport rates, basin physiography and accommodation. The authors show first how these controls can contribute to determine stratal architectures, and then an analysis of the sensitivity of modelled deep-marine sand volumes to these controls (RSL, shelf width, sediment transport rates). A similar method was presented by *Falivene et al.* (2014), but with the addition of an objective function to ensure the included models fit the available data.

2.3 Future developments & thesis motivation

Sequence stratigraphy is a method to explain stratal relationships within a chronostratigraphic framework, and it is widely applied for understanding theoretical and practical problems from reservoir to continental scale. However, the method is based on a single, dominant control of stratal geometries by accommodation variations. An important question is whether the method requires the assumption of a dominant control by accommodation?

Attempting to subdivide observed stratigraphic architectures in to large scale (e.g., global) chronostratigraphic frameworks (e.g., *Simmons et al.*, 2007) based on a single control by accommodation is logically unrealistic given the complexity of a basin's stratigraphic response to allogenic (external to the basin system) and autogenic (internal to the basin system) controls. Some examples of this complexity have been described above (e.g., non-uniqueness, basin response time, delta autoretreat, etc).

It is probably not possible for sequence stratigraphy to accurately break down strata into time units based on a wider consideration of controlling processes aside from simply accommodation variations (e.g., time-variable sediment supply, variable sediment transport rates). A key reason for this is because extracting information from the stratigraphic record is an inverse method which is likely to produce non-unique results (e.g., *Flemings and Grotzinger*, 1996). Given this complexity, a simplifying assumption of control by accommodation has been required for application of the model. Consequently, applying the model may (1) produce correct results because accommodation variations are the dominant control or (2) the results may be correct for other reasons (e.g., non-uniqueness), or (3) the model doesn't produce correct results because the controls are more complicated than the model assumes.

The above mentioned physical and numerical modelling experiments of basin filling give some examples of why the single accommodation control explanation adopted by sequence stratigraphic models to understand the formation of stratal geometries may be an oversimplification.

Going forward and for the purpose of this thesis, (i) further understanding of the controls behind the formation of stratal geometries would be useful for improving a sequence stratigraphic model that does consider multiple controls, not just accommodation variations. Also, (ii) understanding how the current sequence stratigraphic model leads to unreliable interpretations and incorrect predictions is required to elucidate weaknesses of the single control assumption. Both of these points are required to address the question regarding whether sequence stratigraphy requires a simple accommodation dominant control model, and ultimately, move sequence stratigraphy forward.

Chapter 3

Numerical Model Descriptions & Methods

3.1 Introduction

The purpose of this chapter is to provide a description of the numerical stratigraphic forward models (SFMs) used in the thesis, as well as a detailed explanation of a methodology for running multiple model runs. Details of individual model runs, for example how parameter values were selected, are explained within the relevant chapters.

3.1.1 Numerical SFMs for simulating basin-margin stratal geometries

Many different algorithms for representing the erosion and deposition mechanism of sediments involved in basin evolution have been proposed and, broadly speaking, these can be classified into two groups: geometrical models and processed-based models.

The first group use empirical rules to essentially mimic the response of basin filling, but with the limitation that the dynamics of sediment transport are not considered. Often depositional slope angles are specified explicitly and are constant through the duration of the model run. Such examples are described in *Harbaugh and Bonham-Carter* (1981) and *Paola* (2000).

In contrast to geometric models, process-based models represent basin filling using various algorithms without explicit predefined geometric rules (e.g., slope angles), and such

attempts at representing basin filling processes can be further subdivided into fluid-flow models and dynamic-slope models. Fluid-flow models generally use simplified versions of the Navier-Stokes equations (e.g., SEDSIM, described below), and dynamic-slope models use mass conservation combined with a transport relation (e.g., diffusion - Dionisos, also described below) to average the long-term result of various processes of sediment transport. Some examples of available SFMs are listed in Table 3.1.

This thesis is based predominantly on numerical models generated in Dionisos. However, in the following chapter results from Dionisos are compared with some results from SEDSIM. Since SEDSIM and Dionisos are models based on different algorithms with different model assumptions, comparing results from both is a potentially useful way for elucidating unrealistic results. Both Dionisos and SEDSIM are described in detail below.

3.2 Dionisos numerical SFM

3.2.1 Introduction

There are several numerical SFMs available that are capable of simulating basin margin stratal architectures (Table 3.1), of these Dionisos is perhaps the most useful for this thesis because it combines the required spatial (i.e. hundreds of kilometres) and temporal (several millions of years) resolution alongside a relatively user-friendly graphical user interface (GUI) (Figure 3.1). The realism of model results from Dionisos will be discussed in the following chapters.

Dionisos is a 3D numerical SFM developed by the Institut Français du Pétrole (*Granjeon and Joseph*, 1999; *Granjeon*, 2002). The model is capable of creating complex 3D models of siliciclastic (and carbonate) strata through the representation of various sedimentary and tectonic processes. In this thesis the model is used to create various two- and 3D siliciclastic stratal geometries of the type often observed in subsurface datasets on basin-margins.

TABLE 3.1: State of the art numerical SFMs.

Model	***Developers***	***Type***	***Description***	***Reference***
Dionisos	IFP	Processed-based, dynamic-slope	Diffusional model capable of reconstruction clastic and carbonate strata on basin scale...transport and geo time	*Granjeon and Joseph* (1999)
SEDSIM	Stanford Univeristy & CSIRO	Processed-based, fluid-flow, geometric component	SEDSIM simulates deposition and erosion using an approximation to the Navier-Stokes flow equation set coupled with a geometric component determining maximum deposition angles for different facies groups	*Tetzlaff and Harbaugh* (1989) *Griffiths et al.* (2001)
SedFlux	CSDMS	Processed-based, dynamic-slope	Multicomponent high frequency and resolution process-response model	*Hutton and Syvitski* (2008)
Delft3D	CSDMS	Processed-based, fluid-flow	Three-dimensional hydrodynamic model with a number of modules, such as wave-current interaction, hydrostatic flow, salinity, temperature, cohesive sediment transport and more. Online GUI	*Lesser et al.* (2004)
SedPack	University of South Carolina	Geometric	Simulates clastic sediment transport based on slope angles and carbonate production based on water depths	*Kendall et al.* (1989)

3.2.2 Model parameters

Dionisos is operated from a simple graphical user interface (GUI) (Figure 3.1). To complete a single model run, Dionisos creates a **project file** based on the parameters specified by the user in the GUI. A Dionisos project file consists of a list of parameters and their values in a specific order and format. Dionisos reads a project file when a model run is executed. Parameters in a Dionisos project file include:

Model duration

Each simulation is performed from the past up to the present in a sequence of time steps. Each sedimentary layer in Dionisos is defined by the time-step.

Lithologies

For siliciclastic simulations, Dionisos lithologies are associated to grain size ranges. For example, mud =< 0.004 mm. The ratio of, for example, sand to mud, can be specified in the *boundary supplies* parameter (Figure 3.1).

Geometry

Figure 3.1 shows the result of a model run in Dionisos. The simulation area was determined by specifying x and y axis lengths (km) (e.g., large area made up of cells in Figure 3.1). Within this rectangular simulation area a series of regularly spaced square cells (i.e., equal along their x and y axis) were added by a grid point spacing (km) (Figure 3.1).

Boundary supplies

The boundary supplies (Figure 3.2) control panel allows time-variable sediment supply volume and river discharge rate to be specified. User specific input source location and width is also available, together enabling complex basin margin simulation with multiple time-variable supply sources.

Eustasy

Eustasy can be specified by a user-defined curve, cyclic curves, or short- and long-term Haq curves. Composite curves combining user-defined and cyclic curves can also be created.

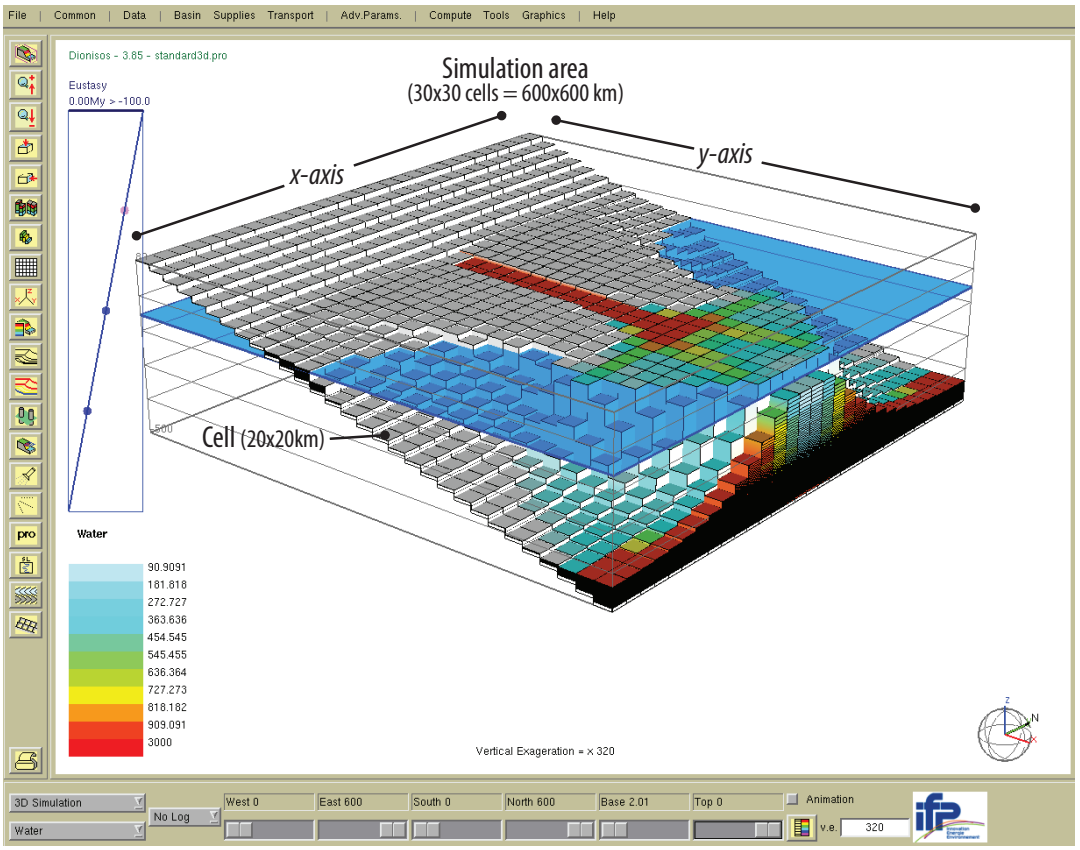

FIGURE 3.1: Example of a Dionisos model run illustrating the graphical user interface, simulation area made up of a grid of cells, and other visualisation tools.

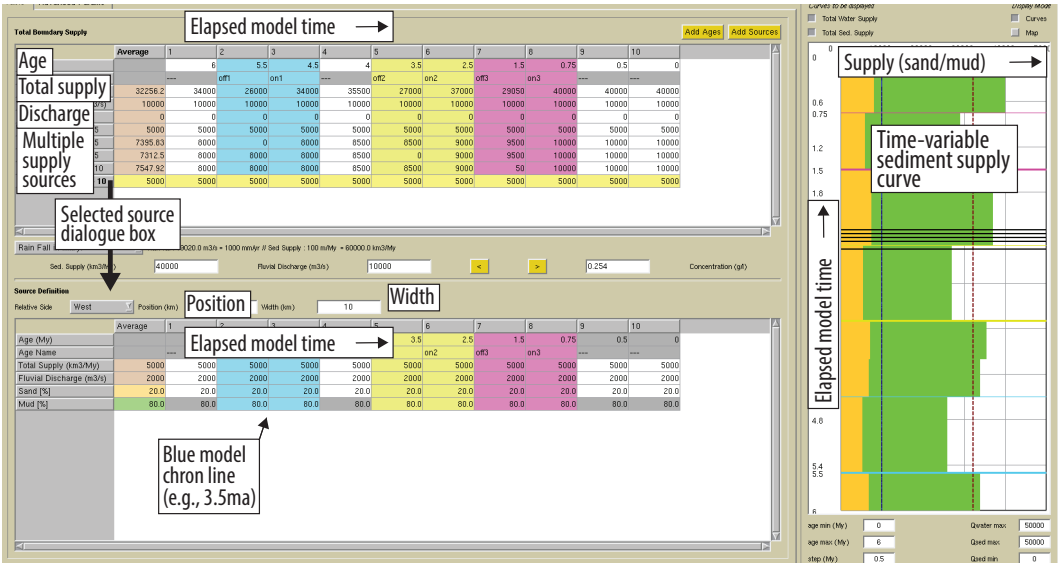

FIGURE 3.2: Sediment supply volume and water discharge rates are specified in the boundary supplies control panel. Multiple source locations and supply volumes can vary spatially through time, allowing relatively complex 3D simulations of basin-margin development.

Subsidence

Spatially varying subsidence rates through time can be simulated using a series of maps for 3D model runs.

Diffusion coefficients

Transport, deposition and erosion of sediment is partly controlled by terrestrial and marine diffusion coefficients for each grain size group. This aspect of the numerical model is described in more detail in the next section.

3.2.3 Sediment transport & numerical solution

Diffusion formulation

Sediment transport is calculated in Dionisos using a generalized modified diffusion formulation, where transport rate for each grain size group at any point on the model grid is dependent on the diffusion coefficient and the topographic gradient (*Granjeon*, 2002, *Granjeon and Joseph*, 1999). Gravity-driven sediment transport is calculated per model cell from

$$Q_s = K_g S \tag{3.1}$$

where Q_s is the sediment transport in square meters per year, K_g is the gravity-only diffusion coefficient in square meters per year, and S is the gradient of the topographic surface at a point in the model grid. Sediment transport also occurs under flowing water, calculated per model cell from

$$Q_s = K_w Q_w S \tag{3.2}$$

where K_w is the water-only diffusion coefficient in square meters per year and Q_w is a dimensionless number representing relative water discharge that is routed across the model grid using a simple steepest-descent algorithm (*Granjeon and Joseph*, 1999). *Rivenæ s* (1992) described a similar method of sediment transport calculation where the partial differential equations are also solved numerically via an implicit finite-difference scheme.

Implicit finite difference scheme

An implicit finite difference scheme is a numerical technique for solving partial differential equations. A partial differential equation is an equation which contains partial derivatives. In contrast to ordinary differential equations (which are centred on the fundamental existence and nonuniqueness theorem (*Ames*, 1977)), a partial differential equation exhibits its own special features reflecting the physical phenomena for which the equation was first used to model. Many founding physical and engineering theories are expressed by means of systems of partial differential equations, for example fluid mechanics is often formulated by the Navier-Stokes equations, electricity and magnetism by Maxwell's equations, and general relativity by Einstein's field equations.

The diffusion equation is an example of a partial differential equation

$$\frac{\partial u}{\partial t} = \frac{\partial}{\partial x}\left(D\frac{\partial u}{\partial x}\right) \tag{3.3}$$

where u is a function of x and t, and D is the diffusion coefficient. An initial value problem is defined because if information on u is given at some initial time t_0 for all x, the equations then describe how $u(x,t)$ propagates itself forward in time (*Press et al.*, 2007).

In Dionisos, partial differential equations at each time-step are solved numerically by using a fully implicit finite difference method, applying a Newton iteration scheme on the non-linear equations. Applying this type of iteration scheme allows progressively more accurate solutions to Dionisos' partial differential equations to be approximated (*Press et al.*, 2007).

In order for Dionisos to solve the partial differential equations at each time-step, a number of starting and boundary conditions are required. The implicit finite difference scheme essentially splits the space between the boundary and starting conditions into a grid of points (i.e., the Dionisos model grid, Figure 3.1) and renders approximate solutions as to the right values for each point in the grid using the Newton iteration scheme.

Figure 3.3 shows a 2D example. Information is known about the upper, right and top boundaries. The implicit method uses information from three points to approximate the next, working along each column and filling estimates for the next until the whole next

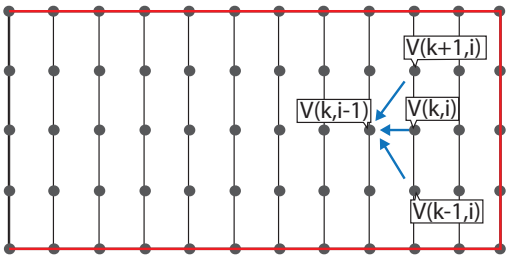

FIGURE 3.3: Simple diagram illustrating how an implicit finite difference scheme makes estimations of points within a 2D grid with known upper, lower and right-side boundary conditions.

column has estimates. The scheme then moves on to the newly calculated column and starts using those values to fill the next column, etc. (Figure 3.3).

Although the implicit finite difference scheme only approximates solutions to partial differential equations at each time step, this method is more appropriate for Dionisos compared to alternative schemes such as an explicit method. The key reason for this is stability. Stability ensures if the error between the numerical solution and the exact solution remains bounded as numerical computation progresses. An explicit finite difference scheme could yield an exact solution directly at each time-step, but a major problem with an explicit scheme is a lack of stability. In contrast to the explicit scheme, a fully implicit finite difference scheme can be unconditionally stable in so much that the time-step can be arbitrarily large. Given the long time-scales required in model runs reproducing basin-margin strata, the implicit scheme has an advantage in this respect. The implicit scheme also has an advantage over other methods (e.g., explicit, Crank-Nicholson) by being computationally efficient, which is a consideration for running large numbers (e.g., tens or hundreds) of model runs (e.g., *Williams et al.*, 2011).

3.2.4 Dionisos output

2D model runs are presented in this thesis as simple side view cross sections (Figure 3.4A), and chronostratigraphic charts are created to illustrate deposition and erosion in the model through time (Figure 3.4B). 3D models are displayed from an aerial view position (Figure 3.4C), and in some cases 3D models are shown in a dip-orientated cross section to illustrate aspects of stratal architecture variability along strike (Figure 3.4D). A number of other illustrative features available with the model are also used. Modelled strata are either classified by bathymetry, where positive bathymetry represents foreset strata and negative bathymetry (including 0) represents topset strata (e.g., grey and green, respectively, in Figure 3.4A), or according to a simple facies scheme based on

a number of parameters (Figure 3.4E). Deposited strata can be assigned to a facies depending on water flow, water depth, percent sand or mud, sediment thickness and age. This is particularly useful for recognising different marine facies and timings of non-deposition. For example, in Figure 3.4B, the red facies distinguishes a subaerial hiatus based on a water depth of < 0 and a sediment thickness of 0.0001 m. Similarly a marine hiatus is distinguished by dark blue in Figure 3.4B and D using the water depth (> 0 m) and sediment thickness (0.0001 m) facies classifications (Figure 3.4E).

3.3 ANALYSE: the multiple model program for Dionisos

3.3.1 Introduction

The principal purpose and importance of the ANALYSE program is that multiple model suites can be run with a range of different controlling parameters to systematically test the response of the model to various parameter value combinations. An advantage of this method is that, not only can different parameters be tested (e.g., eustasy, sediment supply) in terms of response of generated stratal geometries, but for each parameter a wide range of values can also be tested.

For example, using ANALYSE to run multiple numerical model suites in this thesis (chapters 4, 6) with a range of values of diffusion coefficients and a range of relative-sea level histories (e.g., amplitude of fall or rise) is a useful approach because it provides a set of results to determine the types of stratal geometries that can result from the different combinations of diffusion coefficient values and RSL histories.

ANALYSE was originally written by Didier Granjeon (Institut Français du Pétrole) and received subsequent modifications by Peter Burgess (Royal Holloway) and the author to enable quantitative analysis of various geometric relationships resulting from individual model runs with different parameter values. ANALYSE consists of around 1500 lines of C code and its purpose is to automate the running of multiple model suites.

A flow chart illustrating the main components of the program is shown in Figure 3.5, and the the program's input and output files are listed in Table 3.2.

A. Dionisos two-dimensional cross section

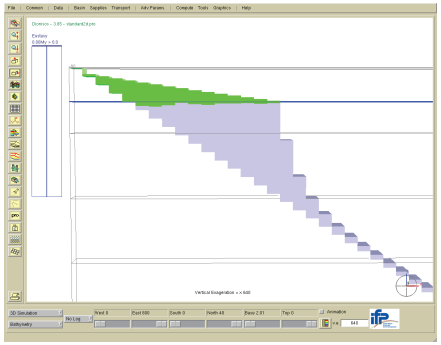

B. Dionisos two-dimensional chronostratigraphic diagram

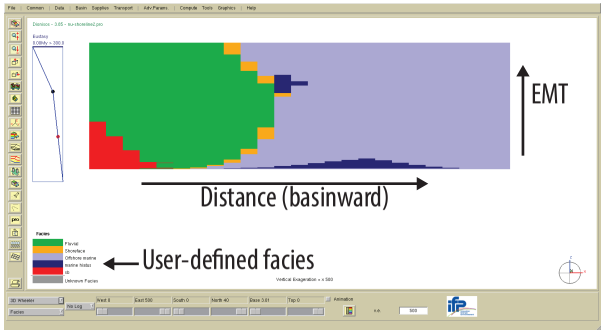

C. Dionisos three-dimensional model view

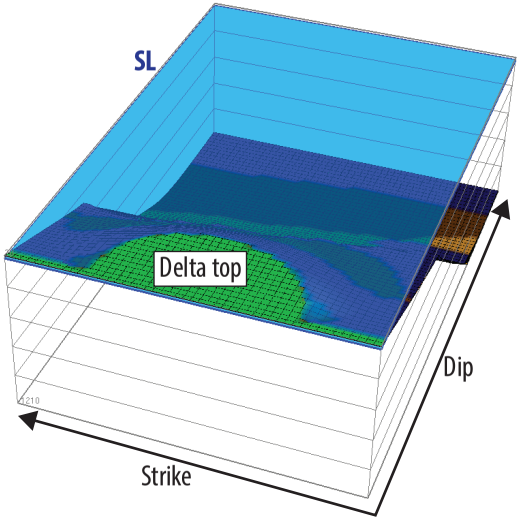

D. Dionisos three-dimensional dip-orientated cross-section

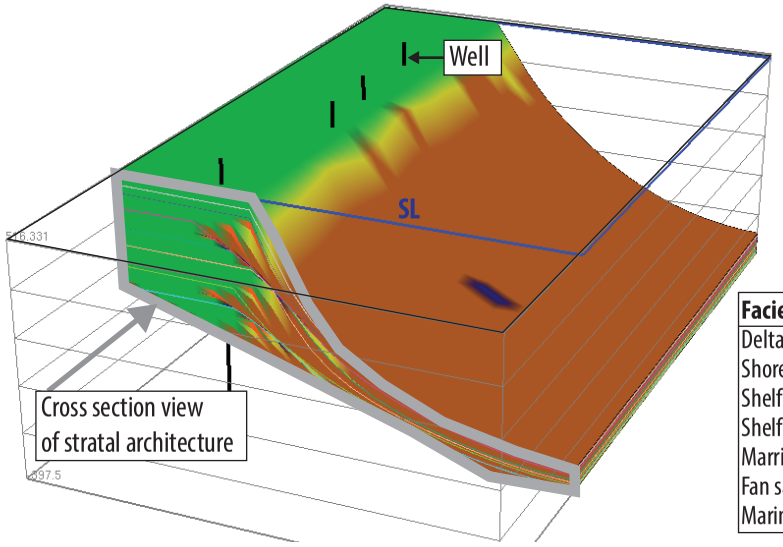

E. Facies scheme for D.

Facies name	colour	Water depth	Sand	Mud	Water Flow (%)	Sed. Thick (m)	Age (My)
Delta top		< 0	0 to100				
Shoreface		0 to 20	20 to 100				
Shelf shale		0 to 600	0 to 40				
Shelf sand		20 to 600	40 to 100				
Marrine shale		600 to 10000	0 to 30				
Fan sand		600 to 10000	30 to 100				
Marine hiatus		> 0	0 to 100			0 to 0.0001	

FIGURE 3.4: (Previous page.) Dionisos simulations can be illustrated in a number of ways: A) 2D model cross section with topset (negative bathymetry) and foreset (positive bathymetry) strata distinguished; B) 2D model run shown with a chronostratigraphic chart, where elapsed model time (EMT) runs vertically, and proximal to distal distance from the supply source runs from left to right, respectively; C) Aerial view of a 3D model run illustrating the delta top morphology; D) Cross section of a 3D model run to illustrate the internal stratal architecture of a modelled basin margin; E) deposited sediment can be interpreted using a range of facies or other classification schemes (e.g., percent sand, water depth, age, etc). Scale in all models is several hundreds of metres vertically by several hundreds of kilometres along dip (and strike in the 3D models).

TABLE 3.2: Files required by the multiple model program Analyse.

File	***Origin***	***Description***
default.pro	User generated and required by the program	Single Dionisos project file designed for the suite of multiple model runs. Aside from parameters iterated by the program (see Figure 3.5), all parameter values in this project file remain constant for the multiple model runs.
results.txt	Generated by the program	Simple text file to store results from the program, including the model run number, the parameters that created the model and the resulting t/f ratio.
_inv.pro	Generated by the program	Temporary project file. Information is copied from default.pro and from the Main Program. _inv.pro creates project files and saves them as 001.pro to 209.pro.
_inv.sav	Generated by the program	Stores simulated model cell information used to calculate cell volume and topset/foreset ratios.
#001.pro to #209.pro	Generated and saved by the program	Dionisos project files generated by the program for each model run.

3.3.2 Program operation

Analyse runs Dionisos from the command line a number of times determined by the user. This is achieved by specifying in the Main Program (Figure 3.5) the number of iterations for the parameters RSL fall (RSLfall in Figure 3.5) and terrestrial diffusion coefficient (Ksand and Kmud in Figure 3.5). For example, the flow chart illustrates how 209 model runs will be executed by looping firstly through 11 iterations of RSLfall, and for each of these cases, 19 iterations of Ksand Kmud (i.e., a nested loop). The number and parameter range of model runs can be increased simply by changing the start, end and increment values in the loops. Additional variable parameters, such as

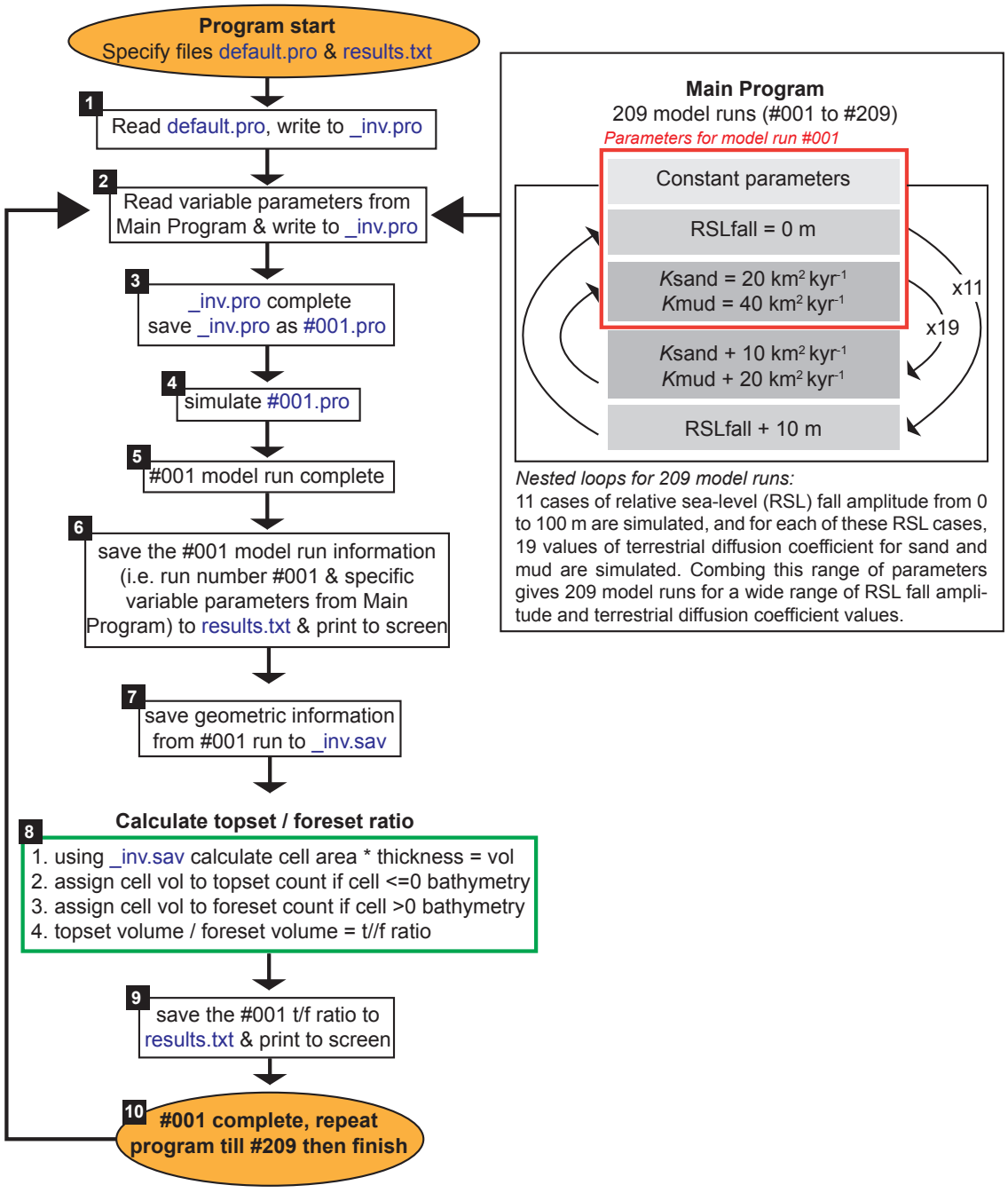

FIGURE 3.5: Flow chart illustrating the Dionisos multiple model run program Analyse. Five files are associated with the program (highlighted in blue text) and these are described in Table 3.2. Main Program controls the number of model runs by looping through parameter values. Parts 2 to 9 in the flow chart illustrate how Analyse copies, writes, executes and saves 209 project files based on the default project (default.pro). Part 8 of the flow chart includes the program's calculation of a t/f ratio.

river discharge rate and sediment supply volume, can be included using more nested loops in the Main Program code.

With reference to Figure 3.5, consider model run number 1 of 209 model runs in Dionisos. When starting ANALYSE, a Dionisos project file called *default.pro* and an output file for storing data called *results.txt* are specified. The Dionisos project file *default.pro* is a simple text file containing all of the parameter information required for a single model run. The project file *default.pro* has been set up specifically for this suite of model runs. All of the parameters (e.g., sediment supply, initial topography, etc) in *default.pro* are constant for the suite of model runs except for Ksand/Kmud and RSLfall. ANALYSE iterates through a range of values for these two the parameters (Ksand/Kmud and RSLfall) (Main Program in Figure 3.5). After specifying the project file *default.pro* and result file *results.txt* and executing ANALYSE from the command line, ANALYSE performs the following to complete model run number 001:

1. writes *default.pro* to a temporary file named *_inv.pro*;
2. stops writing information from *default.pro* to *_inv.pro*. Reads parameter values for RSLfall and Ksand/ Kmud from Main Program and writes this to *_inv.pro*;
3. recommences copying from *default.pro* to *_inv.pro* to make a complete Dionisos project file. *_inv.pro* is copied to a new project file named *#001.pro*;
4. simulates model run number #001 using the project file *#001.pro*, which has just been created based on the standard parameters in *default.pro* and the parameters taken from Main Program (*RSLfall* and Ksand/Kmud);
5. completes model run number #001;
6. prints selected model #001 parameters, including *RSLfall*, Ksand/Kmud, to the screen and to the file *results.txt*;
7. after model run #001 is complete, calculates sediment volume deposited per model cell. This is done by multiplying cell area (i.e., grid point spacing) with cell thickness. This geometric cell information is saved to *_inv.sav*;
8. uses sediment volume per cell from *_inv.sav* to calculate a topset foreset ratio. This ratio characterises the proportion of topset strata deposited in the model run

relative to foreset strata. When no topset strata are preserved the t/f ratio is zero. When topset strata are preserved the t/f ratio is > 0;

9. prints t/f ratio information to screen and to the results file *results.text*.

10. repeats this process until the loops specified in Main Program are complete, and all the parameter values have been simulated.

ANALYSE enables multiple model runs to be executed systematically, so that many hundreds of individual model runs with specific parameter values for terrestrial diffusion coefficients and RSL change can be assessed in terms of their generated stratal geometry. ANALYSE characterises the proportion of topset strata deposited in the modelled stratal geometries from the suite of model runs using a simple topset foreset ratio. This allows the range of values for terrestrial diffusion coefficients and RSL change to be evaluated in terms of their influence for deposition or erosion of topset strata.

3.4 SEDSIM

3.4.1 Introduction

In contrast to the processed-based dynamic-slope model Dionisos, SEDSIM is a 3D processed-based fluid-flow model with a geometric component. SEDSIM was developed initially at Stanford University in the 1980s, with current development ongoing at the Commonwealth Scientific and Industrial Research Organisation (CSIRO). The model includes Fortran 77 programs that incorporate physical laws based on fluid flow dynamics to simulate erosion, transport, and deposition of sediment by flow in open channels (*Martinez and Harbaugh*, 1993). In this thesis a number of single SEDSIM model runs are executed to compare with results from the diffusional SFM Dionisos.

3.4.2 SEDSIM operation

SEDSIM is operated from a DOS command window on a Windows machine. To run a simulation (e.g., delta-project, in Figure 3.6 and Table 3.3), a command file (*delta-project*.sif) and a number of ASCII input files (Table 3.3) are required. The command file contains essential code for the model to run, along with some simple parameters

including model duration and sediment supply. The input files contain further parameter information. For example, a .sl file contains the sea-level parameter values.

Once the command file is set up and SEDSIM is executed from the command line (step 1 in Figure 3.6), the available input files are called by the program. Once SEDSIM has run the simulation, output files are generated (step 2 in Figure 3.6). The .GRAPH output file is used to view the simulation result in the associated program, SEDVIEW. An example of SEDSIM output viewed in SEDVIEW is shown below (Figure 3.7).

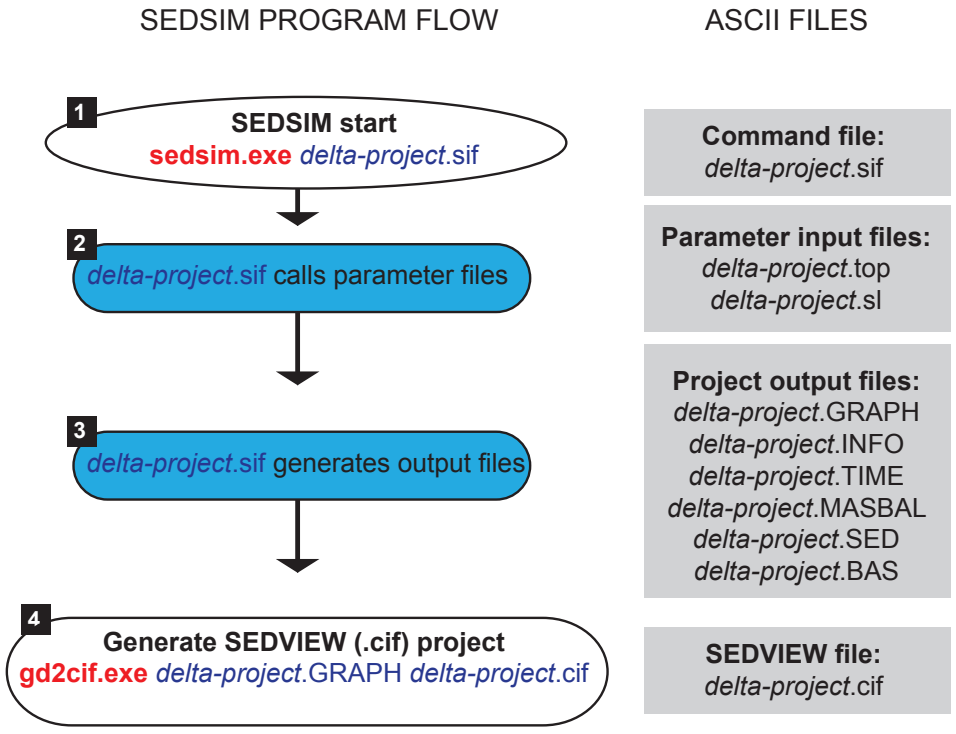

FIGURE 3.6: Simple flowchart summarising the basic operation of SEDSIM SFM. The basic steps are shown on the left, and associated input and output files are on the right. Commands are in red text and key files for SEDSIM and SEDVIEW operation are in dark blue. See text for description.

One of the downsides to SEDSIM's processed-based fluid-flow approach is that the model is computationally intensive. Individual model runs can take several tens of minutes to complete even with reasonable computer processing speed. Therefore, SEDSIM does not lend itself to a multiple model run methodology.

TABLE 3.3: SEDSIM ASCII input and output files.

File	***Origin***	***Description***
project.**sif**	Input	The main command file
project.**top**	Input	Topographic file of the initial surface
project.**sl**	Input	Sea-level elevation through time
project.**tec**	Input	Uplift and subsidence grid files
project.**GRAPH**	Output	Main output file. Contains sedimentation records at each cell and each layer. Can be displayed in SEDVIEW
project.**BAS**	Output	Basement change output file
project.**INFO**	Output	Status of SEDSIM run
project.**TIME**	Output	Information about the time progress of the simulation
project.**SED**	Output	Record of the fluid elements
project.**MASBAL**	Output	Mass balance file containing statistics of sediment budget

3.4.3 Model Parameters

There are a number of parameters available allowing for complex 3D simulations. For simulation of basin-margin stratal geometries, the following SEDSIM parameters are used.

Model duration

Simulation start and end time are specified for each model run. A display interval determines how often the results files are updated, and a flow sampling interval decides how often fluid elements are released from the source.

Sediment supply

Sediments are grouped by grain size. Four grain size groups include Coarse (0.28 mm), Medium (0.15 mm), Fine (0.03 mm) and Finest (0.0003 mm). Multiple sources can be arranged in the model each with a start and end time for sediment supply, a location, discharge rate (m^3/sec), sediment concentration (kg/m^3) and composition (% of each grain size group).

Sediment transport

To represent sediment transport on basin margins SEDSIM applies a simplified version of the Navier-Stokes flow equations. Erosion, transport and deposition of four grain sizes is modelled using semi-empirical relationships to predict the sediment distribution over a given surface (*Griffths and Paraschivoiu*, 1998). Algorithms trace fluid elements across the model grid, and depending on the fluid velocity, grain-size and settling velocity grains are deposited or eroded (*Tetzlaff and Harbaugh*, 1989).

Angle of deposition

SEDSIM has a geometric component for shallow-marine and coastal facies, where erosion and deposition are determined by depositional slope angles defined explicitly and kept constant through the simulation. This 'slope angles' module allow for different grain size groups to have different depositional slope angles.

Initial topography

Initial topography in the SEDSIM model runs is determined by a model grid *.top* file. Grid spacing (m), base level elevation, and number of rows and columns are required parameters. Lower left (SW) corner coordinates can also be specified.

Eustasy

Eustasy is defined in a simple 2 column (elevation and time) text file. Initial base-level elevation is specified in the topography parameter.

3.4.4 SEDSIM output

On completion of a simulation several output files are generated which contain information regarding the fluid element behaviour in the model run. The main output files are listed above in Table 3.3. These files include data on deposition and erosion of sediment, the sediment composition at each layer, surface elevation at each time step, etc. SEDVIEW is an additional desktop application required to visualise results from a SEDSIM simulation.

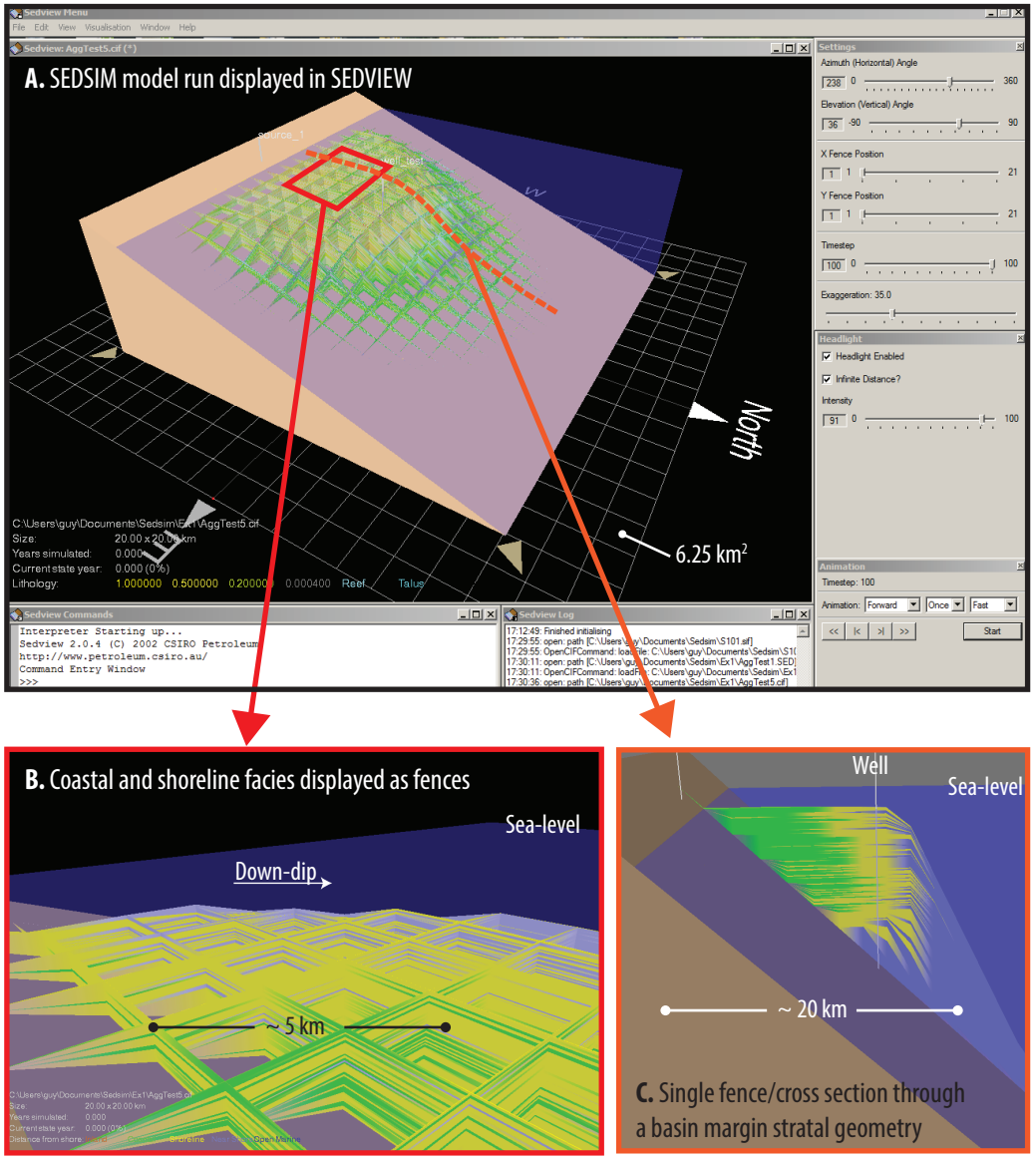

FIGURE 3.7: Example of a SEDSIM model run displayed in SEDVIEW (A). The interface includes a range of display modes to visualise modelled strata, including the ability to evaluate stratal architectures with fences (B) and cross sections (C).

Chapter 4

Numerical Modelling of Falling-Stage Topset Aggradation: Implications for Distinguishing between Forced & Unforced Regressions in the Geological Record

4.1 Introduction

Sequence stratigraphic models make a significant distinction between forced and unforced regressive strata (*Catuneanu et al.*, 2009), the former resulting from relative sea-level (RSL) fall, and the latter from rate of sediment supply exceeding rate of accommodation creation (*Porbski and Steel*, 2003). Forced regressive strata are assumed to contain little or no aggradational topset and display downstepping progradation with development of a descending shoreline trajectory and a subaerial unconformity (Figure 4.1; *Catuneanu et al.*, 2009, *Helland-Hansen and Hampson*, 2009, *Helland-Hansen and Martinsen*, 1996, *Posamentier and Morris*, 2000). In contrast, strata deposited during unforced regressions are assumed to show significant topset aggradation and a horizontal

to ascending shoreline trajectory due to creation of accommodation during progradation (Figure 4.1).

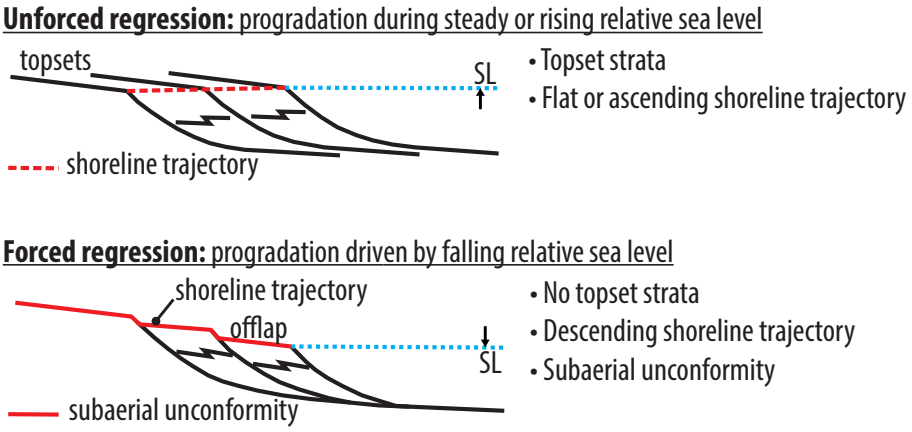

FIGURE 4.1: The conventional genetic types of deposit defined by stratal stacking patterns, modified from *Catuneanu et al.* (2009).

The ability to distinguish between these two possibilities is important, not least because it determines predictions of volume and style of sediment bypass, which may vary significantly between forced and unforced regressive cases. Unfortunately, because present models contain implicit assumptions about sediment supply and the response of coastal plain and fluvial deposystems to falling and rising RSL, it is possible that these two scenarios do not adequately account for the potential variability in strata generated by the mechanisms of forced and unforced regression. Related to this variability, it is also possible that stratal geometries generated by various RSL histories might be non-unique.

A unique stratal geometry is demonstrably different from other stratal geometries and results from only one set of controlling variables with specific values. In contrast, a non-unique stratal geometry can occur as a consequence of many different combinations of controlling variables that all result in similar strata. Non-unique stratal geometries can also occur due to similar results from entirely different processes. A flooding surface is a good example of a non-unique stratal geometry. Flooding surfaces can develop due to an increase in the rate of creation of accommodation during steady sediment supply, or a reduction in sediment supply during a steady increase in accommodation (*Flemings and Grotzinger*, 1996).

There is some compelling evidence to suggest that topset aggradation is non-unique in the sense that significant fluvial deposition can occur during both RSL rise and fall.

Experimental and theoretical studies investigating autogenic responses of fluvio-deltaic systems to changes in RSL have demonstrated that fluvial aggradation can occur during rising and steady RSL but also during RSL fall (e.g., *Burgess and Allen*, 1996, *Helland-Hansen and Martinsen*, 1996, *Johannessen and Steel*, 2005, *Martin et al.*, 2009, 2011, *Muto and Swenson*, 2005, 2006, *Muto et al.*, 2007, *Rittenour et al.*, 2007, *Swenson and Muto*, 2005, 2007). For example, *Muto and Steel* (2004) described fluvial aggradation in flume-tank experiments during steady RSL fall before an autoincision threshold was reached. *Muto and Swenson* (2006) investigated conditions necessary to attain fluvial grade on a simple ramp topography, and showed that rivers can remain aggradational during RSL fall before grade is reached, after which the river becomes degradational. *Muto et al.* (2007) argued that rivers can aggrade throughout the duration of a RSL fall provided that the RSL history does not cross a critical grade curve.

Basin-margin topography is also likely to be a key control on fluvial aggradation versus incision (*Schumm*, 1993). Two simple contrasting scenarios have been considered, one where the shelf gradient (β) is greater than the coastal-plain gradient (α) and one where $\beta < \alpha$. Most studies exploring fluvial response on a basin topography when $\beta > \alpha$ suggest that erosion and incision of the exposed topography is the most likely consequence during RSL fall (e.g., *Blum and Törnqvist*, 2000, *Cant*, 1991, *Leeder and Stewart*, 1996, *Schumm*, 1993, *Wood et al.*, 1993). However, *Leeder and Stewart* (1996) suggested that with high sediment supply fluvial aggradation could occur in a $\beta > \alpha$ case even during RSL fall. Studies investigating basin physiographies with $\beta < \alpha$ suggest that fluvial aggradation will occur with this physiography even during RSL fall (*Blum and Törnqvist*, 2000, *Cant*, 1991, *Heller et al.*, 2001, *Koss et al.*, 1994, *Muto and Swenson*, 2005, *Petter and Muto*, 2008, *Schumm*, 1993, *van Heijst and Postma*, 2001)

Helland-Hansen and Martinsen (1996) considered shoreline trajectory gradients relative to initial basin topography and suggested that topset aggradation is most likely to occur when the gradient of the alluvial plain is steeper than the shoreline trajectory gradient. In contrast, when the shoreline trajectory is steeper than the alluvial gradient (i.e., fast RSL fall and/or low gradient shelf), it is suggested that fluvial erosion and incision is common (*Helland-Hansen and Martinsen*, 1996).

Overall, this previous work suggests the possibility that topset aggradation during RSL fall may be more common in the geological record than is currently commonly assumed.

4.1.1 Aim of this chapter

This work uses a diffusional stratigraphic forward model to build on the work from previous studies and investigate how topset aggradation might develop during RSL fall across a wide range of model parameter values. A metric based on proportions of topset and foreset area or volume is used to analyse the degree of topset aggradation in strata generated in each model run. Several hundred numerical simulations have been run in a stratigraphic forward model called Dionisos to examine the consequences of varying sediment transport rates and the initial topography on forced and unforced regressive strata produced by a range of different magnitudes and different durations of RSL fall. Models generated in 2D are verified with a set of 3D multiple model runs, and a small number of forced regressive stratal geometries are generated in a different stratigraphic forward model called SEDSIM for comparison. The results from this work have important consequences for the sequence stratigraphic model, and how we interpret topset aggradation in ancient strata, with implications for interpretation of sand bypass and for the reconstruction of RSL histories.

4.2 Numerical model descriptions & modelling methods

4.2.1 Dionisos model formulation & parameter values

Dionisos is a 3D stratigraphic forward model developed by the Institut Français du Pétrole (IFP) (*Granjeon and Joseph*, 1999). The model simulates basin-scale sediment transport on geological time scales using a diffusional approach. Erosion, sediment transport, and deposition are modelled based on a modified diffusion formulation where rates of sediment transport for multiple grain sizes are determined by topographic slope, terrestrial and marine diffusion coefficients, and water flow (*Granjeon and Joseph*, 1999; Figure 4.2).

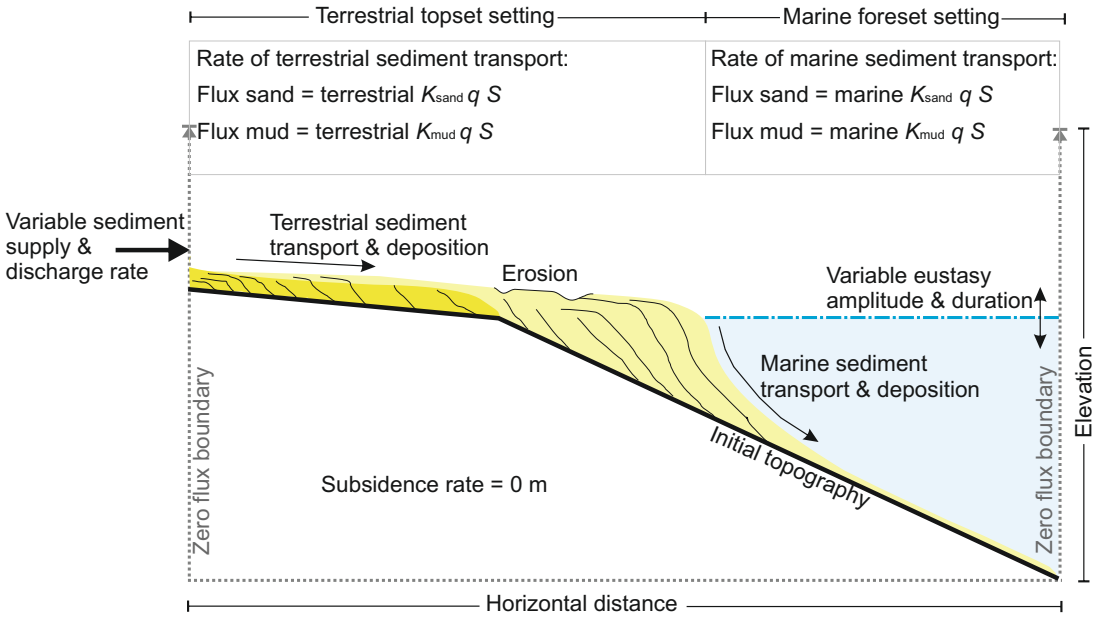

FIGURE 4.2: Components of the Dionisos modelling tool. K = terrestrial or marine diffusion coefficient, q = water discharge, and S = slope. See text for description.

Model Grid Dimensions and Initial Topography

2D models in this work each represent an 800-km-length cross section through a typical basin-margin sediment wedge along the main axis of sediment transport in a delta system. The 2D grid consists of a 1-by-40 grid of cells where each cell has a length of 20 km. 3D models were run on a 40-by-40 grid giving an areal extent of 800 km by 800 km. 2D models were run on a ramp topography and a shelf-slope topography (Figure 4.3) to consider how stratal geometries might be controlled by different initial basin-margin topographies in Dionisos. The shelf-slope topography (Figure 4.3B) was selected to investigate how stratal geometries generated in Dionisos might differ from stratal geometries produced in previously published conceptual and physical modeling studies with a geometrically similar initial basin topography (i.e., $\beta > \alpha$) (e.g., *Leeder and Stewart*, 1996, *Wood et al.*, 1993). Both initial topographies have a total relief of 800 m. The ramp topography has a constant slope angle of 0.06 °, and the shelf-slope topography has a break of slope at initial sea level from a terrestrial angle of 0.06 ° to a marine angle of 0.1 ° (Figure 4.3B). These values are similar to measured gradients from medium-scale to large-scale river-dominated delta systems, for example the GangesBrahmaputra, McKenzie, Po, and Amazon delta plain gradients range from 0.01 to 0.2 m km^{-1} (*Reading and Collinson*, 1996). The same initial ramp topography was

used for the 3D models, but extended along strike with constant geometry.

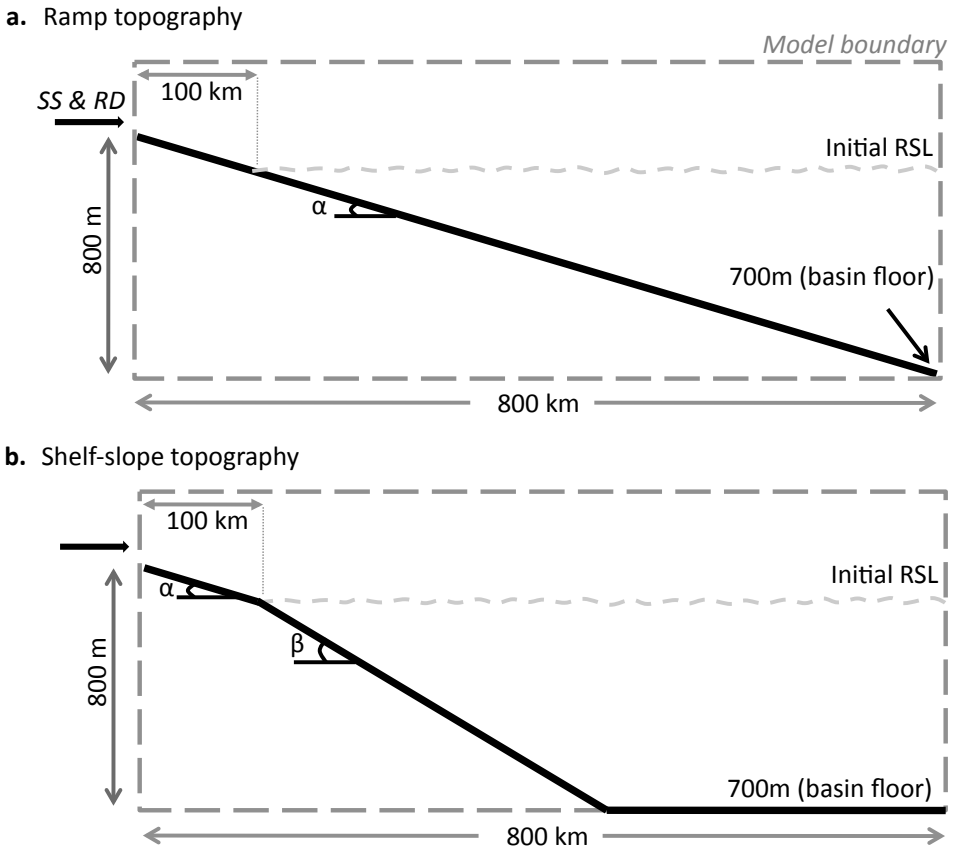

FIGURE 4.3: Dionisos 2D initial topographies: A) ramp topography used for 2 My and 0.4 My duration multiple model runs and B) shelf-slope topography with a change of slope at the point of initial sea level (based on work by *Leeder and Stewart*, 1996, their fig. 1). $\alpha = 0.06\,°$, $\beta = 0.1\,°$, SS = sediment supply, RD = river discharge. Vertical exaggeration approximately X 250.

.

Sediment supply

For the three dimensional models a sediment supply volume of 10000 km^3My^{-1}, and a river discharge value of 9.46 x $10^{13}km^3My^{-1}$ (3000 m^3s^{-1}) were used, representing a typical small to medium sized river system. For example, sediment supply values of 9500 km^3My^{-1} and 10500 km^3My^{-1} are observed for the Volta and Ebro rivers (*Burgess and Hovius*, 1998), and discharge rates of 1500 m^3s^{-1} measured for the Po (*Boldrin et al.*, 2005), 1700 m^3s^{-1} for the Rhone (*Marion et al.*, 2010) and 3000 m^3s^{-1} for the River Nile (*Kundzewicz et al.*, 2009). Sediment supply and fluvial discharge for the 2D model runs were determined by scaling down the values used in the 3D models by a factor of ten to 1000 km^3My^{-1} and 6.31 x $10^{12}km^3My^{-1}$ (200 m^3s^{-1}) respectively. These values

generate similar stratal geometries in the 2D and 3D models when all other parameters are the same, suggesting that they are a reasonable 2D approximation of medium sized river sediment supply. Sediment was delivered to the model at the proximal end of the grid, as a point source in the case of the 3D models. The distal end of the model grid had a closed zero-flux boundary, but was sufficiently distal from the modelled clinoforms that little or no sediment reached this point, so there were no significant edge effects resulting from the zero-flux condition.

Sediment transport

Sediment transport is calculated using a generalized modified diffusion formulation, where transport rate for each grain size group at any point on the model grid is dependent on the topographic gradient at that point and the diffusion coefficient (*Granjeon and Joseph*, 1999). Gravity-driven sediment transport is calculated per model cell from

$$Q_s = K_g S \tag{4.1}$$

where Q_s is the sediment transport in square meters per year, K_g is the gravity-only diffusion coefficient in square meters per year, and S is the gradient of the topographic surface at a point in the model grid. Sediment transport also occurs under flowing water, calculated per model cell from

$$Q_s = K_w Q_w S \tag{4.2}$$

where K_w is the water-only diffusion coefficient in square meters per years and Q_w is a dimensionless number representing relative water discharge that is routed across the model grid using a simple steepest-descent algorithm (*Granjeon and Joseph*, 1999). *Rivenæ s* (1992) described a similar method of sediment transport calculation where the partial differential equations are also solved numerically via an implicit finite-difference method.

Diffusion coefficients for sand are always half the value used for mud in the same setting, reflecting higher rates of transport for finer grained sediment. Terrestrial diffusion coefficients used in this work are higher than marine diffusion coefficients by one to two orders of magnitude to reflect higher rates of transport in a terrestrial topset setting

verses a marine foreset setting. For brevity diffusion coefficient values used in model runs are summarised by giving just the water-driven terrestrial sediment transport rates for sand.

Sediment transport rates used in this work span a range representative of small- to medium-size delta systems (*Kenyon and Turcotte*, 1985). Terrestrial diffusion coefficients range from 20 to 200 km^2ky^{-1} for sand and 40 to 400 km^2ky^{-1} for mud, based on values calculated from a range of modern deltas, for example 30 km^2ky^{-1} for the Rhine delta and 560 km^2My^{-1} for the Mississippi (*Kenyon and Turcotte*, 1985). Note that reducing the diffusion coefficients used in this study lower than 20 and 40 km^2ky^{-1} (for sand and mud, respectively) leads to topset-foreset geometries with unrealistically steep topset slope gradients compared to those observed from a range of coastal systems (*Reading and Collinson*, 1996), providing further constraint on the diffusion coefficient values used.

Weathering and Erosion

Previously deposited sediment can be eroded at rates up to 100 m My^{-1} depending on the local topographic gradient and diffusion coefficient. Eroded material is then available for sediment transport.

Eustacy

Amplitudes and durations of eustatic sea-level fall used in these model runs cover a range based on recent Phanerozoic eustatic curves (*Miller et al.*, 2005). For example, large-amplitude, approximately 100 m oscillations with 100 to 400 ky durations are interpreted to have been dominant through icehouse times such as the Late Neogene and the Late Carboniferous.

Grain size

Basic stratal geometries are approximated using two grain sizes, sand and mud, with a range of diffusion coefficients. In these models sand has a lower diffusion coefficient and therefore a shorter transport distance than mud.

4.2.2 SEDSIM model formulation & parameter values

SEDSIM is a 3D stratigraphic forward model developed originally at Stanford University in the 1980s, with current development ongoing at the Commonwealth Scientific and Industrial Research Organisation (CSIRO). The model includes Fortran 77 programs that incorporate physical laws based on fluid dynamics to simulate erosion, transport, and deposition of sediment by flow in open channels (*Martinez and Harbaugh*, 1993).

Sediment Transport

Sediment transport is calculated using an approximation of the Navier-Stokes equations. Rather than attempting to solve the full 3D form of the Navier-Stokes equations, which describe how the velocity, pressure, temperature, and density of a moving fluid are related, SEDSIMs Lagrangian averaged Navier-Stokes equations are a simplified description of fluid flow that can be simulated in a realistic time scale. The modified Navier-Stokes equations are solved in Sedsim using a Cash-Karp Runge Kutta scheme (*Press et al.*, 2007). A limitation of SEDSIMs hydrodynamic approach is that individual events, such as high-frequency variations in fluid flow, are not modeled. Instead, SEDSIM model runs over geological time scales simulate longterm time-averaged sediment deposition.

Initial Topography

SEDSIM models have been run on a simple initial ramp topography, ranging from 70 m above initial sea level to approximately 130 m below initial sea level.

Angle of Sediment Accumulation

Accumulation of coastal-plain sediments in SEDSIM is restricted to predefined maximum subaerial slope gradients for each grain size. Models presented in this work have a maximum accumulation angle of 0.1 ° for all grain sizes above sea level, which is similar to values observed on medium- to large-scale delta plains and shelf-margin clinoforms (*Porbski and Steel*, 2003, *Reading and Collinson*, 1996).

Grain Size

SEDSIM is capable of simulating multiple grain sizes, including: pebble (4 - 64 mm), granule (2 - 4 mm), very coarse sand (1 - 2 mm), coarse sand (0.5 - 1 mm), medium sand (0.25 - 0.5 mm), fine sand (0.125 - 0.25 mm), very fine sand (0.062 - 0.125 mm),

silt (0.0039 - 0.062 mm), and clay (< 0.0039). For the models in this work, grain size spans four categories of sand: coarse (C), medium (M), fine (F), and very fine (VF).

4.3 Model output

In order to systematically investigate topset aggradation during RSL fall, Dionisos has been run 1264 times to generate 2D and 3D stratal geometries over a range of amplitudes of RSL fall each with a range of sediment transport rates. For example, 209 models have been run with water-driven sediment transport rates ranging from 20 to 200 km^2ky^{-1} for sand and 40 to 400 km^2ky^{-1} for mud (increments of 10 and 20 km^2ky^{-1}, respectively) and with amplitudes of RSL fall ranging from 0 to 100 m (10 m increments). Each model run had either a 2 My duration (e.g., Model Set 1) or a 0.4 My duration (Model Set 2). Details of the 1264 models run are summarized in Table 4.1.

Table 4.1: Summary of the model sets in this chapter.

Set	***SFM***	***2D/3D***	***Runs***	***Model duration***	***Initial topography***
One	Dionisos	2D	209	2My	Ramp
Two	Dionisos	2D	209	0.4My	Ramp
Three	Dionisos	3D	209	2My	Ramp
Four	Dionisos	2D	209	2My	Shelf-slope
Five	Dionisos	2D	418	2My	Shelf-slope & Ramp
Six	Sedsim	3D	10	1My	Ramp

Geometry and extent of topset aggradation is summarized for each model run as a simple ratio between topset volume and foreset volume (t/f ratio). The t/f ratio metric applied in this work is similar to the topset and foreset thickness ratio applied by *Edmonds et al.* (2011) to distinguish between foreset- and topset-dominated deltas. When relatively large volumes of topset strata are present this value is, for example, 0.51. When no topset strata are preserved it is zero. The t/f ratios calculated in Dionisos are plotted against amplitude of RSL fall and sediment transport rate in parameter space plots (e.g., *Edmonds et al.*, 2011, *Williams et al.*, 2011). A grade line (*Muto et al.*, 2007) in the parameter-space plots (e.g., Figure 4.4) indicates the model runs where sediment transport and supply parameters generated rivers that were at grade (Table 4.2). Points

on the plot below this grade line represent an aggradational topset regime (t/f ratio > 0.01), and points above it represent a degradational topset regime (t/f ratio < 0.01, marked in blue). T/f ratios from selected models are also plotted as cross plots.

SEDSIM has also been used to run single 3D models of basic stratal geometries during falling RSL (Table 4.3). The stratal geometries created are presented as fence diagrams (e.g. *Griffiths et al.*, 2001), with estimated t/f ratios displayed and coastal plain, shoreline and marine strata distinguished.

TABLE 4.2: Dionisos standard model parameters.

Parameter	***2D value***	***3D value***
Grid length (x-axis) (km)	800	800
Grid length (y-axis) (km)	40	800
Grid Point Spacing (km)	20	20
Terrestrial transport distance (km)	100	100
Sediment supply (km^3My^{-1})	1000	10000
River discharge (km^3My^{-1})	6.31 x 10^{12}	9.46 x 10^{13}
Gravity weathering rate (m My^{-1})	1	1
Water weathering rate (m My^{-1})	100	100
Composition of sediment supply (sand, mud) (%)	20, 80	20, 80
Gravity-driven terrestrial k sand (km^2ky^{-1})	4	4
Gravity-driven terrestrial k mud (km^2ky^{-1})	8	8
Gravity-driven marine k sand (km^2ky^{-1})	0.05	0.05
Gravity-driven marine k mud (km^2ky^{-1})	0.1	0.1

4.4 Analysis of regressive geometries in Dionisos

4.4.1 Model Set One: 2D 2 My duration forced regressions

Model Set One consists of 209 2D model runs, each with a 2 My duration and spanning a range of RSL fall amplitudes from 0 to 100 m and a range of diffusion coefficients from 20 to 200 km^2ky^{-1} (Table 4.4). These runs generate strata with t/f ratios ranging from 0 to 0.51 (Figure 4.4). The proportion of topset strata in these models is a function of both

TABLE 4.3: Parameter values for SEDSIM model runs - Model Set Six.

Parameter	***Value***
Grid length (*x-axis*) (km)	50
Grid length (*y-axis*) (km)	50
Grid Point Spacing (km^{-2})	1
Model duration time (My)	1
Display interval (Ky)	10
Velocity at source (vx, vy) (m/s)	0, 10^{-7}
Sediment concentration (Kg/m^3)	0.027
River discharge (km^3My^{-1})	9.46 x 10^{13}
Sediment composition (C, M, F, VF) (%)	15 20, 25, 30
Diameter of each grain size (C, M, F, VF) (mm)	1, 0.5, 0.2, 0.0004
Suspension (1) or bed load (0) transport	0, 1, 1, 1
Maximum terrestrial gradient (degrees)	0.01

the magnitude of RSL fall and the diffusion coefficient, the latter determining the rate of sediment transport. For model runs with low sediment transport rates due to a diffusion coefficient of 30 km^2ky^{-1} (labelled a to e in Figures 4.4, 4.5), t/f values range from 0.37 in the case with no RSL fall, to 0.1 in the case with a 100 m amplitude RSL fall. A value of 0.37 results from a significant proportion of accumulated sediment being deposited as topset strata during normal regression (*sensu Catuneanu et al.*, 2009). For a RSL fall of 50 m the t/f ratio is reduced to 0.22. Although this is lower than during normal regression, a t/f ratio of 0.22 still represents significant topset aggradation despite a falling shoreline trajectory (Figures 4.4, 4.5 profile c). Increasing the amplitude of RSL fall to 100 m decreases the t/f ratio to 0.1. Topset aggradation has decreased in this case, but note that this relatively limited topset aggradation prevents formation of the subaerial unconformity that is assumed to develop during falling RSL (*Catuneanu et al.*, 2009).

Increasing the value of the diffusion coefficient tends to decrease topset aggradation. In contrast with examples a to e in Figure 4.4 and Figure 4.5, models runs with the same range of amplitudes of RSL fall but a higher sediment transport rate of 150 km^2ky^{-1} (labelled f to j in Figure 4.5) show t/f values ranging from 0.08 in the case with no RSL fall, to zero in the case with a 100 m RSL fall (*sensu Catuneanu et al.*, 2009). The

relationship between t/f values for a particular diffusion rate and amplitude of RSL fall is approximately linear (Figure 4.6).

TABLE 4.4: Parameter values for Dionisos Model Set One (ramp topography) and Dionisos Model Set Four (shelf-slope topography).

Parameter	***Value***
Grid length (x-axis) (km)	800
Grid length (y-axis) (km)	40
Grid Point Spacing (km)	20
Model duration time (My)	2
Model chron interval (My)	0.01
Sediment supply (km^3My^{-1})	1000
River discharge (km^3My^{-1})	6.31 x 10^{12}
Composition of sediment supply (sand, mud) (%)	20, 80
Water-driven terrestrial diffusion coefficient for sand (km^2ky^{-1})	20 to 200
Water-driven terrestrial diffusion coefficient for mud (km^2ky^{-1})	40 to 400
Relative sea-level amplitude (m)	0 to -100

4.4.2 Model Set Two: 2D 0.4 My duration forced regressions

In order to test the impact of higher rates of RSL fall, Model Set Two has a duration of 400 ky and runs span a range of RSL fall amplitudes from 0 to 100 m and a range of diffusion coefficients from 20 to 200 km^2ky^{-1} (Table 4.5). These model runs generate strata with t/f ratios ranging from 0 to 0.36 (Figure 4.7). These ratios are lower than ratios from the 2 My duration runs because faster rates of RSL fall tend to decrease preservation of topset strata. Consequently, increasing the rate of RSL fall by a factor of five in the 400 ky runs significantly reduces the volume of topset strata deposited during forced regression. However, as with the 2-My-duration examples, even low volumes of topset aggradation during RSL fall imply that incision and fluvial valley formation would likely not occur because for the lowest sediment transport rates (diffusion coefficient of 20 km^2ky^{-1}) topset aggradation, with a t/f greater than 0.1, still occurs even with RSL fall amplitudes of up to 100 m (Figures 4.7, 4.8).

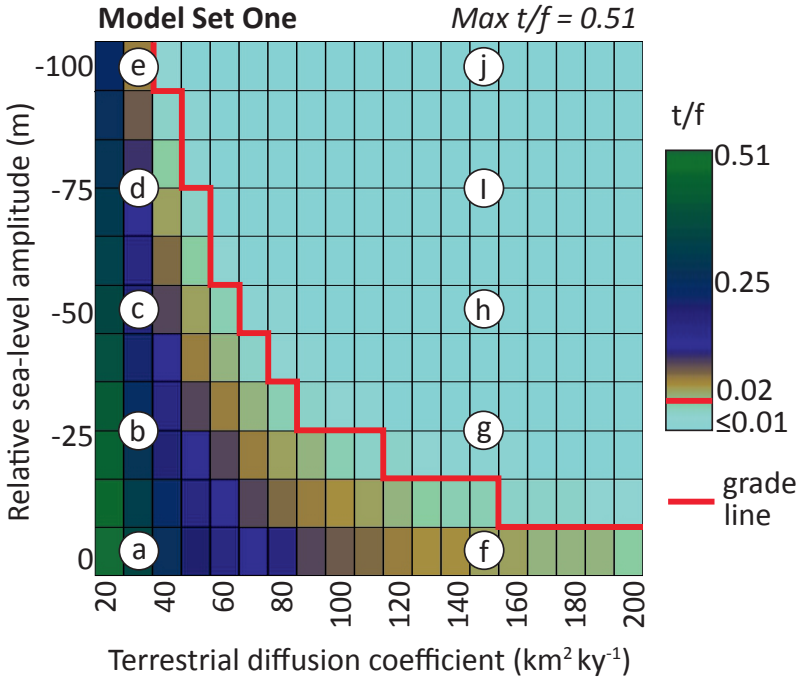

FIGURE 4.4: Parameter space plot for Model Set One. Model sets are listed in 4.1. Labels a to j refer to labels on Figure 4.5 and are referred to in the text. Max refers to the maximum t/f ratio generated by this set of model runs. Values of RSL amplitude range from 0 to 100 m (*y axis*) and terrestrial diffusion coefficient values range from 20 to 200 km^2ky^{-1} (*x axis*). The t/f ratio scale is 0 to 0.51. The parameter-space plot has a grade line (red), which is marked to distinguish between model runs that generate a stratal geometry with net aggradation (t/f ratios > 0.01) from stratal geometries that display net degradation (t/f ratio $=< 0.01$).

TABLE 4.5: Parameter values for Dionisos Model Set Two (ramp-topography): 2D 0.4 My multiple model runs.

Parameter	***Value***
Grid length (x-axis) (km)	800
Grid length (y-axis) (km)	40
Grid Point Spacing (km)	20
Model duration time (My)	0.4
Model chron interval (My)	0.002
Sediment supply (km^3My^{-1})	1000
River discharge (km^3My^{-1})	6.31 x 10^{12}
Composition of sediment supply (sand, mud) (%)	20, 80
Water-driven terrestrial diffusion coefficient for sand (km^2ky^{-1})	20 to 200
Water-driven terrestrial diffusion coefficient for mud (km^2ky^{-1})	40 to 400
Relative sea-level amplitude (m)	0 to -100

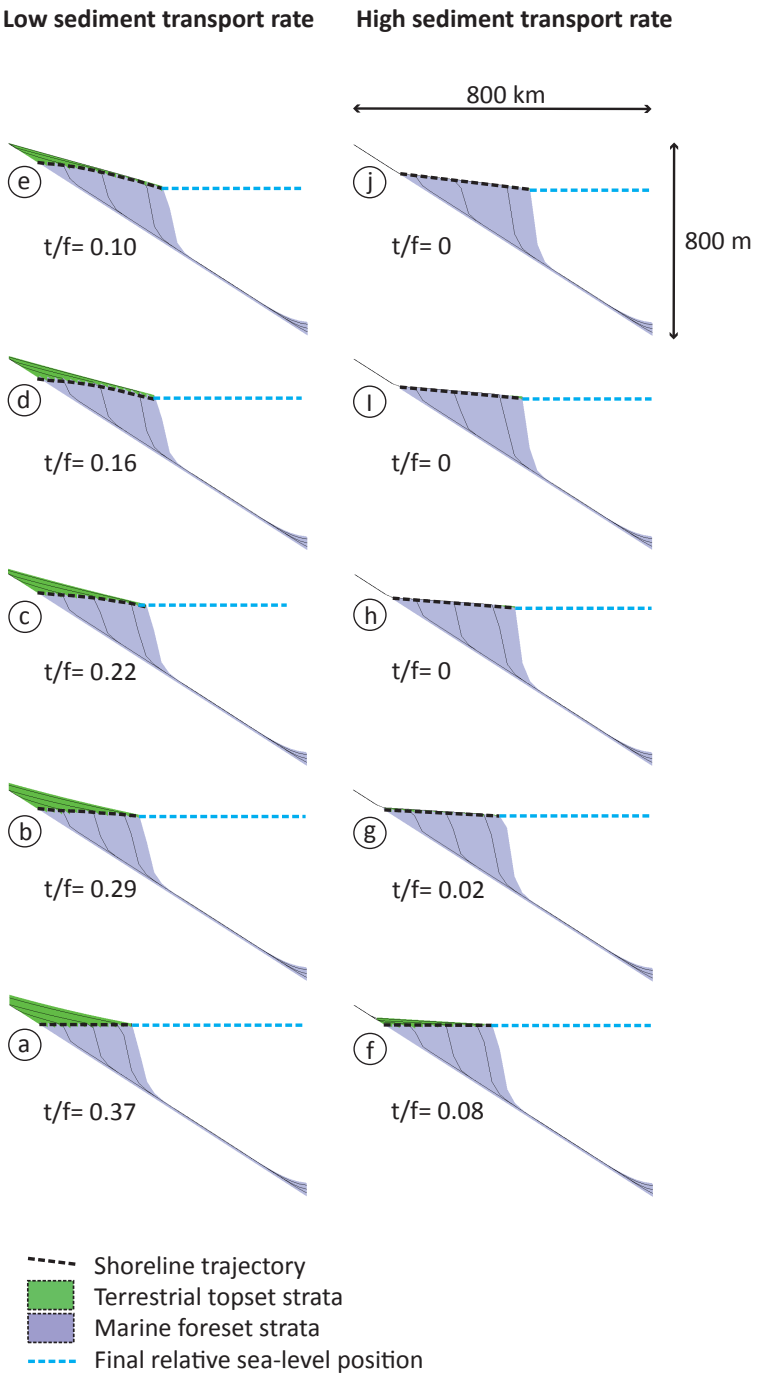

FIGURE 4.5: 2D Dionisos profiles created with different amplitudes of RSL fall over 2 My duration, and either relatively low or high terrestrial diffusion coefficients. Each of the 10 profiles has an associated position on the parameter space plot (Figure 4.4), highlighting the corresponding parameter values used for the terrestrial diffusion coefficient and amplitude of RSL fall.

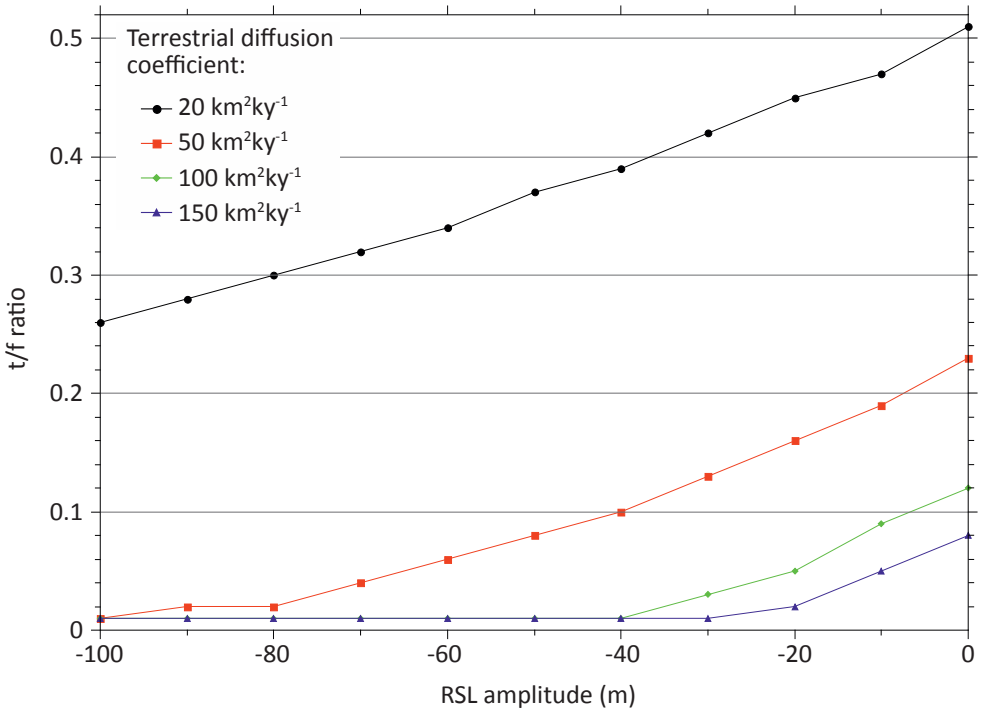

FIGURE 4.6: Cross plot of t/f ratios resulting from 2D 2 My duration models (Figures 4.4, 4.5) for selected terrestrial diffusion coefficients (marked by color) and for a range of amplitudes of RSL fall from 0 to 100 m.

4.4.3 Model Set Three: comparison of 2D & 3D regressive geometries

Results from 3D multiple model runs with a 2 My duration, spanning the same range of RSL fall amplitudes and diffusion coefficients as Model Set One and Model Set Two (parameters listed in Table 4.6), generate strata with t/f ratios ranging from 0 to 0.22 (Figure 4.9).

A 3D model run with low sediment transport rates (terrestrial diffusion coefficient of 20 km^2ky^{-1}), generates a t/f ratio of 0.22 (point i, Figure 4.9). This is due to accumulation of topset strata during normal regression. A t/f ratio of 0.03 results from a 100 m RSL fall (point iii, Figure 4.9). The amount of topset strata deposited in cases with no RSL fall has decreased from the equivalent 2D t/f ratio of 0.51 (Figure 4.4), to a t/f ratio of 0.22 (point i, Figure 4.9). For a 50 m RSL fall the t/f ratio is reduced to 0.08 (point ii, Figure 4.9). This is a relatively low volume of topset aggradation compared to the volume of sediment transported to the delta foresets, but topset strata are still present across the entire topset throughout the falling-stage. Increasing the magnitude of RSL

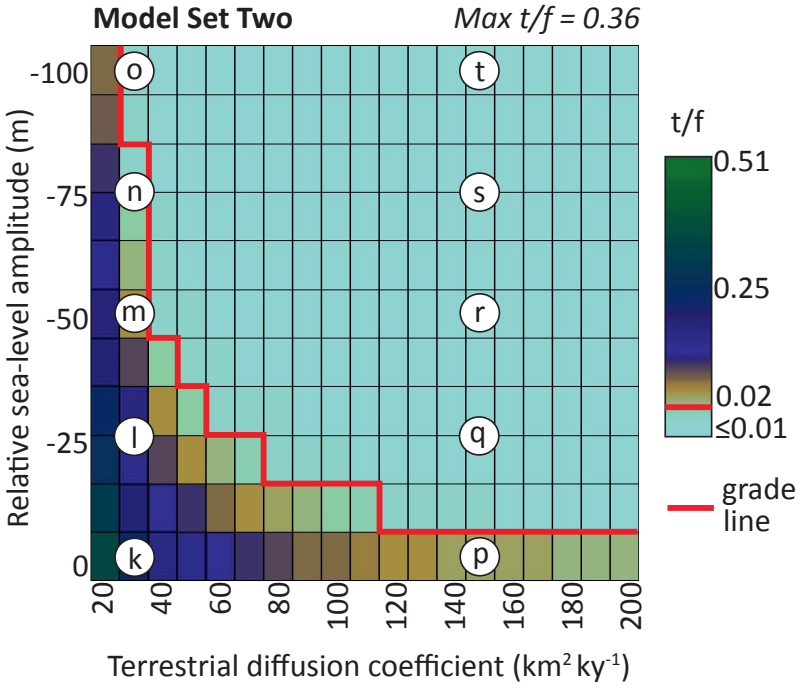

FIGURE 4.7: Parameter space plot for Model Set One. Model sets are listed in 4.1. Labels k to t refer to labels on Figure 4.8 and are referred to in the text. Max refers to the maximum t/f ratio generated by this set of model runs. Values of RSL amplitude range from 0 to 100 m (*y axis*) and terrestrial diffusion coefficient values range from 20 to 200 km^2ky^{-1} (*x axis*). The t/f ratio scale is 0 to 0.51. The parameter-space plot has a grade line (red), which is marked to distinguish between model runs that generate a stratal geometry with net aggradation (t/f ratios > 0.01) from stratal geometries that display net degradation (t/f ratio $=< 0.01$).

TABLE 4.6: Parameter values for Dionisos Model Set Three (ramp-topography): 3D 2 My multiple model runs.

Parameter	***Value***
Grid length (x-axis) (km)	800
Grid length (y-axis) (km)	800
Grid Point Spacing (km)	20
Model duration time (My)	2
Model chron interval (My)	0.01
Sediment supply (km^3My^{-1})	10000
River discharge (km^3My^{-1})	9.46 x 10^{13}
Composition of sediment supply (sand, mud) (%)	20, 80
Water-driven terrestrial diffusion coefficient for sand (km^2ky^{-1})	20 to 200
Water-driven terrestrial diffusion coefficient for mud (km^2ky^{-1})	40 to 400
Relative sea-level amplitude (m)	0 to -100

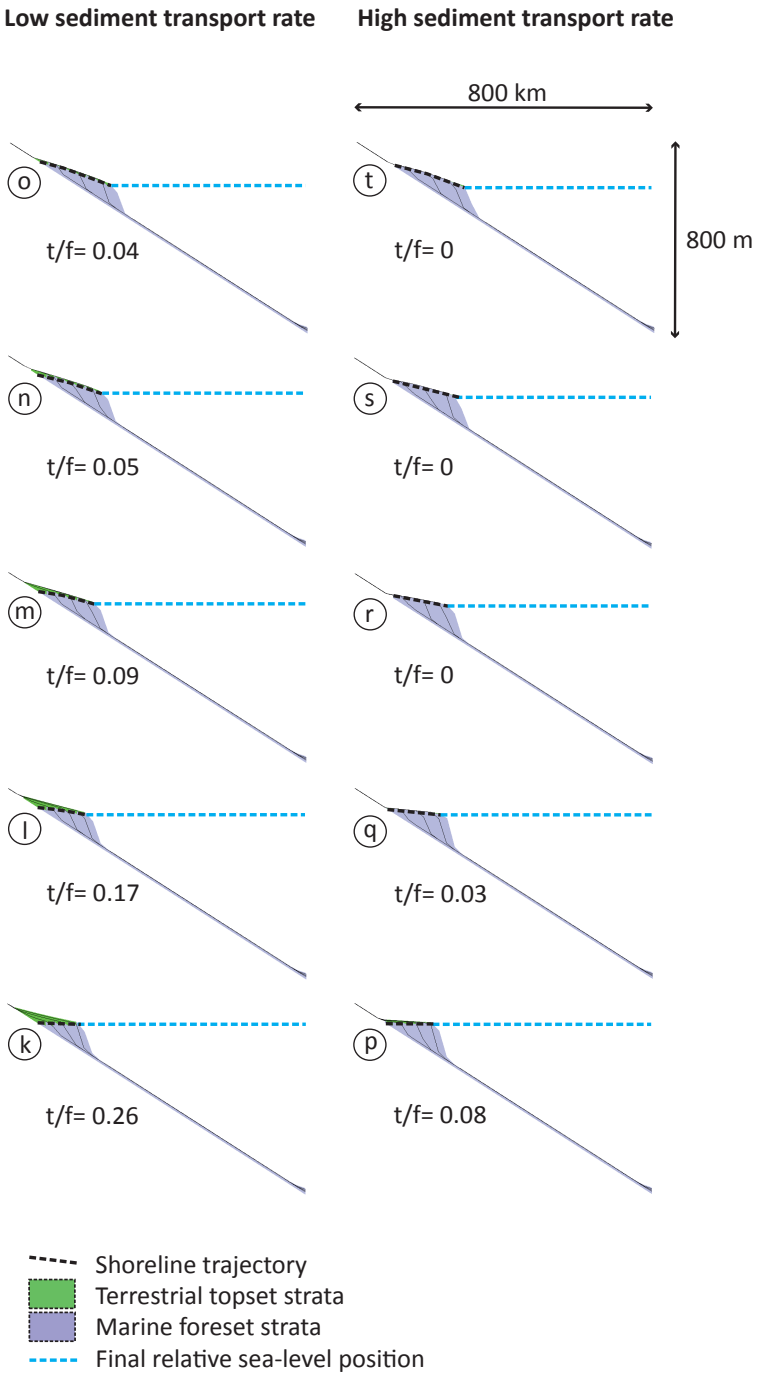

FIGURE 4.8: 2D Dionisos profiles created with different amplitudes of RSL fall over 0.4 My duration, and either relatively low or high terrestrial diffusion coefficients. Each of the 10 profiles has an associated position on the parameter space plot (Figure 4.7), highlighting the corresponding parameter values used for the terrestrial diffusion coefficient and amplitude of RSL fall.

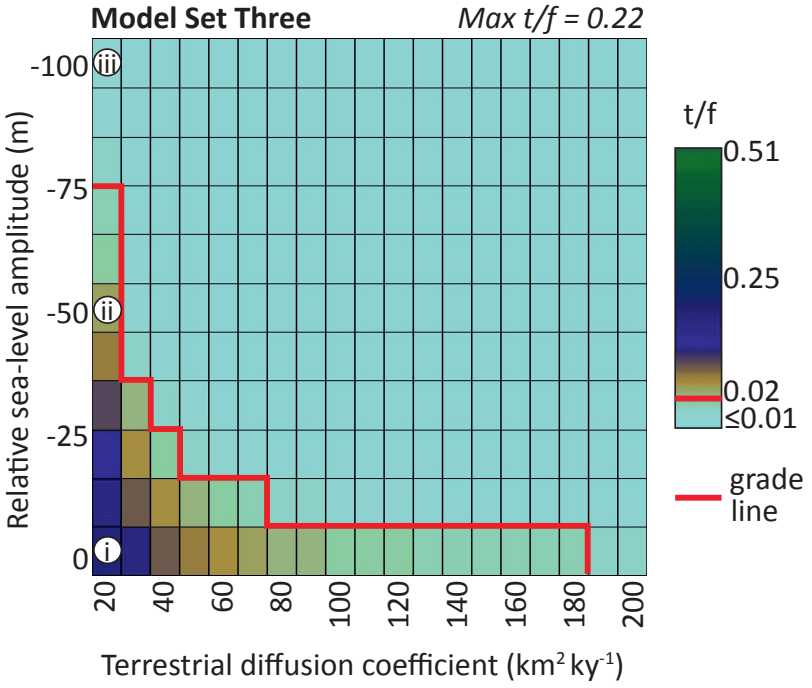

FIGURE 4.9: Parameter space plot for Model Set Three. Model sets are listed in 4.1. Labels i to iii are referred to in the text. Max refers to the maximum t/f ratio generated by this set of model runs. Values of RSL amplitude range from 0 to 100 m (*y axis*) and terrestrial diffusion coefficient values range from 20 to 200 km^2ky^{-1} (*x axis*). The t/f ratio scale is 0 to 0.51. The parameter-space plot has a grade line (red), which is marked to distinguish between model runs that generate a stratal geometry with net aggradation (t/f ratios $>$ 0.01) from stratal geometries that display net degradation (t/f ratio $=<$ 0.01).

.

fall to 100 m decreases the t/f ratio to 0.03 (point iii, Figure 4.9), reflecting a scenario of limited topset aggradation during a high amplitude fall in RSL.

In general, the reduced values of the t/f ratio are a consequence of measuring the point-source fan geometry of the topset strata in 3D rather than 2D; for example, 0.22 is approximately 0.51^2. However, there are other differences in the 3D models associated with channel incision and some complex routing of river flow across previously incised and/or aggraded topography, which also influence the t/f ratio in individual model runs. Despite these points, the results from the 3D model support the basic validity of the 2D models.

4.4.4 Model Set Four: analysis of regressive geometries on initial shelf-slope topography

Model Set Four repeats the 209 model runs described above in Model Set One but with an initial topography that has a change of slope gradient at the point of initial sea-level elevation (shelf-slope topography, Figure 4.3B). Parameters for this set of model runs are listed in Table 4.4.

T/f ratios from Model Set Four show that stratal geometries generated in Dionisos on an initial topography with a break in slope tend to have lower t/f ratios than stratal geometries generated on an initial ramp topography. For example, the highest t/f ratio in Model Set Four resulting from an unforced regression with relatively low sediment transport rates is 0.29 (Figure 4.10), compared to a t/f ratio of 0.51 from the equivalent run in Model Set One (Figure 4.4). The key reason for this difference in t/f ratio is the greater progradation distances formed on the initial ramp topography, in both cases of falling and stationary RSL. This provides a larger area for topset aggradation, leading to a relatively low gradient on the topset, reducing the sediment transport rate of the system and favouring aggradation. Compared to stratal geometries created on the ramp topography, progradation is limited on the shelf-slope topography because of increased marine sediment transport rates, a result of the greater slope gradient below initial sea-level elevation (Figure 4.3B). Despite the lower t/f ratios in the shelf-slope topography runs, significant topset aggradation still occurs during falling RSL. For example, the t/f ratio in profile v (Figure 4.11) is 0.07 with a minimum thickness of 2 m on the topset.

Previous diffusional modeling studies suggest that a break in slope gradient of the initial topography (i.e., when $\alpha < \beta$ in Figure 4.3) will encourage river incision during RSL fall, commencing at the shelf-slope break (*Leeder and Stewart*, 1996). Results from this work suggest that this is not always the case. *Leeder and Stewart* (1996) modeled a system with low sediment supply and high transport rates. The cases modeled here with higher sediment supply show that a break in slope of the initial topography does not always lead to significant erosion at the slope break. The main reason for this, in contrast with model results from *Leeder and Stewart* (1996), is due to topset aggradation during RSL fall, especially with relatively low values of terrestrial diffusion coefficient.

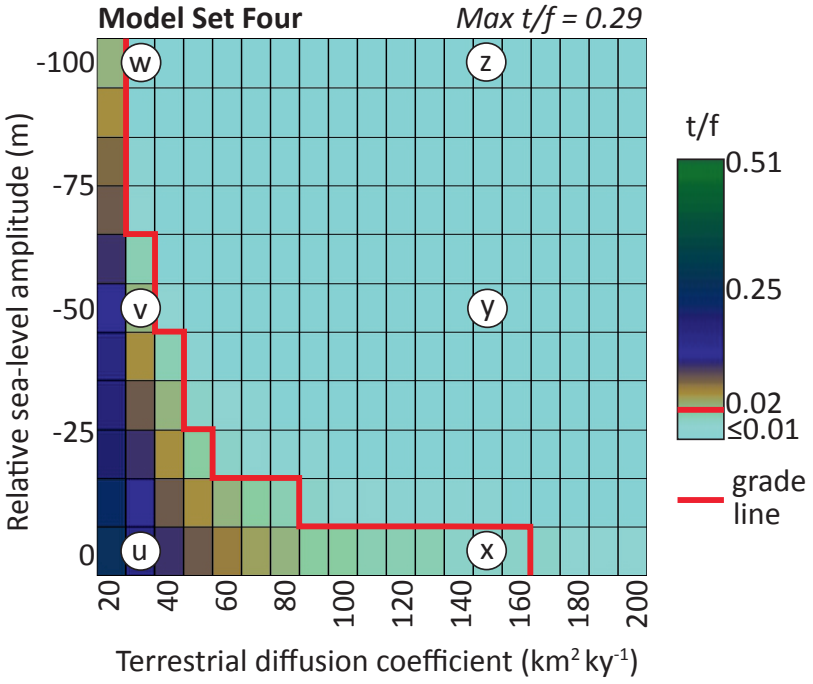

FIGURE 4.10: Parameter space plot for Model Set Four. Model sets are listed in 4.1. Labels u to z refer to labels on Figure 4.11 and are referred to in the text. Max refers to the maximum t/f ratio generated by this set of model runs. Values of RSL amplitude range from 0 to 100 m (*y axis*) and terrestrial diffusion coefficient values range from 20 to 200 km^2ky^{-1} (*x axis*). The t/f ratio scale is 0 to 0.51. The parameter-space plot has a grade line (red), which is marked to distinguish between model runs that generate a stratal geometry with net aggradation (t/f ratios > 0.01) from stratal geometries that display net degradation (t/f ratio $=< 0.01$).

.

4.4.5 Model Set Five: high sediment supply rates on ramp & shelfslope break physiographies

To assess the impact of greater sediment supply on topset aggradation versus erosion and incision on both initial topographies (ramp and shelf-slope, Figure 4.3), Model Set Five consists of 209 Dionisos model runs on both the shelf-slope and the ramp initial topographies (418 model runs in total, Table 4.1) (e.g., Figure 4.13). These multiple model runs cover the same model parameters as Model Set 1 (Table 4.4), with the addition of a high-case sediment-supply value of 1500 km^3My^{-1}. Results are presented as parameter-space plots in Figure 4.12.

For the same range of diffusion coefficients used in previous model runs (20 to 200 km^2ky^{-1}), a larger sediment supply volume of 1500 km^3My^{-1} increases t/f ratios for

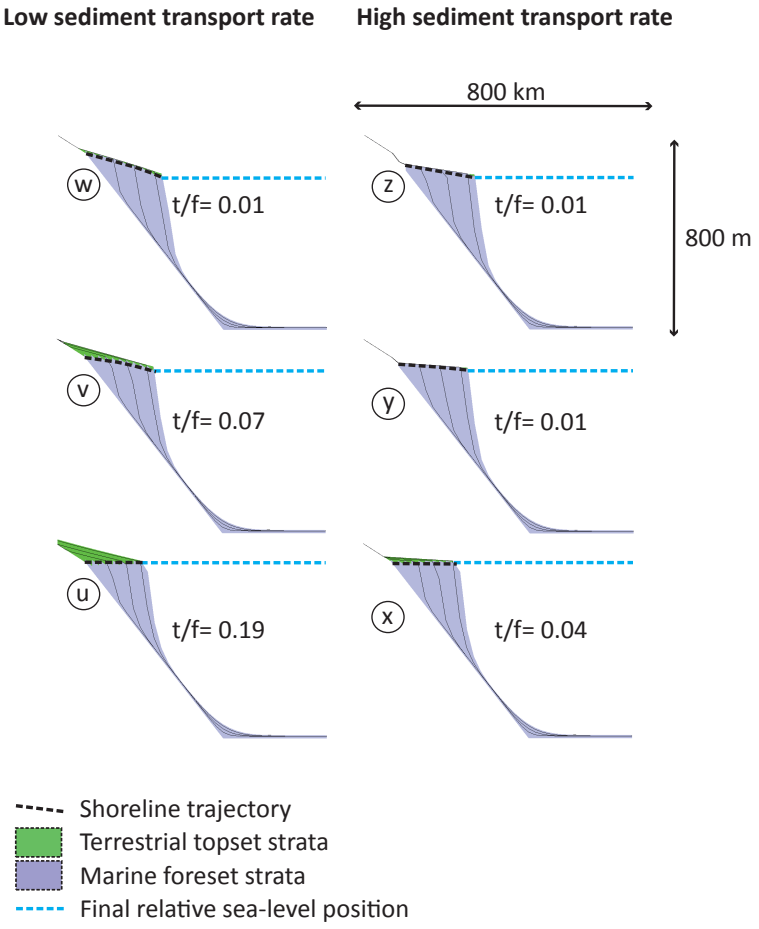

FIGURE 4.11: 2D Dionisos profiles created with different amplitudes of RSL fall over 2 My duration, and either relatively low or high terrestrial diffusion coefficients. Each of the 6 profiles has an associated position on the parameter space plot (Figure 4.10), highlighting the corresponding parameter values used for the terrestrial diffusion coefficient and amplitude of RSL fall.

models run on both topographies (ramp and shelf-slope) for the whole range of amplitudes of RSL fall tested (Figure 4.12. As might be expected, t/f ratios calculated from stratal geometries generated on the initial shelf-slope topography are lower than t/f ratios generated on the initial ramp topography (Figure 4.12B compared to Figure 4.12A). However, a greater sediment supply volume increases the t/f ratio more on the shelf-slope topography than on the ramp topography.

For example, for model runs on the shelf-slope topography with a 50 m-amplitude RSL fall and low-case sediment transport rate (30 km ^{2}ky^{-1} terrestrial diffusion coefficient), a supply volume of 1500 km^{3}My^{-1} generates a t/f ratio of 0.22 (profile 8, Figure 4.13). In contrast, the same parameters on the ramp topography created a t/f ratio of 0.44 (profile 2, Figure 4.13). For the sediment supply rates of 1000 and 1500 km^{3}My^{-1}, t/f

ratio increased by a factor of $\tilde{3}$ on the shelf-slope topography (from 0.07 in profile v, Figure 4.11), compared to a factor of 2 on the initial ramp topography (from 0.22, profile c, Figure 4.5).

4.4.6 Model Set Six: 3D regressive geometries in SEDSIM

Dionisos models presented in this work suggest that topset aggradation can occur during falling RSL when sediment transport rates are relatively low or sediment supply is relatively high (e.g., Figures 4.4, 4.12). A set of model runs with falling RSL have been conducted with another stratigraphic forward model, SEDSIM (Table 4.3) for comparison, to establish if a model with quite different governing equations and founding assumptions also generates falling-stage topset aggradation. Importantly, SEDSIM is not a diffusional model but instead uses a hybrid hydrodynamic and geometric approach to model erosion, transport, and deposition of strata (*Tetzlaff and Harbaugh*, 1989). Deposition in SEDSIM is controlled largely by threshold gradients of deposition specified for each grain size modeled in terrestrial and marine settings. For example, the maximum gradient of terrestrial sediment accumulation is 0.01 °. Five SEDSIM model runs were calculated with a range of amplitudes of RSL fall from 10 to 50 m and a duration of 1 My. Modeled strata from each run are displayed in Figure 4.14 as fence diagrams.

SEDSIM strata from all five model runs show preserved aggradational topset strata deposited during RSL fall. Fluvial incision also occurs in each of the model runs (marked A to E, Figure 4.14) and decreases preservation of up-dip coastal-plain deposits along the main axis of sediment transport (e.g., model D, Figure 4.14), but does not remove all of the topset. Unlike in the Dionisos models, in the SEDSIM models the proportion of topset strata compared to foreset strata does not decrease with increasing amplitude of RSL fall. For example, model A (Figure 4.14) was generated with a 10-m-amplitude RSL fall over 1 My and has a t/f ratio of 0.08, but profile D, generated with a 40-m-amplitude RSL fall over 1 My, has a higher t/f ratio of 0.13. This is due to the threshold angle for terrestrial sediment accumulation specified in the model runs. With steady RSL, the area for subaerial deposition is defined by the angle of the initial topography and the angle of sediment accumulation above sea level. However, when RSL falls, the delta can deposit subaerial strata over a greater area. For example, a RSL fall of 10 m increased the area for subaerial deposition by 61.25 km^2 (1.75 km shoreline regressive

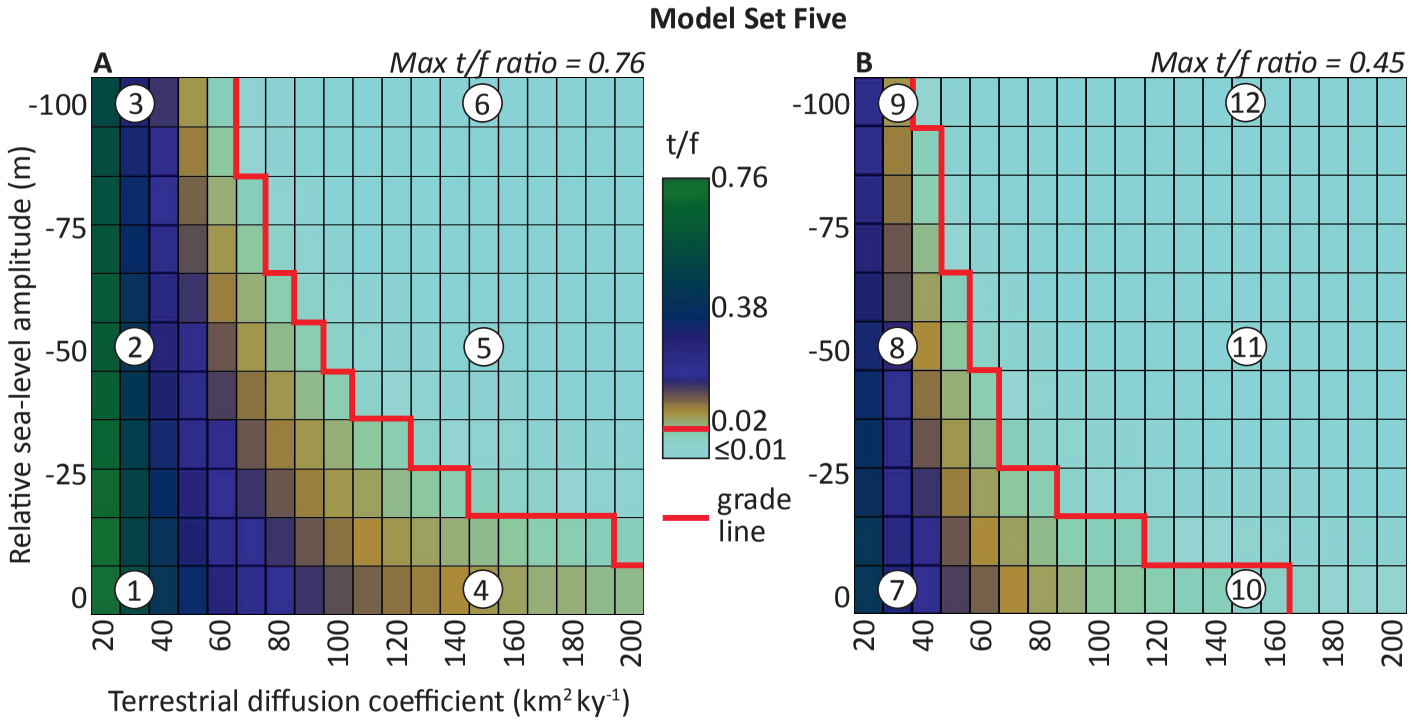

FIGURE 4.12: Parameter space plot for Model Set Five. Model sets are listed in 4.1. Labels 1 to 12 across both the plots refer to labels on Figure 4.13 and are referred to in the text. Max refers to the maximum t/f ratio generated by this set of model runs on the two initial topographies. Values of RSL amplitude range from 0 to 100 m (*y axis*) and terrestrial diffusion coefficient values range from 20 to 200 km^2ky^{-1} (*x axis* on both plots). Note that the t/f ratio scale for this set of model runs is greater, from 0 to 0.76. The parameter-space plots have a grade line (red), which is marked to distinguish between model runs that generate a stratal geometry with net aggradation (t/f ratios > 0.01) from stratal geometries that display net degradation (t/f ratio $=< 0.01$).

.

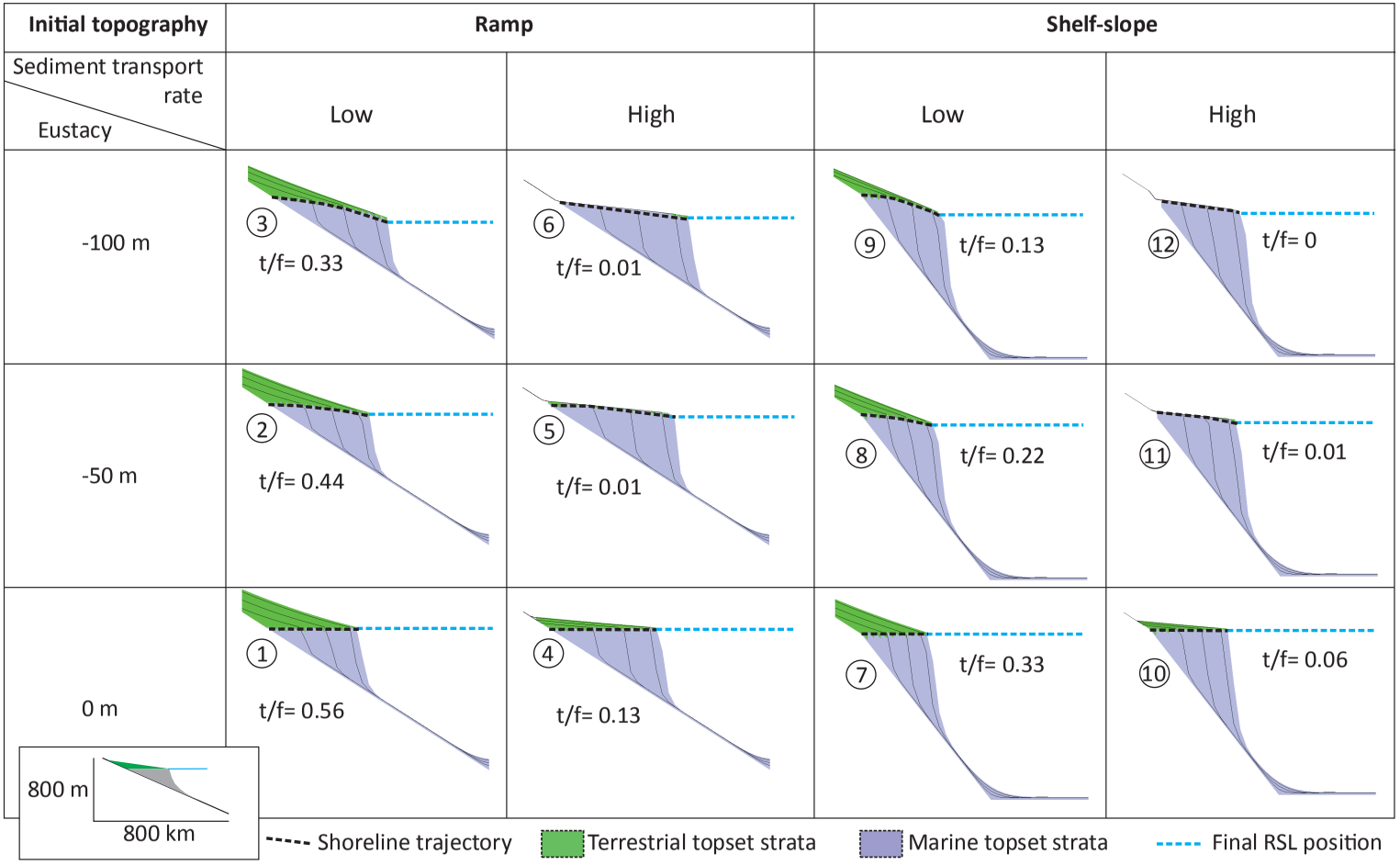

FIGURE 4.13: 2D Dionisos profiles created with a high case sediment supply value of 1500 km^3My^{-1} on both initial ramp and break of slope topographies, and for each of these cases with different amplitudes of RSL fall over 2 My duration, and either relatively low or high terrestrial diffusion coefficients. Each of the 12 profiles has an associated position on the parameter-space plots in Figure 4.12), highlighting the corresponding parameter values used for the terrestrial diffusion coefficient and amplitude of RSL fall.

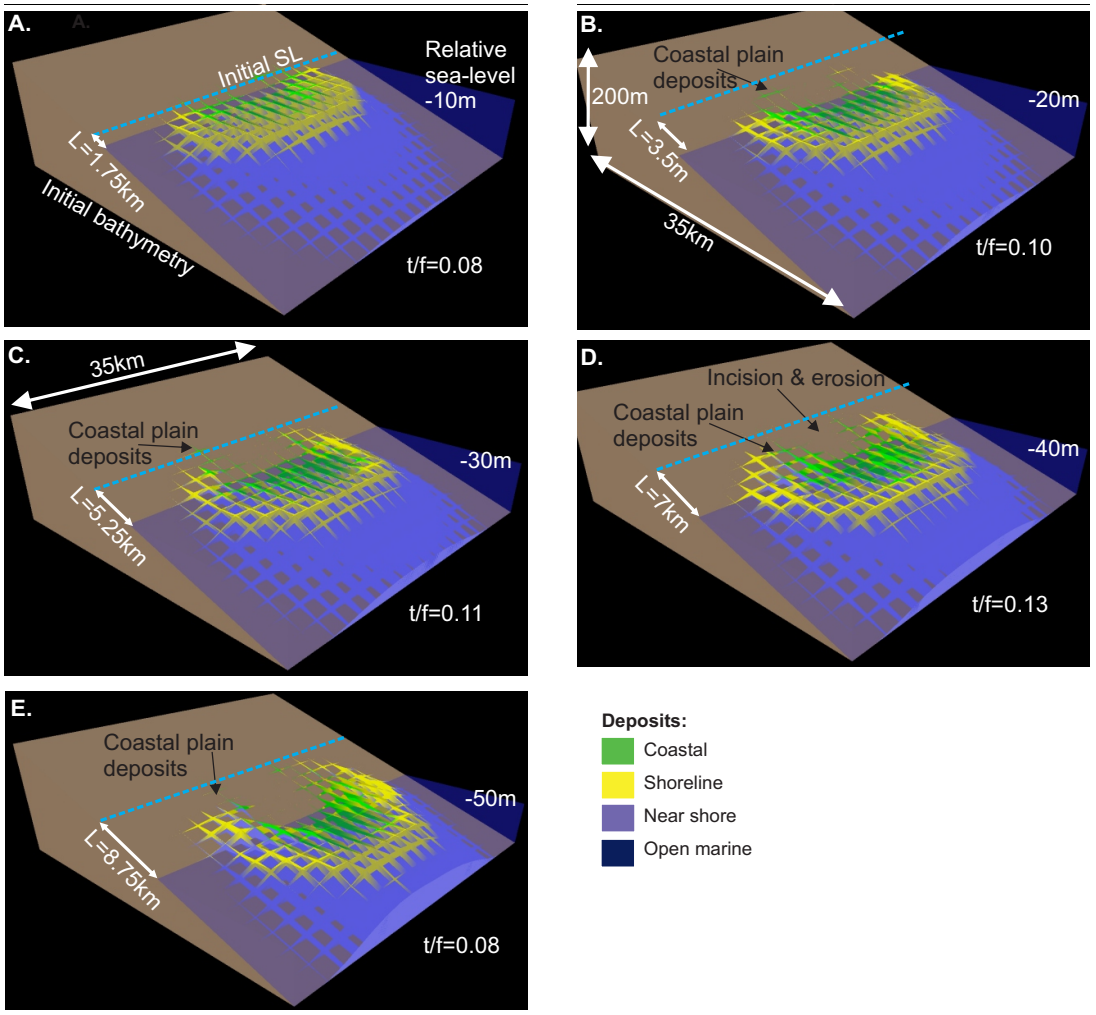

FIGURE 4.14: Five single model runs from SEDSIM, generated with 10 to 50 m amplitudes of RSL fall (models A to E). Stratal geometries are displayed as fence diagrams, with initial sea level marked in dash blue. L = distance of shoreline migration. The models show that topset aggradation occurs in SEDSIM during falling RSL.

transit over a 35 km model width) in model run A (Figure 4.14). A 40-m-amplitude RSL fall increased the area for subaerial (coastal plain) deposition by 245 km^2 (7 km shoreline transit over a 35 km model width) in model run D (Figure 4.14).

Although the SEDSIM model runs described above are relatively simple (e.g., *Griffiths et al.*, 2001), they do demonstrate that topset aggradation occurs in SEDSIM during RSL fall. The fact that topset aggradation occurs during falling RSL in both Dionisos and SEDSIM suggests that the phenomenon is not simply a consequence of one set of model assumptions, increasing the likelihood that it is an important scenario that should be accounted for in sequence stratigraphic models.

4.5 Discussion

This work uses numerical forward models to investigate what stratal geometries could occur during falling and steady RSL in basin-margin depositional systems, with a ramp initial topography and a shelf-slope-break initial topography, and with different rates of sediment transport. In contrast to other studies focussed on a small number of forward model simulations (e.g., *Burgess and Steel*, 2008) or other useful approaches such as flume-tank modeling (e.g., *Muto and Steel*, 2001), here we have used many hundreds of runs analyzed through simple metrics using a parameter-space-plot approach (e.g., *Williams et al.*, 2011).

4.5.1 Are these model results realistic enough to be useful?

As with any model result, assumptions and limitations inherent in the model formulation should be carefully taken into account. In the case of Dionisos, an important assumption is that diffusion indirectly but accurately represents various processes of sediment transport, such as suspension and fluvial bedload transport, hyperpycnal flows, etc., at a temporal and spatial scale suitable for reproduction of basin-margin stratal geometries. There is some evidence that this is a reasonable assumption. *Paola et al.* (1999) presented a diffusion-based model and tested it on a mine-tailings fan, which provided a simple field-scale example of a fluvial fan-delta system with measured accommodation, sediment flux, water discharge, and calculated diffusion coefficients from measurements of the river network. Through this study the authors showed that a simple diffusion-based model could be used to predict the steady-state topography given known input parameters. Results similar to those presented here have also been generated in other numerical models and supported with scaled flume-tank work (e.g., *Swenson and Muto*, 2007). Based on this, diffusion is probably a reliable method for the long-term large-scale simulation of sediment transport processes and reconstructions of basin stratigraphy.

Another area of concern regarding realism of forward-modeling results is the parameter values used in the modeling. Here we have used parameter values for sediment supply, river discharge rates, and diffusion coefficients from previously published work (*Burgess and Hovius*, 1998, *Kenyon and Turcotte*, 1985, *Marion et al.*, 2010) to represent a typical medium-size river system similar to, for example, the Rhone, Volta, and Ebro rivers. If

these types of rivers are representative of the types of fluviodeltaic systems responsible for depositing ancient strata, the model results presented here should be useful for interpreting such strata.

In order to run many models quickly, most of these results are based on 2D model runs. An important consideration is how the results would vary in 3D models, and if these 3D models are more realistic. 3D model runs are generally a more realistic representation of the real world, but a key question is what critical processes occur in 3D that cannot be represented in 2D. Multiple model runs on a 2D model grid (Model Set One) were repeated on a 3D model grid (Model Set Three). Topset aggradation during falling RSL also occurred in the 3D model runs, but t/f ratios were reduced simply because of an area-to-volume scaling factor. In 3D there was also the added complication of water-flow response to previous topography, leading to more complex incision patterns and more spatially variable t/f ratios in individual model runs. However, these complications did not refute the basic observation of topset aggradation during falling RSL. As a further test of the impact of model assumptions, we ran similar 3D experiments in a second forward model SEDSIM. The results from SEDSIM show that topset aggradation also occurs during falling RSL despite the fact that the two models contain quite different assumptions and representations of sediment transport. Of course, both models could still be wrong in predicting falling-stage topset aggradation, but the likelihood of two independently constructed and quite different models being wrong in this way might be considered less than the probability of just one model being wrong.

4.5.2 Implications of falling-stage topset aggradation for sequence stratigraphic methods

Within siliciclastic systems, the term highstand systems tract is commonly used to indicate an aggradational to progradational topsetforeset stratal geometry assumed to have formed during the late stage of RSL rise. The term falling-stage systems tract is used to indicated a purely regressive stratal geometry capped by an erosional unconformity assumed to have formed during falling RSL (Figure 4.1) (*Catuneanu*, 2006). Implicit in this systems-tract terminology is the critical assumption that topset aggradation occurs only during steady to rising RSL and not during RSL fall. Like many of the implicit assumptions in the sequence stratigraphic models, this is a model-driven assumption with

little or no independent evidence to support it (*Thorne*, 1992). Note that the frequency with which this interpretation is applied does not qualify as supporting evidence; in the absence of independent evidence for sea-level history combined with high-resolution biostratigraphic data to prove correlation between strata and known sea-level history, interpretations of topset aggradation as highstand rather than falling-stage or lowstand are entirely the consequence of a conceptual model which, though popular, may not be accurate. Very few examples of this kind of independent evidence exist, partly because it is very difficult to determine past RSL without circular reasoning (*Burton et al.*, 1987), and partly because sufficiently precise biostratigraphic data to unequivocally demonstrate correlation with proposed histories of frequency of sea-level oscillations are rare (*Miall*, 2010).

The results presented in this work show that modeled stratal geometries generated with low sediment transport rates contain significant proportions of topset strata relative to foreset strata even during high-amplitude, fast RSL fall (e.g., Figures 4.4 to 4.13). The importance of falling-stage topset aggradation is summarized by the two stratal geometries created with the same sea-level curve and constant rate of sediment supply volume, but with differing terrestrial diffusion coefficients, and hence different rates of sediment transport (Figure 4.15). Stratal geometry A in Figure 4.15 was created with a diffusion coefficient of 100 km^2ky^{-1}, reflecting a mid-case rate of sediment transport for the range of terrestrial diffusion coefficients tested in this work (*Kenyon and Turcotte*, 1985). The systems tracts in geometry A were defined by their position on the input eustatic sea-level curve (Figure 4.15). The stratal geometries of each systems tract in geometry A (Figure 4.15) look very similar to stratal geometries in the conceptual sequence stratigraphic model (e.g., *Catuneanu*, 2006). Stratal geometry B in Figure 4.15 was created with a low-case sediment transport rate by applying a terrestrial diffusion coefficient of 20 km^2ky^{-1}. Stratal geometry B also has systems tracts defined by positions on the input eustatic sea-level curve (Figure 4.15). However, in stratal geometry B, the falling-stage systems tract shows a high rate of aggradation. This is due to falling-stage topset aggradation resulting from low rates of sediment transport represented by a terrestrial diffusion coefficient of 20 km^2ky^{-1}. Sensitivity testing with thousands of individual model runs spanning a broad range of sediment transport and sea-level parameter values shows that this phenomenon of falling-stage topset aggradation occurs frequently in these model runs, implying that falling-stage topset aggradation can be

much more likely in the ancient record than has been generally believed.

Based on this, topset aggradation may be another good example of a non-unique stratal geometry, forming under more than one set of controlling parameter values, and therefore not uniquely indicative of particular parameter values. If topset aggradation is not uniquely indicative of steady or rising RSL, then this has important consequences for our ability to accurately distinguish highstand strata from falling stage strata, and to reliably identify systems tracts. It suggests that reconstruction of RSL histories based on identification and mapping of systems tracts is unlikely to be accurate. Falling-stage topset aggradation also has important consequences for prediction of sediment bypass and deposition of sand-grade sediment to deepwater deposystems. If topset aggradation occurs in forced regressive strata, volumes of deepwater sand deposition would be reduced, limiting the potential for deepwater sand reservoirs in the ancient record during periods of sea-level lowstand.

Another key component to sequence stratigraphic model predictions of sediment bypass is the concept of graded fluvial profiles. A graded river has a balance between gradient, discharge, and channel form that allows it to transport its sediment load without net aggradation or degradation (*Mackin*, 1948, *Muto and Swenson*, 2006). Conventional sequence stratigraphy is based on the assumption that rivers in deltaic settings aggrade during RSL rise and degrade during RSL fall (Figure 4.1), implying that fluvial grade is attained with steady RSL. Recent studies have questioned this conventional model, suggesting that rivers can become graded only during RSL fall (*Muto and Swenson*, 2005, 2006). For example, *Muto and Swenson* (2006) suggested that, with a simple initial ramp topography, fluvial grade can be attained with any constant rate of RSL fall. In general, results from our modeling support this conclusion. However, our work also has implications for the likely frequency of occurrences of graded profiles in natural river systems. Considering Model Set One as an example, only 4 of the total 209 model runs generate a graded fluvial profile, because, as the definition of grade suggests, an equilibrium grade state requires quite specific values of sediment transport rates for any particular rate of RSL fall, sediment supply, and initial topography. This suggests that graded fluvial profiles are likely to be rare in natural systems.

One important addition to the original sequence stratigraphic methodology has been

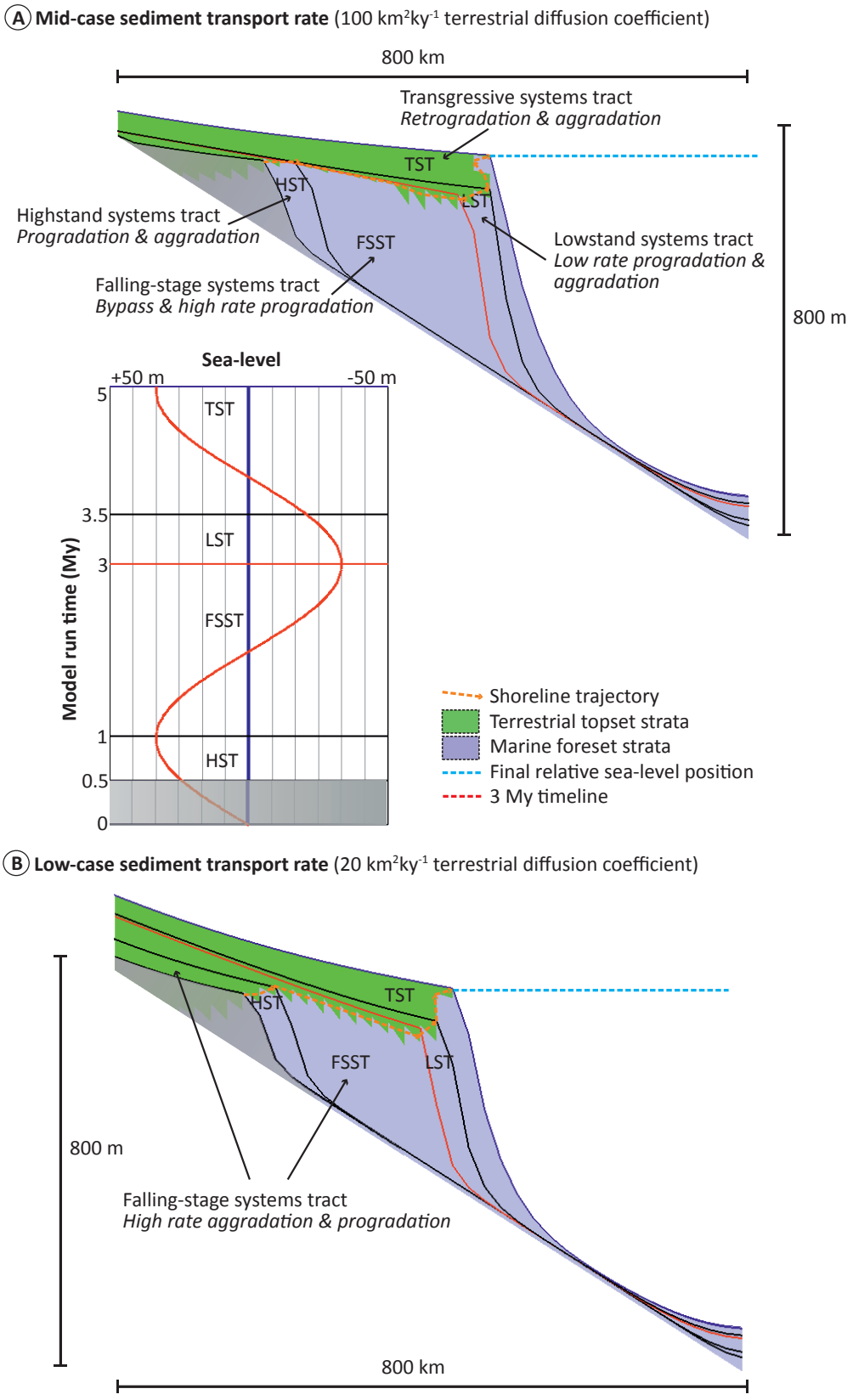

FIGURE 4.15: Caption next page.

FIGURE 4.15: (Previous page.) Reconstruction of systems tracts in Dionisos with A) a mid-case sediment transport rate (terrestrial diffusion coefficient of 100 km^2ky^{-1}) and B) a low-case case sediment transport rate (20 km^2ky^{-1}), reflecting relatively low and moderate rates of sediment transport for a small to medium-size delta system (*Kenyon and Turcotte*, 1985). Sediment supply was constant in both 5 My duration models (A and B) and a eustatic sinusoidal sea-level curve ranges from +40 to -40 m. The major difference between the two models is that model A, with a mid-case sediment transport rate, creates systems tracts similar to the conceptual model (e.g., *Catuneanu*, 2006), whereas the low-case sediment transport model creates a falling-stage systems tract with high rates of aggradation due to topset aggradation during falling RSL.

the development of the concepts and methods of shoreline-trajectory analysis (*Helland-Hansen and Hampson*, 2009, *Helland-Hansen and Martinsen*, 1996). This method is important because it requires fewer implicit assumptions than a systems-tract approach, which assumes dominant control by accommodation variations and is interpretive rather than observational even in its basic nomenclature (e.g., lowstand systems tract). Shoreline trajectories are less interpretive and have the potential to objectively distinguish between falling-stage and highstand topset aggradation. A descending shoreline trajectory associated with topset aggradation would indicate falling-stage, while a horizontal or rising trajectory would indicate highstand. Also, it has been suggested that the gradient of a descending shoreline trajectory relative to the alluvial gradient could be a control on fluvial aggradation versus erosion and incision during RSL fall (*Helland-Hansen and Martinsen*, 1996). However, results in this work show that this may not be the case, because fluvial aggradation occurs when the shoreline trajectory gradient is lower (e.g., profile e, Figure 4.5) or higher (FSST, Figure 4.15B) than the alluvial gradient.

Unfortunately, distinguishing horizontal or rising trajectories from descending trajectories in ancient strata requires knowledge of the paleohorizontal datum. Identification of this datum can be difficult when tectonic tilting or differential compaction has occurred, as shown in Figure 4.16, where a horizontal and a descending trajectory generated in Dionisos are subjected to differential compaction under overburden (*Helland-Hansen and Hampson*, 2009). It is difficult to see how the post-compaction forced and unforced regressive trajectories could be reliably distinguished in ancient strata in these cases without very detailed 2D and 3D backstripping.

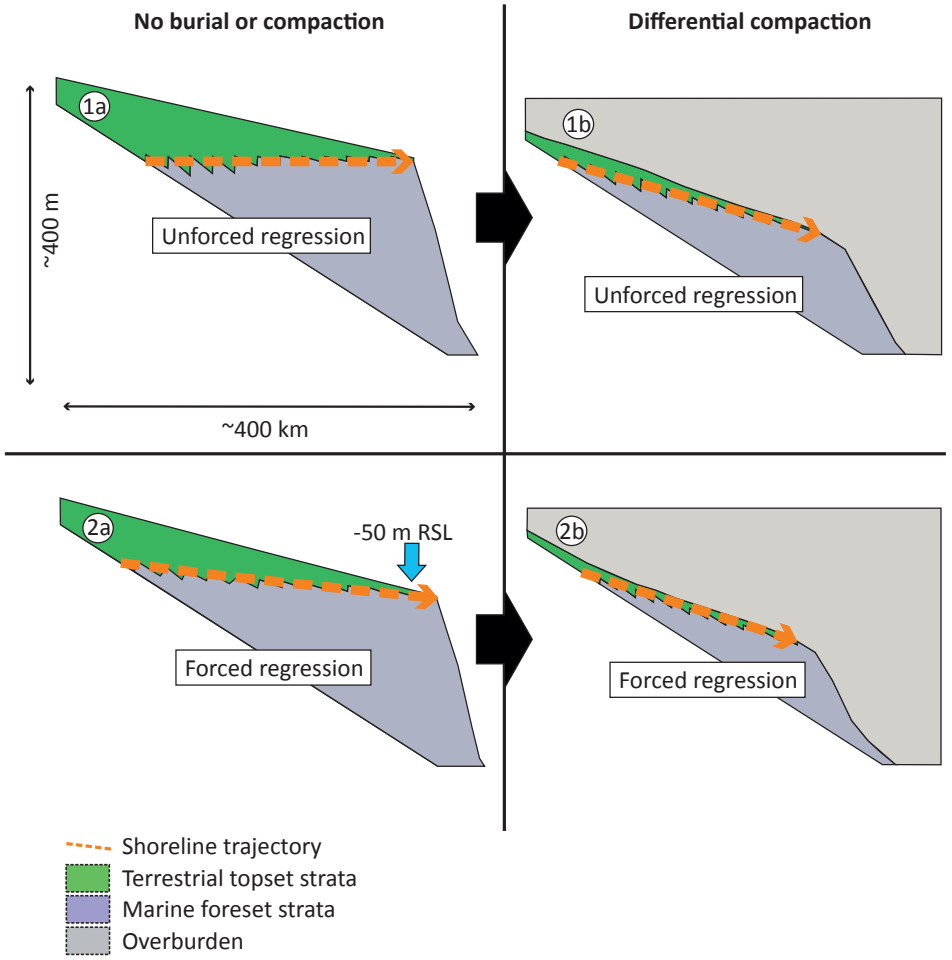

FIGURE 4.16: Comparison of uncompacted (1a and 2a) and compacted (1b and 2b) shoreline trajectories reconstructed from Dionisos 2-My duration model runs. Stratal geometry 1a was generated with steady RSL and has a horizontal shoreline trajectory. Stratal geometry 2a was generated with a 50-m-amplitude RSL fall and has a descending shoreline trajectory. After differential compaction from overburden the horizontal shoreline trajectory in 1a appears descending (geometry 1b), and the descending shoreline trajectory in geometry 2a is exaggerated.

4.6 Conclusions

Numerical modeling of forced and unforced regressive strata, generated with a range of amplitudes and durations of RSL fall and a range of sediment transport rates, supports previous work suggesting that topset aggradation can occur during falling relative sea level.

Several hundred numerical simulations on a simple ramp topography and on a topography with a shoreline break of slope demonstrate that topset aggradation during RSL

fall occurs across a wide range of values of terrestrial diffusion coefficients, and of amplitudes and durations of RSL fall. Topset aggradation during falling relative sea level is particularly prevalent in models with sediment transport rates at the low end of what is observed in modern delta systems. These results suggest that falling-stage topset aggradation is likely to be common in ancient strata.

Across the suite of model runs, falling-stage topset aggradation is difficult to distinguish from highstand topset aggradation. If falling-stage topset aggradation commonly occurs in ancient strata, this nonuniqueness has serious implications for the reliable identification of systems tracts, for reconstruction of RSL curves, and for predictions of sediment bypass into deep-marine settings.

Careful analysis of shoreline trajectories may help alleviate this non-uniqueness problem, but processes like differential compaction may complicate this by making rising and falling trajectories difficult to distinguish.

Chapter 5

Formation & Preservation of Shoreline Trajectories: Implications for Shoreline Trajectory Analysis

5.1 Introduction

Shoreline trajectories describe the migration history of a shoreline in a cross sectional depositional-dip section (e.g., Figure 5.1, 5.3). Since they are understood to be a function of bathymetry, sediment supply, eustatic sea-level change and subsidence or uplift (*Helland-Hansen and Gjelberg*, 1994; *Helland-Hansen and Hampson*, 2009), shoreline trajectories are useful geomorphic features for analysis of stratigraphic architectures observed in 2D and 3D data (e.g., *Loseth et al.*, 2006; *Kertznus and Kneller*, 2009; *Hampson et al.*, 2009).

5.1.1 The shoreline trajectory method

Clinoform rollovers and shoreline trajectory classes

Shoreline (or shelf-edge) trajectories are recorded in the ancient record by geomorphic breaks in slope that are associated with changes in depositional processes and products

that occur at the shoreline (Figure 5.1). They can be reconstructed from observed clinoforms by interpreting consecutive maximum breaks in clinoform slope (Figure 7.13a) known as clinoform rollovers.

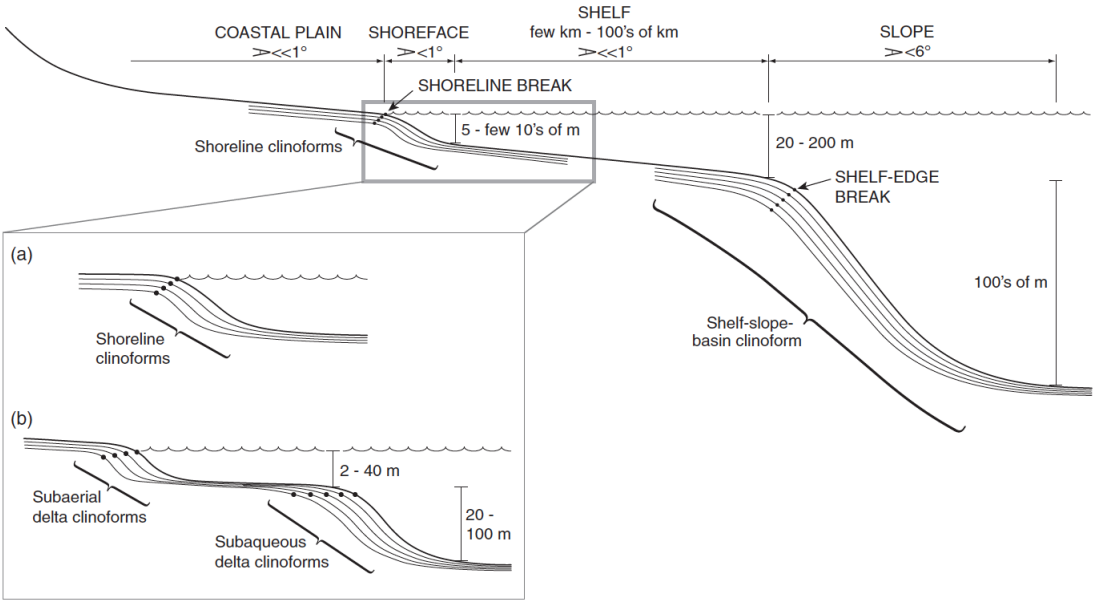

FIGURE 5.1: Depositional dip profile with a break in slope at the shoreline and shelf-break. Shoreline clinoforms are on a scale of tens of metres in thickness compared to larger shelf-slope-basin clinoforms which are on scales of hundreds of metres in thickness. (a) Shoreline trajectories are interpreted by identifying successive clinoform maximum breaks in slope (i.e. the topset-foreset clinoform roll-over position). In some cases subaqueous delta clinoforms are laterally separated from the shoreline. Figure reprinted with permission, from *Helland-Hansen and Hampson* (2009).

Interpreting shoreline trajectories from seismic data can be difficult because the scale of shoreline clinoforms is relatively small (10s of metres in thickness). Often it is shelf-margin clinoforms and the shelf-edge trajectory that is interpreted from seismic datasets (e.g., *Kertznus and Kneller*, 2009). However, if shoreline clinoforms are well imaged, shoreline trajectories can be interpreted, as shown in Figure 5.2. Deciding on the maximum break in slope of the clinoform, however, can be an ambiguous task.

Trajectory classes describe shoreline trajectories in a vertical and horizontal perspective (Figure 5.3). Descending regressive class indicates shoreline regression in response to a fall in RSL. Ascending regressive and transgressive classes indicate shoreline regression and transgression in response to RSL rise. A stationary shoreline trajectory class recognises periods when shorelines are stablised for long periods of time fronting deep basinal waters with accompanying large volumes of sediment bypass (*Helland-Hansen and Hampson*, 2009). In addition to these classes, an accretionary shoreline trajectory

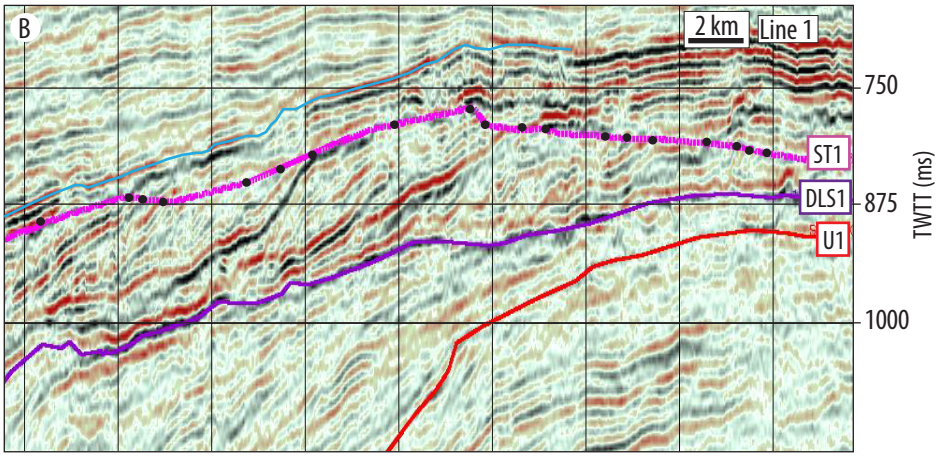

FIGURE 5.2: Depositional dip orientated 2D seismic line, from the Northern Carnarvon Basin. The shoreline trajectory has been interpreted from maximum breaks in slope of the shoreline clinoforms. The line has not been flattened on a datum surface, which is required for reliable interpretation of shoreline trajectories. Dark blue line is an underlying downlap surface. Line courtesy of Geoscience Australia.

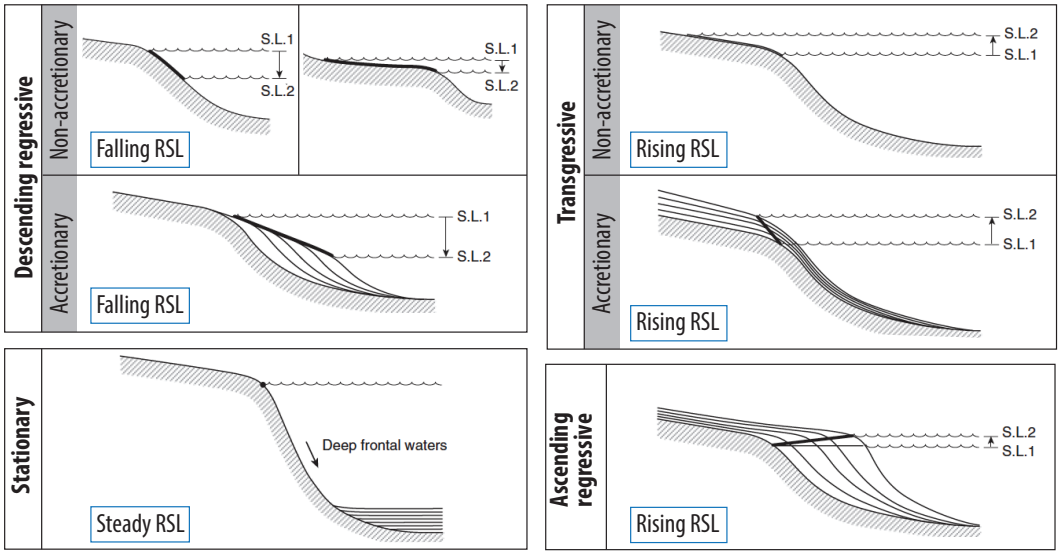

FIGURE 5.3: Shoreline trajectory classes indicating RSL and sediment supply history . Heavy lines indicate shoreline trajectory. Modified from *Helland-Hansen and Hampson* (2009).

describes a scenario when sediment supplied to the shoreline participates in determining the shoreline trajectory, whereas a non-accretionary shoreline trajectory describes a scenario when the existing topography has determined the style of shoreline trajectory (*Helland-Hansen and Gjelberg*, 1994; Figure 5.3).

Application of the shoreline trajectory method

Reconstruction of shoreline trajectories can aid analysis of stratigraphic architectures

observed in outcrop, well-log or seismic data, which can improve our understanding of controls on ancient strata (*Helland-Hansen and Hampson*, 2009). For example, recent studies have applied the trajectory concept to make predictions on shoreline tongue lateral extent (*Loseth et al.*, 2006) and thickness (*Hampson et al.*, 2009), predict the absence or presence of extensive erosional surfaces and make predictions on basin-floor fan systems (*Helland-Hansen and Hampson*, 2009). What makes the trajectory concept particularly important is that, unlike conventional sequence stratigraphic models, shoreline trajectory analysis does not rely on simplifying assumptions such as a dominant control by accommodation variations or constant rate of sediment supply through time. Instead, the analysis of shoreline trajectories requires a more intuitive, observational approach (e.g., ascending versus descending shoreline trajectory trend) compared to the more interpretative nature of conceptual sequence models (e.g., *Posamentier et al.*, 1988).

5.1.2 Complications for shoreline trajectory analysis

An additional control by the rate of sediment transport

It is widely understood that shoreline trajectories are controlled by sediment supply, RSL and initial bathymetry (*Helland-Hansen and Gjelberg*, 1994). However, some evidence also suggests that sediment transport rates play an important controlling role on development of shoreline trajectories. For example, Chapter 4 demonstrated that sediment transport rates in the terrestrial environment influence extent of erosion versus aggradation at the shoreline; high sediment transport rates at the shoreline lead to erosion and low sediment transport rates at the shoreline encourage fluvial aggradation. This is likely to have an impact on the resulting shoreline trajectory. This point was highlighted by *Rivenæ s* (1997), who suggested that efficient sediment transport systems can reduce preservation potential of non-marine sediments. In addition to a control by terrestrial sediment transport rates, *Burgess and Steel* (2008) showed that marine sediment transport rates may also be an important control on shoreline trajectories because higher marine sediment transport rates encourage transgression of the shoreline by removing sediment from the delta front and transporting it to the marine environment.

If sediment transport rates can control the amount of sediment deposition versus erosion at the shoreline and the distribution of sediment across the different marine environments, from shelf to slope and deeper water, then this suggests an additional control

on shoreline trajectories. For example, high sediment transport rates increase rates of progradation by preventing topset deposition and transferring sediment to the marine slope. And higher sediment transport rates have been shown to encourage shoreline transgression during constant rising RSL (*Burgess and Steel*, 2008).

These examples suggest different shoreline trajectories can result from similar combinations of supply and accommodation history, because of variations in sediment transport rate. This could complicate RSL reconstructions. For example, different trajectory classes interpreted along a basin margin may lead to different supply and accommodation reconstructions; interpreting an ascending regressive class in one location and an ascending transgressive in an another (Figure 5.3) would lead to alternative interpretation regarding sediment supply and accommodation histories, when in reality different sediment transport rates could be the cause of the two different shoreline trajectories observed.

Modification by differential compaction

As demonstrated in Chapter 4, differential compaction has the potential to alter shoreline trajectories to the extent that different trajectory classes are difficult to tell apart. This could pose a problem for the shoreline trajectory analysis method given that restoration of clinoform geometries using paleo-horizontal datum surfaces is a difficult process (*Helland-Hansen and Hampson*, 2009).

Non-uniqueness

An additional issue presented by the complications above (i.e. sediment transport rates as a control on shoreline trajectories and modification of shoreline trajectories by differential compaction) is the possibility of non-unique shoreline trajectories. Non-unique shoreline trajectories will exist when similar shoreline trajectories are generated with different parameter values. This contrasts to a unique shoreline trajectory, which is easily distinguished from other shoreline trajectories and formed from only one set of parameter values (e.g., sediment transport rate, amplitude of RSL variations, etc) of controlling processes.

Aforementioned work suggests that, in addition to variations in volume of sediment supply, RSL fluctuations and initial bathymetry, terrestrial and marine sediment transport rates and differential compaction may be an important control on shoreline trajectories. If this is the case, shoreline trajectories generated with identical accommodation

and sediment supply histories could look different. This is important because different shoreline trajectories may lead to different interpretations of sediment supply and accommodation histories which may influence RSL reconstructions and related predictions of stratigraphic architecture elsewhere in the basin.

5.1.3 Aim of this chapter

In this chapter shoreline trajectories are calculated from stratal geometries generated with a numerical stratigraphic forward model to investigate (i) how terrestrial and marine sediment transport rates can influence shoreline trajectories and (ii) if differential compaction during burial will compromise shoreline trajectory reconstruction, making shoreline trajectories generated with different parameter values difficult to distinguish.

5.2 Method and model parameter values

In this chapter shoreline trajectories are calculated from basin-margin stratal geometries generated in a numerical stratigraphic forward model. The numerical model is described in detail in Chapter 3 and the parameter values for the different model runs in this chapter fall within the standard parameter values previously discussed (Table 5.1).

Eustasy

Amplitude and durations of sea-level rise and fall in this chapter, for simple 2 My and complex 6 My RSL curves, cover the same range investigated in Chapter 4. These values are from published amplitudes and durations interpreted through the Phanerozoic (*Miller et al.*, 2005).

Initial topography

All modelled stratal geometries, from which shoreline trajectories are calculated, were generated on a simple ramp topography (illustrated in Figure 5.4). The initial topographic slope is used as a reference datum to correct shoreline trajectories to true horizontal at the end of the model runs. This initial topographic surface has a low paleo-seaward dip of $\alpha = 0.06^\circ$ (Figure 5.4) which is similar to measured gradients from medium- to large-scale river-dominated delta systems (Chapter 4; *Reading and*

TABLE 5.1: Dionisos standard model parameter values.

Parameter	*2D value*
Grid length (x-axis) (km)	800
Grid length (y-axis) (km)	40
Grid Point Spacing (km)	20
Terrestrial Transport Distance (km)	100
Sediment supply (km^3My^{-1})	1000
River discharge (m^3s^{-1})	200
Gravity weathering rate (m My^{-1})	1
Water weathering rate (m My^{-1})	100
Composition of sediment supply (sand, mud) (%)	20, 80
Gravity-driven terrestrial K sand (km^2ky^{-1})	4
Gravity-driven terrestrial K mud (km^2ky^{-1})	8
Gravity-driven marine K sand (km^2ky^{-1})	0.05
Gravity-driven marine K mud (km^2ky^{-1})	0.1

Collinson, 1996).

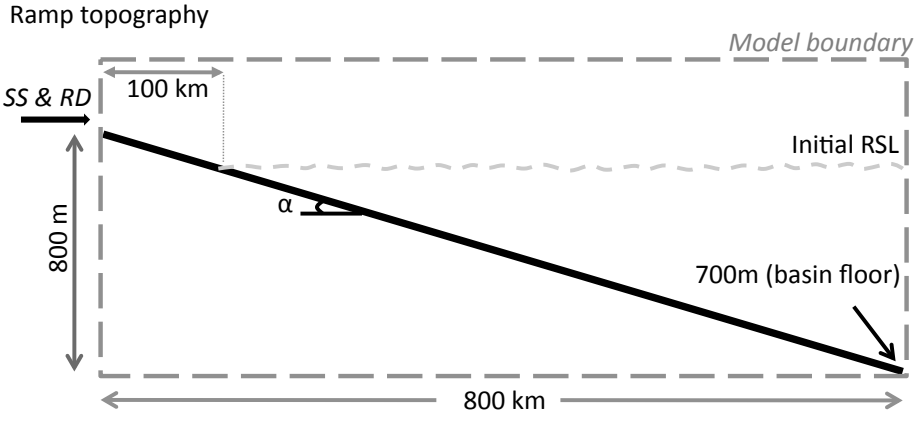

FIGURE 5.4: Illustration of the Dionisos 2D initial ramp topography used for this chapter. $\alpha = 0.06\,°$, SS = sediment supply, RD = river discharge. Verticle exaggeration approximately = x 250. Basin floor reflects 700 m initial water depth.

Sediment supply

Sediment input was constant through each model run unless specified. As with the multiple model runs discussed in the previous chapter, the constant parameter value

for sediment supply volume was 1000 km^3My^{-1} and for river discharge rate it was 200 m^3s^{-1}.

5.3 Model Output

Shoreline trajectories are plotted from stratal geometries generated in Dionisos for a selection of 2D model runs, including simple 2 My duration RSL histories and 6 My duration RSL histories. These shoreline trajectory plots are displayed as (i) shoreline trajectory cross sections (horizontal distance versus vertical elevation) and (ii) shoreline trajectory time plots (horizontal position versus elapsed model time). A selection of stratal geometries are compacted to investigate the consequences of post-depositional compaction for shoreline trajectory preservation. These compacted geometries are shown as annotated cross sections from the numerical model.

5.4 Analysis of shoreline trajectories

5.4.1 Model Set One: simple shoreline trajectories from 2 & 0.4 My models

Figure 5.5 shows shoreline trajectories calculated from a selection of model runs. These models were generated and discussed in Chapter 4 (Model sets one & two in Chapter 4). Shoreline trajectories were calculated from models of both 2 My and 0.4 My durations, for 0 m, 50 m and 100 m amplitudes of RSL fall, and for each of these cases, diffusion coefficients of 20 and 200 km^2kyr^{-1}, representing relatively low and high sediment transport rates, respectively (*Kenyon and Turcotte*, 1985). Comparison of the shoreline trajectories from the low and high sediment transport cases for the different amplitudes of RSL fall indicates that sediment transport rate can be an important control on the preserved shoreline trajectory. For example, for the 100 m RSL fall case for a 2 My duration model, preserved shoreline trajectories are quite different for the two cases with different sediment transport rates. The key reason for the two different trajectories is the topset aggradation in the model with a diffusion coefficient of 20 km^2kyr^{-1} versus topset erosion in the model with a diffusion coefficient of 200 km^2kyr^{-1}. In the

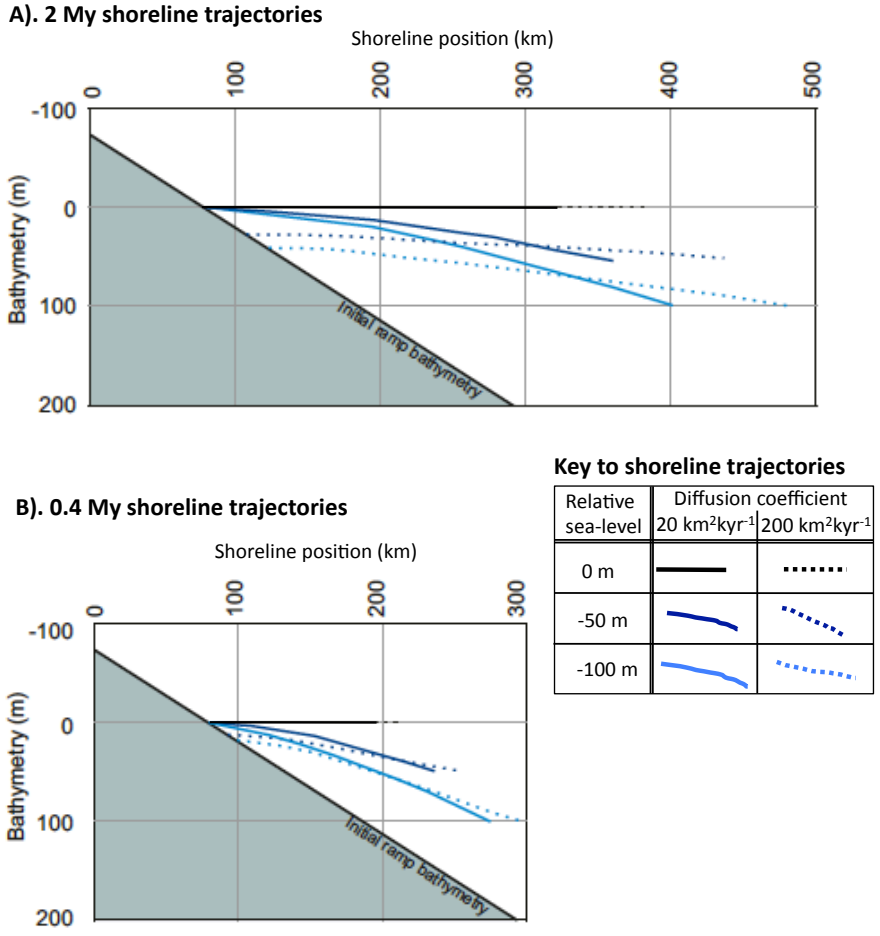

FIGURE 5.5: Shoreline trajectories reconstructed from 2 My (A) and 0.4 (B) My duration Dionisos simulations. On both cross sections (A & B) shoreline trajectories were created with different RSL histories (denoted by colour: black = 0 m, dark blue = 50 m, light blue = 100 m) and low or high terrestrial diffusion coefficients (denoted by solid or dash lines). Solid lines represent shoreline trajectories reconstruction from models with relatively low sediment transport rates (20^2kyr^{-1} diffusion coefficient) and dotted lines represent trajectories reconstructed from models with high sediment transport rates (200^2kyr^{-1} diffusion coefficient). Initial ramp topography was used as a surface to assure true horizontal. Initial RSL begun at 0 m elevation. Shoreline trajectories generated with relatively high diffusion coefficients (dotted lines) and large amplitude RSL fall plot below initial RSL position and hence are inaccurate. This is a consequence of erosion during RSL fall.

latter case, higher sediment transport rates lead to erosion, with the resulting reconstructed shoreline trajectory appearing to start below initial sea-level. Comparison with the shoreline trajectories reconstructed from no RSL fall (black dotted and solid lines on Figure 5.5) is also informative. In these two cases, the shoreline trajectories for the different sediment transport rates are similar. Based on these comparisons of high and low sediment transport cases for the different RSL fall amplitudes and durations, it is clear that sediment transport rate, as well as amplitude of RSL fall and sediment supply rate, control the shoreline trajectories.

An important question is what effect different sediment transport rates can have on more complex shoreline trajectories created by RSL oscillations over longer durations. Do different sediment transport rates lead to different regressive and transgressive shoreline transits? And how might these different shoreline trajectories lead to different RSL history reconstructions based on interpretation of clinoforms rollovers?

5.4.2 Model Set Two: shoreline trajectories reconstructed from 2D models with sinusoidal RSL curves

To investigate shoreline trajectory reconstruction from more complex relative sea level histories, Model Set Two consists of eight Dionisos models that have been run with an oscillating sea-level curve over a 6 My duration (Figure 5.6). The eight models were created with terrestrial diffusion coefficients of 20, 80, 140 and 200 km^2kyr^{-1} and for each of these cases, a marine diffusion coefficients of 0.5 and 4 km^2kyr^{-1} (note that these values are for sand, coefficients for mud were double these values), representing a range from relatively low to high terrestrial sediment transport rates (*Kenyon and Turcotte*, 1985), and a low case and a high case of sediment transport in the marine environment. Shoreline trajectories reconstructed from Model Set Nine are plotted on two cross sections and two shoreline trajectory plots. In the plots (Figure 5.6) shoreline trajectories generated by different terrestrial diffusion coefficients are distinguished by colour. Figure 5.6 is further divided, labelled A and B, for two of the marine diffusion coefficients tested. The shoreline trajectories in the cross sections were reconstructed from modelled stratal geometries at the end of the 6 My model runs, illustrating the position of the shoreline break of slope through time. One stratal geometry is also presented in screen captures, with wells taken at points of interest (Figure 5.7).

Model runs with identical 6 My duration RSL histories and differing terrestrial and marine diffusion coefficients generate different shoreline trajectories (Figure 5.6). Shoreline trajectories in Figure 5.6 display varying durations of progradation, aggradation and retrogradation, as shown by the cross sections and shoreline trajectory plots. The shoreline trajectories are described in detail in the following sections.

0 - 1.5 My simulation time

Figure 5.6a shows that after initial progradation during rising RSL, a model run with a terrestrial diffusion coefficient of 20 km^2kyr^{-1}, representing a relatively low terrestrial sediment transport rate, generates a stratal geometry that displays an ascending shoreline trajectory for 0.5 My of simulation time. This contrasts with shoreline trajectories reconstructed from model runs generated with a higher terrestrial diffusion coefficient, which show little or no ascent, and descend continuously for the first 1.5 My of simulation time. This difference in initial shoreline trajectory is a result of the sediment transport rate in the model run: a lower terrestrial diffusion coefficient, and therefore lower terrestrial sediment transport rate, is less efficient at transporting sediment from the delta topsets (coastal plain area) to the delta forsets (marine shelf - slope environment), and consequently more sediment is deposited as topset strata, leading to a more aggradational stacking pattern and an ascending shoreline trajectory. In contrast, a higher terrestrial diffusion coefficient creates a delta environment with higher terrestrial sediment transport; more sediment is deposited to the delta foresets and the shoreline trajectory is predominantly progradational (e.g., black shoreline trajectory in plot a, Figure 5.6). At 1.5 My, a time of RSL lowstand, a clear difference between the reconstructed shoreline trajectories is that the blue trajectory (created with a low, 20 km^2kyr^{-1} diffusion coefficient) has prograded 325 km basinward, compared to shoreline trajectories created with higher rates of terrestrial diffusion coefficient which have prograded an additional 60 km, to a delta front shoreline position of 385 km (Figure 5.6a).

1.5 - 2.5 My simulation time

During a second, larger amplitude RSL rise of 100 m over 1 My, each shoreline trajectory displays an aggradational phase shortly followed by retrogradation. In these cases retreat of the shoreline is driven either by delta autoretreat, due to insufficient sediment supply to maintain progradation during rising RSL (*sensu Muto and Steel*, 1997), or simply retrogradation driven by RSL rise. An obvious disparity between the shoreline

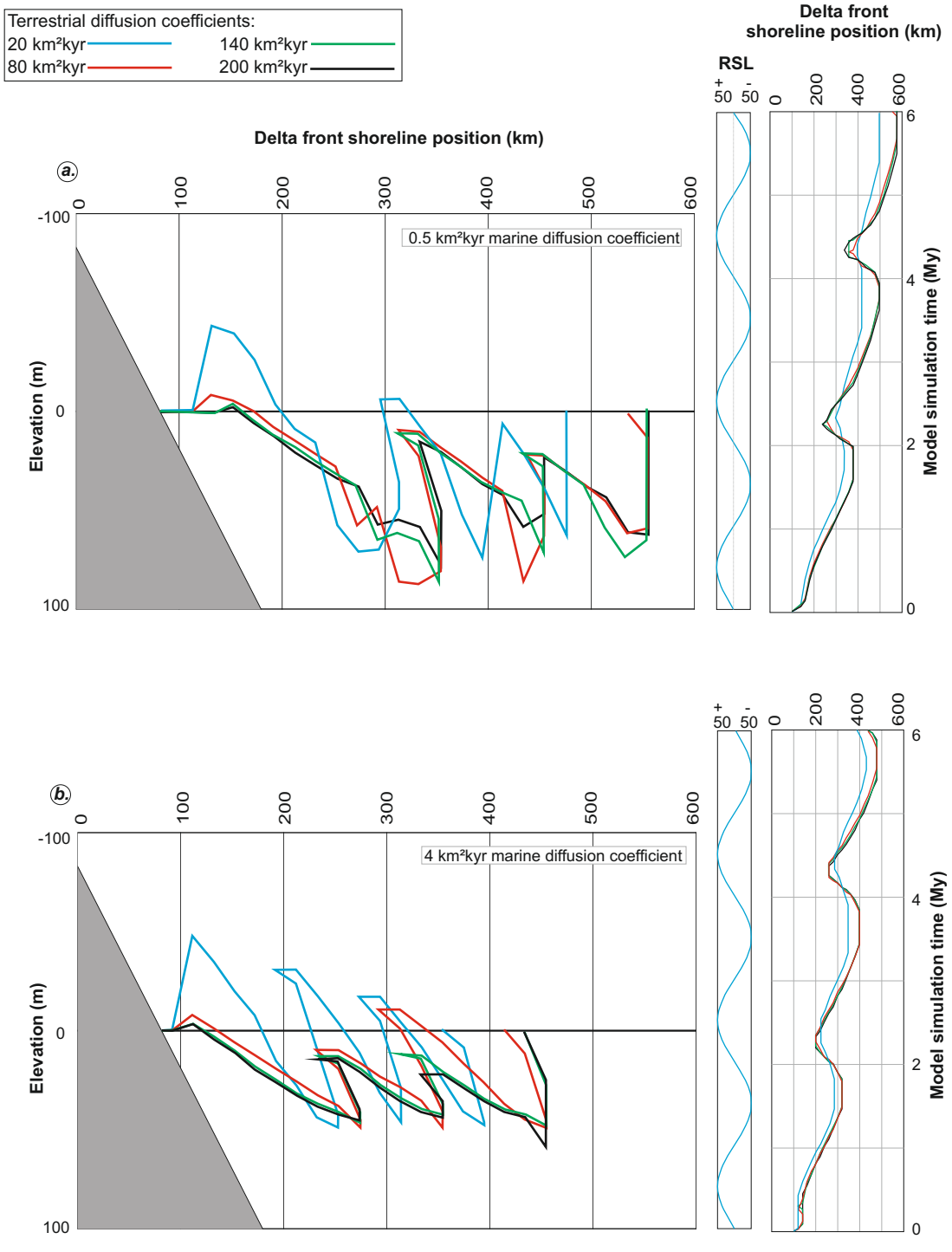

FIGURE 5.6: Shoreline trajectories reconstructed from 6 My model runs. Different colour lines represent shoreline trajectories generated with different terrestrial diffusion coefficients. Plot A consist of shoreline trajectories created with the standard marine diffusion coefficients (Table 5.1), B contains shoreline trajectories reconstructed from model runs with increased marine diffusion coefficients. A RSL curve and shoreline-time plot are positioned to the left of the larger, main cross sections.

trajectories during this aggradational to retrogradational phase is that the blue shoreline trajectory (resulting from a terrestrial diffusion coefficient of 20 km^2kyr^{-1}) does not maintain its aggradational phase for as long as shoreline trajectories reconstructed from model runs with higher diffusion coefficients (green, red and black), nor does it appear to flood back as far over its coastal plain, which was deposited during the previous phase of progradation (Figure 5.6a).

2.5 - 6 My simulation time

During this interval RSL fall forces the shoreline in model runs with terrestrial diffusion coefficients of 80, 140 and 200 km^2kyr^{-1} to prograde further basinward than the shoreline in the model run with a lower, 20 km^2kyr^{-1} diffusion coefficient. This is because the model simulation with 20 km^2kyr^{-1} diffusion coefficient does not provide sufficient sediment transport for removal of sediment from the delta topset to the foresets despite RSL fall. This is a scenario of topset aggradation during RSL fall (Chapter 4 and references therein). Subsequent RSL rise, to a highstand at 4.5 My simulation time, causes the three trajectories with 80 km^2kyr^{-1} or higher to aggrade for a similar distance before retrograding. In contrast, the shoreline trajectory generated by a lower terrestrial diffusion coefficient (20 km^2kyr^{-1}, blue line) does not display retrogradation at 4.5 My of simulation time. Finally, a RSL fall and subsequent rise causes shoreline trajectories generated with 80 km^2kyr^{-1} terrestrial diffusion coefficient or higher to prograde to approximately 560 km, compared to the blue shoreline trajectory, created with 20 km^2kyr^{-1} terrestrial diffusion coefficient, that progrades to nearly 500 km. Only a shoreline trajectory generated with a 80 km^2kyr^{-1} diffusion coefficient goes into retrogradation in the final 50 m amplitude RSL rise (Figure 5.6a).

Reconstructed shoreline trajectories presented in Figure 5.6a demonstrate that the terrestrial sediment transport rate is an important control on regressive and transgressive shoreline shifts in Dionisos. Shoreline trajectories generated with a low terrestrial diffusion coefficient of 20 km^2kyr^{-1}, representing a relatively low rate of terrestrial sediment transport in deltaic environments (*Kenyon and Turcotte*, 1985), show less transgressive and regressive shoreline travel distances than trajectories generated with higher terrestrial diffusion coefficients (e.g., 200 km^2kyr^{-1}). This is because a lower terrestrial diffusion coefficient, and therefore a lower terrestrial sediment transport rate in the model runs, leads to topset aggradation rather than sediment transport and deposition on the delta foresets. This situation is reflected by t/f ratios calculated from stratal geometries

in Chapter 4; stratal geometries created with low diffusion coefficients had higher t/f ratios than stratal geometries created with higer terrestrial diffusion coefficients. Based on this analysis of shoreline trajectories resulting from a range of terrestrial diffusion coefficients in Dionisos, it seems probable that the sediment transport rate of a delta system exherts some control on the transgressive and regressive shifts of the shoreline due to the amount of sediment deposited as topset strata versus foreset strata.

Comparison between shoreline trajectory reconstruction and shoreline-time plots

Comparing a shoreline trajectory reconstructed in cross section with its position on the shoreline-time plot in Figure 5.6 can give conflicting information on delta front shoreline position. For example, the shoreline-time chart (Figure 5.6a) indicates that at approximately 2.25 My, shoreline trajectories generated in model runs with 80, 140 and 200km^{2}kyr^{-1} (red, green and black, respectively) are shown to retrograde back to a delta front position of 250 km. However, these shoreline trajectories (red, green and black) reconstructed and illustrated in the cross section in Figure 5.6a do not transgress back to this delta front position. The reason for this difference is because in the final (i.e., 6 My EMT) modelled stratal geometry, no marine strata deposited during the 2.5 EMT transgression (and shown on the shoreline-time plot) is preserved beyond a delta front shoreline position of approximately 310 km.

This problem is illustrated in Figure 5.7, which shows a screen shot at 2.5 My and a screenshot at 4.5 My simulation time, from the same single model run with 200 km^{2}kyr^{-1} diffusion coefficient, representing a relative high rate of terrestrial sediment transport. Well HST_1 intersects a point of maximum flooding resulting from a highstand of RSL that occurred at 0.5 My EMT (red time line). Well HST_2 intersects a second highstand event at 2.5 My (orange time line).

In Figure 5.7a at 2.5 My EMT, the shoreline position is above well HST_2 and has flooded approximately 100 km back over the coastal plain. However, no marine strata has been deposited and preserved on the previous coastal plain deposits during this RSL rise. This is because the terrestrial diffusion coefficient of 200 km^{2}kyr^{-1}, representing relatively high sediment transport, has prevented deposition of strata at the coastline. Without the current position of RSL shown, the only evidence of marine transgression in the simulation is truncation of the previously deposited topset strata (green). In Figure

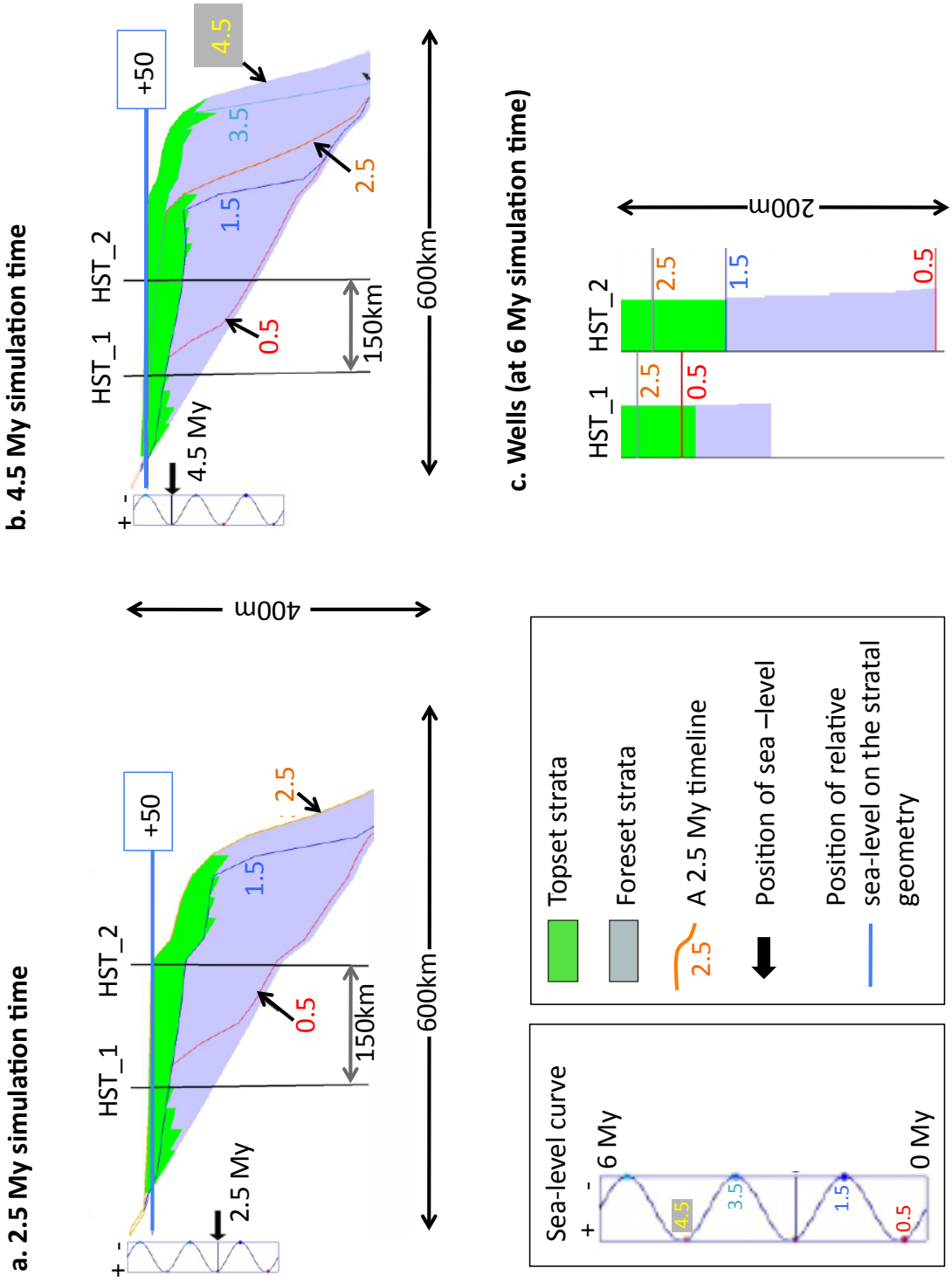
a. 2.5 My simulation time
b. 4.5 My simulation time
c. Wells (at 6 My simulation time)
+50
HST_1
HST_2
2.5
1.5
0.5
150km
600km
400m
2.5 My
4.5 My
4.5
3.5
200m
Topset strata
Foreset strata
A 2.5 My timeline
Position of sea –level
Position of relative sea-level on the stratal geometry
Sea-level curve
6 My
0 My

FIGURE 5.7: (Previous page.) Screen shots at 2.5 (a) and 4.5 My (b), with well transects taken at the end of the 6 My duration model run in Dionisos (c). Sediment transport was relatively high, represented by a diffusion coefficient of 200 km^2kyr^{-1}. The screen shots of the SFM run illustrate that no marine strata was deposited at the location of well HST_2 after 2.5 My EMT, despite a RSL rise at 4.5 My EMT.

5.7b, a screen shot from 4.5 My EMT shows that no marine strata was deposited during a subsequent RSL fall after 2.5 My EMT (i.e., above the 2.5 time line). An important question is whether this marine transgression, from 2 to 2.5 My simulation time, would be recognisable without deposition of marine strata. Figure 5.7c shows that well HST_1 has marine strata deposited close to the 0.5 time line, a time of initial RSL highstand, but no marine strata, or any evidence of truncation, is present in well HST_2 (Figure 5.7).

Influence of marine sediment transport rates

Comparing shoreline trajectories reconstructed from model runs with the same range of terrestrial diffusion coefficients, but with a higher marine diffusion coefficients (Figure 5.6b), suggests that sediment transport rates in the marine environment also influence shoreline trajectories (*Burgess and Steel*, 2008). For example, comparison of shoreline trajectories in Figure 5.6a & b shows that higher rates of marine sediment transport (Figure 5.6b) generally lead to transgression of the shoreline during periods of rising RSL (also shown by *Burgess and Steel*, 2008). This implies that a retrogradational shoreline trajectory (e.g., on Figure 5.6 b at 6 My EMT) could result from either a sufficiently high amplitude and duration RSL rise (*sensu Muto and Steel*, 1992) with relatively low marine sediment transport rates, or from a low amplitude RSL rise with sufficiently high marine sediment transport rates. Conversely, an aggradational shoreline trajectory might result from a steady rising RSL with low marine sediment transport rates such to prevent retreat of the shoreline, or high amplitude RSL rise with sufficiently low marine sediment transport rates to maintain aggradation.

Shoreline trajectories generated with identical RSL and sediment supply histories, but different terrestrial and marine sediment transport rates show important differences. The key reason for the different shoreline trajectories is due to the amount of topset aggradation compared to erosion occuring at the shoreline and basinward transport of sediment. This difference in aggradation versus erosion and sediment transport is a consequence of the diffusion coefficients used in the model run. Low terrestrial and

marine diffusion coefficients lead to more topset aggradation (and a higher t/f ratio, e.g., Figure 4.4 in Chapter 4) and a more aggradational shoreline trajectory, compared to a shoreline trajectory which shows greater transgressive to regressive shifts due to higher marine and terrestrial diffusion coefficients.

Different shoreline trajectories generated by different sediment transport rates but similar RSL and sediment supply histories (Figure 5.6) are important because they give conflicting information about RSL and sediment supply history. Interpretation of different shoreline trajectories from seismic or outcrop in the geological record commonly leads to different interpretations of sediment supply and RSL histories. However, results discussed above suggest that this is not necessarily always correct. In addition variations in shoreline trajectories due to sediment transport rates, a crucial process capable of altering shoreline trajectories and complicating shoreline trajectory reconstruction further, is differential compaction during burial.

5.4.3 Model Set Three: post-depositional compaction of 2 My shoreline trajectories

Post depositional compaction has the potential to alter stratal geometries therefore affect how shoreline trajectories are preserved. Differential compaction occurs when strata varies in thickness or compactibility due to porosity variation. This has the potential to cause problems for reconstruction of shoreline trajectories (e.g., *Helland-Hansen and Hampson*, 2009). In Dionisos, compaction is quantified by using porosity-burial depth laws, which assume a relationship between sediment, porosity and burial depth. This relationship is an exponential curve defined, for sand and mud respectively, by initial porosities of 40% and 70%, residual porosities of 10% and 5% and exponential decay depths of 2000 m and 500 m (Figure 5.8).

Figure 5.9 shows an uncompacted profile (numbered 1-3) and an equivalent compacted profile (1a-3a) created in Dionisos, under conditions of rising, steady and falling RSL. Each of the six model runs presented in Figure 5.9 were created on a 2 My duration (as indicated by RSL curves, Figure 5.9) with relatively low rates of sediment transport (diffusion coefficient of 30 km^2kyr^{-1}). Compacted profiles (1a-3a) have been subjected to 1 km of burial over an additional 0.1 My, at the end of the 2 My model run, with

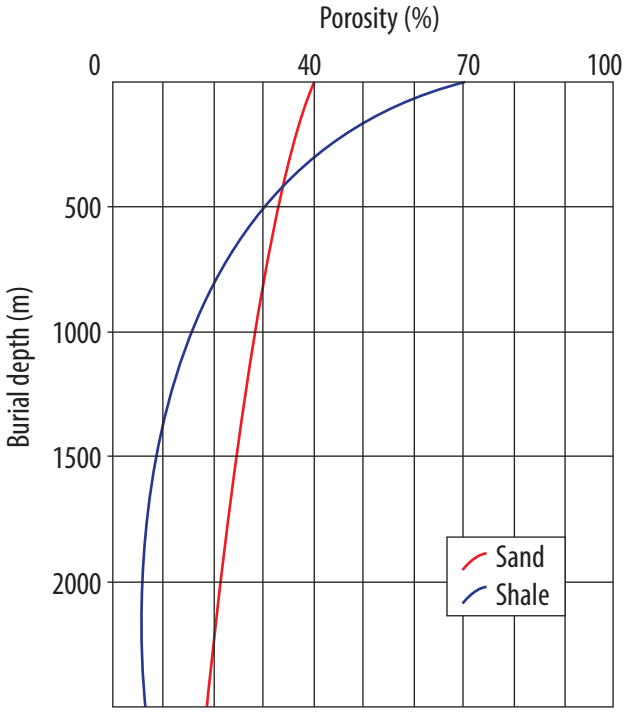

FIGURE 5.8: Dionisos compaction curves for sand and mud.

typical porosity decay rates and residual porosities for sand and mud (*Allen and Allen*, 2005).

Figure 5.9 shows that stratal geometries created without any compaction display a shoreline trajectory directly indicative of the RSL history. For example, profile 1 displays an ascending shoreline trajectory due to rising RSL. Profile 2 was created with steady RSL and therefore displays a horizontal shoreline trajectory. Profile 3 displays a descending shoreline trajectory as a result of falling RSL (Figures 5.9, profiles 1, 2 & 3).

In direct contrast with profile 1, profile 1a displays a descending shoreline trajectory despite its formation during rising RSL. The trajectory of the shoreline has changed from its initial path, which ascended from 0 to +25 m over a horizontal distance of 350 km in profile 1, to appear descending from 0 to -100 m over 350 km in profile 1a. This is a consequence of differential compaction, which has occurred because distal, more muddy foreset strata underlying the shoreline trajectories in models 1 has compacted more than proximal, sandy underlying topset strata. As a result of differential compation the original geometry of the shoreline trajectory has rotated. This is also the case with shoreline trajectories in models 2a and 3a (Figure 5.9). Profile 2a displays a descending shoreline trajectory, though it was created with steady RSL (profile 2). Profile 3a displays a descending trajectory, which is a combined result of RSL fall (profile 3) and

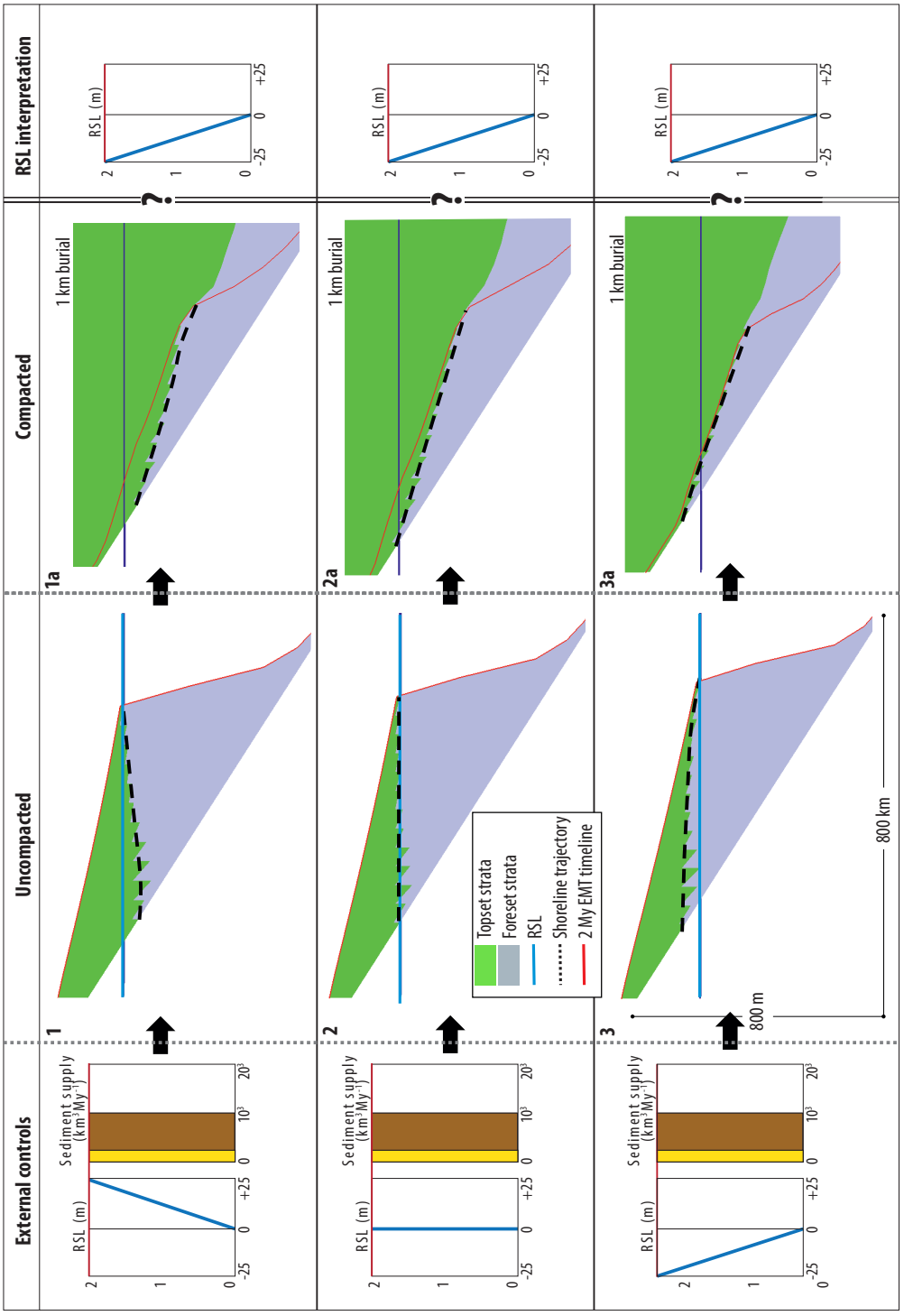
External controls
Uncompacted
Compacted
RSL interpretation
1
1a
2
2a
3
3a
1 km burial
800 m
800 km
Sediment supply (km³My⁻¹)
RSL (m)
Topset strata
Foreset strata
RSL
Shoreline trajectory
2 My EMT timeline
?

FIGURE 5.9: (Previous page) Comparison of uncompacted and compacted shoreline trajectories generated in Dionisos. Model runs 1 to 3 were of 2 My duration, with relatively low rates of sediment transport represented by a 30 km^2kyr^{-1} terrestrial diffusion coefficient for sand (double for mud), and a constant sediment supply of 1000 km^2My^{-1}. Stratal geometry 1 and 1a were created with a steady 25 m RSL rise, stratal geometries 2 and 2a with steady RSL and 3 and 3a with a 25 m RSL fall. Stratal geometries 1, 2 and 3 were not subjected to compaction in Dionisos. Stratal geometries 1a, 2a and 3a were generated with identical parameters as 1, 2 and 3, respectively, but with an additional 0.1 My time step with increased sediment supply values to achieve 1 km burial. Suggested RSL interpretations for each compacted example (1a to 3a) on the right hand side of the figure illustrates how differential compaction could modify shoreline trajectories so that actual RSL histories may be difficult to interpret.

the affects of differential compaction (Figure 5.9). The results suggest that it would be difficult to tell apart shoreline trajectories generated with different RSL histories (Profiles 1, 2 and 3) after modification by differential compaction (Profiles 1a, 2a and 3a). However, an important question is how differential compaction might complicate more complex shoreline trajectories generated from, for example sinusoidal RSL curves.

5.4.4 Model Set Four: post-depositional compaction of 6 My shoreline trajectories

Figure 5.10 shows an uncompacted (black line) and a compacted shoreline trajectory (red line) reconstructed from two different model runs. One model run was created with relatively low sediment transport rate (plot a, with 40 km^2kyr^{-1} terrestrial diffusion coefficient) and the other with a relatively high sediment transport rate (plot b, 140 km^2kyr^{-1} terrestrial diffusion coefficient). Both models were 6 My in duration and were generated with a sinusiodal sea-level curve shown in Figure 5.10c (2 My phase and 50 m amplitude). The stratal geometries were generated with the standard model parameters listed in Table 5.1.

Plots a and b (Figure 5.10) show that RSL histories are reflected in the generated shoreline trajectories if the stratal geometries are not subjected to burial and compaction. For example, until a delta shoreline position of approximately 400 km, both uncompacted shoreline trajectories (black lines in plots a and b) show repeated ascending regressive trajectory trends due to steady sediment supply and RSL rise, though as noted previously there is some variation due to different sediment transport rates. After the delta front has reached approximately 400 and 450 km in the low and high case sediment transport rates (plots a and b, respectively), the delta switches to an aggradational

phase when RSL rises, rather than prodradational, because volume of sediment supply is not sufficient to maintain progradation with rising RSL in deeper water. This occurs when RSL rises at 3.5 My and at 5.5 My EMT (Figure 5.10c).

Shoreline trajectories reconstructed from modelled stratal geometries subjected to burial and compaction in Dionisos generally show predictable differences compared to the shoreline trajectories reconstructed from uncompacted stratal geometries (Figure 5.10). Overall, differential compaction modifies the shoreline trajectories for the two sediment transport cases (a and b in Figure 5.10) so that amplitude of RSL change might be difficult to extract, but the general pattern of regressive and transgressive shoreline transits is quite clear in the compacted cases.

The only significant difference between the uncompacted and compacted shoreline trajectories is the preservation of ascending regressive trajectory trends in the uncompacted cases due to steady sediment supply and RSL rise, compared to descending regressive trajectory trends in the compacted shoreline trajectories due to steady sediment supply, RSL rise and differential compaction. This suggests shoreline trajectories interpreted from seismic or outcrop data that have been influenced by differential compaction could lead to incorrect interpretation of accommodation versus sediment supply history. Figure 5.10 suggests this issue is less significant for interpretations of shoreline trajectories that show repeated regressive to transgressive transits, compared to interpretations of individual trajectory transits shown in Figure 5.9.

5.4.5 Model Set Five: Differential compaction of shoreline trajectories generated with different sediment supply & accommodation histories

Burial of stratal geometries created by simple (Figure 5.9) and complex (Figure 5.10) RSL histories show that reconstruction of shoreline trajectories could be unreliable. This is because shoreline trajectories can be rotated during burial due to differential compaction. This has important implications for how we interpret, and make predictions from shoreline trajectories.

Shoreline trajectories reflect changes in rate of sediment supply as well as changes in accommodation at the shoreline. Considering how shoreline trajectories can be altered

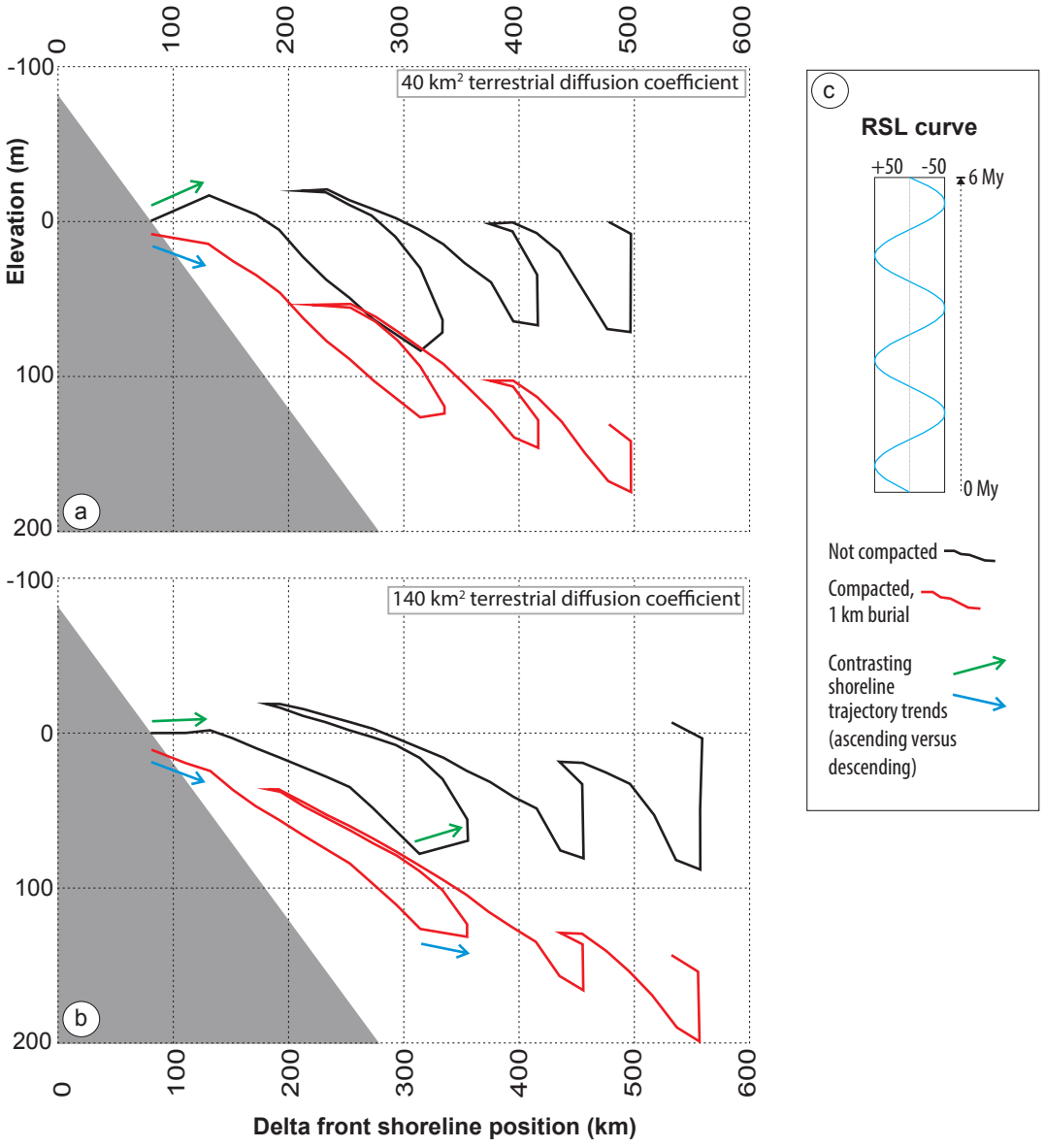

FIGURE 5.10: Comparison of compacted and uncompacted shoreline trajectories reconstructed from Dionisos model runs. Model runs were 6 My (uncompacted shoreline trajectories, black lines) and 6.1 My durations (compacted shoreline trajectories, red lines), generated with 40 and 140 $km^2 kyr^{-1}$ diffusion coefficients (a and b) and a sinusoidal sea-level curve.

due to differential compaction (e.g., Figure 5.9), it is possible that shoreline trajectories created by different sediment supply and RSL histories could look very similar after modification during burial. To investigate this 2 model runs created with different sediment supply rates and RSL histories are subjected to burial and compared.

Figure 5.11 shows 2 different model runs before burial (1 and 2), and the same two model runs after burial (1a and 2a, respectively). Models 1 and 2 were created with the same sediment transport rates but different RSL and sediment supply histories. Profiles 1a and 2a have undergone an additional 0.1 My of burial by approximately 2 km of sediment. Porosity values for sand and mud are the same as previously described for Model Set Eleven.

Profile 1 in Figure 5.11 was created with steadily rising RSL (at a rate of 16.6 m/My). Sediment supply was relatively high, at 2500 km^2kyr^{-1} (*Burgess and Hovius*, 1998), decreases to 50 km^2kyr^{-1} to represent a period of sediment supply shut down, before returning to 2500 km^2kyr^{-1}. As a result of steady RSL rise and the sediment supply history, profile 1 displays initial progradation until 1.4 My EMT, a short-lived transgression due to shut down of sediment supply during steady RSL rise, followed by progradation due to sufficient sediment supply until 6 My EMT. This is reflected by the shoreline trajectory, which is horizontal to transgressive and finally ascending regressive.

Profile 2 in Figure 5.11 was created with constant sediment supply (750 km^2kyr^{-1}) and a sinusoidal sea-level curve (50 m amplitude, 4 My period). After initial progradation, the shoreline trajectory is descending regressive due to RSL fall until 3 My EMT. However, because of relatively low sediment transport rates, topset aggradation occurs during this RSL fall which prevents formation of a subaerial unconformity. At 3 My the shoreline trajectory turns around due to RSL rise. Finally, the shoreline trajectory is forced to descend again due to a short period of RSL fall until 6 My EMT.

When shoreline trajectories in profiles 1 and 2 are buried by approximately 2 km of sediment, they look very similar. Because the shoreline trajectories have been rotated, ascending trajectory trends in profile 1, created during rising RSL, appear to be descending in profile 1a. This is a result of differential compaction. The shoreline trajectories in profiles 1a and 2a appear to have the same trajectory trends despite formation during quite different RSL and sediment supply histories.

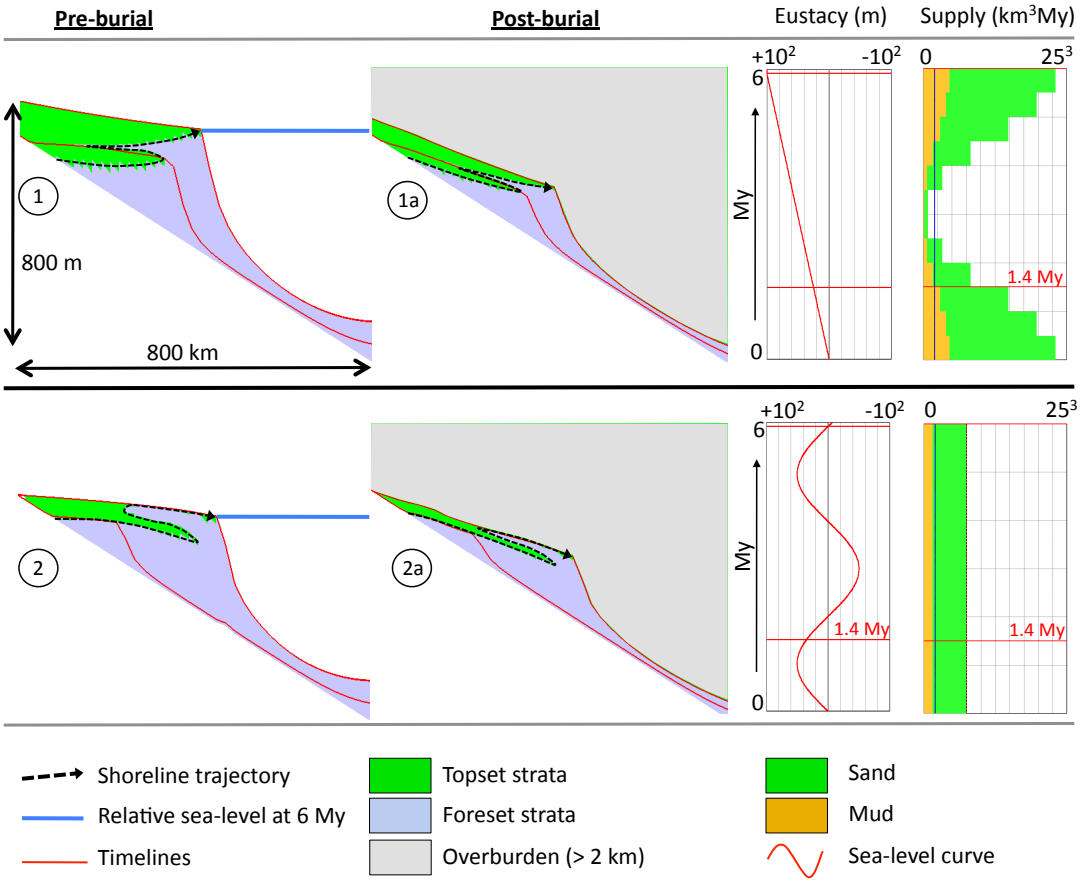

FIGURE 5.11: Comparison of shoreline trajectories generated with (1) variable sediment supply and steady RSL rise, and (2) constant sediment supply and a sinusoidal sea-level curve. The two shoreline trajectories shown on stratal geometries 1 and 2 are compared after burial and compaction in stratal geometries 1a and 2a, respectively. Due to differential compaction after burial, shoreline trajectories show important similarities. Topset aggradation during falling RSL, as well as rising RSL, due to low sediment transport rates (Chapter 4) is also part of the reason for the similarity between the two shoreline trajectories. Stratal geometries were created with the same sediment transport rates (40 $km^2 kyr^{-1}$ terrestrial diffusion coefficient). Porosity values for sand and mud respectively: initial porosity values of 40 and 70%, residual porosities of 10 and 5% and decay depths of 2000 and 500 m.

.

5.5 Discussion

Work in this chapter involved using a numerical stratigraphic forward model to investigate how shoreline trajectories could be controlled by terrestrial and marine sediment transport rates. The role differential compaction could play in modification of shoreline trajectories has also been investigated. In contrast to the many hundreds of simple model runs in the previous chapter, the analysis in this work focussed on a small number of more complex model runs, from which shoreline trajectories were calculated. Results

described above suggest that interpreting shoreline trajectories from 2D or 3D data could be more difficult than commonly assumed because sediment transport rates are an important control. The impact differential compaction has on preservation of shoreline trajectories also has important implications for distinguishing between forced and unforced regressive strata. The results suggest that it may be difficult to distinguish between simple shoreline trajectory trends (ascending, descending, horizontal), as well as recognise more subtle changes in trend from complex shoreline trajectories.

5.5.1 Reliability of model results in this study

The reliability of modelled stratal geomtries in this work hinges on the critical assumption that diffusion indirectly but accurately represents various processes of sediment transport that contribute to form basin-margin stratal geometries in the real world (e.g., saltation, suspension, hypopycnal flows, etc). Unfortunately, to consider any model run analogous to a real physical experiment requires the processes to be completely known. This is obviously not possible for the models in this work, because the physical processes involved in the formation of basin margin stratal geometries are not fully understood (*Paola*, 2000). Nevertheles, the scaled down physical experiment by *Paola et al.* (1999) described previously in Chapter 4 provides a valuable test of a simple diffusional based model against a field-scale example of a delta system with known input parameters. In this case diffusion could be used to predict steady-state basinal topography, suggesting that diffusional models are probably a reliable method for simulating basin-margin stratal geometries.

As discussed in Chapter 4, another important consideration for the plausibility of forward modelling results is the parameter values applied in the experiments. For the stratal geometries and shoreline trajectories generated in this work as well as values used for compaction, the parameter values are similar to values of porosity, sediment supply, river discharge rates and diffusion coefficients from previously published work (*Allen and Allen*, 2005; *Burgess and Hovius*, 1998; *Marion et al.*, 2010; *Kenyon and Turcotte*, 1985). The applied values (Table 5.1) are considered to be representative of a medium sized river system. If this is the case, and such rivers deposited strata in the geological record, then model results in this work should be useful for comparison with shoreline trajectories identified from subsurface and outcrop data.

3D model runs are probably a more realistic representation of the real world. However, for simplicity results in this work are based on 2D model runs. Comparing shoreline trajectories from 2D model runs rather than from 3D model runs omits the problem of shoreline trajectory trend variation along strike, and also reduces computer simulation time. As described in Chapter 3, there is also some complex routing of water across the 3D models which leads to more complicated model results. This complexity is not relevant for the basic question regarding impact of sediment transport efficiency on shoreline trajectories investigated in this chapter.

In Chapter 4 parameter values from published work (*Allen and Allen*, 2005; *Burgess and Hovius*, 1998; *Marion et al.*, 2010; *Kenyon and Turcotte*, 1985) were used to generate a set of 3D model runs. These 3D results were then compared with 2D model runs and it was concluded that the 2D model runs in this work are essentially cross sections through larger, 3D models, representing the main sediment transport axis of a fluvial-dominated delta system.

A common problem involved with shoreline trajectory analysis from outcrop or subsurface data is the choice and availability of a reliable reference datum (*Helland-Hansen*, 2009). Reconstruction of shoreline trajectories from modelled stratal geometries in this work, however, was not complicated by this problem because the initial topographic surface in each model provided a reliable and consistent reference datum (see Figure 5.4). Interpreting the maximum break of slope, or the topset foreset clinoform rollover, in outcrop or subsurface data can also be difficult. In this work shoreline trajectories were calculated from contact between terrestrial (above 0 m elevation) and marine (below 0 m elevation) strata in each model run, further reducing any uncertainty in calculated shoreline trajectories in this work.

5.5.2 Implications of unreliable shoreline trajectories for distinguishing between forced & unforced regressions

The concepts and methods of shoreline trajectory analysis are a useful addition to the conventional sequence stratigraphic theory. The methodology of shoreline trajectory analysis is based on fewer implicit assumptions than the conceptual systems tract models which, critically, assume a dominant control by variations in accommodation. An important difference between a systems tract approach and shoreline trajectory analysis

is that the latter is more observational and enables basic geometries (i.e. ascending versus descending shoreline trajectories) to be directly distinguished. Shoreline trajectories are particularly important with the possibility of topset aggradation during falling RSL considered (e.g., *Prince and Burgess*, 2013 and references therein). In this regard, shoreline trajectories have the potential to objectively distinguish between falling stage and highstand topset aggradation. A descending shoreline trajectory associated with topset aggradation would indicate falling stage, while a horizontal or rising trajectory would indicate highstand.

However, modelling results in this work suggest that distinguishing between horizontal or ascending shoreline trajectories is not straight forward. In addition to changes in accommodation and rate of sediment supply, results described above suggest that sediment transport rates are an important control on shoreline trajectories. Different terrestrial and marine sediment transport rates modelled by using a range of terrestrial and marine diffusion coefficients causes different amounts of topset aggradation and erosion at the shoreline. Low sediment transport rates lead to net aggradation at the shoreline, high sediment transport rates lead to net degradation at the shoreline. In 2 My model runs this leads to subtle, differences in modelled shoreline trajectories despite identical accommodation and sediment supply histories. In more complex, 6 My model runs, different sediment transport rates also generate shoreline trajectories with distinct differences. For example low sediment transport rates due to low terrestrial diffusion coefficients lead to prolonged periods of aggradation, rather than switching to retrogradational phases as is the case with higher sediment transport rates. Similar results have been reached in other studies (*Burgess and Steel*, 2008, *Rivenæ s*, 1997). If sediment transport rates control shoreline trajectories in the geological record, then reconstructions of RSL curves from trajectory trends becomes more ambiguous. For example, is an aggradational to transgressive shoreline shift a result of an increase in rate of accommodation, delta autoretreat (*Muto and Steel*, 1997), or is it possible that the sediment transport rates of the shelf system determined the shoreline shift?

Marine sediment transport rates represented in Dionisos by the marine diffusion coefficient also affects shoreline trajectories. Shoreline trajectories reconstructed from 6 My model runs, created with a sinusoidal RSL curve and a range of terrestrial diffusion coefficients, show that when marine sediment transport rates are high the frequency of transgressive shoreline shifts are greater due to increased marine sediment transport

acting on the marine slope, delivering sediment to the lower delta foresets (*Burgess and Steel*, 2008). This could also be a problem for extracting information on accommodation and sediment supply histories from shoreline trajectories.

Differential compaction adds a further problem to the reliability of shoreline trajectory reconstructions. In Dionisos, ascending shoreline trajectories resulting from a constant RSL rise and horizontal shoreline trajectories resulting from steady RSL appear descending after rotation during differential compaction. When stratal geometries generated by complex, 6 My duration RSL histories are buried, the shoreline trajectories are more subtlety modified: ascending trajectory trends are rotated and appear descending or remain ascending but to a lesser degree; horizontal trajectory trends are modified to appear descending; descending trends appear steeper; and aggradational phases are reduced by compaction. The results suggest that modification by differential compaction may compromise reconstruction of individual shoreline transits, but large scale sediment wedges displaying multiple regressive-transgressive shoreline transits may still enable an overall accommodation and sediment supply history reconstruction.

The scenario of topset aggradation during RSL fall complicates the use of shoreline trajectory analysis for interpretation of RSL histories. This is because neither presence or absence of topset aggradation can be used as a feature indicative of a particular RSL history. The complication arises if there is any doubt on the trajectory trend (i.e., ascending, horizontal or descending) for the shoreline trajectory reconstructed. For example, assuming the scenario of topset aggradation during falling, steady or rising RSL, would a descending shoreline trajectory with associated topset strata be a result of (i) forced regression, or (ii) unforced or normal regression which has undergone subsequent modification by differential compaction (e.g., Figure 5.9 1 & 1a)? It is also possible that, with topset aggradation during falling RSL, accretionary transgressive and forced regressive shoreline trajectories could be confused. This is because both of these shoreline trajectories with contain topset aggradation and both shoreline trajectories would appear to descend paleo-basinward.

5.5.3 Implications for reconstructing RSL histories

Results in this work show that along with changes in sediment supply and accommodation, sediment transport rates are an important control on shoreline trajectories. This

is important for how we interpret shoreline trajectories in the ancient record and how we use these shoreline trajectories as a tool for RSL reconstruction. For example, are different shoreline trajectories necessarily a consequence of different accommodation versus sediment supply histories, or could different shoreline trajectories be the result of variations in sediment transport rates? Conversely, are similar shoreline trajectories necessarily the result of a similar interaction between accommodation and sediment supply histories, or is it possible that similar shoreline trajectories exist due to variations in sediment transport rates, rather than differing RSL and supply histories.

Simple 2 My model results in this chapter have shown that sediment transport rate can be an important control on shoreline trajectories. Models with relatively high sediment transport rate, represented by a terrestrial diffusion coefficient at the high end of the modelled range in this work, lead to net erosion at the shoreline, whereas low sediment transport rates lead to net aggradation at the shoreline. For these two cases of low and high sediment transport rate, different shoreline trajectories are created despite identical sediment supply and accommodation histories. This demonstrates that sediment transport rate can influence shoreline trajectories and complicate reconstruction of RSL histories. Further testing of terrestrial diffusion coefficients and shoreline trajectories for more complex RSL histories shows that the sediment transport rates, as well as rate sediment supply and changes in accommodation, will influence the transgressive and regressive shifts of the shoreline.

5.6 Conclusions

Shoreline trajectories calculated from models generated in Dionisos with identical RSL and sediment supply histories look different due to variations in sediment transport rate. This is because in the model runs the terrestrial diffusion coefficient, which largely controls terrestrial sediment transport, controls how much topset aggradation or erosion occurs at the shoreline. In model runs with falling RSL, high terrestrial diffusion coefficient and therefore relatively high terrestrial sediment transport rates leads to net erosion at the shoreline, but low terrestrial sediment transport rates expressed by a low terrestrial diffusion coefficient leads to net deposition at the shoreline during falling RSL. This suggests that sediment transport rates are an important control on shoreline trajectories.

Reconstructing RSL histories from generated shoreline trajectories that have undergone differential compaction can be problematic. This is because ascending and horizontal shoreline trajectory trends can appear to be descending after differential compaction during burial.

Results suggest that differential compaction of more complicated shoreline trajectories, that experienced repeated regressive and transgressive transits, will still exhibit the same general shoreline trajectory trend. However, interpreting likely amplitudes of RSL variations may be unreliable.

The complexity of shoreline trajectory formation and preservation demonstrated, due to an additional control by sediment transport rates and post depositional modification by differential compaction, means that shoreline trajectories could be an example of a non-unique stratal geometry. This is due to two shoreline trajectories looking similar after generation with different parameter value combinations of RSL, supply, sediment transport rate and differential compaction. Such non-uniqueness would pose a problem for extracting reliable RSL and supply histories from the ancient record.

Chapter 6

Impact of Non-uniqueness for Sequence Stratigraphic Interpretation

6.1 Introduction

Considerable evidence exists to suggest that large scale (i.e., 10s metres to kilometres thick) basin-margin stratal geometries are a consequence of the interplay of several factors including changes in accommodation and supply (e.g., *Carvajal and Steel*, 2009, *Flemings and Grotzinger*, 1996, *Helland-Hansen and Gjelberg*, 1994, *Schlager*, 1993), sediment transport rates (e.g., *Burgess and Steel*, 2008, *Meijer*, 2002, *Paola et al.*, 1999, *Prince and Burgess*, 2013) and initial basin-margin topography (*Leeder and Stewart*, 1996, *Petter and Muto*, 2008, *Schumm et al.*, 1987). Despite this evidence, studies investigating controls on deposition and erosion of basin-margin strata are frequently based on conceptual sequence stratigraphic models which assume a dominant control by accommodation variations (e.g., *Neal and Abreu*, 2009, *Plint and Nummedal*, 2000, *Posamentier et al.*, 1988, *Van Wagoner et al.*, 1990). Assuming a dominant control by accommodation variations has been known for some time to be an oversimplification (*Burton et al.*, 1987), but little work has been done to reveal the limitation of this assumption for sequence stratigraphic interpretation.

The widespread dependence on sequence stratigraphic conceptual models has masked the problem of non-uniqueness (*Burgess and Allen*, 1996, *Burton et al.*, 1987, *Cross and Lessenger*, 1999, *Flemings and Grotzinger*, 1996). By definition a unique stratal geometry must be demonstrably different from other stratal geometries and result from only one set of controlling processes with specific parameter values. Non-unique stratal geometries are not demonstrably different from one another, and can occur as a consequence of different parameter values of controlling processes, or simply from entirely different controlling processes. If several factors, not simply accommodation variations, can control formation of basin-margin stratal geometries, it seems likely that similar stratal geometries could result from different combinations of these controlling factors, suggesting that non-unique stratal geometries could be common in the stratigraphic record.

Previous numerical modelling work has suggested that non-unique stratal geometries exist and present a serious problem for sequence stratigraphy. For example, *Burton et al.* (1987) modelled similar stratal geometries from different combinations (their family of solutions) of parameter values for sedimentation and RSL. They suggested that true inversion of stratigraphic data is not possible due to lack of sufficient information to enable separation of effects of individual controlling processes. *Cross and Lessenger* (1999) took a more positive view and discussed some non-uniqueness issues resulting from an automated method for inversion of stratigraphic data. Non-uniqueness was also discussed by *Heller et al.* (1993), along with their proposal of a stratigraphic solution set to represent possible parameter explanations for any specific stratal geometry.

Studies have also addressed non-uniqueness with respect to specific stratal geometries. Using a numerical stratigraphic forward model *Flemings and Grotzinger* (1996) demonstrated that similar sequence bounding unconformities can be non-unique, due to generation either by time-variable accommodation or sediment supply. Experimental and theoretical studies have demonstrated that fluvial aggradation can occur during rising and steady RSL but also during RSL fall (e.g., *Burgess and Allen*, 1996, *Helland-Hansen and Martinsen*, 1996, *Johannessen and Steel*, 2005, *Martin et al.*, 2009, 2011, *Muto and Swenson*, 2005, 2006, *Muto et al.*, 2007, *Prince and Burgess*, 2013, *Rittenour et al.*, 2007, *Swenson and Muto*, 2005, 2007), suggesting that stratal geometries usually interpreted as normal regressive strata (or highstand) could be non-unique and also form during falling RSL (Chapter 4).

6.1.1 Aim of this chapter

This work applies the diffusional stratigraphic forward model Dionisos to investigate how non-unique stratal geometries can form. Previous examples of non-unique stratal geometries are explored, and a new example is demonstrated. In both of these cases the purpose is to further evaluate how non-uniqueness occurs and elucidate the consequences of various non-unique stratal geometries for sequence stratigraphic models and methods.

Four common types of stratal geometry are investigated, including (i) maximum transgressive surfaces, (ii) sequence boundaries, (iii) aggradational topset strata and (iv) shoreline trajectories. Modelled stratal geometries generated by different parameter values of controlling processes are compared using stratigraphic forward model cross sections, chronostratigraphic charts, synthetic well log correlations and shoreline trajectory plots. A metric based on proportions of topset and foreset strata (used in Chapter 4) is also applied to analyse the degree of topset aggradation in strata generated from 399 model runs.

6.2 Modelling methods

6.2.1 Dionisos model description

Dionisos is a three dimensional stratigraphic forward model that simulates basin-scale sediment transport on geological time-scales (*Granjeon and Joseph*, 1999). As described in Chapter 3, Dionisos simulates long-term sediment distribution by a gravity- and water-driven diffusion equation. Sediment transport is defined by the topographic slope, diffusion coefficient and water discharge (Chapter 3).

As well as simulating sediment transport on geological time scales using a finite difference solution of a modified classic diffusion equation, Dionisos also represents other processes essential for the generation of large scale basin margin stratal geometries. In this Chapter, accommodation variations are modelled by combining spatially and temporally variable total subsidence with eustatic sea-level curves to create both either simple of complex RSL histories. Sediment supply is either constant through model runs or variable through time. In 3D model runs sediment supply varies spatially.

TABLE 6.1: Dionisos default model parameters.

Parameter	***2D value***
Grid length (x-axis) (km)	500
Grid length (y-axis) (km)	40
Grid Point Spacing (km)	20
River discharge (km^3My^{-1})	6.31 x 10^{12}
Gravity weathering rate (m My^{-1})	1
Water weathering rate (m My^{-1})	100
Composition of sediment supply (sand, mud) (%)	20, 80
Gravity-driven terrestrial k sand (km^2ky^{-1})	4
Gravity-driven terrestrial k mud (km^2ky^{-1})	8
Gravity-driven marine k sand (km^2ky^{-1})	0.05
Gravity-driven marine k mud (km^2ky^{-1})	0.1

6.2.2 Model sets

Statal geometries in this work are investigated using both individual and multiple model runs, the former consisting of a low number of relatively complex 2D or 3D model runs and the latter involving several hundred simple 2D model runs. The model runs in this work are executed to investigate the consequences of particular parameter combinations of accommodation, sediment supply, and sediment transport rates. Some analysis presented required more model runs, and for these cases several hundred 2D model runs were executed and analysed quantitatively using a metric described previously in Chapter 4 (the t/f ratio). This allowed a particular aspect of the generated stratal geometries to be characterised. The model sets described in detail below are summarised in Table 6.2.

6.3 Non-unique maximum transgressive surfaces (MTS)

Cross sections and chronostratigraphic diagrams of two stratal geometries generated in Dionisos after 2 My of simulated time are shown in Figure 6.1. Model parameter values used to generate both stratal geometries are listed in Table 6.1. RSL and sediment

Table 6.2: Summary of the model runs.

Model name	***Stratal Geometry investigated***	***Number of model runs***	***Model run duration***	***Time-variable parameters***
SG1	MTS	1	2 My	RSL
SG2	MTS	1	2 My	Sediment supply
Model set 1	Topset aggradation	399	2 My	RSL, terrestrial k
SG3	Sequence boundary	1	3 My	RSL
SG4	Sequence boundary	1	3 My	RSL, terrestrial k
SG5	Progradational to retrogradational shoreline trajectory	1	3 My	RSL
SG6	Progradational to retrogradational shoreline trajectory	1	3 My	RSL, sediment supply
SG7	MTS	1	6 My	Sediment supply

supply parameter values differ for the two modeled stratal geometries. Correlated well sections (Figure 6.1c, g) from Stratal Geometry 1 (SG1) and SG2 are displayed for comparison.

6.3.1 Stratal Geometry 1: Accommodation-driven MTS

In Figure 6.1, SG1 was generated with constant sediment supply and a time-varying rate of RSL rise (Figure 6.1a). Rate of RSL rise increased at 0.9 My EMT from 100 m My^{-1} to 400 m My^{-1}. From 1 to 1.25 My EMT rate of RSL rise drops to 25 m My^{-1} before returning to the initial rate of 100 m My^{-1} (Figure 6.1a). Terrestrial and marine diffusion coefficients for mud and sand were constant through generation of SG1 and SG2 (Table 6.1).

The cross section (Figure 6.1d) and chronostratigraphic diagram (Figure 6.1b) show that after initial supply-driven progradation, the stratal stacking pattern in SG1 becomes aggradational at 0.5 My EMT. This short-lived aggradational phase represents a period when rates of sediment transport and sediment supply were sufficient to maintain aggradation, compared to the constant rate of accommodation creation. At 0.9 My

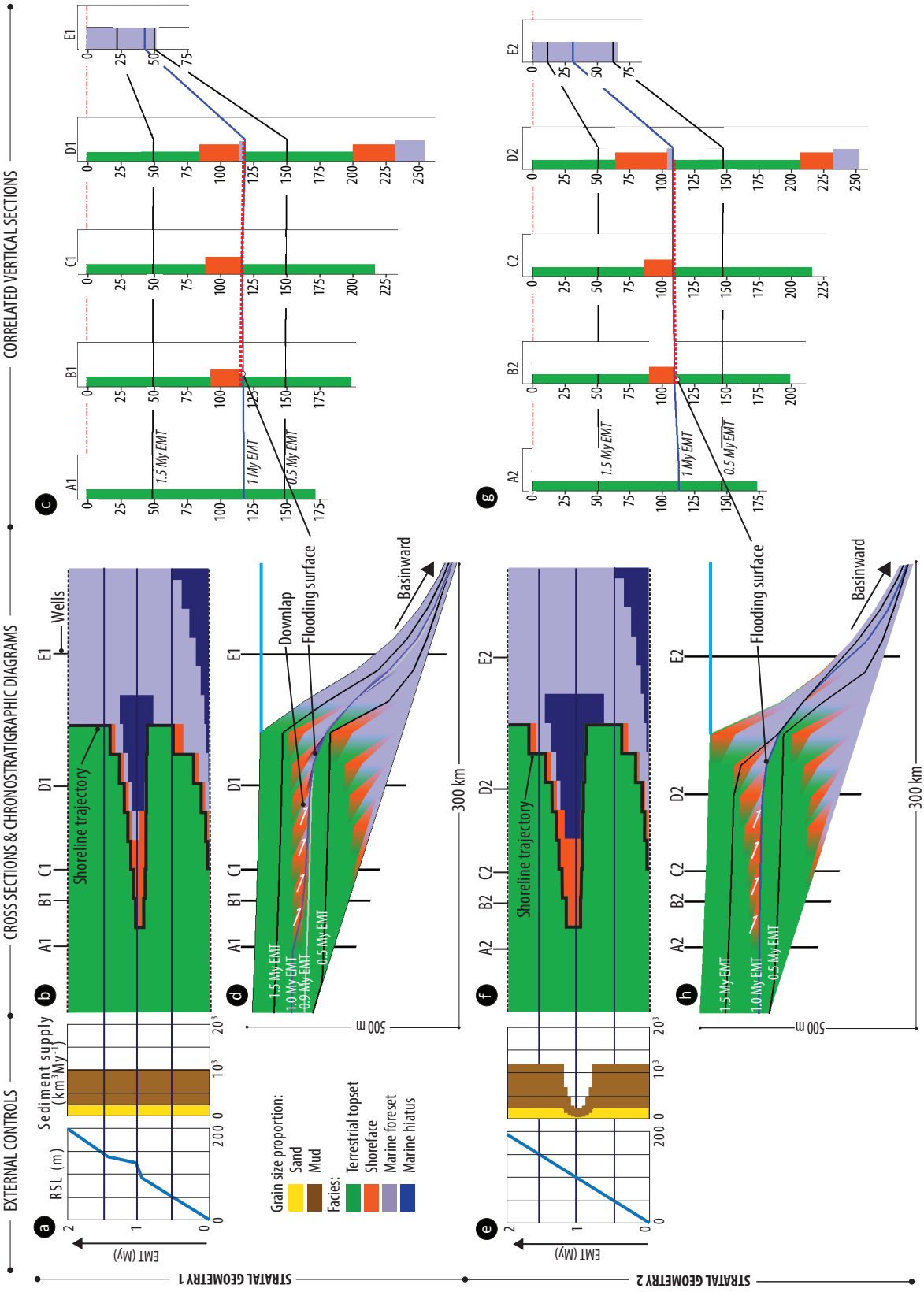
EXTERNAL CONTROLS
CROSS SECTIONS & CHRONOSTRATIGRAPHIC DIAGRAMS
CORRELATED VERTICAL SECTIONS
STRATAL GEOMETRY 1
STRATAL GEOMETRY 2
a
RSL (m)
Sediment supply (km³My⁻¹)
EMT (My)
b
Wells
Shoreline trajectory
c
1.5 My EMT
1 My EMT
0.5 My EMT
d
Downlap
Flooding surface
Basinward
1.5 My EMT
1.0 My EMT
0.9 My EMT
0.5 My EMT
500 m
300 km
Grain size proportion:
Sand
Mud
Facies:
Terrestrial topset
Shoreface
Marine foreset
Marine hiatus
e
f
g
h

FIGURE 6.1: (Previous page.) Stratal geometry 1 (SG1) and stratal geometry 2 (SG2) shown in cross section (d and h), as chronostrat digarams (b and f) and as correlated vertical sections (c and g), have similar MTSs despite being generated with different RSL and sediment supply curves (a and e).

EMT, rate of accommodation creation increases due to a faster rate of RSL rise (Figure 6.1a) and the stacking pattern becomes retrogradational. Figure 6.1d and d show that the retrogradational phase continues until 1 My EMT, at which time the shoreline has transgressed back to approximately 50 km. This transgression of the shoreline causes development of a transgressive surface (Figure 6.1d) and a switch from retrogradational to progradational stacking when rate of accommodation creation is reduced at 1 My EMT. The MTS generated in SG1 is similar to the conformable downlapped MTS described in sequence stratigraphic literature (*Catuneanu*, 2006, *Catuneanu et al.*, 2009, 2010, 2011). A high rate of progradation occurs after 1 My EMT in SG1 due to sedimentation outpacing the low rate of accommodation creation (25 m My^{-1}). By 1.5 My EMT the stacking pattern returns to aggradation due to an apparent equilibrium state between sediment transport rate, sediment supply and rate of accommodation creation.

6.3.2 Stratal Geometry 2: Supply-driven MTS

In contrast to SG1, SG2 was generated with a constant rate of RSL rise and a time varying rate of sediment supply. From 0.75 to 1 My EMT sediment supply drops from 1200 to 250 km^3 My^{-1}. At 1 My EMT sediment supply returns to 1200 km^3 My^{-1}. All other model parameters, such as marine and terrestrial diffusion coefficients, are the same as values used to generate SG1 (Table 6.1).

Despite generation with different accommodation and sediment supply histories to SG1, SG2 is significantly similar to SG1 (Figure 6.1d compared to Figure 6.1h). For example, as with SG1, after initial supply driven progradation the stacking pattern in SG2 becomes retrogradational. However, unlike shoreline transgression in SG1 which is driven by a change in the rate of accommodation, shoreline transgression in SG2 is driven by a reduction in rate of sediment supply during constant rate of RSL rise. The chronostratigraphic diagram (Figure 6.1f) shows that the shoreline reaches maximum landward extent at approximately 50 km at 1 My EMT, after which retrogradation changes to supply-driven progradation due to an increase in sediment supply rate during constant

rate of RSL rise. A MTS is generated in SG2 at 1 My EMT because of a reduction in rate of sediment supply during steady RSL rise. This MTS is preserved and downlapped by strata formed due to an increase in sediment supply rate during steady accommodation creation.

6.3.3 Comparison of Stratal Geometries 1 & 2

MTSs generated in SG1 and SG2 exhibit several diagnostic characteristics identical to the MTS described in the various sequence stratigraphic depositional models (e.g., *Catuneanu*, 2006). For example, in both SG1 and SG2, the stacking pattern below and above the MTS is retrogradational and progradational, respectively. In both modeled cases (Figure 6.1) the MTS is downlapped by the overlying progradational strata. Wells intersecting the MTS observed in SG1 and SG2 (Figure 6.1c, B1 to D1, and Figure 6.1h B2 to D2) display a sharp facies transition from fluvial to shallow marine strata. Finally, the MTS in SG1 and SG2 is conformable except for a marine hiatus on the outer shelf, which together are indicative of a rapid increase in rate of accommodation creation. However, all these characteristics were generated by two different controlling processes (Figure 6.1a, e). This demonstrates that a MTS can be a non-unique stratal geometry, generated by either changes in rate of accommodation during steady sediment supply, or by changes in the rate of sediment supply during a steady increase in accommodation. An important consequence of non-unique MTSs is how the correlation properties in the different non-unique cases generated and described above might contrast.

6.4 Non-unique sequence bounding unconformities

An integral element of sequence models is that subaerial erosion surfaces form during RSL fall, which are assumed to occur due to fluvial incision of the exposed continental shelf (*Catuneanu*, 2006, *Catuneanu et al.*, 2009, *Posamentier and Morris*, 2000, *Posamentier et al.*, 1988, 1992). However, some field based studies and recent numerical and analogue work has investigated this element of the sequence models and suggest that the traditional assumption may be an oversimplification (*Best and Ashworth*, 1997, *Martin et al.*, 2011, *Schumm*, 1993, *Strong and Paola*, 2008, *Woolfe et al.*, 1998).

To investigate how sequence bounding unconformities generated by fluvial incision may be non-unique due to formation during different RSL histories and sediment transport rates, two stratal geometries SG3 and SG4 are presented. Cross sections and chronostratigraphic diagrams from two different stratal geometries (SG3 and SG4) generated in Dionisos after 3 My of simulated time are shown in Figure 6.2. Parameter values of controlling processes (RSL, sediment supply, terrestrial diffusion coefficients) (Figure 6.2a, e) and well logs shown with time lines (Figure 6.2c, g) taken from the SFM cross sections are illustrated. Additional model parameters identical across both models are listed in Table 6.1. Both models were run for an initial 1 My EMT with constant sediment supply and steady RSL, but different terrestrial diffusion coefficients (Figure 6.2a, e), during which time they generated similar overall unforced regressive stratal geometries (grey shaded area, Figure 6.2d, h). After 1 My EMT, SG3 was generated with a 50 m My^{-1} fall for 1 My followed by a 50 m My^{-1} rise for 1 My, with terrestrial diffusion coefficients of 100 km^2ky^{-1} for sand and 200 km^2ky^{-1} for mud (Figure 6.2a). In contrast, SG4 was generated with steady RSL for 1 My followed by a 50 m My^{-1} rise for 1 My, with higher rates of terrestrial diffusion coefficient of 200 km^2ky^{-1} for sand and 400 km^2ky^{-1} for mud. Formation of SG3 and SG4 between 1 and 3 My EMT, are described below.

6.4.1 Stratal Geometry 3: Accommodation controlled SBs

The chronostratigraphic diagram (Figure 6.7b) and SFM cross section (Figure 6.7d) show the development and final stratal geometry of a sequence boundary. This sequence boundary is analogous to sequence bounding unconformity described in sequence stratigraphic models and interpreted from subsurface and outcrop data (e.g., *Catuneanu et al.*, 2009). RSL fall from 1 to 2 My EMT (Figure 6.7a) results in subaerial exposure of the previously deposited topset region. The sequence boundary (subaerial unconformity surface) develops due to non-deposition, erosion and sediment bypass (Figure 6.7b), extending basinward during falling RSL and reaches its maximum extent at the end of RSL fall at 2 My EMT (Figure 6.7a, b). Correlated well sections show that between 1 and 2 My EMT sediment is deposited into the marine environment reflecting sediment shelf-bypass and deposition into deep-water deposystems. At 2 My EMT RSL rises and topset strata are deposited, preserving the sequence boundary formed between 1 and 2 My EMT (Figure 6.7a, b, c).

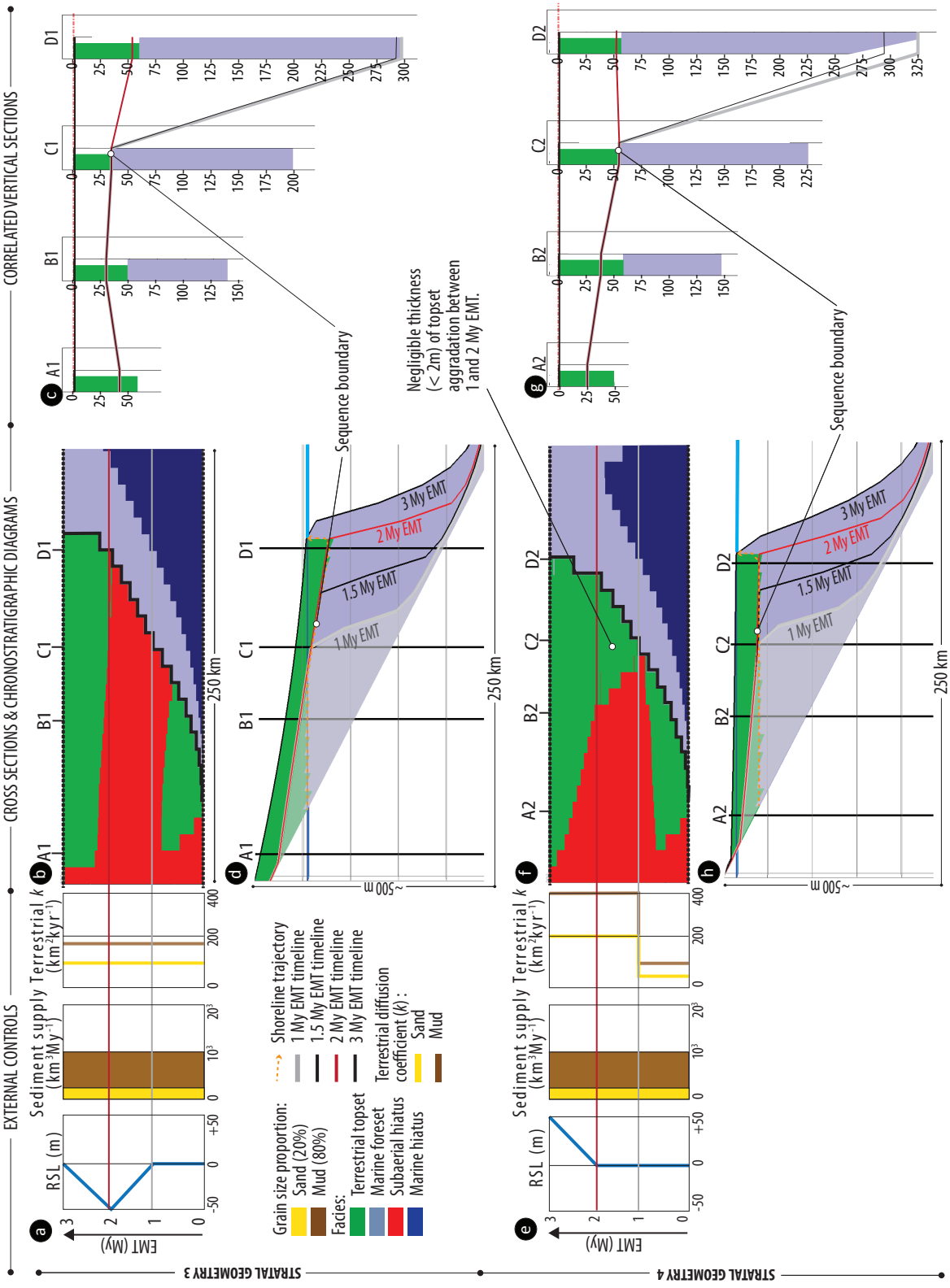
EXTERNAL CONTROLS
CROSS SECTIONS & CHRONOSTRATIGRAPHIC DIAGRAMS
CORRELATED VERTICAL SECTIONS
STRATAL GEOMETRY 3
STRATAL GEOMETRY 4
EMT (My)
RSL (m)
Sediment supply (km³My⁻¹)
Terrestrial k (km²kyr⁻¹)
Grain size proportion:
Sand (20%)
Mud (80%)
Facies:
Terrestrial topset
Marine foreset
Subaerial hiatus
Marine hiatus
Shoreline trajectory
1 My EMT timeline
1.5 My EMT timeline
2 My EMT timeline
3 My EMT timeline
Terrestrial diffusion coefficient (k):
Sand
Mud
Sequence boundary
Negligible thickness (< 2m) of topset aggradation between 1 and 2 My EMT.
3 My EMT
2 My EMT
1.5 My EMT
1 My EMT
250 km
~500 m
A1
B1
C1
D1
A2
B2
C2
D2

FIGURE 6.2: (Previous page.) Stratal Geometry 3 (SG3) and Stratal Geometry 4 (SG4) have similar sequence boundaries shown in cross section (d and h), in chronostratigraphic diagrams (b and f) and as correlated vertical sections (c and g) despite being generated with different parameter values for RSL and sediment transport rates (a and e). Note that differences in the most distal part of the sequence bounding unconformity between the two cases are more significant in time than in thickness; approximately 1 My of EMT in SG4 (f) is represented by only 2 m of preserved sediment thickness (h and g) meaning that SG3 and SG4 are very similar in both cross section (b and h) and in vertical sections (c and g). Accommodation history is shown by RSL curves (a and e).

6.4.2 Stratal Geometry 4: Sediment transport rate controlled SBs

In contrast to SG3, formation of SG4 sequence boundary is not driven by RSL fall, instead SG4 is driven by high sediment transport rates by higher terrestrial diffusion coefficients (Figure 6.2e, h). Increased terrestrial diffusion coefficients for sand and mud at 1 My EMT reflect higher sediment transport rates in the terrestrial topset environment, for example reflecting an increase in the size of the river system with greater water discharge rate. As a result, the topography is eroded and bypassed and a subaerial unconformity develops during steady RSL. The chronostratigraphic diagram (Figure 6.2f) shows that a subaerial hiatus initially extends across the entire topset to the shoreline. In contrast to the sequence boundary in SG3, topset aggradation across the outer topset region between approximately 1.1 and 2 My EMT. However, the cross-section and well C2 indicate that this aggradation was low, at less than 2 m (stacked timelines 1 to 2 My EMT in well C2, Figure 6.2), and the majority of sediment bypasses the topset region between 1 and 2 My EMT. As with SG3, fluvial aggradation during a rise in RSL at 2 My EMT buries the SG4 unconformity surface.

6.4.3 Summary of Stratal Geometries 3 & 4

Model cross sections, chronostratigraphic charts and wells in Figure 6.2 demonstrate how increased sediment transport rates in the terrestrial topset environment could lead to sediment bypass and erosion even during steady RSL (Figure 6.2 SG4). SG3 and SG4 display similar stratal geometries with sequence boundaries, which in both cases are indicated by an unconformable surface, truncating strata below and onlapped by strata above, and a shallowing up of facies. Without independent information on RSL history and sediment transport rate, the only feature that serves to tell apart these two stratal

geometries is the shoreline trajectory. In SG3 the shoreline trajectory between 1 and 2 My EMT is descending regressive, due to falling RSL. In contrast, for the same interval in SG4 the shoreline trajectory is horizontal, indicating steady RSL. However, it would not be straightforward to distinguish these two shoreline trajectories in ancient strata that have undergone differential compaction (Chapter 4, 5) or where a reliable regional paleohorizontal datum is difficult to define (*Helland-Hansen and Hampson*, 2009).

6.5 Non-unique topset aggradation

Chapter 4 investigated topset aggradation during RSL fall through a multiple modelling approach. Figure 6.3 shows results from a similar set of experiments. As with Chapter 4, a topset/foreset ratio (t/f ratio) summarises the proportion of topset strata relative to foreset strata deposited in individual model runs (when no topset strata is present the t/f ratio is 0, presence of topset strata = t/f ratio > 0). The t/f ratios calculated from 399 different model runs are displayed in a parameter space plot (Figure 6.3a). The 399 model runs in Model Set 1 cover a range of amplitudes of RSL fall from 0 to 100 m and a range of amplitudes of RSL rise from 10 to 100 m (10 m increments). For each of these RSL cases a range of terrestrial diffusion coefficients for sand and mud from 20 to 200 km^2kyr^{-1} and 40 to 400 km^2kyr^{-1}, respectively, are also tested. Amplitudes and the durations of RSL fall and rise in this work cover a range similar to recent Phanerozoic eustatic curves (*Miller et al.*, 2005) and the terrestrial diffusion coefficients span a range of values representative of small- to medium-sized delta systems (*Kenyon and Turcotte*, 1985). Additional model parameters, such as sediment supply and river discharge rate, are listed in Table 6.1. Selected SFM cross sections from model runs in Model Set 1 are shown in Figure 6.3b, with their t/f ratio and parameter values detailed.

Figure 6.3 shows that from the range of terrestrial diffusion coefficient and amplitudes of RSL fall and rise tested, proportions of topset strata are highest in model runs with low values of terrestrial diffusion coefficient and high amplitudes of RSL rise. This is reflected by model profile 1 (Figure 6.3b) which has the highest t/f ratio of all 399 model runs after generation with RSL rise of 100 m and a terrestrial diffusion coefficient of 20 km^2kyr^{-1} for sand.

a
b
Relative sea-level amplitude (m)
Unforced regression
Forced regression
100
75
50
25
0
-25
-50
-75
-100
Terrestrial diffusion coefficient (k) for sand (km²ky⁻¹)
Increasing sediment transport rate
20
40
60
80
100
120
140
160
180
200
t/f = > 0
Topset aggradational regime
t/f = 0
Topset degradational regime
Fluvial grade line
1
2a
2b
3a
3b
3c
3d
4a
4b
4c
4d
T/F RATIO
0.89
0.67
0.45
0.23
0
Increasing volume of topset strata
800 km
800 m
Shoreline trajectory
Terrestrial topset strata
Marine foreset strata
Final RSL position
Terrestrial diffusion coefficient
Topset/foreset ratio
Relative sea-level amplitude
k
t/f
RSL
t/f = 0.89
k = 20
RSL = +100
t/f = 0.68
k = 20
RSL= +50
t/f = 0.32
k = 20
RSL= -70
t/f = 0.32
k = 110
RSL = +50
t/f = 0.14
k = 30
RSL = -80
t/f = 0.14
k = 90
RSL = 0
t/f = 0.68
k = 60
RSL = +100
t/f = 0.32
k = 40
RSL = +10
t/f = 0.32
k = 200
RSL = +60
t/f = 0.14
k = 70
RSL = -10
t/f = 0.14
k = 180
RSL = +20

FIGURE 6.3: (Previous page.) (a) Nearly 400 models from Model Set 1 plotted as colour-coded values of the t/f ratio in a sediment transport rate and RSL amplitude parameter space plot. High t/f ratios represent models with topset strata approaching the same volume as foreset strata. Low to zero t/f ratio occurs for higher rates of sediment transport or for high amplitudes of RSL fall. The fluvial grade line indicates the points in the parameter space where models develop fluvial profiles that are at grade, with neither accumulation or erosion of strata, just bypass of all sediment to the shoreline (b) Cross sections from a subset of model runs are shown with shoreline trajectory, t/f ratio, terrestrial diffusion coefficient value (k) and RSL amplitude labelled. The position of each cross section is labelled on the parameter space plot in (a). Note that cross sections with the same number label are considered non-unique sets with similar geometries yet generated by different RSL and terrestrial diffusion coefficient parameter values.

Together the parameter space plot and selected profiles illustrate that the same volume of topset strata can occur in model runs that are generated with different parameter values Figure (6.3a, b). For example, profiles 4a to 4d all have t/f ratios of 0.14 despite being generated with different RSL histories. Profile 4d was generated with a 20 m RSL rise, but profile 4a was generated with an 80 m RSL fall. As with stratal geometries described from the previous model sets, results in Model Set 1 suggest that topset aggradation is also an example of a non-unique stratal geometry. Similar examples of non-uniqueness can be seen across the rest of the parameter space plot (e.g., positions 3a to 3d, Figure 6.3).

If topset aggradation is a non-unique stratal geometry, occurring during falling RSL as well as during steady to rising RSL, then this has important implications for how we interpret topset aggradation in ancient strata. For example, presence of topset aggradation is generally taken to be indicative of highstand systems tract, whereas absence of topset aggradation indicates falling-stage. However, if topset aggradation is non-unique as described above then it would not a reliable indicator for distinguishing between these two systems tracts. As with the sequence boundaries discussed SG3 and SG4, only the shoreline trajectories remain to distinguish between the stratal geometries created with different RSL histories (Figure 6.3b).

6.6 Non-unique shoreline trajectories

The method of shoreline trajectory analysis has an advantage over other elements of sequence stratigraphy because, generally, the method is more directly based on observation and requires fewer *apriori* assumptions in its application. However, some of the

examples presented above suggest that non-uniqueness may also be an issue for reliable analysis of shoreline trajectories. To explore this issue four similar shoreline trajectories (SG1, SG2, SG5 and SG6) are generated in Dionisos with different RSL and sediment supply histories.

Figure 6.4 and 6.5 show cross sections and shoreline trajectory plots from four different stratal geometries generated in Dionisos. The RSL curve, sediment supply history and marine diffusion coefficients specified to generate SG1, SG2, SG5 and SG6 (Figure 6.4 and 6.5) are illustrated along with calculated shoreline trajectories plotted as chronostratigraphic shoreline charts (Figure 6.4a and 6.5b) and simple shoreline position plots (Figure 6.4d and 6.5c). SG5 and SG6 result from 3 My duration model runs (Figure 6.4), whereas SG1 and SG2 result from 2 My duration model runs discussed previously (Figure 6.1). Shoreline trajectories generated from model runs of the same duration are compared below.

6.6.1 Non-unique shoreline trajectories from SG5 & SG6

SG5 was generated with a constant rate of sediment supply and a time-varying rate of rising RSL (Figure 6.4 a). From 0 to 2 My EMT, RSL rises at a rate of 50 m My^{-1}. From 2 to 3 My EMT rate of RSL rise is 100 m My^{-1}. Initial progradation resulting from steady RSL rise (50 m My^{-1}) and constant sediment supply is reflected by an ascending regressive trajectory trend for the first 1 My of simulated time (Figure 6.4c, e). During this initial 1 My EMT the shoreline trajectory steepens, reflecting a reduction in progradation rate and a switch from progradational to aggradational stacking. At 1.5 My EMT the shoreline transgresses due to delta autoretreat (*Muto and Steel*, 1992, 1997).

Autoretreat has occurred in this model run because, as the delta prograded into deeper water the effective area of the deltas foreset increased, such that the constant rate of sediment supply (Figure 6.4a) was not sufficient to maintain slope accretion (*Muto and Steel*, 1992). When rate of RSL rise is doubled to 100 m My^{-1} at 2 My EMT, retrogradational stacking is encouraged and hence a transgressive shoreline trajectory trend is generated.

Comparing the shoreline trajectory calculated from SG5 with the shoreline trajectory calculated from SG6 is interesting because, despite different accommodation and supply histories (Figure 6.4a), the shoreline trajectories look similar. For the first 1 My EMT, the shoreline trajectory in SG6 shows an ascending regressive trend much like the trajectory calculated from SG5. However, for the first 1 My EMT, SG6 was generated with a higher and more complex history of sediment supply during a rate of rising RSL double that of SG5. This demonstrates that different rates of RSL rise can lead to very similar shoreline trajectories. Shoreline trajectory from SG6 also looks similar to SG5 after 1 My EMT; from 1 to 3 My EMT SG6 shoreline trajectory shows an aggradational to accretionary transgressive trajectory trend. In contrast to SG5 shoreline trajectory, this transgressive trajectory trend was generated with a slower rate of RSL rise and a lower volume of sediment supply.

There are also some important differences to observe from the two shoreline trajectories. Unlike the SG5 transgression described above which is initiated by delta autoretreat, shoreline transgression in SG6 is driven by a reduction in sediment supply during rising RSL. Without independent knowledge of sediment supply and RSL history, it would be difficult to tell these different shoreline trajectories apart.

The shoreline trajectories calculated from SG5 and SG6 demonstrate how different sediment supply and RSL histories can lead to shoreline trajectories that look the same. The results suggest that inferring reliable accommodation and sediment supply history from simple shoreline trajectories interpreted in the ancient record could be difficult. An important consideration is if more complex shoreline trajectories, for example displaying repeated regressive or trangressive transits, can still look similar when generated by different sediment supply and accommodation histories.

6.6.2 Non-unique shoreline trajectories from SG1 & SG2

Shoreline trajectories SG1 and SG2 shown in Figure 6.5, display closely matching regressive and transgressive transits and similar overall geometries. However, these two geometrically similar shoreline trajectories were generated by quite different sediment supply rates and different rates of RSL rise (Figure 6.5).

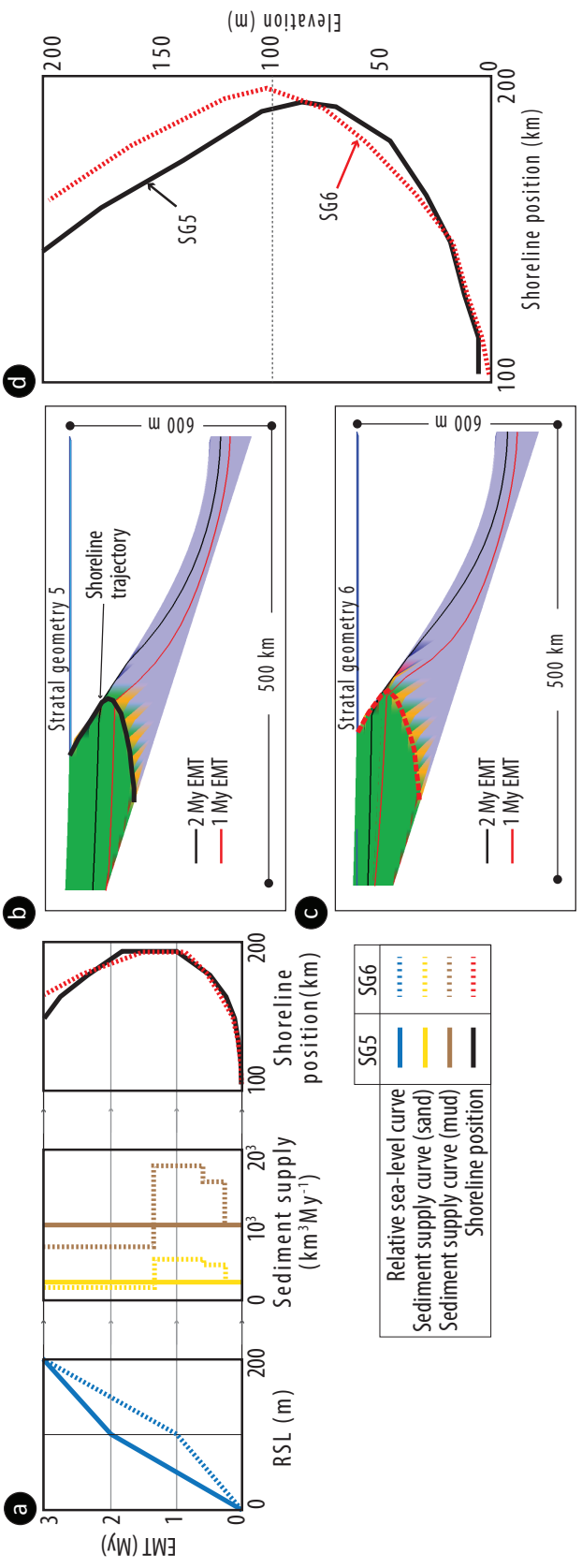

FIGURE 6.4: Stratal Geometry 5 (SG5) and Stratal Geometry 6 (SG6) have similar shoreline trajectories (b, c and d) generated with different RSL and sediment supply histories (a).

Stratal geometry 1 was generated with constant sediment supply and a variable rate of RSL rise (Figure 6.5a). Transgression of the shoreline at 0.9 My EMT was driven by an increase in rate of RSL rise from an initial 100 m My^{-1} to 400 m My^{-1}. As a result the shoreline trajectory trend is accretionary transgressive (*Helland-Hansen and Hampson*, 2009). At 1 My EMT the shoreline trajectory switches to an ascending regressive trend due to a reduction in rate of RSL rise to 25 m My^{-1} during constant sediment supply. Progradation is initially fast due to low rate of RSL rise (Figure 6.5) and sufficient sediment supply, until 1.4 My EMT when rate of RSL rise increased to 100 m My^{-1} and the shoreline trajectory becomes predominantly aggradational.

In contrast to the shoreline trajectory calculated from SG1, the shoreline trajectory calculated from SG2 was generated with constant rate of RSL rise and variable rate of sediment supply volume. As with the shoreline trajectory from SG1 described above, after initial supply-driven progradation (normal regression), the shoreline transgresses at 0.8 My EMT. Critically, the transgression in SG2 is driven by a reduction in sediment supply volume during constant rate of RSL rise, as apposed to the accommodation-driven transgression described for SG1. The transgression in SG2 leads to a shoreline trajectory closely matching the shoreline trajectory in SG1 (Figure 6.5). After transgression of the shoreline, progradation is driven by a rapid increase in sediment supply, again creating a very similar shoreline trajectory to SG2 but due to different parameter values.

The shoreline trajectories calculated from SG1 and SG2 demonstrate that extremely similar, complex shoreline trajectories can be produced by disparate RSL and sediment supply histories. If these modeled stratal geometries are reasonable reconstructions of stratal geometries interpreted in the sedimentary record then the results suggest that shoreline trajectories recognised in subsurface or outcrop data could be non-unique. If shoreline trajectories can be non-unique than this has important implications for how we interpret these types of stratal geometries.

6.7 Discussion

Non-unique stratal geometries look extremely similar, but can form from distinctly different parameter values of controlling processes (e.g., different RSL histories). Unique stratal geometries are distinguishable from other stratal geometries and result from

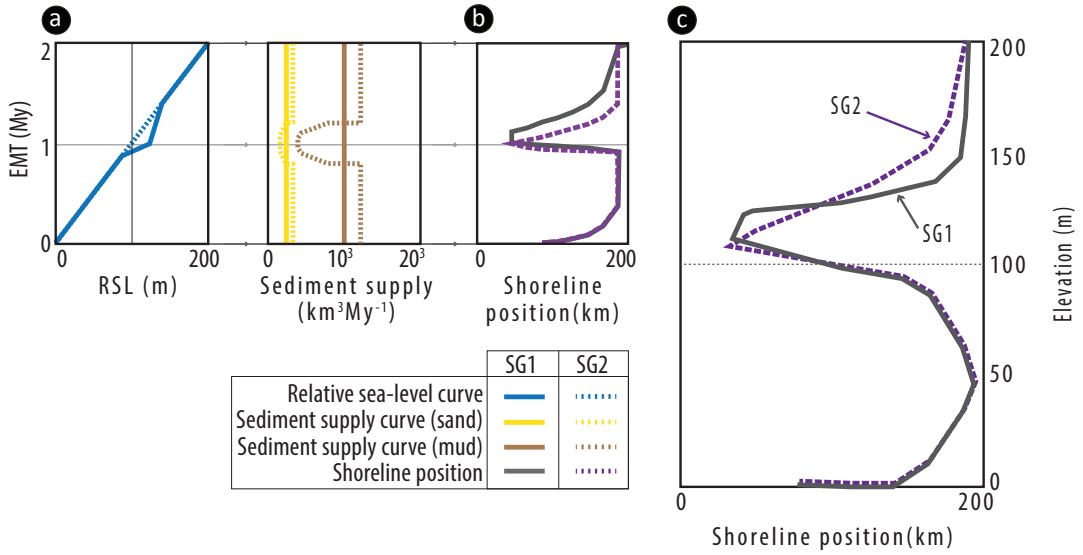

FIGURE 6.5: RSL and sediment supply curves (a) for SG1 and SG2 that generate similar shoreline trajectories in time (b) and in elevation (c).

one set of parameter values of controlling processes. Non-unique stratal geometries are difficult to tell apart despite formation as a result of different parameter values of controlling process, or different process entirely. In this work a numerical stratigraphic forward model has been used to investigate how four types of stratal geometry could be non-unique due to generation of similar stratal geometries with different parameter values.

6.7.1 How realistic are the stratal geometries generated in this work?

Realism of stratal geometries generated in this work derives from the assumptions and limitations of the stratigraphic forward model, as well as parameter values applied. Dionisos ability to reproduce accurate and meaningful stratal geometries has been discussed in Chapter 4 and much of the points raised in that chapter apply here, too. Some important points regarding the realism of Dionisos are summarised here.

Dionisos uses a modified diffusion equation of sediment transport to represent sediment transport processes that contribute to formation of stratal geometries in basin-margin settings. A key question is whether this representation is realistic. Diffusional models have been shown to accurately reproduce basin topography (*Flemings and Jordan*, 1989), and have lead to similar predictions as made by conventional geological models

(e.g., *Sinclair et al.*, 1991. Though these cases support the plausibility of diffusional models generally, they do not illustrate an example where a diffusional model has been tested with respect to the realism of the model results. This is because the model predictions in the above mentioned examples are not compared with data independent from that used to define the model parameters. In contrast, *Paola et al.* (1999) tested a diffusional model (*Parker et al.*, 1998) on a fluvial fan in a mine-tailings basin with known input parameters. The depositional profile developed in the mine-tailings basin could be closely matched by a calculated profile from a diffusional solution (*Paola et al.*, 1999), showing that for this example diffusion could be used to predict basinal topography given independently constrain input parameters. The different studies described above suggest that diffusional models are a relatively reliable method for reproducing stratal geometries. However, it is important to emphasise the point that any model is only as good as its assumptions. For this work, the major assumption is that the model reliably represents a limited set of sediment transport processes at a particular spatial and temporal scale.

As discussed in Chapter 4, parameter values applied in any model experiments should be considered in respect to real-world systems. Parameter values and model grid sizes used in this work are similar to those described in Chapter 4, which represent values of a typical medium-sized river system similar to, for example, the Rhone and Ebro rivers (*Burgess and Hovius*, 1998, *Kenyon and Turcotte*, 1985, *Marion et al.*, 2010).

6.7.2 Non-uniqueness of modeled stratal geometries in this work

The four stratal geometry examples modelled in this work, including the MTS, sequence bounding unconformity, topset aggradation and shoreline trajectory, are examples of non-uniqueness because for each example similar stratal geometries have been generated by more than one set of parameter values. In SG1 and SG2 similar MTSs were generated by an increase in the rate of accommodation creation during constant sediment supply (SG1) but also due to a shut-down in sediment supply during a constant rate of accommodation creation (SG2). Similar sequence bounding unconformities were generated by a fall in RSL with a mid case rate of terrestrial sediment transport (SG3) but also by a high case rate of terrestrial sediment transport (*Kenyon and Turcotte*, 1985) during steady RSL (SG4). Several hundred model runs demonstrated that topset

aggradation can be non-unique in the sense that, for different rates of terrestrial sediment transport, the same volume of topset aggradation can occur in strata generated by falling, steady and rising RSL (Model Set 1). Finally, geometrically similar pairs of shoreline trajectories were generated in the numerical model with distinctly different accommodation and sediment supply histories (SG5 compared to SG6, and SG1 compared to SG2). These four examples of non-uniqueness have important implications for sequence stratigraphy.

6.7.3 Implications of along-strike sediment supply variations for MTS correlation

Correlation of stratal geometries that represent changes in depositional environment is a primary application of sequence stratigraphy. Depending on suspected timing and mode of formation, different stratal geometries serve as stratigraphic markers for correlation. In this sense MTSs are important because they are suspected to form uniquely as a result of an increase in rate of accommodation creation, which is likely to be a regional event. However, results presented above show how MTSs are not unique, because they can also form due to reductions in sediment supply during a constant increase in accommodation. The modelled stratal geometries discussed above also illustrate that MTSs formed by these different mechanism (accommodation driven or supply driven) would be difficult to tell apart in the ancient record because they look similar. This non-uniqueness is a major problem for correlation because MTSs formed by reductions in sediment supply are unlikely to be contemporaneous. To illustrate this correlation issue Figure 6.6 shows how MTSs can form at different times within a basin due to local variations in sediment supply during steady RSL rise (Figure 6.6a).

Previous work has mentioned that along strike variability of sediment supply can cause an MTS to be diachronous (*Catuneanu et al.*, 2009). However, the implications of variable sediment supply through time and consequent non-uniqueness is more serious than diachronous surfaces (*Martinsen and Helland-Hansen*, 1995, *Wehr*, 1993). The problem arises because MTSs formed by reductions in sediment supply (e.g., SG2 in Figure 6.1) may be indistinguishable in form from and therefore correlated with accommodation-driven MTSs (e.g., SG1 in Figure 6.1), despite the fact that they are unlikely to be contemporaneous. To illustrate this correlation SG7 in Figure 6.6 shows how MTSs can

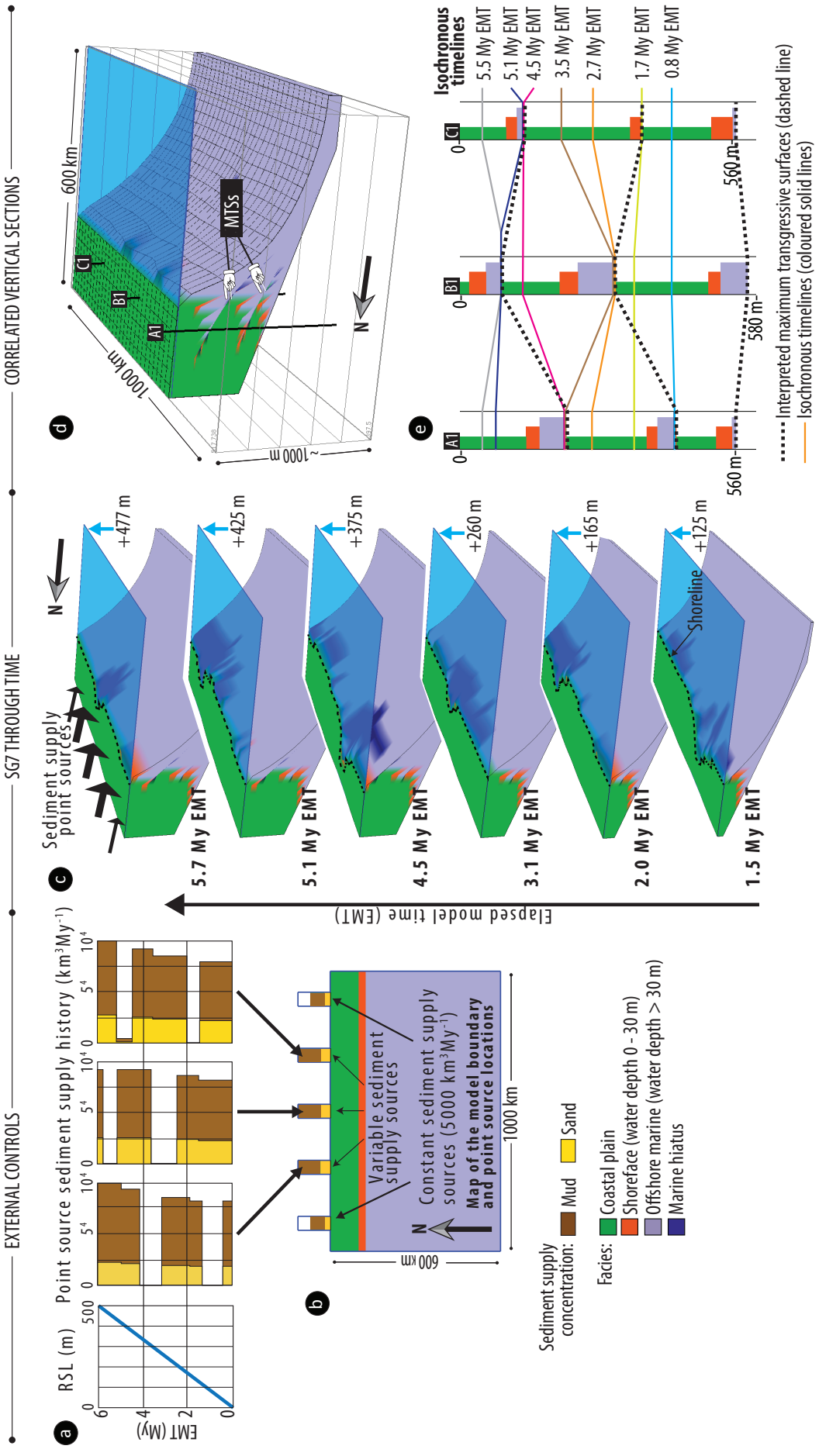
EXTERNAL CONTROLS
SG7 THROUGH TIME
CORRELATED VERTICAL SECTIONS
a
RSL (m)
Point source sediment supply history (km³My⁻¹)
EMT (My)
b
Variable sediment supply sources
Constant sediment supply sources (5000 km³My⁻¹)
Map of the model boundary and point source locations
600 km
1000 km
Sediment supply concentration:
Mud
Sand
Facies:
Coastal plain
Shoreface (water depth 0 - 30 m)
Offshore marine (water depth > 30 m)
Marine hiatus
c
Sediment supply point sources
N
+477 m
+425 m
+375 m
+260 m
+165 m
+125 m
Shoreline
5.7 My EMT
5.1 My EMT
4.5 My EMT
3.1 My EMT
2.0 My EMT
1.5 My EMT
Elapsed model time (EMT)
d
600 km
1000 km
~1000 m
C1
B1
A1
MTSs
N
e
Isochronous timelines
5.5 My EMT
5.1 My EMT
4.5 My EMT
3.5 My EMT
2.7 My EMT
1.7 My EMT
0.8 My EMT
560 m
580 m
560 m
Interpreted maximum transgressive surfaces (dashed line)
Isochronous timelines (coloured solid lines)

FIGURE 6.6: (Previous page.) Selected input parameters and output from the 3D SG7 model run showing how variable sediment supply histories (a) at multiple point sources (b, d) lead to strongly diachronous maximum transgressive surfaces that can be mistaken for a single correlative chronostratigraphic surface (e). The model run has constant rising RSL (c) but sediment supply varies through time (a) and each sediment input point has a different sediment supply history (b).

form at various times along a basin margin as a result of local variations in sediment supply (*Martinsen and Helland-Hansen*, 1995) (Figure 6.6a, b, c, d) during a steady RSL rise (Figure 6.6a). MTSs form at various times along this basin margin due to shut-downs of sediment supply sources. Wells from positions A1 to C1 in Figure 6.6d each show three MTSs that could be correlated. If an interpretor assumed that these surfaces are the result of regional changes in accommodation creation, the correlation would be considered chronostratigraphically significant because surfaces are assumed to be isochronous. This scenario is represented in the correlation panel, by black dashed lines in Figure 6.6e. The correlation panel also illustrates the actual position of the time lines in the model (coloured lines in Figure 6.6e), and comparison of these time lines with the possible MTS correlation shows that the correlation lines are diachronous by up to 1.9 My. This mis-correlation could be greater. For any case where MTSs are correlated based on the sequence stratigraphic approach of assuming a dominant control of MTSs by regional variations in accommodation, this kind of mis-correlation demonstrated in Figure 6.6 could occur unless accommodation-driven and supply-driven MTSs can be reliably distinguished.

6.7.4 Complications of non-unique sequence boundaries for sand bypass predictions

Predicting siliciclastic sediment partitioning in the different depositional environments, from coastal plain to deep marine, is a fundamental purpose of sequence stratigraphic models. For example, sequence models predict that sand deposition to deepwater deposystems occurs during RSL lowstands, when rivers bypass the topset area and deliver sediment to shelf-edge deltas, from where it can be routed to deep marine environments (*Catuneanu*, 2006). Related to this prediction is the assumption that rivers aggrade during RSL rise and degrade during RSL fall, leading to deposition of topset strata in the former case and the development of a subaerial unconformity in the latter. Hence, development of sequence bounding unconformities is associated with sand bypass (*Catuneanu*

et al., 2009). However, this model prediction has been shown to be an oversimplification because significant of sand bypass can occur at any position on a RSL curve (e.g., *Burgess and Hovius*, 1998, *Carvajal et al.*, 2009, *Carvajal and Steel*, 2006, *Covault and Graham*, 2010, *Helland-Hansen and Gjelberg*, 1994). Given this, it is interesting to consider the sand partitioning of the two non-unique SBs in Figure 6.2, which were generated with different RSL histories. For example, if sequence boundaries are non-unique, forming during steady or rising RSL as described above, then similar styles and volumes of sand bypass could occur for different reasons, for example climate versus accommodation driven. Alternatively, sequence boundaries formed by different mechanisms could lead to styles of sediment bypass with important differences.

To investigate the sand partitioning implications from the two non-unique SBs (Figure 6.2), Figure 6.7 illustrates percent sand distribution for SG3 and SG4. SG3 and SG4 are composed of 20% sand and 80% mud, the sand fraction is partitioned according to the diffusion coefficients used in the model runs to calculate sediment transport rates. Interestingly, comparison of the sand from SG3 and SG4 in cross section and vertical well sections shows that sand paritioning for the two non-unique shoreline trajectories is similar. For example, during formation of the unconformity surfaces due to either RSL fall (SG3) or steady RSL with higher sediment transport rates (SG4), the majority of the sand is restricted to the upper delta foresets with limited volumes reaching the deep-water toesets (Figure 6.7g). During subsequent RSL rise in both modelled stratal geometries SG3 and SG4, the majority of sand is restricted to the proximal delta topsets. This similar sand distribution is interesting because it shows how the non-uniqueness of SBs described above could extend to sand partitioning, suggesting that sequence boundaries formed by RSL fall and by an increase in sediment transport rates during steady RSL could have similar implications for sand bypass.

Identification of shoreline trajectory trends may help to distinguish between sequence boundaries formed during steady and falling RSL. Sequence boundaries formed during steady RSL would display a horizontal trajectory trend, sequence boundaries formed during falling RSL would display a descending trend. However, because original geometries of shoreline trajectories are likely to be modified by ubiquitous process during burial, for example rotation due to differential compaction (Chapter 4), distinguishing between these different sequence boundaries using the trajectory concept may be problematic.

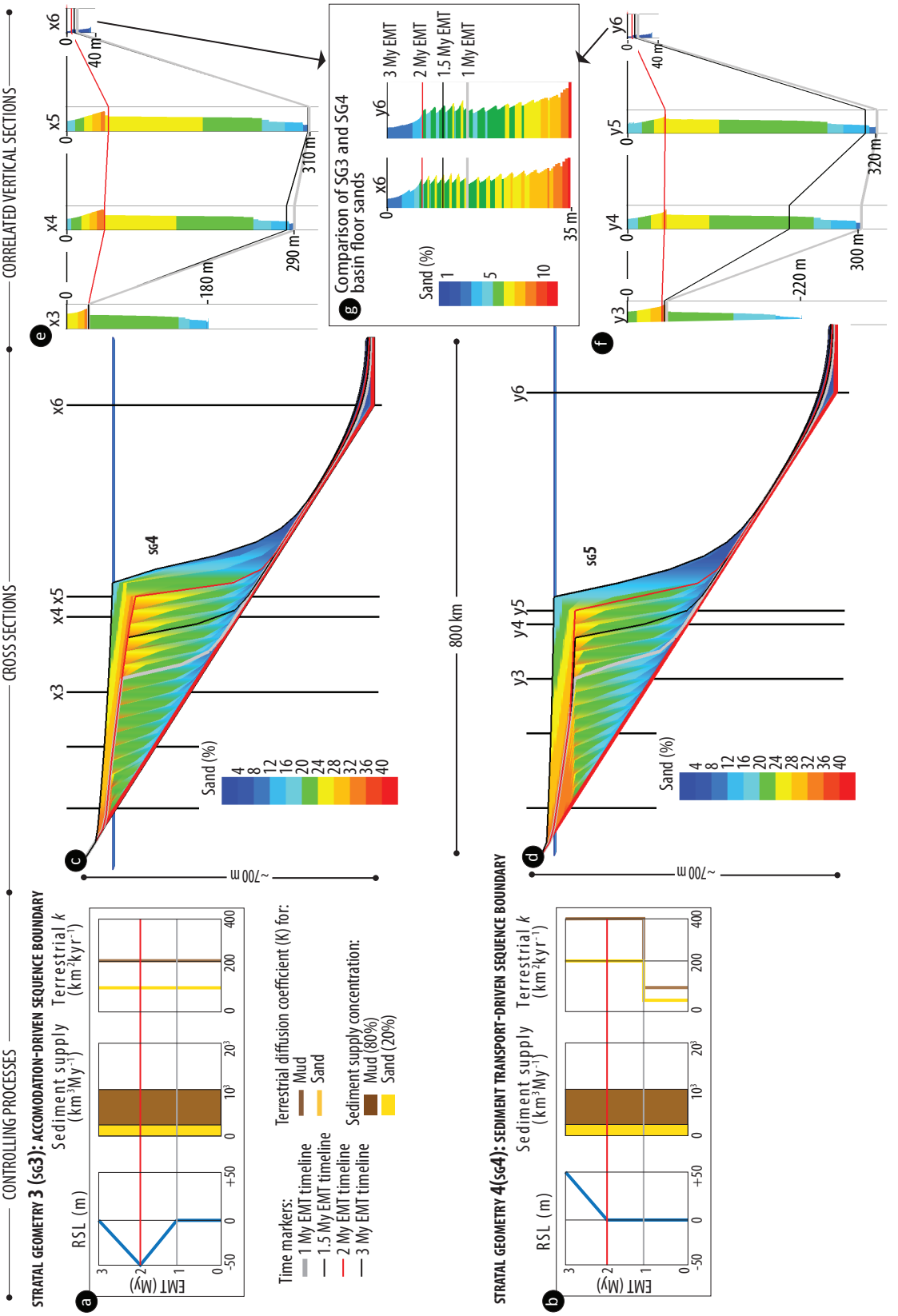
CONTROLLING PROCESSES
CROSS SECTIONS
CORRELATED VERTICAL SECTIONS
STRATAL GEOMETRY 3 (sg3): ACCOMODATION-DRIVEN SEQUENCE BOUNDARY
STRATAL GEOMETRY 4(sg4): SEDIMENT TRANSPORT-DRIVEN SEQUENCE BOUNDARY
RSL (m)
EMT (My)
Sediment supply (km³My⁻¹)
Terrestrial k (km²kyr⁻¹)
Time markers:
1 My EMT timeline
1.5 My EMT timeline
2 My EMT timeline
3 My EMT timeline
Terrestrial diffusion coefficient (K) for:
Mud
Sand
Sediment supply concentration:
Mud (80%)
Sand (20%)
sg4
sg5
800 km
~700 m
Sand (%)
Comparison of SG3 and SG4 basin floor sands
3 My EMT
2 My EMT
1.5 My EMT
1 My EMT
40 m
310 m
290 m
180 m
35 m
320 m
300 m
220 m

FIGURE 6.7: (Previous page.) Stratal geometry 4 (SG4) and stratal geometry 5 (SG5) shown with strata colour coded for proportion of sand content in cross section (c and d) and vertical sections (e, f and g). Although the overall stratal geometries are very similar (see also figure 3) there are some differences in sand content of the strata. Sand content is higher in SG5 in the proximal coastal plain (d) leading to less sand bypass and slightly lower sand proportion in deep-water toeset strata (g).

6.7.5 Implications of non-unique topset aggradation & shoreline trajectories for sequence stratigraphy

Recent numerical modelling of topset aggradation during RSL fall suggests that falling stage topset aggradation is probably more common in the ancient record than currently realised (*Petter and Muto*, 2008, *Prince and Burgess*, 2013, *Swenson*, 2005, *Swenson and Muto*, 2007). Results from Model Set 1 expand on this work by including a set of model results with a range of amplitudes of rising RSL. The results demonstrate non-uniqueness because identical volumes of topset strata occur in modelled stratal geometries resulting from rising, steady and falling RSL depending on the sediment transport rate. This non-uniqueness is important because it suggests that topset aggradation can occur as a result of many different parameter values of RSL history, and is not a unique product of steady to rising RSL as is usually assumed (*Catuneanu*, 2006, *Catuneanu et al.*, 2009). If topset aggradation can occur during RSL fall as well as steady and rising RSL then this has important consequences for our ability to recognize systems tracts (e.g., Chapter 4, Figure 4.15) and reconstruct RSL histories based on mapping of systems tracts. For example, strata deposited during falling RSL with topset aggradation (falling stage systems tract) could look similar to strata deposited during steady or rising RSL with topset aggradation. The only feature that could, if reliably preserved, distinguish between these two cases is the shoreline trajectory. Topset aggradation with a descending shoreline trajectory would indicate falling RSL, whereas topset aggradation with a flat or rising shoreline trajectory would indicate steady or rising RSL. In addition, if topset aggradation during falling RSL is common in the geological record, then volumes of sand bypass during suspected timings of RSL lowstand would be lower, reducing the potential for deepwater sand reservoirs during periods of sea-level lowstand.

Shoreline trajectory analysis (*Helland-Hansen and Gjelberg*, 1994, *Helland-Hansen and Hampson*, 2009, *Helland-Hansen and Martinsen*, 1996) has been an important addition to the original sequence stratigraphic methodology. Compared to sequence models,

fewer implicit assumptions are required for shoreline trajectory analysis and the method is generally more observational than interpretational (*Helland-Hansen and Hampson*, 2009). However, shoreline trajectories calculated in this work show a strong degree of non-uniqueness, because similar shoreline trajectories have been generated by different parameter values of sediment supply and RSL history (Figure 6.4, 6.5). This non-uniqueness, combined with the problem of differential compaction during burial (Chapter 4, 5), has important implications for trajectory analysis, not least because it complicates our ability to extract reliable information from shoreline trajectories in ancient strata.

6.8 Conclusions

Numerical stratigraphic forward model results presented in this chapter show how a maximum transgressive surface (MTS), a sequence bounding unconformity (SB), topset aggradation and shoreline trajectories can be non-unique stratal geometries that for each example are generated by more than one set of parameter values. MTSs are generated due to an increase in rate of RSL rise during constant sediment supply and an increase in rate of sediment supply during steady rise in RSL. SBs are generated due to falling RSL with relatively low rates of sediment transport and steady RSL with relatively high rates of sediment transport. Similar volumes of topset strata are generated in model runs with a range of amplitudes of rising and falling RSL, depending on the sediment transport rate. This non-uniqueness of topset strata suggests that distinguishing between systems tracts generated by rising and falling RSL using presence of topset aggradation is not reliable. Results have also demonstrated how similar shoreline trajectories are generated in models with different sediment supply and accommodation histories, suggesting that extracting reliable information from shoreline trajectories could be difficult.

Non-uniqueness presents a serious problem for sequence stratigraphy because it challenges our ability to extract a single, unique solution from the stratigraphic record. If these model results are realistic and the four stratal geometries investigated in this work are non-unique, then information extracted from the stratigraphic record using these non-unique stratal geomtries, for example to better understand sediment bypass and RSL histories, is not likely to be reliable. Non-uniqueness also makes it difficult to assign chronostratigraphic significance to stratigraphic surfaces which has implications for our ability to correlate strata.

Based on the results presented here, what is required to move sequence stratigraphy forward is a methodology which considers the multiple possible scenarios that may exist for the formation of different stratal geometries. One step towards achieving this may be through combining sequence stratigraphy with recent methods and developments in numerical stratigraphic forward modelling.

Chapter 7

Seismic Interpretation of Middle-Miocene to Pliocene Siliciclastics in the Northern Carnarvon Basin, North West Shelf Australia

7.1 Introduction

Previous studies in the Northern Carnavon Basin (NCB), North West Shelf of Australia (Figure 7.1) have identified late-middle Miocene siliciclastics which occur above the pre-existing Miocence carbonate shelf (e.g., *Cathro and Austin*, 2001, *Cathro et al.*, 2003, *Moss et al.*, 2004, *Sanchez et al.*, 2012,). It has been suggested that these upper-middle Miocene siliciclastics, identified as the Bare Formation in several industry wells and seismic reflection data (*Cathro et al.*, 2003, *Wallace et al.*, 2003), were delivered from an antecedent of the modern Fortescue River (Figure 7.1) and represent an interval of deltaic progradation across the middle-outer portions of the pre-existing carbonate platform (*Sanchez et al.*, 2012,).

With seismic coverage and well data within the region made available by Geoscience Australia (Figure 7.3), these previously documented Neogene prograding siliciclastic sediments provide a case study for testing some of the ideas explored in this thesis, for example non-unique stratal geometries (Chapter 6). This data may also provide an opportunity for testing hypothesise regarding occurrence and progradation history of reported deltaic siliciclastics (e.g., *Sanchez et al.*, 2012). This chapter presents the seismic interpretation of the NCB's late-middle Miocene siliciclastic sediments, allowing the following chapter to discuss the possible evolution of siliciclastics in this region and analyse some of the stratal geometries interpreted from the seismic data in the NCB.

7.1.1 Aim of this chapter

This chapter describes a seismic interpretation study completed for the Neogene siliciclastic sediments in the NCB. Main aims of this study are:

- to utilise available 2D seismic and well data to confirm the presence of the late-middle Miocene siliciclastic sediments above the pre-existing Miocene carbonate platform;
- to identify and map any unconformities within the study area;
- to interpret any siliciclastic clinoforms identified in the dataset to confirm if previously documented delta lobes are present;
- to map any delta lobes identified in the dataset;
- to interpret successive topset foreset rollovers from suitable dip-orientated 2D seismic lines for shoreline trajectory analysis.

7.2 Geological setting of the NCB, Australian Northwest Shelf

7.2.1 Tectonic history

The NCB is located within the North West Shelf of Australia. Since formation by extension in the late Paleozoic (*Driscoll and Karner*, 1998), the NCB has experienced a

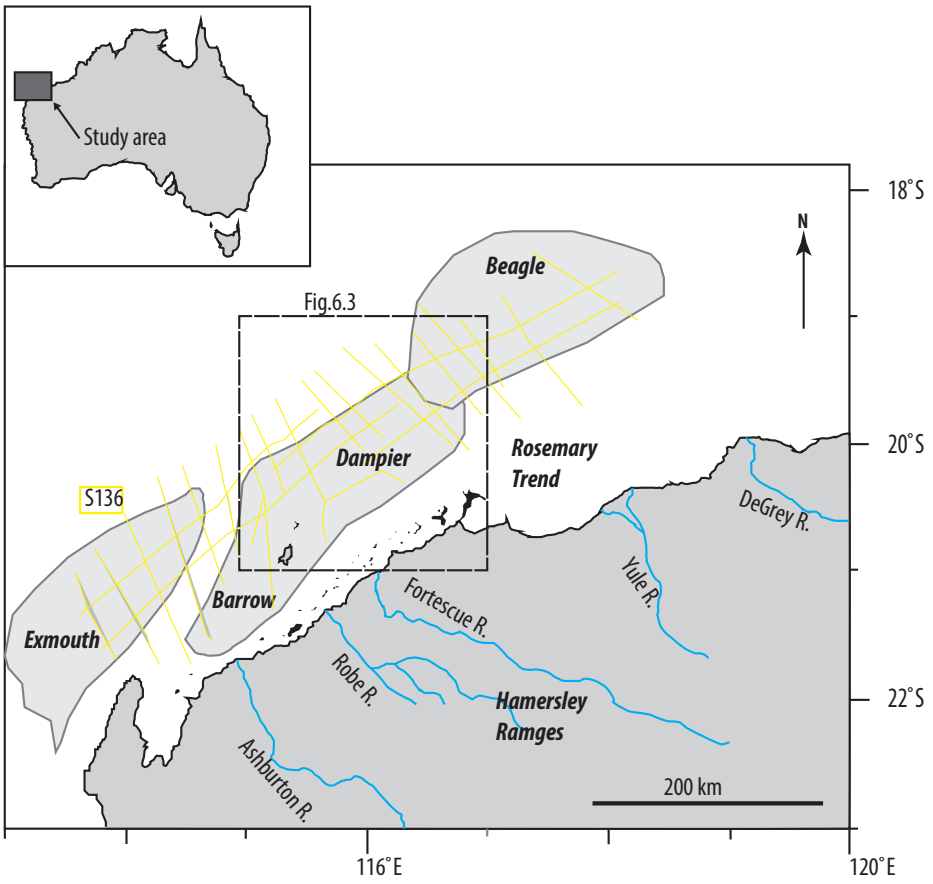

FIGURE 7.1: Map of the NCB, composed of four Mesozoic depocentres including the Exmouth, Barrow, Dampier and Beagle sub-basins. Box-out refers to the area investigated in this study.

complex Mesozoic - Cenozoic evolution due to multiple inversion and reactivation events. Inversion in the Turonian followed post-Valanginian regional subsidence (*Driscoll and Karner*, 1998). It is thought that collision of the Indo-Australian Plate with the Pacific and Eurasion plates to the north of the NCB initiated in the late Oligocene (*Pigram and Davies*, 1987).

Formation of the NCB is the result of three rift phases that influenced the North West Shelf of Australia, from the Late Permian to the Late Jurassic (*Bradshaw et al.*, 1988). After multiple rifting phases, thermal subsidence occurred (*Cathro and Karner*, 2006), and there is evidence to suggest that this thermal subsidence was interrupted by inversion, dated between the Cenomanian and Campanian as a result of collision between the Banda Arc and Australia (*Bradshaw et al.*, 1988, *Driscoll and Karner*, 1998).

7.2.2 Stratigraphy

Siliciclastic sedimentation dominated the North West Shelf during the Mesozoic, but a change to predominately carbonate sedimentation in the Cenozoic occurred as a result of continued northward drift of the Australian Plate to lower latitudes, which initiated in the Mesozoic (*Bradshaw et al.*, 1988). In the NCB, *Cathro et al.* (2003) documented an Eocene-Recent progradational succession of shelf-margin scale clinoforms, which consists of predominately carbonate sediments, such as hetorozoan carbonates in the Oligocene to mid-Miocene.

The middle-upper Miocene Stratigraphy in the NCB has been divided based on previous well-data studies. Divisions include the middle Miocene Trealla Limestone, made up of skeletal packstones to grainstones and offshore marls (*Hocking et al.*, 1987), and the late middle to late Miocene Bare Formation, consisting of well-sorted, medium-grained mature quartz sandstones interbedded with fine-grained calcarenites and dolomites incorporating scattered quartz grains (*Heath and Apthorpe*, 1984). The Bare Formation has been interpreted from well data in the NCB as coastal deposits, based on lack of preserved fauna, presence of interbedded dolomites and occurrence of mature, quartz-rich sandstones (*Heath and Apthorpe*, 1984, *Sanchez et al.*, 2012, *Wallace et al.*, 2003); Figure 7.2).

7.3 Data

Approximately 4000 line-km of 2D multichannel seismic profiles, covering the Dampier and part of the Barrow and Beagle basins (Figures 7.1 and 7.3) was made available for this study by Geoscience Australia. Pg93, the main 2D survey interpreted in this study, has a central frequency around 25-35 Hz and was acquired and processed by Geoscience Australia between 1991 and 1994. Vertical resolution is about 23-32 m at 1 s two-way traveltime (TWT) (*Cathro et al.*, 2003). Well completion reports from 4 industry wells, namely Eaglehawk-1, Goodwyn-2, Goodwyn-6 and Goodwyn-7 (Figures 7.1 and 7.3) confirm lithologies reported previously within the study area (e.g., *Sanchez et al.*, 2012).

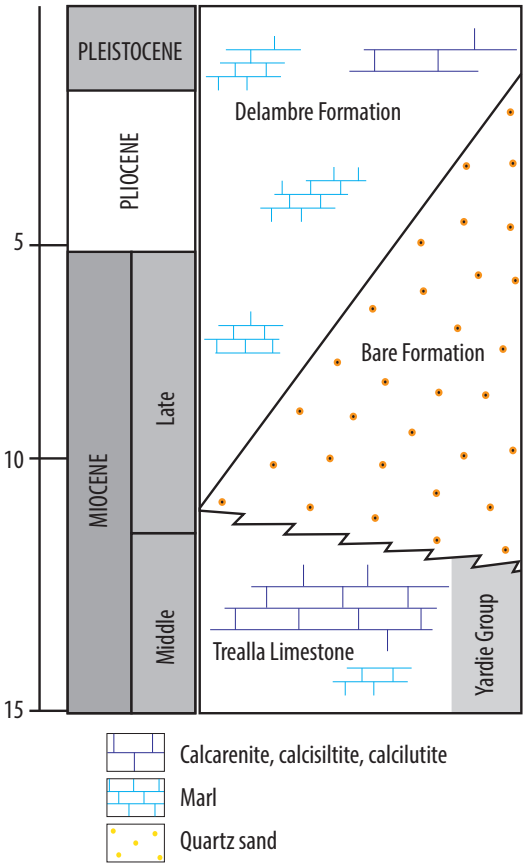

FIGURE 7.2: Simplified Miocene-Pleistocene stratigraphy recognised in the NCB. The middle Miocene Trealla Limestone consists of Skeletal packstones to grainstones and offshore marls (*Hocking et al.*, 1987). The late middle to late Miocene Bare Formation consists of well-sorted, medium-grained mature quartz sandstones interbedded with fine-grained calcarenites and dolomites incorporating scattered quartz grains (*Heath and Apthorpe*, 1984; *Sanchez et al.*, 2012). Figure modified from *Sanchez et al.* (2012).

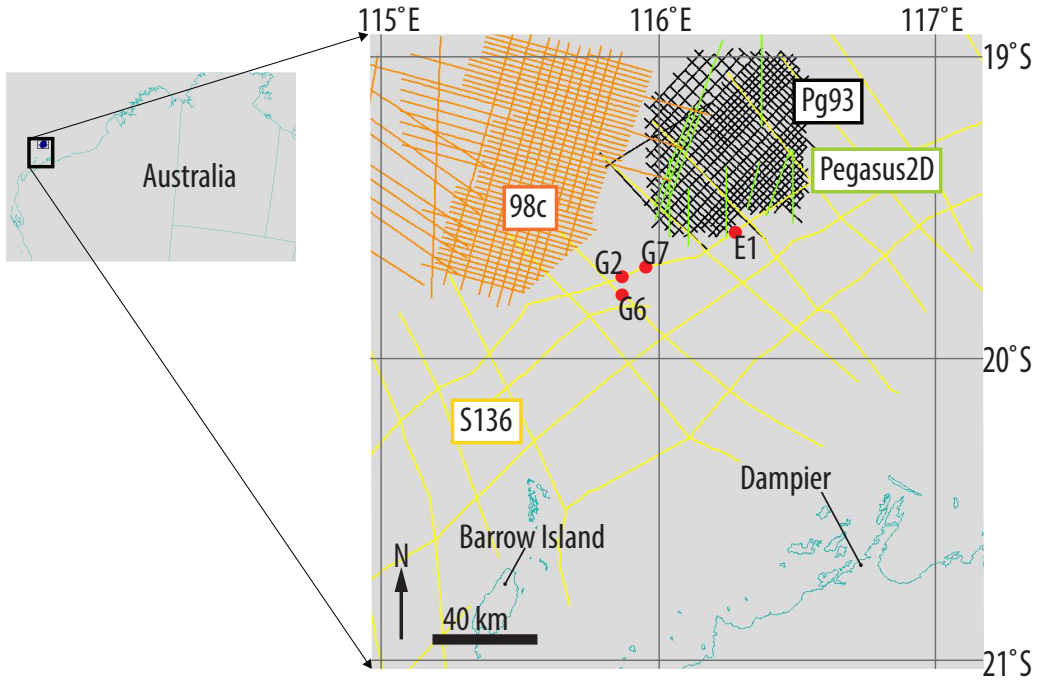

FIGURE 7.3: Map showing the location of four 2D seismic surveys and four wells available for interpretation in this chapter. Well names are Eaglehawk-1 (E1), Goodwyn-2 (G2), Goodwyn-6 (G6) and Goodwyn-7 (G7).

7.4 Methodology

7.4.1 Interpreting seismic profiles

Seismic data provided by Geoscience Australia enabled the subdivision of mappable units bounded by unconformities (e.g., Fig. 7.6). Using seismic interpretation software GeoFrame®, unconformities were mapped across the 2D profiles in surveys Pg93 and Pegasus2D (Figure 7.3). A number of intersecting profiles from surveys S136 and 98c were also used where possible to confirm horizon ties (Figure 7.3). Seismic observations of onlap, truncation and toplap where used to identify unconformities (Figure 7.4).

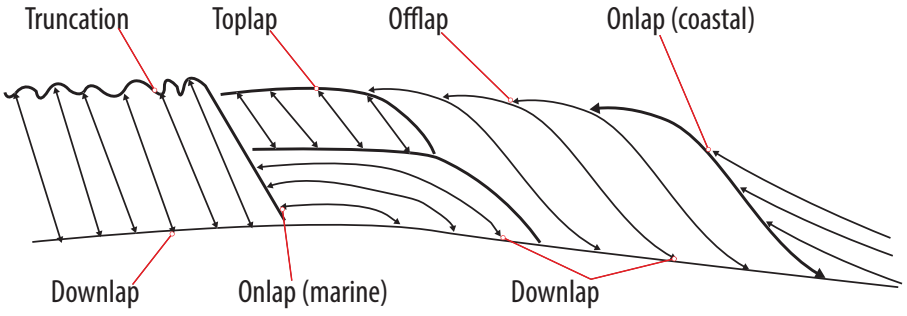

FIGURE 7.4: Types of stratal terminations observed from seismic data in this study to interpret seismic unconformities (modified from *Emery and Myers*, 1996 and *Catuneanu*, 2006).

7.4.2 Distinguishing between carbonate & siliciclastic strata

Siliciclastic and carbonate facies described in the well-completion report for Eaglehawk-1 (Figure 7.5) correlate with seismic facies observed in 2D seismic profiles. For example, thick continuous intervals of well-sorted, medium-grained mature quartz sandstones interbedded with fine-grained calcarenites and dolomites were observed between depths of approximately 1800 to 3600 ft (e.g., in well Eaglehawk-1, Figure 7.5). Dolomites are present in the lower section of this interval (Figure 7.5). According to the time-depth curve provided with the well report for Eaglehawk-1, which was constructed from check-shot and sonic (acoustic) data, 3600 ft occurs at about 900 ms two way travel time. This correlates with expecting seismic reflection response on 2D profiles intersecting Eaglehawk-1. For example, high amplitude reflections and oblique to sigmoidal geometries, indicative of siliciclastic strata, are observed between approximately 550 and 900

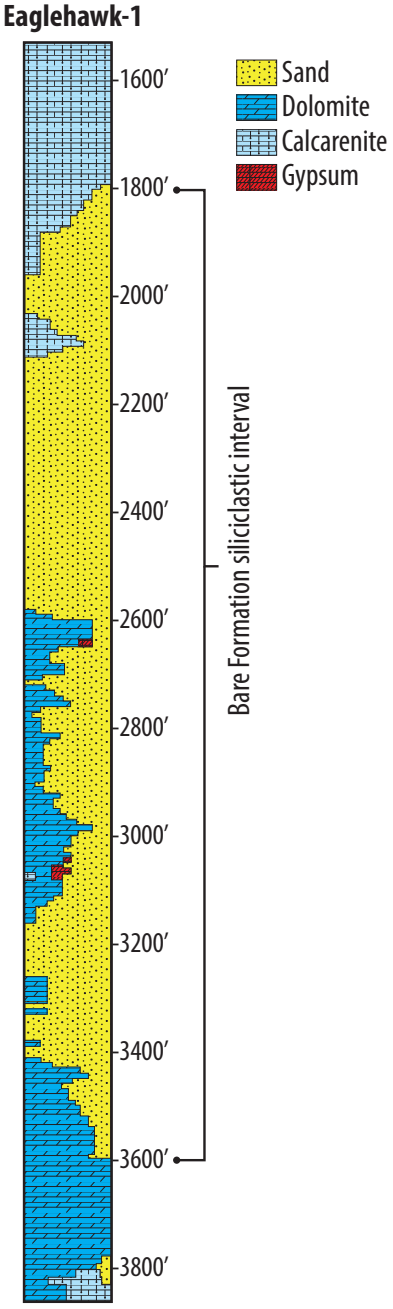

FIGURE 7.5: Lithological information for well Eaglehawk-1 between 1600 and 3600'. Formation descriptions indicate that the sand for this interval is made up of well-sorted, medium-grained mature quartz. Sand is interbedded with fine-grained calcarenites and dolomites, though quartz grains are present throughout the 1800-3600' interval. Well location: Latitude 19° 30' 29.7" S, longitude 116° 16' 36.8 E. Figure based on information provided by Geoscience Australia.

TWT on line 1 in Figure 7.8B. In contrast, thick and homogenous carbonate intervals show low amplitude reflections and a more continuous and parallel geometry, for example above horizon U2 in Figure 7.8B. These contrasting siliciclastic and carbonate seismic facies are compared in Figure 7.7.

7.4.3 Identifying clinoforms & clinoform sets

Shoreline clinoforms were interpreted within the siliciclastic interval based on the observation of strong amplitude, sigmoid - oblique reflections which often display a strong topset -foreset- toeset geometry (e.g., Figure 7.6). These clinoforms are on scales of 10's of metres thick, indicative of shoreline clinoforms (*Helland-Hansen*, 2009).

Seismic observations of toplap and downlap (Figure 7.4) enabled toplap and downlap surfaces to be interpreted, respectively. These surfaces allowed individual shoreline clinoforms to be grouped into clinoforms sets (Figure 7.6). After correlating each clinoform set's bounding toplap and downlap surfaces across intersecting 2D dip- or strike-orientated seismic lines, the sets were then mapped using the most basinal clinoform topset-foreset rollover (e.g., point n in Figure 7.6).

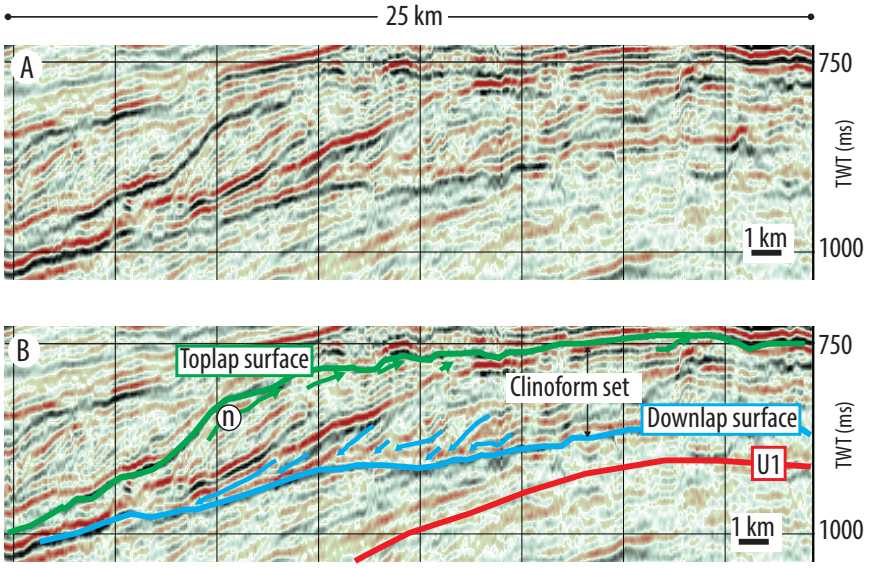

FIGURE 7.6: A) Uninterpreted seismic line and B) the same line with clinoforms interpreted. In B, shoreline clinoforms are grouped by downlap and toplap stratigraphic surfaces. Clinoforms are between 40 and 100 m high, indicative of shoreline clinoforms (*Helland-Hansen and Hampson*, 2009), and terminate against the toplap and downlap surfaces showing tolap and downlapping, respectively. Point n represents the most basinward observed clinoform topset - foreset rollover - a feature used to map clinoform sets in the study area (*Sanchez et al.*, 2012).

7.4.4 Shoreline trajectories

Using the concepts developed by *Helland-Hansen and Gjelberg* (1994) and *Helland-Hansen and Martinsen* (1996) for analysis of shoreline trajectories, geomorphic breaks

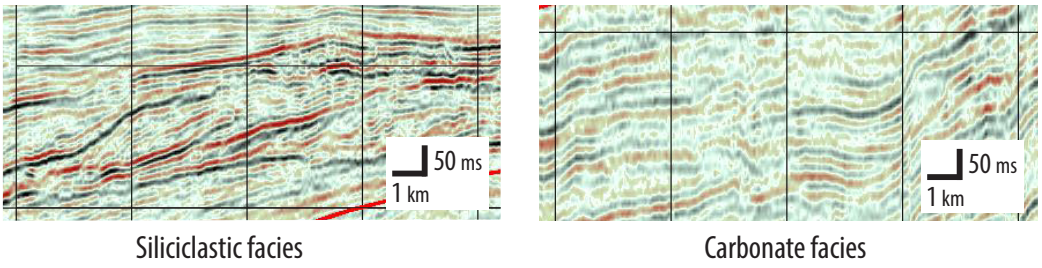

FIGURE 7.7: Comparison of siliciclastic and carbonate seismic facies identified from 2D seismic profiles. Siliciclastic facies is characterised by moderate- to high-amplitude seismic reflections and an oblique or sigmoidal geometry, often with a distinct topset, foreset and bottomset clinoform. As a result of clean and vertically homogenous carbonate lithologies, carbonate clinoform facies is characterised by generally low-amplitude seismic reflections, which are often parallel and continuous, particularly in strike orientated sections.

in slope identified on 2D depositional dip profiles along the Northern Carnarvon system can give an indication into rates of sediment supply, rates of sediment transport and the position of RSL during the late-middle Miocene for this region. For example, ascending and descending regressive shoreline trajectories indicate progradation during rising and falling RSL, respectively. Transgressive shoreline trajectories are indicative of rising RSL and retrogradation, but as discussed previously in Chapter 6, similar looking transgressive shoreline trajectories can result from variations in sediment supply during rising RSL, as well as from an increase in the rate of RSL rise during constant rate of sediment supply.

Reliable analysis of shoreline trajectories is dependent on the use of well-defined datum surfaces because clinoform geometries and thus shoreline trajectories can be altered by processes such as tectonic tilting and differential compaction (e.g., *Helland-Hansen and Hampson*, 2009, *Prince and Burgess*, 2013; Chapter 5). Ideally, datum surfaces are laterally extensive, have a sub-horizontal palaeodip and lie relatively close to the clinoforms under investigation (*Helland-Hansen and Hampson*, 2009). If datum surfaces are recognised on seismic data, for example MTSs and coal seams can qualify as datum surfaces, shoreline trajectory angles can be quantified from successive positions of the shoreline break-in-slope. Once an appropriate datum surface is selected and the seismic line is flatten on this surface, shoreline trajectory angles can be calculated.

Quantitative trajectory analysis of clinoforms observed on seismic data has generally focussed on larger scale shelf-edge trajectories and associated shelf-margin clinoforms

(e.g., *Kertznus and Kneller*, 2009). Previous studies have analysed shoreline trajectories quantitatively based on outcrop and well data to aid understanding of changing palaeoenvironmental and lithological conditions through time (e.g., *Hampson et al.*, 2009, *Loseth et al.*, 2006), but few quantitative examples of shoreline trajectory analysis from seismic data exist (*Mø ller et al.*, 2009).

In this chapter shoreline trajectories observed from three dip-orientated profiles were interpreted. These profiles were selected from different positions along strike to observe how the shoreline trajectories might vary in 3D in this system. After comparison, one of these shoreline trajectory cases was analysed quantitatively adopting the methods of *Helland-Hansen and Hampson* (2009) described above regarding selection of datum surfaces and shoreline trajectory calculations. The seismic profile under quantitative analysis was converted from time to depth using an average velocity of 2000 m/s. Mean, maximum and minimum shoreline trajectory angles for observed trajectory classes are summarised.

7.5 Results

7.5.1 Unconformities

Unconformities U1 and U2 mark the base and top respectively of a late-middle Miocene - Pliocene siliciclastic interval at well Eaglehawk-1 (Figure 7.8). This is part of the interval previously interpreted as the Bare Formation (*Cathro et al.*, 2003, *Wallace et al.*, 2003; Figure 7.2). Within this siliciclastic interval high amplitude sigmoidal reflections interpreted as shoreline clinoforms are bound by downlap and toplap stratigraphic surfaces (Figure 7.6).

Unconformity U1, which lies at the base of the quartz sands in Eaglehawk-1 (Figure 7.8B), is recognised away from Eaglehawk-1 by seismic reflection terminations. U1 truncates strata below and is onlapped by seismic reflections above (green and blue arrows, respectively, Figures 7.8C and 7.9). The Trealla limestone is recgonised below U1 in the well completion report for Eaglehawk-1. One complication from the interpretation shown in Figure 7.8C and E is that the siliciclastic facies identified in the well bound below by U1 extends into a seismic unit expanding down dip into what appears to be a

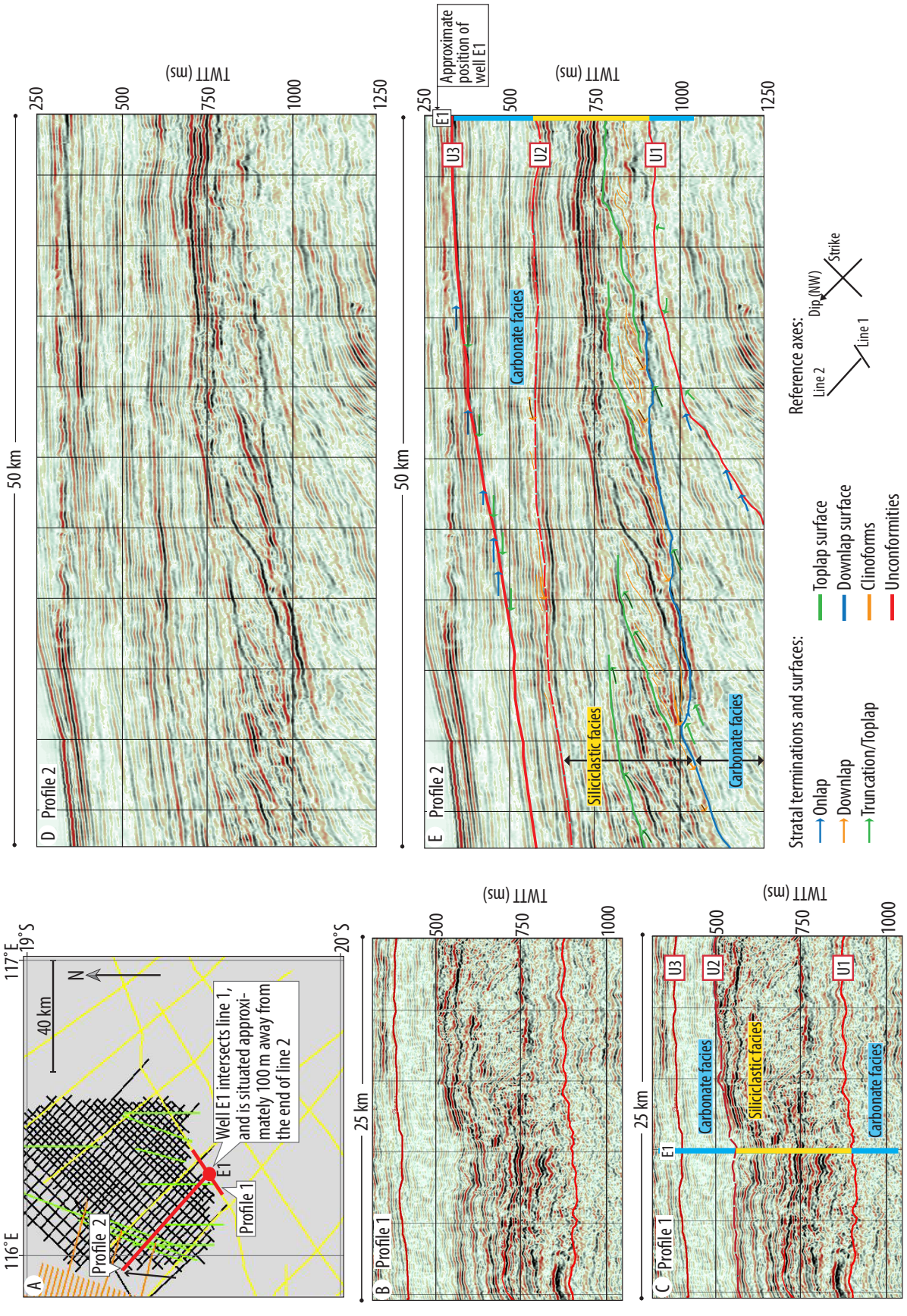
A
117° E
116° E
19° S
20° S
40 km
N
Profile 2
Profile 1
E1
Well E1 intersects line 1, and is situated approximately 100 m away from the end of line 2
B Profile 1
25 km
TWTT (ms)
500
750
1000
C Profile 1
25 km
TWTT (ms)
500
750
1000
U3
U2
U1
E1
Carbonate facies
Siliciclastic facies
Carbonate facies
D Profile 2
50 km
TWTT (ms)
250
500
750
1000
1250
E Profile 2
50 km
TWTT (ms)
250
500
750
1000
1250
Approximate position of well E1
E1
U3
U2
U1
Carbonate facies
Siliciclastic facies
Carbonate facies
Reference axes:
Dip (NW)
Strike
Line 2
Line 1
Stratal terminations and surfaces:
Onlap
Downlap
Truncation/Toplap
Toplap surface
Downlap surface
Clinoforms
Unconformities

FIGURE 7.8: (Previous page.) Example 2D seismic profiles with time converted well log from industry well Eaglehawk-1 (E1). The profiles show interpreted seismic facies and bounding unconformities (U1 - U3) mapped across the study area, and observed siliciclastic and carbonate lithologies from the E1 well completion report. (A) Map of seismic surveys Pg93 (black profiles) and S136 (yellow profiles) (Figure 7.3) interpreted in this study, with the location of well E1. Strike-orientated Profile 1 is intersected by E1. Depositional dip-orientated Profile 2 is approximately 100 m northwest from E1. (B) Uninterpreted section of a 2D regional profile from survey S136, referred to in this study as Profile 1. Interpreted Profile 1 shown with the time-converted well log from E1 and unconformities U1 to U3. Seismic facies are also indicated (C). Uninterpreted Profile 2 (D) and interpreted Profile 2 (E). In the well log, yellow refers to quartz rich sandstone and blue refers to carbonate lithology. Unconformities U1 and U3 mark the Miocene - Pliocene stratigraphic interval, with estimated ages of 12.7 +/-2.5 to 1.5 +/- 1.5 Ma (*Sanchez et al.*, 2012). Unconformities were tied from E1 and mapped across the study area using observations of toplap, truncation and onlap (Figure 7.4), and seismic facies (Figure 7.7).

carbonate facies. One explanation for this is that Bare Formation represents a proximal coastline to an offshore carbonate ramp. This interpretation is supported by previous work described above, which suggests that the Bare Formation siliciclastic interval as a coastal facies, and by the fact that the well report describes Dolomite beds in the lower section of well E1 (Figure 7.5).

Unconformity U2, marking the top of the siliciclastic interval observed in Eaglehawk-1, also shows a high amplitude reflection. As with U1, U2 has been mapped across the study area using observations of truncation and toplap below, and onlap and downlap above. The well completion report confirms that U2 separates siliciclastic strata below from carbonate strata above. Seismic facies (Figure 7.7) are used to confirm this interpretation away from Eaglehawk-1. Unconformity U3 is also recognised in the vicinity of Eaglehawk-1 by toplap and trunction of reflections below and onlap above (Figure 7.8C&E).

Biostratigraphic constraint

Foraminiferal zones were defined in several exploration wells in the NCB by *Moss et al.* (2004) and *Cathro et al.* (2003). Based on this biostratigraphic information and identification of siliciclastics in wells Goodwyn-2 to Goodwyn-7 to the southwest of Eaglehawk-1 (Figure 7.3), *Sanchez et al.* (2012,) assigned the U3 unconformity to the top of the Bare Formation. Therefore, the U3 unconformity has also been mapped across the study area to add constraint to the presence of the Bare Formation siliciclastic interval.

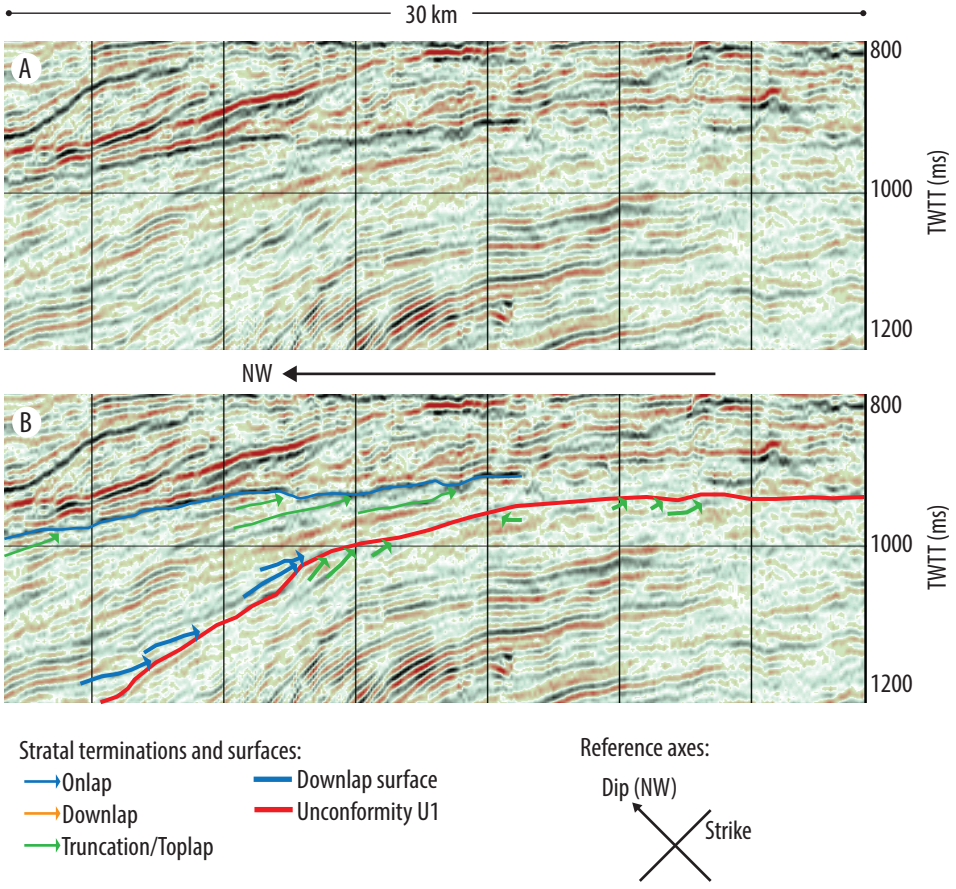

FIGURE 7.9: Seismic reflection terminations of truncation (green arrows) and onlap (blue arrows) identify unconformity U1 away from well Eaglehawk-1 (Figure 7.8).

.

7.5.2 Clinoform sets

Mapping of clinoform sets across the study area shows that these features have either a strike-elongate or lobate structure in plan-view (Figure 7.10). Ten clinoform sets are mapped across the study area as shown in Figure 7.10. Clinoforms sets are grouped from 1 through to 10, from oldest (set 1) to youngest (set 10).

Large strike-elongate clinoform sets

Clinoform sets 1 to 5 display a strike elongate character. For example, Figure 7.11 shows a dip-orientated profile that intersects lobes 1 to 4 (Figure 7.10). These sets are upto 300 m thick, with individual clinoforms over 100 m in thickness in some cases. Strike (SW - NE) orientated seismic lines intersecting these lines show that clinoform sets 1 to 5 are larger than clinoform sets 6 to 10 located in the northeast of the study area.

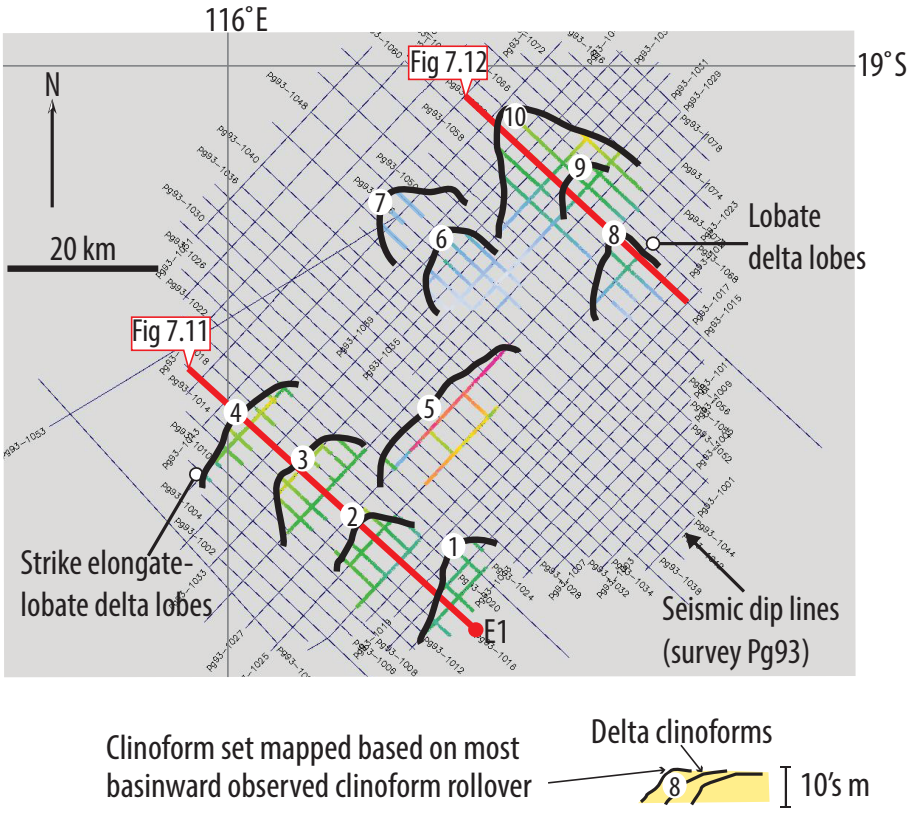

FIGURE 7.10: Sets of shoreline clinoforms interpreted as delta lobes are shown in plan view, along with the position of intersecting dip lines displayed in Figures 7.11 & 7.12. Delta lobes are defined by the most basinward (northwest) clinoform topset-foreset rollover.

Lobate clinoform sets

In contrast to sets 1 to 5, mapped clinoform sets 6 to 10 display a lobate shape in plan view (Figure 7.12). For example, Figure 7.12 is a dip orientated profile intersecting clinoform sets 8 to 10 (Figure 7.10). Clinoform set 8 is less than 100 m thick and is of limited areal extent. In plan view this clinoform set has a strongly lobate shape (Figure 7.10). Clinoform sets 9 and 10 are difficult to distinguish; different downwlap surfaces are recognised but defining the clinoform sets toplap surfaces is not as clear (Figure 7.12).

7.5.3 Shoreline trajectories observed from dip-orientated seismic profiles

Shoreline trajectories have been interpreted from depositional dip orientated 2D seismic profiles (e.g., Figure 7.13). In Figure 7.13, three dip profiles are shown with shoreline

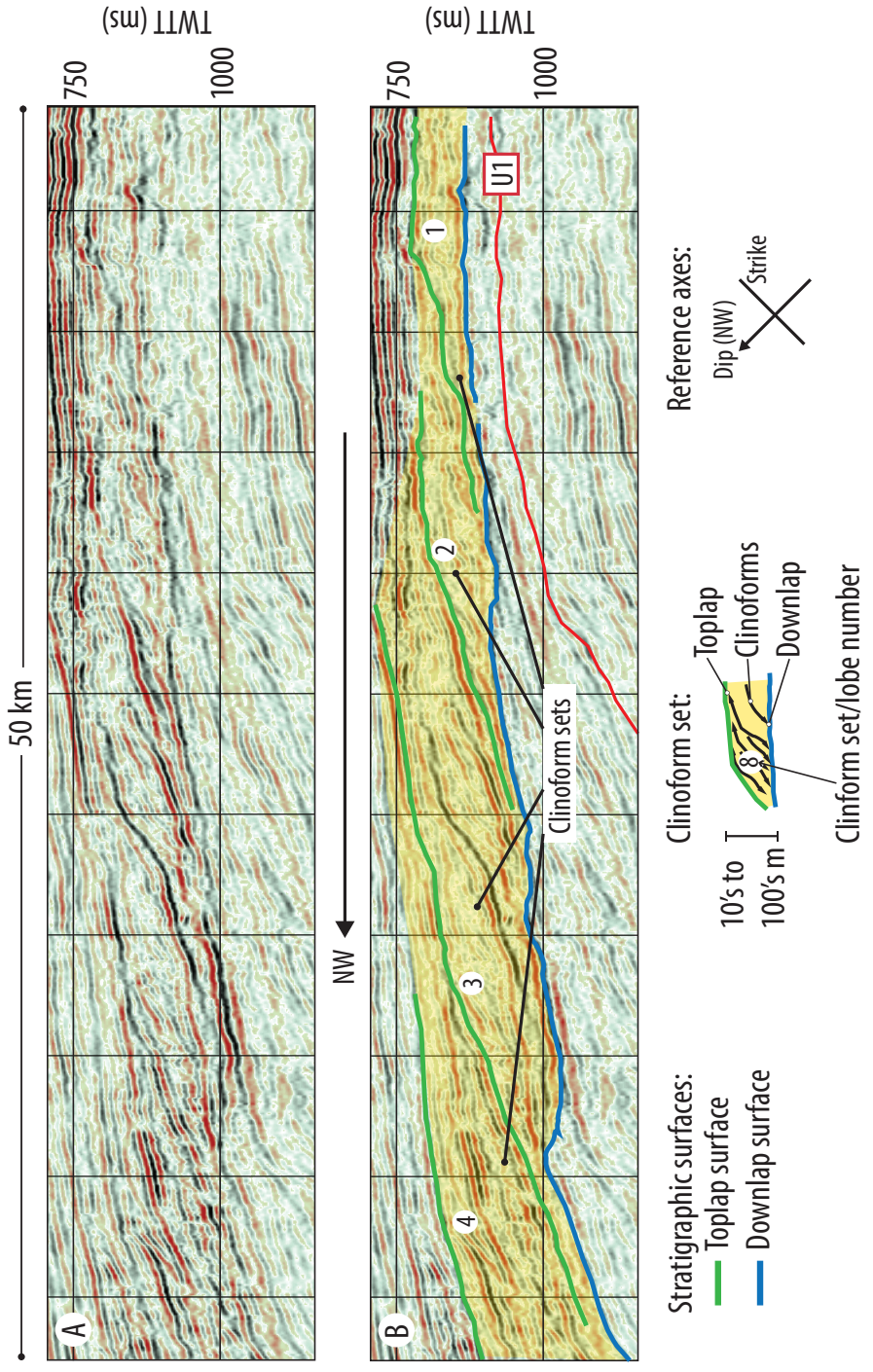

FIGURE 7.11: Shoreline clinoform sets 1 to 4 bounded by toplap and downlap surfaces. Location of the dip line with respect to delta lobes 1 to 4 is shown in Figure 7.10. The reference axis indicates that the seismic line is intersecting clinoforms in a dip orientation, but the extent to which clinoforms may actually be intersected obliquely to true dip direction is difficult to establish.

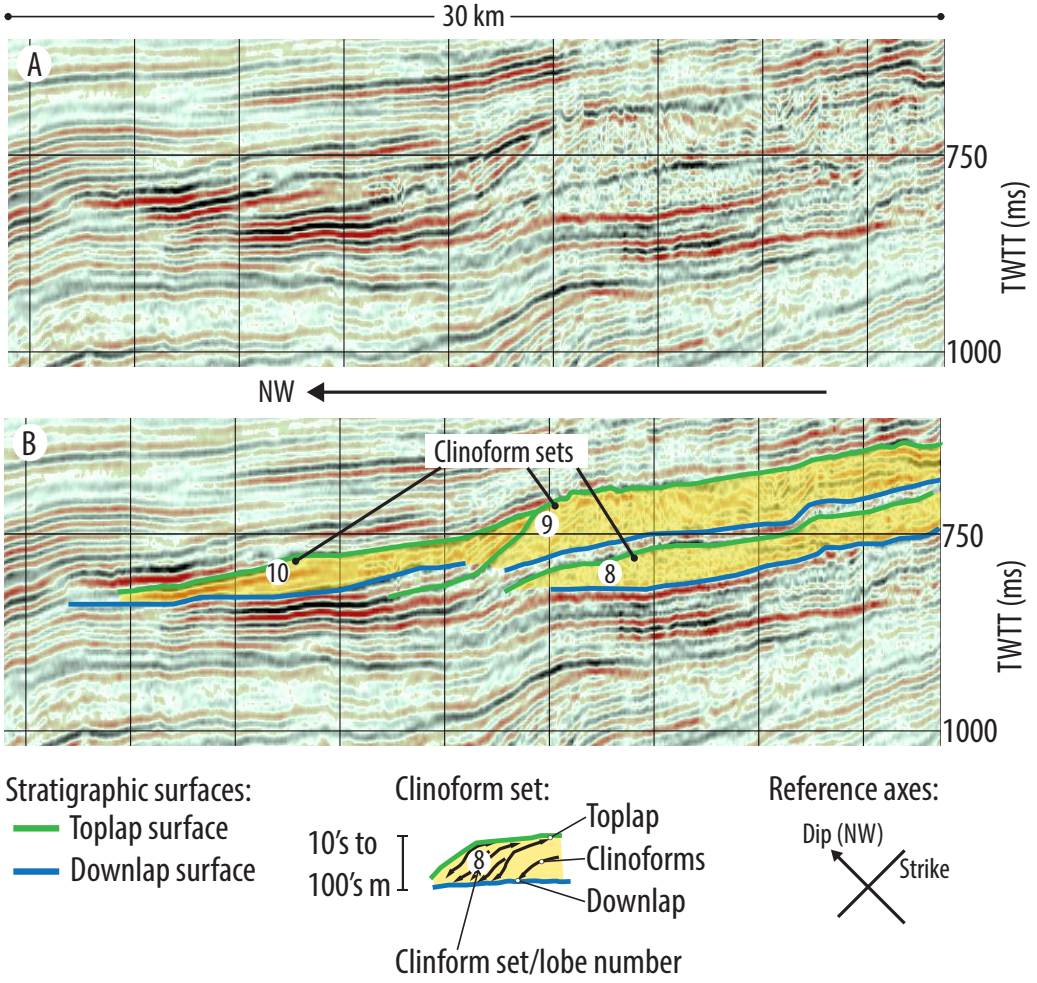

FIGURE 7.12: Shoreline clinoform sets 8 to 10 bounded by toplap and downlap surfaces.

trajectories highlighted, and their locations with respect to seismic survey Pg93 and interpreted clinoform sets are illustrated.

Shoreline trajectory interpretation from Line 1

In Figure 7.13B clinoforms are relatively well imaged, have moderate to strong amplitudes, and sigmoid to oblique geometries. The interpreted interval is overlain by a series of continuous strong reflections. The shoreline trajectory class is initially ascending before reaching its most elevated (shallowest) point approximately half-way along the interpreted profile. From this point, the shoreline trajectory descends by 130 TWT ms from approximately 755 to 885 TWT ms.

Shoreline trajectory interpretation from Line 2

Clinoforms in seismic line 2 are not as well imaged as those observed in line 1 (Figure

7.13C). As with line 1, the shoreline trajectory displays an initial ascent before reaching its highest position. The trajectory then descends by approximately 130 ms, from 710 to 840 ms. After tracing successive clinoforms in a basinward depositional dip direction (NW), it eventually becomes too difficult to identify the topset-foreset rollovers.

Shoreline trajectory interpretation from Line 3

Amplitudes of seismic reflections in line 3 are not as high as line 1 (Figure 7.13D). For this interpretation, the better imaged line 1 can serve as a type line because the overlying, more continuous reflections can also be observed above the interpreted interval in line 3. In contrast to the ascending shoreline trajectory paths described above for line 1 and line 2, the shoreline trajectory in line 3 becomes sub-horizontal after an initial ascent. After approximately 10 km progradation (NW), the shoreline trajectory reaches a high point due to a brief ascent. Then, from approximately 640 ms, the shoreline trajectory descends to 810 ms. After this point, it becomes difficult to identify any breaks in slope that may indicate a shoreline trajectory, either because of poor imaging or because clinoforms are not present.

Summary of interpreted shoreline trajectories

Each of the three shoreline trajectory described above have been interpreted from a depositional-dip orientated 2D profile intersecting delta clinoforms. For each of these three cases, classes of shoreline trajectories indicate a strongly progradational history with steady to rising RSL followed by falling RSL. Shoreline trajectories interpreted from the different dip orientated seismic profiles (Figure 7.13A) display very similar overall geometries despite being from different positions along strike (15 - 20 km strike separated). This tends to suggests that the observed stratal archtectures containing shoreline clinoforms were controlled predominately by regional changes in accommodation. However, the shoreline trajectories from lines 1 to 3 have not yet been corrected to palaeo-horizontal. This is an important step before quantifying trajectory angles (*Helland-Hansen and Hampson*, 2009). An key consideration for the trajectory method is how restoration using a datum surface will effect the trajectory classes described above.

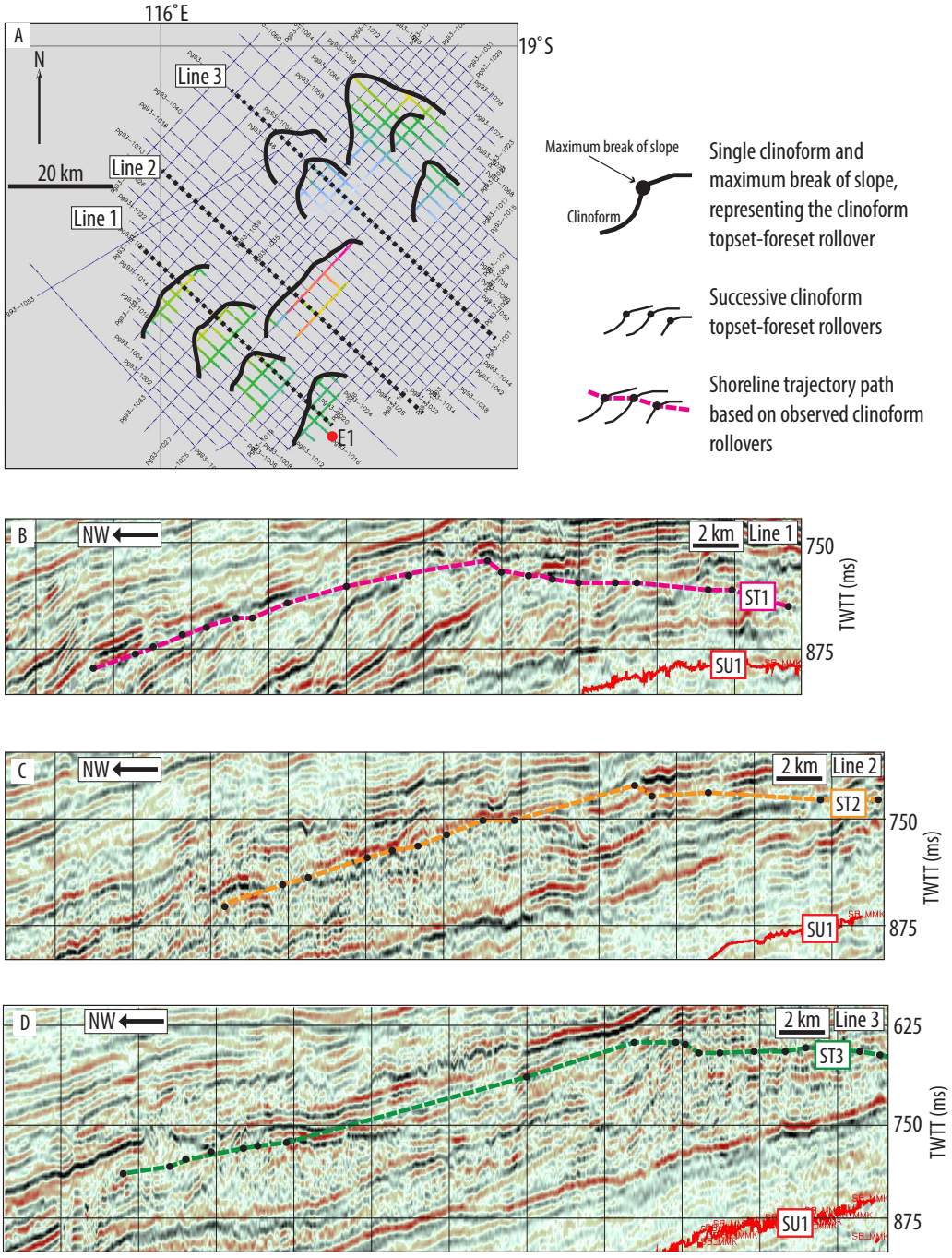

FIGURE 7.13: Shoreline trajectories interpreted from 2D depositional dip orientated profiles. The shoreline trajectory paths (dash lines) in each profile are based on identification of topset - foreset clinoform rollover points (black dots). The shoreline trajectories in each case display both ascending and descending regressive classes (*Helland-Hansen and Martinsen*, 1996) indicating rising and falling RSL, respectively.

7.5.4 Quantitative shoreline trajectory analysis

To further investigate and quantify the shoreline trajectories described above, consideration of a paleo-horizontal surface is required. This is because post-depositional processes such as differential compaction are capable of significantly altering shoreline trajectories to the extent that it becomes difficult to discern ascending from descending trajectory classes (e.g., *Helland-Hansen and Hampson*, 2009; Chapter 5).

In Figure 7.13 shoreline trajectories were shown to have similar overall geometries. Figure 7.14 shows Line 1 (see Figure 7.13 for location) with a downlap surface (DLS1) interpreted below the siliciclastic interval and shoreline trajectory. This surface is suitable as a datum for shoreline trajectory analysis in each of the dip lines (lines 1 to 3 in Figure 7.13) because it is in close proximty to the shoreline trajectory, is laterally continuous, and likely had a depositional angle close to horizontal. For each line, flattening on this surface has a similar effect on the geometry of shoreline trajectories ST1 to ST3.

Flattening line 1 on DLS1 shows that the geometry of the shoreline trajectory was significantly affected after deposition. Comparing the shoreline trajectory in line 1 before and after burial would lead to quite different interpretations of accommodation and sediment supply history. After flattening the seismic line on the datum surface DLS1, the shoreline trajectory shows an initial ascent for approximately 12 km of progradation. The average angle of the ascending trajectory for this 12 km is approximately 3 degrees (Figure 7.14D). After 12 km the shoreline trajectory fluctuates betweem low angle acsending and descending trajectory classes. The maximum descending and ascending trajectory angles are -9 and 9 degrees, respectively (Figure 7.14).

7.6 Discussion

7.6.1 Reliability of the well to seismic tie

The well report for Eaglehawk-1 clearly shows that approximately 1800' (549 m) of well-sorted, medium-grained mature quartz sandstone is present between 1800 and 3600' (549 and 1097 m) (Figure 7.5). Although the tie between this observed interval in the well report with the seismic TWT has been done without the use of a synthetic seismogram, the tie can be considered reliable because (1) the time-depth chart provided with the

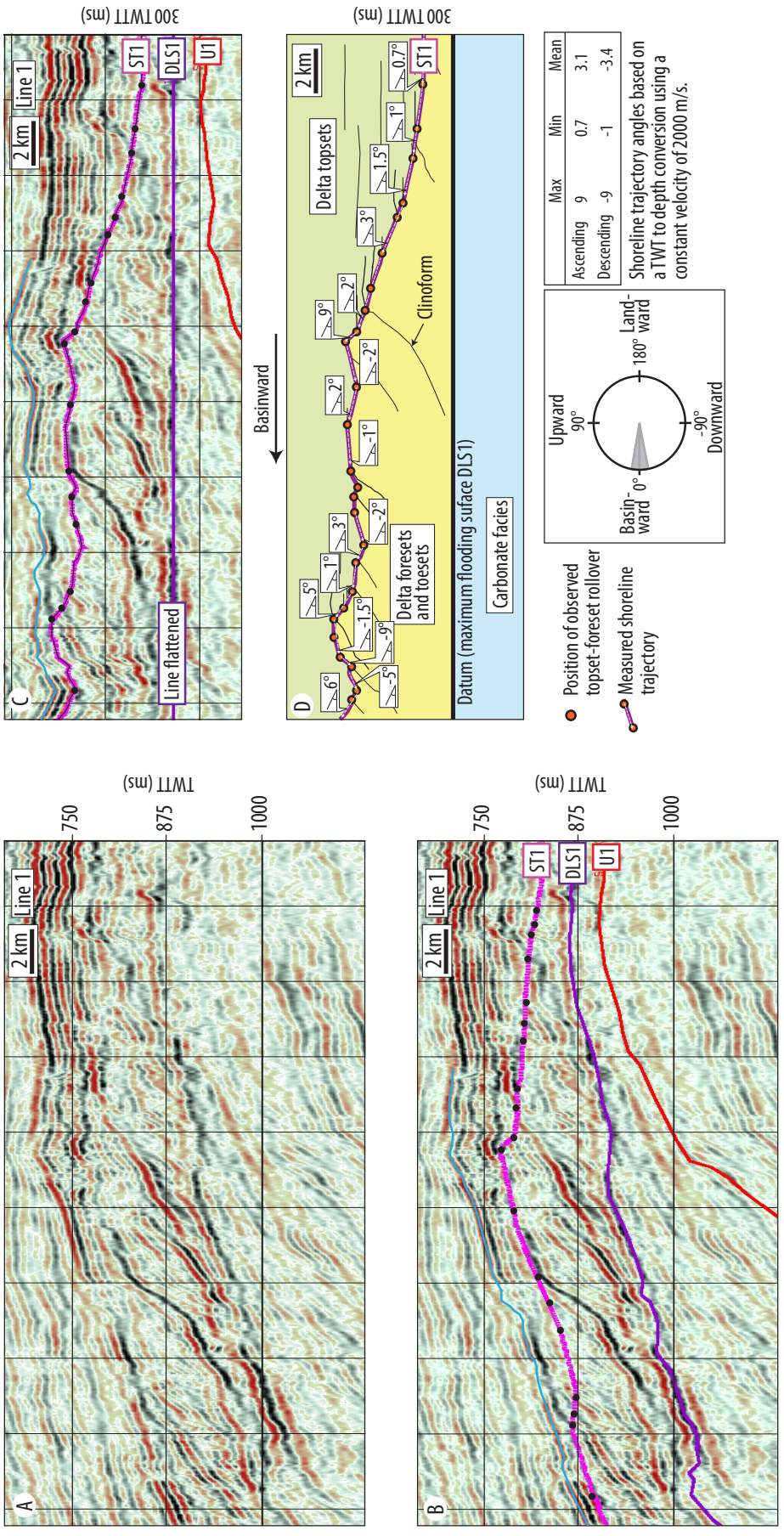
A
B
C
D
Line 1
2 km
TWTT (ms)
750
875
1000
ST1
DLS1
U1
Line flattened
Basinward
Delta topsets
Clinoform
Delta foresets and toesets
Carbonate facies
Datum (maximum flooding suface DLS1)
Upward
Landward
Basinward
Downward
Position of observed topset-foreset rollover
Measured shoreline trajectory
Max Min Mean
Ascending 9 0.7 3.1
Descending -9 -1 -3.4
Shoreline trajectory angles based on a TWT to depth conversion using a constant velocity of 2000 m/s.

FIGURE 7.14: (Previous page.) Analysis of shoreline trajectory interpreted in Line 1. A) uninterpreted Line 1; B) shoreline trajectory and downlap surface used for a palaeo-horizontal datum; C) shoreline trajectory after flattening the line on the downlap surface DLS1; D) schematic diagram of flattened line 1 with shoreline trajectory angles calculated for a range of trajectory trends.

well report shows unequivocally that the siliciclastic to carbonate transition depth of 3600' occurs at 900 TWT (ms), and because (2) this lithological boundary is supported by observed siliciclastic and carbonate seismic facies.

There are also some issues with the well to seismic tie. U1 marks the base of the siliciclastic Bare Formation at the location of well E1, however, down dip U1 is overlain by a different seismic character interpreted to represent a carbonate lithology (Figure 7.8). This observation is described above and interpreted to represent a proximal sandstone to offshore carbonate ramp. Presence of Dolomite within the Bare Formation (Figure 7.5), along with other evidence to suggest that the Bare Formation was deposited in a coastal environment, helps to support this interpretation.

Lack of available data regarding the detail and extent of the Bare Formation also raises some uncertainty. Interpretation of this siliciclastic interval away from the limited well data is speculative because it is based solely on seismic facies and mapping of unconformities above and below the interval of interest. Given the shelf setting and large thickness of siliciclastic material observed in Eaglehawk-1, it is not unlikely that this siliciclastic interval occurs elsewhere on the NCB's shelf, and over the approximately 40 by 40 km ^{2} described and mapped in this work.

7.6.2 Shoreline trajectory interpretation difficulties

Shoreline clinoforms are on scales of 10's of metres in thickness, therefore identifying these features and their maximum break of slope is dependent on seismic data with sufficient resolution. If seismic resolution is sufficient, picking a suitable shoreline trajectory based on maximum breaks of slope is open to interpretation. It is therefore likely that multiple possible interpretations exist. Interpretation is also complicated because shoreline trajectories can be modified by tectonic influence or compaction processes, or both. This modification problem has been highlighted already in this thesis (e.g., Chapter 5).

Following the methods outlined by *Helland-Hansen and Hampson* (2009), flattening on suitable datum surfaces can help alleviate this interpretation problem.

7.6.3 Obliquity of shoreline trajectories

Establishing a precise dip-orientated section through delta clinoforms is rarely (ever?) likely to be possible. It is more likely that delta clinoforms intersected by a cross section are done so at an oblique angle (as suggested in Figure 7.11). This obliqueness could lead to problems when attempting to obtain information regarding sediment supply and accommodation using the methods of shoreline trajectory analysis, because clinoform geometries are likely to show variability along strike due to lateral variations in sediment supply (e.g., Figure 7.10 *Martinsen and Helland-Hansen*, 1995).

7.7 Conclusions

The Bare Formation siliciclastic interval has been mapped across the study area by correlation of bounding unconformities defined by reflection terminations, well data and seismic facies. This has enabled analysis of clinoforms in the region.

Individual shoreline clinoforms have been subdivided into larger clinoform sets bound by onlap and downlap surfaces. Mapping of these clinoform sets in the study area reveals that these sets are likely to be of deltaic origin, primarily due to their lobate shape. Ten delta lobes have been mapped and their character is different, from larger lobate to strike-elongate delta lobes in the southwest to smaller more lobate lobes in the north east.

Analysis of shoreline trajectories in the study area shows that dip-orientated shoreline trajectories located at up to 20 km intervals along strike look similar. This tends to suggests that accommodation was a key control on the evolution of delta lobes observed in the region.

Chapter 8

Two-Dimensional Shoreline Trajectory Reconstruction & Comparison with Three-Dimensional Clinoform Development

8.1 Introduction

Shoreline trajectories describe the nature of shoreline migration through time in 2D. They are useful for unravelling RSL and sediment supply histories at the shoreline, and predicting variability of stratal architectures in other depositional systems. Interpreting shoreline trajectories is closely tied to interpreting clinoform geometries because shoreline trajectories are recorded by clinoform topset-forset rollovers (*Helland-Hansen and Hampson*, 2009; Chapter 5 and 7). However, because stratal architectures observed in siliciclastic basin-margin settings often show significant strike variability (*Helland-Hansen and Martinsen*, 1996, *Martinsen and Helland-Hansen*, 1995), shoreline trajectories interpreted from individual cross sections (i.e. 2D seismic profiles) are limited in respect to understanding and predicting stratal geometries in strongly 3D systems. To circumvent this 2D limitation of single shoreline trajectory examples, comparison of

multiple shoreline trajectories from strike-offset cross-sections is required. Such comparative analysis has not been performed from seismic data, suggesting that the limitation of using shoreline trajectories from single cross-sections for interpreting 3D systems is often overlooked.

Concepts and methods of shoreline trajectory analysis relies on the assumption that clinoform geometries can be described, at least approximately, in 2D. If this assumption is correct then it should be possible to reconstruct shoreline trajectories and related clinoform geometries interpreted from seismic data in a 2D numerical model. To investigate this possibility the first analysis in this chapter will involve a 2D Dionisos reconstruction of a shoreline trajectory interpreted from seismic data in the NCB (Chapter 7). Reconstructing stratal geometries observed in the ancient record, either from seismic or outcrop data, is a useful method for better understanding what controls formation of various stratal geometries (including shoreline trajectories). Accurately reconstructing observed stratal geometries is also a positive step for validating the realism of a particular numerical model (*Paola et al.*, 1999), not least because in order for stratigraphic forward models to be realistic they first need to be capable of reproducing observed stratal geometries.

Leading on from this 2D shoreline trajectory reconstruction, three different delta systems will be simulated in a 3D numerical forward model and, for each of these cases, different dip-oriented shoreline trajectories will be interpreted and compared to demonstrate how shoreline trajectories can vary along strike in different delta systems (*Martinsen and Helland-Hansen*, 1995). Results from this analysis are compared with the shoreline trajectories interpreted from dip-orientated seismic lines in the NCB (Chapter 7) to consider how the NCB system may have formed. The work suggests that comparing dip-orientated shoreline trajectories that are from different positions along strike could be a useful method for better understanding and predicting stratal architectures in 3D.

8.1.1 Aims

In the previous chapter seismic interpretation of the NCB included analysis of shoreline trajectories from three dip-orientated seismic profiles. Sets of shoreline clinoforms interpreted as delta lobes were also interpreted and mapped. The main aims in this chapter are:

- to reconstruct one shoreline trajectory from the NCB interpretation in the numerical model Dionisos.
- to illustrate the issues regarding interpretation of obliquely intersected clinoform rollovers for shoreline trajectory analysis.
- to numerically model with Dionisos three different scenarios of delta progradation, from simple delta progradation to complex lobe switching.
- to calculate shoreline trajectories from different dip-orientated cross sections taken from scenarios above.
- to compare strike-offset shoreline trajectories calculated from modelled delta scenarios with shoreline trajectories interpreted from the NCB to better understand the evolution of the NCB delta system.

8.2 Model description

Dionisos is a numerical stratigraphic forward model (described in Chapter 3) capable of simulating clinoform development in 2D and 3D, and its application in this chapter is to investigate the consequences of using 2D shoreline trajectories for attempting to understand 3D clinoform geometries.

In this chapter 2D and 3D modelling analysis are described separately. The method, parameter values (Table 8.1) and results from a 2D modelling analysis are covered before the 3D modelling analysis (Table 8.2). Model results are shown in cross section and in plan view for the 3D model runs. Selected cross sections show shoreline trajectories interpreted from clinoform topset-foreset rollovers.

8.3 Analysis Part I: 2D shoreline trajectory reconstruction

8.3.1 Outline

2D cross sections are often used to interpret shoreline trajectories and thus describe 3D clinoform geometries. For example, an ascending shoreline trajectory describes overall rising clinoform topset-foreset rollovers deposited during rising RSL. However, a critical

assumption of the shoreline trajectory method is that 3D clinoform geometries can be approximately described from 2D cross sections.

To investigate the reliability of this 2D assumption inherent to the current shoreline (and shelf-edge) trajectory method, the first analysis in this chapter involves a 2D Dionisos reconstruction of a shoreline trajectory interpreted from 2D seismic data in the NCB. Assuming that Dionisos can accurately reconstruct clinoform geometries in 2D and 3D, and that clinoform geometries can be described in 2D, a 2D Dionisos model should therefore be capable of reconstructing a shoreline trajectory interpreted from seismic data.

8.3.2 2D modelling method & parameter values

Model grid dimensions and initial topography

For the first analysis in this chapter, which focussed on shoreline trajectory reconstruction in a 2D Dionisos model, a 2D model was completed on a 1-by-80 grid of 1 km^2 cells, giving an areal extent of 1 km by 80 km (Figure 8.1). The model was run on a simple shelf-slope topography which had a total relief of approximately 400 m. Slope angles for the initial topography are as high as approximately 0.4 °, which is at the upper end of what is observed on modern continental shelves and marine slopes (*Reading and Collinson*, 1996).

Diffusion coefficients and sediment supply

Realistic clinoform geometries can be reconstructed in 2D Dionisos model runs, but this requires careful selection of parameter values. In Chapter 4, 2D models were compared with cross sections from the main axis of sediment transport in 3D models. This comparison showed that stratal architectures in these two cases looked similar, suggesting that the 2D model runs can be considered as a representation of the main axis of sediment transport. Parameter values used for the 2D model runs in this chapter are modified from the values used in Chapter 4 because of a reduction in the size of the model grid (800 km length in Chapter 4, 80 km length in this chapter). For example, values for the diffusion coefficients are lower because the transport distances are smaller, and sediment supply and river discharge values are lower because of the smaller volume required.

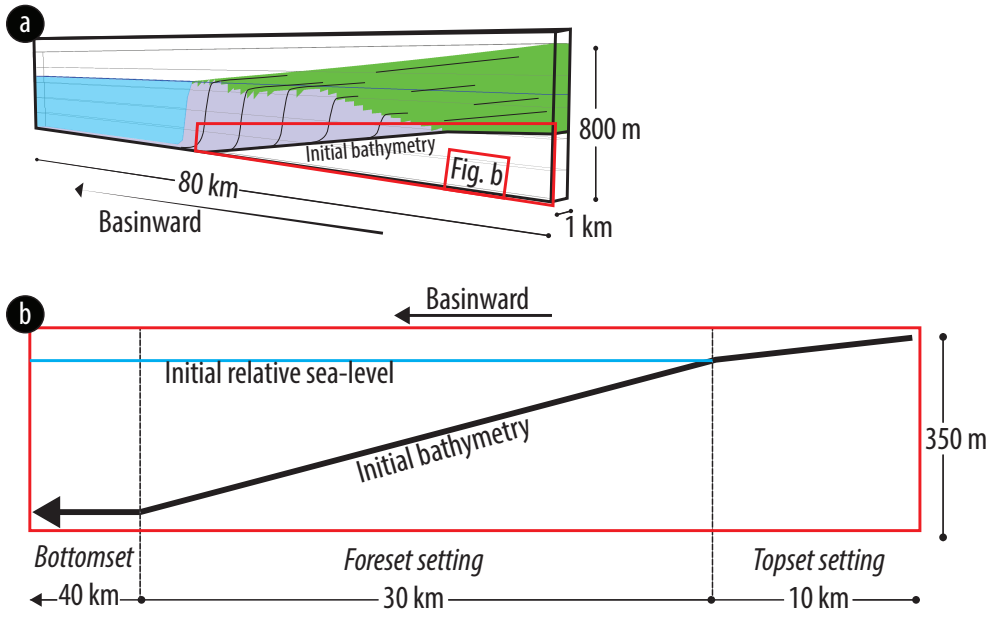

FIGURE 8.1: Initial bathymetry used for the 2D modelling analysis. a) Completed model run illustrating preserved topset (green) and foreset (grey) strata on the 2D initial bathymetry. b) Side view of the initial ramp bathymetry. Note that the horizontal bottomset extends for 40 km. Maximum slope is approximately 0.4 °. This bathymetry was used for several tens of model runs in the 2D modelling analysis.

Relative sea-level

In Chapter 7, the shoreline trajectory (ST1) interpreted from seismic data, which is under investigation in this chapter, was quantified in terms of trajectory angles and elevation. To reconstruct this shoreline trajectory, the shoreline in the model run must span the same elevation range as the observed seismic example as well as similar ascending and descending shoreline trajectory angles. To achieve this the RSL curve specified in the model run was calculated from successive elevation positions of ST1 down dip when the trajectory changed class, for example when switching from descending to horizontal, or descending to ascending, etc.

Time-variable sediment supply

Shoreline trajectories are not controlled purely by changes in accommodation (*Burgess and Steel*, 2008, *Helland-Hansen and Hampson*, 2009, *Helland-Hansen and Martinsen*, 1996). The sediment supply history for NCB through the late Miocene to Plio-Pliestocene is not known (*Cathro et al.*, 2003), so a time-variable sediment supply curve was developed alongside the RSL curve to generate a geometrically similar shoreline trajectory to the seismic example.

TABLE 8.1: Parameter values for 2D shoreline trajectory reconstruction.

Parameter	**Value**
Model dimensions & basin geometry (km)	
Grid length (x-axis)	80
Grid length (y-axis)	1
Grid point spacing	1
Terrestrial transport distance	10
River discharge & supply	
Total sediment supply (km^3My^{-1})	t
River discharge rate (m^3s^{-1})	t
Sediment composition (sand, mud) (%)	20, 80
Weathering rates ($m\ My^{-1}$)	
Gravity weathering rate	1
Water weathering rate	100
Sediment transport rates (km^2ky^{-1})	
Gravity-driven terrestrial k sand	4
Gravity-driven terrestrial k mud	8
Gravity-driven marine k sand	0.05
Gravity-driven marine k mud	0.1
Water-driven terrestrial k sand	8
Water-driven terrestrial k mud	16
Water-driven marine k sand	0.005
Water-driven marine k mud	0.01

t = time-variable
k = diffusion coefficient

8.3.3 Results from 2D shoreline trajectory reconstruction

The seismic line in Figure 8.2a shows a shoreline trajectory (purple, labelled ST1) interpreted from identifying successive shoreline clinoform rollovers. This seismic line has been flattened on an underlying downlap (datum) surface (DLS1), interpreted as an MTS, to help account for any geometric modification the clinoforms may have incurred since deposition through processes such as tectonic tilting and differential compaction. After flattening the shoreline trajectory on the datum surface DLS1, ST1 has been quantified by measuring angles of ascending and descending shoreline trajectory paths (Chapter 7). Figure 8.2b is a schematic diagram of the seismic line in Figure 8.2a with trajectory angles labelled. Overall, the shoreline trajectory from this 30 km dip-orientated seismic line is strongly progradational with ascending and descending trajectory classes averaging $3.1\,^\circ$ and $-3.4\,^\circ$, respectively (Figure 8.2b).

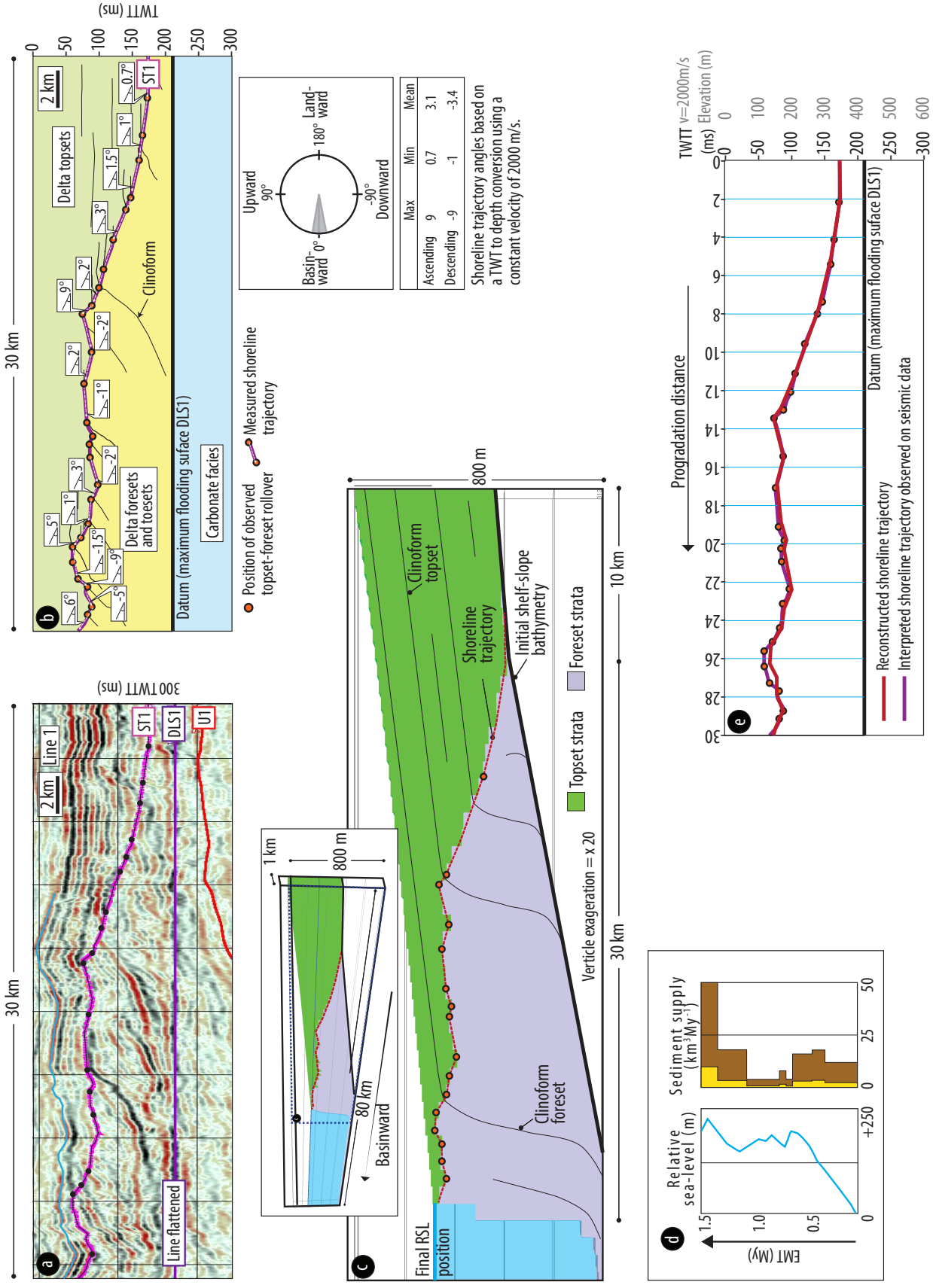
a
30 km
2 km
Line 1
300 TWTT (ms)
ST1
DLS1
U1
Line flattened
b
TWTT (ms)
0
50
100
150
200
250
300
30 km
2 km
Delta topsets
Clinoform
Delta foresets and toesets
Carbonate facies
Datum (maximum flooding suface DLS1)
ST1
Position of observed topset-foreset rollover
Measured shoreline trajectory
Upward 90°
Basin-ward 0°
180° Land-ward
-90° Downward
Max Min Mean
Ascending 9 0.7 3.1
Descending -9 -1 -3.4
Shoreline trajectory angles based on a TWT to depth conversion using a constant velocity of 2000 m/s.
c
1 km
800 m
80 km
Basinward
800 m
Clinoform topset
Shoreline trajectory
Initial shelf-slope bathymetry
Foreset strata
Topset strata
Clinoform foreset
Final RSL position
Verticle exageration = x 20
30 km
10 km
d
Relative sea-level (m)
1.5
1.0
0.5
EMT (My)
+250
0
Sediment supply (km³My⁻¹)
25
50
e
TWTT v=2000m/s (ms) Elevation (m)
Progradation distance
Datum (maximum flooding suface DLS1)
Reconstructed shoreline trajectory
Interpreted shoreline trajectory observed on seismic data

FIGURE 8.2: (Previous page.) Reconsructed shoreline trajectory. A) Flattened shoreline trajectory interpreted from seismic data and (B) quantification of this shoreline trajectory. C) Stratal geometry generated in a 2D Dionisos model with time-variable RSL and sediment supply (D). The modelled shoreline trajectory and the seismic shoreline trajectory show clear similarities (E).

ST1 has been reconstructed in Dionisos to test if the stratigraphic forward model is capable of reconstructing specific stratal geometries observed in the ancient record, thus helping to validate the diffusional representation of sedient transport and deposition in Dionisos. Reconstruction of ST1 is also an investigation into what parameter values for sediment supply, RSL and sediment transport rate are required to generate this shoreline trajectory observed in the NCB (Figure 8.2c). For example, was ST1 controlled predominantly by RSL oscillations or did time-variable sediment supply play an equally important role?

From the multiple experiments required to generate a shoreline trajectory that appeared geometrically similar to ST1 (Figure 8.2a), a time-variable sediment supply history was required (Figure 8.2d). With constant sediment supply the modelled shoreline trajectory looked significantly different to the seismic example despite multiple tests with different durations of RSL change. This in itself is an interesting result, and contradicts the critical implicit assumption of constant sedimentation in sequence stratigraphic models *Catuneanu* (2006), *Catuneanu et al.* (2009, 2011). Direct comparison of ST1 with the modelled reconstruction (generated with time-variable sediment supply) using a simple cross plot shows that they are similar (Figure 8.2e).

The Dionisos reconstruction in Figure 8.2 is founded on the assumption that ST1 is intersecting clinoforms along a progradational axis (*Sydow and Roberts*, 1994), rather than cutting clinoforms obliquely. In practise distinguishing whether a 2D section is intersecting clinoforms obliquely or directly along a progradational axis is likely to be difficult, and interpretations from these different cases may yield quite different interpretations for RSL and supply histories in the system. This issue is illustrated in Figure 8.3, where 4 cross sections W, X, Y and Z intersect clinoforms of a delta at different positions.

Intersecting clinoform rollovers

In Figure 8.3 it is assumed for simplicity that clinoforms 1 to 5 contained within the delta each have a topset-foreset rollover that exhibits no elevation variation along strike. This

is not always the case, for example in some modern high energy settings subaqueous delta clinoforms exist because the shoreline and topset-foreset rollover are laterally separated (e.g., *Cattaneo and Steel*, 2003, *Driscoll and Karner*, 1999). Section W intersects the delta through the main axis of progradation and therefore clinoforms interpreted from this section are likely to give the most accurate account of sediment supply and RSL changes through time (i.e plot W in Figure 8.3B).

Sections X, Y and Z, however, intersect clinoforms obliquely to the main delta progradation axis. Section X is parallel to the main sediment transport axis, but when compared to the clinoforms intersected by section W, it leads to a different shoreline trajectory interpretation and therefore a different reconstruction of sediment supply and RSL change through time. For example, shoreline trajectory from section W suggests either a faster rate of RSL rise or lower sediment supply rate (or both) when compared to the shoreline trajectory in section X (Figure 8.3B). Comparing the shoreline trajectory from section Z with the shoreline trajectory from section W presents a similar issue.

Interpreting a shoreline trajectory from section Y presents a more serious complication for reconstructing RSL and sediment supply histories. Section Y does not intersect the same age clinoforms as W, and this leads to a different shoreline trajectory interpretation. Shoreline trajectory Y has a descending trajectory trend followed by a horizontal and then ascending trajectory trend, indicative of falling, steady and rising RSL history. This contrasts to shoreline trajectory W that displays a steady to rising shoreline trajectory trend and is indicative of steady to rising RSL.

Even assuming identical elevations along strike for each clinoform topset-foreset rollover (elevation labelled 1 to 5 vertically in Figure 8.3B), shoreline trajectories interpreted from oblique sections (X, Y, Z) are different from section W that intersects clinoforms along the main axis of progradation (Figure 8.3E). The examples shown from oblique sections X and Z in Figure 8.3 are relatively simplistic when compared to oblique section Y in the sense that clinoforms ages are intersected from old to young (i.e. 1 to 5). As a result, sections X and Z do produce different shoreline trajectories compared to the axis parallel shoreline trajectory (W), but it is section Y that leads to the most dissimilar shoreline trajectory and hence has the most significant implication for shoreline trajectory analysis and associated stratigraphic interpretation (Figure 8.3C).

Given that many delta systems contain delta lobe complexes caused by river avulsions (e.g., the Mississippi River Delta), it is easy to see how a complicated and oblique cross section, such as Y in Figure 8.3, could be encountered in subsurface datasets. For example, interpreting shoreline trajectories from cross sections through such complex delta lobe systems as shown in Figure 8.4 could be complicated. Some clinoforms, such as those from lobe 4 in Figure 8.4 may be intersected close to the progradational axis, where as other clinoforms may be intersected obliquely (e.g., lobe 3 clinoforms). In yet more complicated settings, where delta lobe evolution is more varied, shoreline trajectory paths could be taken through strata of random ages as a result of delta lobe switching. In contrast to the simple delta lobe case or progressive progradation (albeit from different lobes) in Figure 8.4, the schematic map of the Mississippi River Delta (Figure 8.5) shows a section through lobes of various ages. This cross section could lead to a complicated and somewhat misleading shoreline trajectory because the section intersects delta clinoforms of various ages.

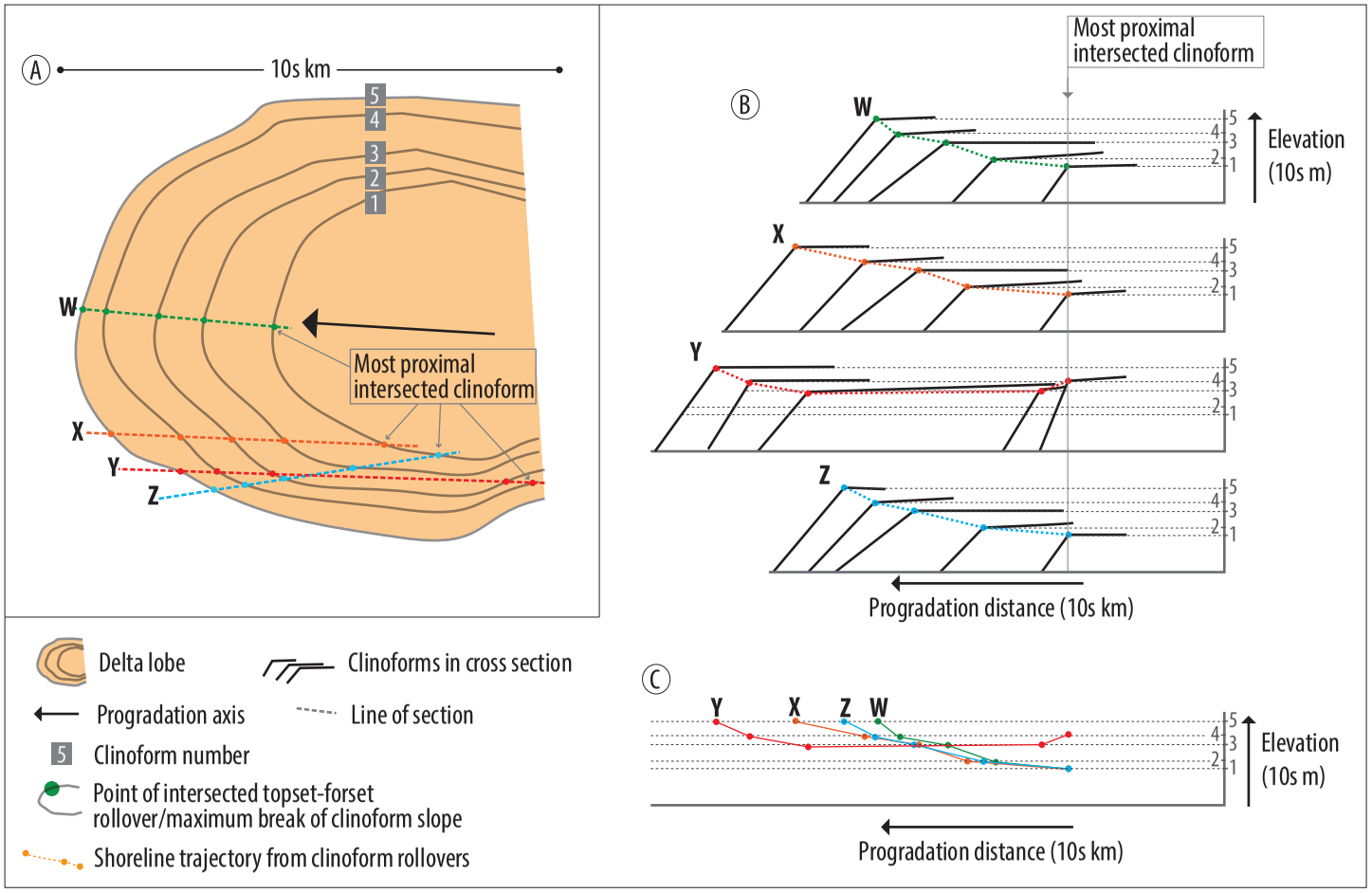

FIGURE 8.3: A) Simplified map of a delta lobe with prograding delta clinoforms. For simplicity, within the delta lobe, clinoform rollovers 1 to 5 are each assumed to have constant elevations along stike (i.e. elevations 1 to 5 in B to E). In A, dip-orientated 2D sections intersect clinoforms of a delta lobe down the main axis of progradation (line X) or obliquely (line Y and Z). Lines Y and Z cross cut clinoform rollovers obliquely, and as a result the shoreline trajectories suggest higher rates of progradation for sections Y and Z compated to X (B to E).

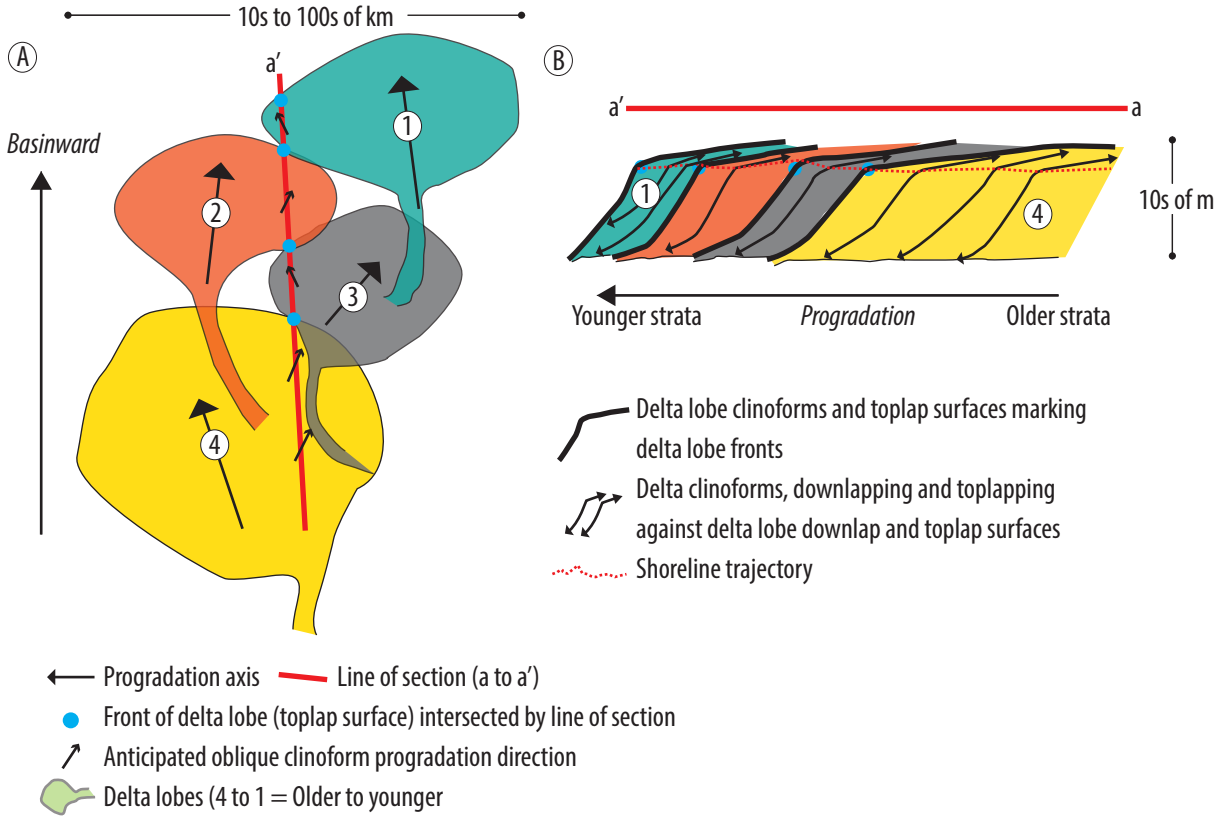

FIGURE 8.4: Cartoon illustrating the potential obliquity of delta clinoforms from 2D cross sections through delta lobe complexes. A) Four delta lobes labelled 1 to 4 each have a central axis of progradation. Cross section from a to a' through these delta lobes does not intersect clinoforms along ther progradation axis. Instead, clinoforms are intersected obliquely. B) Obliquely intersected clinoforms might be difficult to recognise in cross section, and could lead to unreliable interpretations of accommodation and supply history.

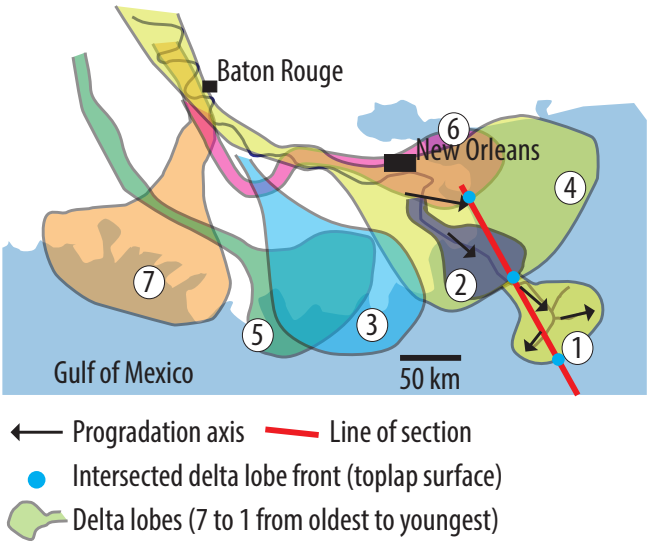

FIGURE 8.5: Schematic map of the Mississippi delta lobes. Modified from *Day et al.* (2007).

8.4 Analysis Part II: Comparison of 2D shoreline trajectories from 3D clinoform geometries

8.4.1 Outline

To investigate consequences of interpreting shoreline trajectories from 2D sections intersecting 3D clinoforms obliquely, rather than along the main axis of sediment transport, 3D numerical modelling of clinoform development is required. Three scenarios of delta progradation are modelled in 3D. The scenarios represent delta progradation of varying complexity, from simple delta progradation to random delta lobe switching. For each of these scenarios shoreline trajectories are interpreted from dip-orientated (strike separated) cross sections and compared to evaluate how shoreline trajectories can vary along strike in different deltaic systems.

8.4.2 3D modelling method & parameter values

Model grid dimensions and initial topography

3D models in this chapter were run on a 40-by-40 grid of 20 km^2 cells, giving a areal extent of 800 km by 800 km. Each model run was executed on a simple ramp topography which has a total relief of 800 m. As with previous multiple model runs described in Chapter 4, this initial ramp topgraphy has a constant slope angle of 0.06 ° which is similar to measured gradients from medium-scale to large-scale river-dominated delta systems (*Reading and Collinson*, 1996).

Sediment supply

For each of the 3D models sediment supply and river discharge rates are similar to values observed from modern rivers (Table 8.2).

River avulsion

Delta lobes are generated by river avulsion in Dionisos, which is simulated using a stochastic random walk parameter. Random walk is analogous to the diffusion process (*Hughes*, 1995), and it can be described as a process of random steps of a defined length (*Weiss*, 1994).

TABLE 8.2: Parameter values for modelled delta scenarios.

Parameter	**Value**		
	Modelled delta scenarios:		
	One	*Two*	*Three*
Model dimensions & basin geometry (km)			
Grid length (x-axis)	800	800	800
Grid length (y-axis)	800	800	800
Grid point spacing	20	20	20
Terrestrial transport distance	100	100	100
Fluvial supply & location			
Total sediment supply (km^3My^{-1})	t	t	6000
River discharge rate (m^3s^{-1})	t	t	1000
Sediment composition (sand, mud) (%)	20, 80	20, 80	20, 80
Weathering rates (m My^{-1})			
Gravity weathering rate	1	1	1
Water weathering rate	100	100	100
Sediment transport rates (km^2ky^{-1})			
Gravity-driven terrestrial k sand	4	4	4
Gravity-driven terrestrial k mud	8	8	8
Gravity-driven marine k sand	0.05	0.05	0.05
Gravity-driven marine k mud	0.1	0.1	0.1
Water-driven terrestrial k sand	75	75	75
Water-driven terrestrial k mud	150	150	150
Water-driven marine k sand	0.05	0.05	0.05
Water-driven marine k mud	0.1	0.1	0.1
Delta lobe switching:			
Random walk:	on	off	off

t = time variable
k = diffusion coefficient

8.4.3 Results: Strike separated shoreline trajectories

Shoreline trajectories interpreted from the Northern Carnarvon Basin

The reconstructed shoreline trajectory in Figure 8.2 is one of three geometrically similar shoreline trajectories interpreted and discussed in the previous chapter (Chapter 7). These three shoreline trajectories are all dip-orientated, but separated along strike by approximately 10 to 20 km. Previous studies have not compared strike-separated shoreline trajectories, but doing so may help to elucidate the style of deltaic progradation and the formation of delta lobes in the NCB during the Plio-Pleistocene.

Previous authors have suggested that delta progradation and formation of strike-separated delta lobes on the pre-existing carbonate ramp in the NCB is a consequence of sediment

supply from a single river and migration of deltaic lobes due to wave influence during rising RSL (*Sanchez et al.*, 2012). However, given the similarity in observed shoreline trajectories, is it possible that this deltaic progradation occurred under different conditions?

Comparison of shoreline trajectories from modelled delta scenarios

To investigate the controls behind the development of similar strike-separated shoreline trajectories in the NCB, three scenarios of delta progradation are illustrated in Figure 8.6. Each scenario has been generated in Dionisos, and the parameter values are listed in Table 8.2. In Scenario One a delta lobe complex is generated by river bifurcation and avulsion during RSL oscillations (Figure 8.6). Scenario One is represented by the Mississippi River Delta, where several delta lobes have been identified and the current birds foot geometry is sourced from the Mississippi River. In contrast, Scenario Two is a simple prograding delta driven by a single point source fluvial feeder during RSL oscillations. This scenario is perhaps best represented by a single delta lobe of the Mississippi River Delta. Scenario Three illustrates a case where three rivers form individual deltas. Though it is more complex, the upper Texas coast within the Gulf of Mexico illustrates this scenario where deltas are fed by the Colorado, Guadalupe and Nuecces rivers.

Scenario One: Delta lobes

The 3D model Scenario One shows a delta lobe complex with an overall fan shape geometry resulting from sediment supply from a single point source. The delta formed during RSL oscillations and the single fluvial feeder has been set to random walk to allow river avulsion and development of delta lobes. Shoreline trajectories are interpreted from three down-dip seismic lines (indicated in red lines in Figure 8.6). Shoreline trajectories interpreted by identifying clinoform rollovers from the different locations look different, and in section b they are difficult to interpret. Scenario One suggest that for a delta with a complex delta lobe system, shoreline trajectories identified in dip-orientated cross-sections from different positions along strike would look different because the cross sections are intersecting clinoforms of various ages. The shoreline trajectory in each section would be determined by the RSL and supply history operating during the deposition of the intersected clinoforms.

Scenario Two: Simple delta or individual delta lobe progradation

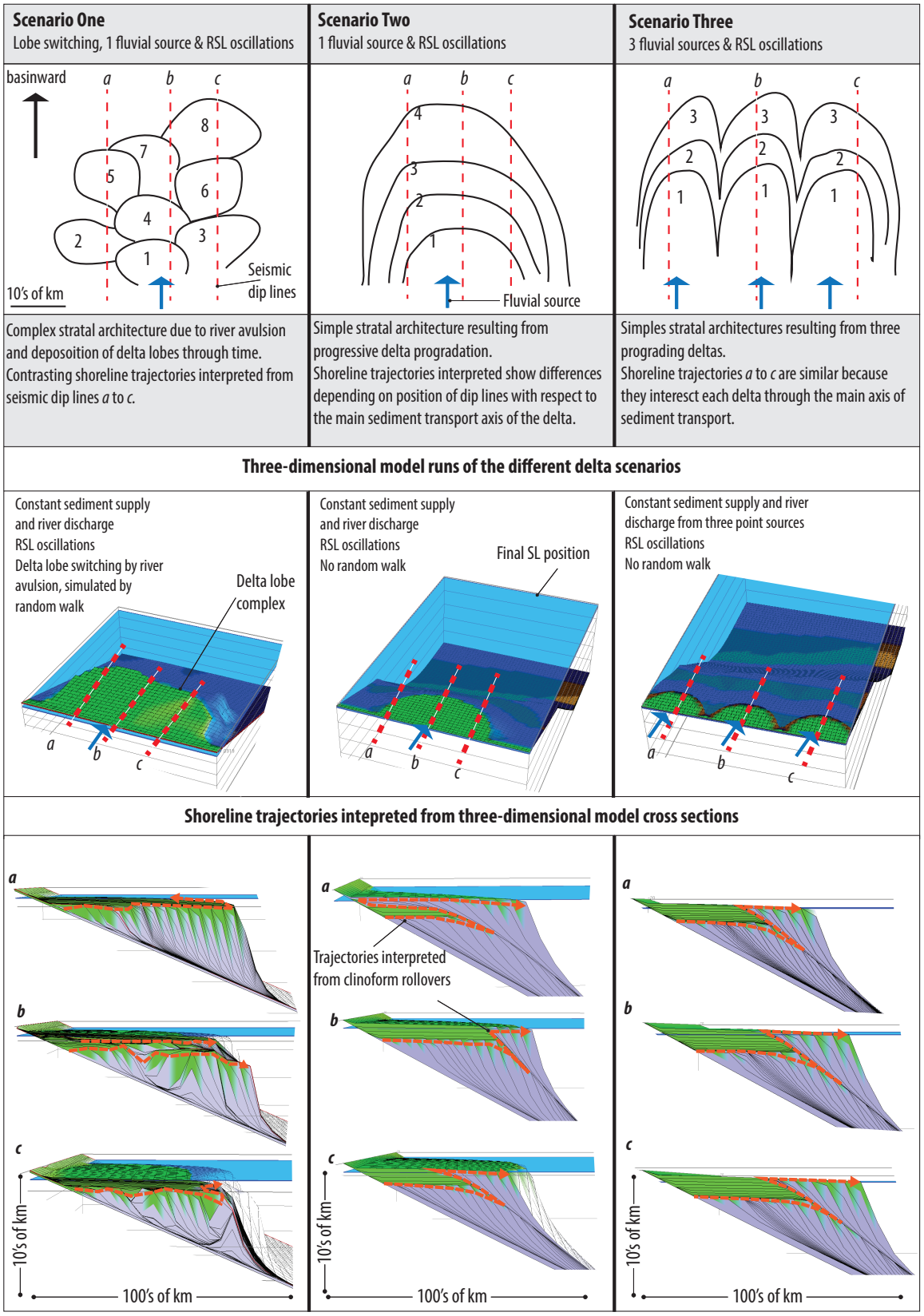

FIGURE 8.6: 3D model scenarios each showing different degrees of shoreline trajectory variability along strike. For each scenario RSL is a sinusoid curve with an amplitude of 25 m over a 2 My period. Sediment supply in each is constant. Parameter values are listed in Table 8.2.

In this scenario the overall shoreline trajectory paths would be expected to look somewhat similar. Shoreline trajectories a to c all show progradation followed by transgression and development of MTSs and then a switch back to progradation. However, sections a and c imply a different magnitude of RSL rise or sediment supply reduction by a more extensive flooding surface compared to the shoreline trajectory in section b. This is because section b intersects clinoforms along the main progradation axis, whereas sections a and c intersect clinoforms obliquely and away from the progradation axis, where sediment supply is reduced. Shoreline trajectories from sections a and c would show more significant differences to shoreline trajectory from section b if the sections where not parallel to the sediment transport axis. This scenario was suggested earlier along with Figure 8.3, where various clinoform ages where intersected by a strongly oblique section (Y in Figure 8.3), and this lead to a quite different shoreline trajectory.

Scenario Three: 3 simple river deltas

With no delta lobe formation and identical sediment supply from 3 point sources along this basin margin, cross sections a to c from Scenario Three all lead to similar shoreline trajectories. This is because shoreline trajectories are interpreted from clinoform rollovers that are along the main progradation axis of each delta, where RSL and sediment supply history are the same for each case (a to c, Figure 8.6; Table 8.2).

8.5 Discussion

Results from a 2D model have demonstrated that Dionisos is capable of reconstructing a shoreline trajectory that closely resembles a shoreline trajectory observed in seismic data. Problems with interpreting shoreline trajectories from obliquely intersected clinoforms have also been highlighted. 3D model runs in Dionisos have shown the potential variability of shoreline trajectories from different positions along strike in a given delta system. In contrast, modelled scenarios have shown situations where shoreline trajectories from different positions along strike can look similar.

8.5.1 Implications of strike variable shoreline trajectories

Depending on the evolution of a deltaic system, strike variable shoreline trajectories could represent a major problem for the method of trajectory analysis (*Helland-Hansen*

and Hampson, 2009). This problem is likely to be greatest in systems which contain strong three-dimensionality, for example due to high-frequency delta lobe switching. The position of the depositional dip orientated cross section will determine how delta clinoforms are intersected, either obliquely or parallel to a progradation axis, which influences the shoreline trajectory interpretation. In most cases, it seems that comparison of shoreline trajectories from different locations along strike is essential to the trajectory method.

8.5.2 Application of along-strike comparative shoreline trajectory analysis

Based on the modelled delta scenarios in this work, similar shoreline trajectories observed in the NCB from different positions along strike suggest that the system was likely to have been fed by more than one river. This contradicts previous studies which interpret delta evolution as a result of sediment supply from one river (*Sanchez et al.*, 2012,). There are other possible explanations for similar shoreline trajectories in this case study. Firstly, multiple shoreline trajectory interpretations may exist for one 2D section due to the descriptive nature of the method (i.e. where exactly is the maximum break in slope?). Secondly, it is possible that Scenario One described in this work (Figure 8.6) is capable of producing similar shoreline trajectories along strike, despite river avulsion operating. In this situation the shoreline trajectories would be the same due to non-uniqueness, being formed by different combinations of parameter values for sediment supply, avulsion, sediment transport and RSL.

8.5.3 Can oblique shoreline trajectories be modelled?

The 2D model shoreline trajectory in this work represents a shoreline trajectory from a progradation axis. However, it also resembles a real world example. An important question is whether it is possible to tell if the real world example is cutting clinoforms obliquely or not. This question relates to reconstruction of delta lobes generally. River avulsion in Dionisos is a stochastic process, and consequently it is not possible to accurately reconstruct a particular delta lobe system. There are alternative stratigraphic forward models but few offer options for deterministic delta lobe modelling. So the shoreline trajectory reconstructed in Dionisos may look similar to the seismic example from

the NCB, however, like all seismic to model reconstructions, it could be non-unique in the sense that it is hard to distinguish between the geometries of the modelled and seismic shoreline trajectory, but they have formed by quite different processes or parameter values.

8.6 Conclusions

Shoreline trajectories are potentially limited for stratigraphic interpretation because they are 2D, yet these features are often used to describe processes of clinoform development occurring in 3D which may lead to significant variability of stratal architectures.

Successful reconstruction of a shoreline trajectory interpreted from seismic in a 2D model suggests that shoreline trajectories may be useful for describing clinoform development in 3D. However, it does not adequately account for clinoform strike variability resulting from variations in volume and style of sediment supply and deposition.

Different scenarios of delta progradation have been modelled in 3D, and shoreline trajectories from different positions along strike in each model have been interpreted and compared. This modelling demonstrates how shoreline trajectories can show significant variability along strike, depending on the nature of delta deposition. Dip-orientated, strike-separated sections through a complex delta lobe system will commonly intersect clinoforms of various ages and hence various RSL and supply histories. Therefore, shoreline trajectories interpreted from these sections will look different, and commonly lead to contrasting RSL and sediment supply reconstructions. In contrast, similar dip-orientated shoreline trajectories along strike may indicate more than one fluvial feeder for the system with similar supply and RSL histories.

Based on the modelled delta scenarios and anticipated shoreline trajectories in this work, similar dip-orientated and strike-separated shoreline trajectories interpreted from the Northern Carnarvon Basin suggests that a history for the region involving complex delta lobe switching sourced by one river is unlikely.

Chapter 9

Thesis Summary

9.1 Introduction

Stratal geometries identified on basin margins are often assumed to be predominately controlled by variations in accommodation (*Catuneanu et al.*, 2009). However, there is increasing evidence to suggest that other controls are also responsible for the formation of stratal geometries (reviewed in Chapter 2). Using a numerical stratigraphic forward model this thesis has investigated the consequences of varying multiple controlling process parameter values on basin-margin stratal geometries, and demonstrated how stratal geometries generated by multiple controls can have implications for sequence stratigraphic methods. This final chapter first summarises the results and analysis presented in each chapter in this thesis. Following these summaries some further analysis will be presented regarding the combined implications of the different results for sequence stratigraphic methods, and for making petroleum system element predictions.

9.2 Summary of Chapter 4 Numerical modelling of topset aggradation

Distinguishing between forced and unforced regressive strata is important for identification of systems tracts, prediction of sediment bypass, and reconstruction of RSL histories. As discussed in Chapter 4, conventional sequence stratigraphic models distinguish between forced and unforced regressive strata through the presence of aggradational topset

(no aggradation during forced regression) and style of shoreline trajectory (descending in forced regressive strata and flat to rising in unforced regressive strata). However, because conventional models contain implicit assumptions about sediment supply and the response of coastal-plain and fluvial deposystems to falling and rising RSL, it is probable that these two scenarios are an oversimplification of a more complex reality.

With a simple diffusional stratigraphic forward model, this chapter investigated how topset aggradation might develop during RSL fall using 1264 model runs with different initial topographies and combinations of parameter values. Model runs were executed on 2D and 3D model grids on both a ramp topography and a topography with a break of slope at the shoreline. Parameter values covered a range of RSL fall amplitudes from 0 to 100 m on both 0.4 and 2 My durations, and for each of these cases, a range of terrestrial diffusion coefficient values from 20 to 200 km^2 kyr^{-1} for sand and 40 to 400 km^2 kyr^{-1} for mud, representing a range of sediment transport rates from low to high based on comparison with modern delta systems (*Kenyon and Turcotte*, 1985). Proportion of deposited and preserved topset strata relative to foreset strata was characterised for each model run using a topset foreset ratio (t/f ratio). When topset strata were present in model runs the t/f ratio was > 0, when no topset strata were present the t/f ratio was zero. This allowed a simple quantitative comparison of topset aggradation across the suite of model runs (e.g., Figure 4.4). To add validation to the hundreds of diffusional modelling results, five single model runs were also executed in a geometric model to establish if topset strata was preserved during RSL fall in an alternative model formulation (Figure 4.14). Finally, three simple shoreline trajectories were subjected to burial in the diffusional numerical model to establish how ascending, horizontal and descending shoreline trajectories might aid distinguishing between forced and unforced regressive strata after differential compaction (Figure 4.16).

The several hundred model runs in Chapter 4 demonstrated that topset aggradation during RSL fall occurs across a wide range of values of terrestrial diffusion coefficients, and across a wide range of amplitudes and durations of RSL fall. Topset aggradation during falling RSL was particularly prevalent in models with sediment transport rates at the low end of what is observed in modern delta systems. The results in Chapter 4 (e.g., Figure 4.4) suggest that falling-stage topset aggradation is likely to be common in ancient strata, and that shoreline trajectories are unlikely to be reliable for aiding distinction

between falling and rising RSL histories because differential compaction during burial modifies original geometries.

9.3 Summary of Chapter 5 Numerical Modelling of Shoreline Trajectories

Shoreline trajectory analysis is an important addition to the original sequence stratigraphic method, not least because it requires fewer implicit assumptions than the original systems-tract approach, which assumes a dominant control of stratal architectures by simple accommodation variations (*Catuneanu*, 2006; Chapter 2). Shoreline trajectories are generally understood to be controlled by bathymetry and variations in supply and accommodation, and are recorded by geomorphic breaks of slope between the sub-horizontal clinoform topset and the dipping foreset (known as clinoform rollovers). Identification of successive clinoform rollovers marks the shoreline migration history (trajectory) and can be used to aid reconstruction of sediment supply and RSL histories. For example, ascending shoreline trajectories suggest supply-driven progradation during rising RSL, whereas descending shoreline trajectories indicate falling RSL.

To add some complication to the concepts of trajectory analysis (*Helland-Hansen and Gjelberg*, 1994), previous work has suggested that, in addition to controls by bathymetry and accommodation and sediment supply variations, sediment transport rates also play a role in determining shoreline trajectory geometries (*Burgess and Steel*, 2008). Furthermore, as highlighted in Chapter 4, post-depositional process during burial, such as tectonic tilting and differential compaction, have the ability to modify shoreline trajectories. Consequently, shoreline trajectory analysis is highly dependent on use of reliable datum surfaces to enable descending, horizontal and ascending trajectory trends (indicative of falling, steady and rising RSL, respectively) to be distinguished.

Chapter 5 applied Dionisos to investigate the impact of variable sediment transport rates on shoreline trajectories. Sets of single model runs were executed with the same time-variable sediment supply and accommodation histories, but differing terrestrial and marine sediment transport rates. To build on work in Chapter 4 regarding burial and post depositional compaction of simple shoreline trajectories, a number of more

complicated shoreline trajectory transits (i.e. repeated progradation and transgression) were modelled and then buried and compacted.

The results demonstrated that sediment transport rates are an important control on shoreline trajectories, because shoreline trajectories created with different sediment transport rates clearly differ from one another despite all other parameters being equal in these runs (Figure 5.6). Burial led to differential compaction of shoreline trajectories, which was shown to have implications for distinguishing between simple trajectory trends (i.e. single descending, horizontal or ascending transits) because ascending and horizontal trajectories were modified to appear descending (Figure 5.9). More complex shoreline trajectories retained their original regressive and transgressive relationships, but any interruption of these shoreline transits (e.g., by growth faults, or imaging problems) would likely lead to interpretation problems (Figure fig:6MyDiffComp). Such modification by differential compaction in the ancient record would be hard to recognise and account for, particularly given the difficulty of accurately backstripping using potentially unreliable paleo-datum surfaces.

9.4 Summary of Chapter 6 Non-unique stratal geometries

Sequence stratigraphy assumes a dominant control by accommodation changes in an attempt to analyse strata within a time-stratigraphic framework of repetitive, genetically related depositional units bounded by surfaces of non-deposition or erosion (*Catuneanu*, 2006, *Catuneanu et al.*, 2009, *Galloway*, 1989, *Posamentier et al.*, 1988). Although advocates of sequence stratigraphy often acknowledge additional controls on formation of stratal geometries, for example by variations in sediment supply, little attempt has been made to consider the implications of variations in multiple controls for the sequence stratigraphic method and model. As a result, non-uniqueness has not received sufficient attention. In the context of siliciclastic sequence stratigraphy, non-uniqueness occurs when similar looking stratal geometries result from different sediment supply and/or accommodation histories. This contrasts to unique stratal geometries, which can only be generated from one possible history of sediment supply and accommodation.

Chapter 6 used Dionisos to address the non-uniqueness issue by investigating the outcome of variations in sediment supply, accommodation and sediment transport rates on the development of four stratal geometries that are integral to sequence stratigraphic interpretation. Modelled stratal geometries included maximum transgressive surfaces (MTS), sequence bounding subaerial unconformities, topset aggradation and shoreline trajectories.

The four stratal geometries were shown to be non-unique because for each surface, stacking pattern and shoreline trajectory, similar stratal geometries were created by different combinations of parameter values. Non-uniqueness for each stratal geometry is summarised below.

Non-unique maximum transgressive surfaces

The MTS was non-unique in the model because similar MTSs were generated either by an increase in the rate of accommodation creation during steady sediment supply (accommodation-driven) or by a reduction in sediment supply during steady increase in accommodation (supply-driven). A similar result was also demonstrated by *Flemings and Grotzinger* (1996). The investigation of non-unique MTSs went further by highlighting the consequences for sequence stratigraphy, concluding that correlation of flooding surfaces not uniquely driven by regional accommodation variations could lead to erroneous correlation of diachronous surfaces.

Non-unique sequence boundaries

Sequence bounding subaerial unconformities were reconstructed in the model by falling RSL or relative high rates of sediment transport during steady RSL. In both cases fluvial incision occurred, creating an erosion surface that when buried formed a sequence bounding unconformity surface. The two cases would be difficult to tell apart in the geological record unless the shoreline trajectory could be reliably interpreted to indicate steady or falling RSL. In both the non-unique cases, sediment partitioning was similar, suggesting that similar styles and volumes of sand can be partitioned across basin-margin stratal geometries for alternative reasons to that suggested by sequence models; as well as sand bypass driven by RSL fall, sand bypass may be driven by changes in climatic conditions and related increases in river discharge rates.

Non-unique topset aggradation

Non-uniqueness of topset aggradation was suggested in Chapter 4. In Chapter 6, non-uniqueness of topset aggradation was taken a step further to show that identical proportions of topset strata were deposited in model runs with either rising, steady or falling RSL, depending on the sediment transport rate. If similar proportions of topset strata can occur across a wide range of RSL histories, this has important implications for how we recognise systems tracts. This issue will be discussed below.

Non-unique shoreline trajectories

Sediment transport rates were shown to be an important control on shoreline trajectories in Chapter 4. This was due to the amount of deposition versus erosion and incision occurring at the shoreline; high sediment transport rates led to erosion at the shoreline and transport of sediment into deeper water depositional systems, whereas low sediment transport rates increased deposition at the shoreline. Non-unique shoreline trajectories, formed by different parameters of RSL, sediment supply and sediment transport rate as well as effects by differential compaction, were then suggested in Chapter 5). Then, in Chapter 6, non-uniqueness of shoreline trajectories was investigated more thoroughly. A simple progradational to retrogradational geometry and a more complex geometry were generated with quite different parameter values demonstrating the exent to which shoreline trajectories may be non-unique (e.g., Figure 6.5). This suggests that extracting reliable information from a given shoreline trajectory may be difficult because multiple possible non-unique solutions may exist.

9.5 Summary of Chapter 8 Reconstruction of a 2D shoreline trajectory & comparison with 3D clinoform geometries

The shoreline trajectory analysis concept relies on the ability to describe 3D clinoform geometries in 2D. However, stratal architectures observed in basin-margin settings often show significant strike variability. Consequently, using shoreline trajectories interpreted from cross sections for understanding and predicting stratal geometries in strongly 3D systems may be more limited than often assumed.

Chapter 8 tested the potential 2D limitation of the shoreline trajectory concept and method by reconstructing a shoreline trajectory interpreted from seismic data using a 2D

numerical model. The logic behind this experiment was that if (as shoreline trajectory analysis assumes) 3D clinoform development can be described accurately with a 2D shoreline trajectory, it should also be possible to accurately describe the progradation of 3D clinoforms using a 2D numerical model.

Following this 2D numerical reconstruction of a shoreline trajectory interpreted from seismic data, three different delta scenarios (delta lobe switching, single point source, and multiple point source) were modelled in 3D to consider how dip-oriented strike-separated shoreline trajectories might differ in a range of deltaic scenarios. For each of these delta scenarios shoreline trajectories were interpreted from dip-orientated strike-separated cross sections, and compared to consider the impact different styles of delta progradation have for obtaining reliable information regarding sediment supply and RSL history from shoreline trajectories.

The numerical model Dionisos was capable of accurately reconstructing in 2D the shoreline trajectory interpreted from seismic data (Figure 8.2). Accurate reconstruction of 3D clinoform development in 2D suggests that the concept of shoreline trajectory analysis (i.e. that 3D clinoform developent can be described in 2D) is a reasonable assumption. However, the 3D modelling of the three delta scenarios and comparison of strike-separated shoreline trajectories for the different cases does not support this assumption.

Variability of dip orientated shoreline trajectories along strike in delta scenarios one and two demonstrate that assuming a single 2D shoreline trajectory can describe 3D clinoform development is not reliable (Figure 8.6). So, although it may be possible to reconstruct a single shoreline trajectory in 2D with specific parameters of RSL and sediment supply, this 2D model is unlikely to fit other 2D shoreline trajectories in a 3D system.

Considering any scenario of delta lobe switching (e.g., Scenario One in Figure 8.6) highlights the problem with the 2D assumption of shoreline trajectories described above. This is due to the temporal and spatial variability of sediment deposition and erosion occurring during formation of each lobe; cross sections intersecting various lobes will consequently have different shoreline trajectories.

Scenario Two illustrated that different shoreline trajectories can also occur in a simple case of delta progradation (or an individual delta lobe), because shoreline trajectories

are likely to intersect clinoform rollovers at different obliquities to the central progradation axis. For the simple delta progradation scenario (Scenario Two), a more extreme case of oblique clinoform intersection and resulting shoreline trajectory was illustrated schematically by section Y in Figure 8.3. The reason for the variability of section Y's shoreline trajectory was because section Y intersected clinoforms of various ages. This contrasts to a shoreline trajectory from a section through the main axis of delta progradation (e.g., section W in Figure 8.3), which is more likely to intersect clinoforms aged from old to young.

Scenario Three illustrated an exception to this 3D variability. Dip-orientated shoreline trajectories from different positions along strike looked similar. This was because the sections intersected three deltas along their main progradation axis, and because each delta had an identical supply and was influenced by an identical RSL history.

Considering the three delta scenarios in Figure 8.6, and comparison of their dip-orientated shoreline trajectories described above (Figure 8.6), similar shoreline trajectories observed from different positions along strike in the NCB dataset in Chapter 7 suggest an alternative interpretation for the deltaic evolution in the NCB. Previous studies advocate a complex history of delta lobe switching and northwest, along strike lobe migration (e.g., *Sanchez et al.*, 2012), but it seems unlikely that similar shoreline trajectories could be generated in this scenario (e.g., Scenario One, Figure 8.6).

Analysis in Chapter 8 suggested that using single 2D shoreline trajectory examples to describe 3D clinoform development is unlikely to be realistic. This is because shoreline trajectories from sections through simple cases of delta progradation or through more complex delta lobe architectures will intersect clinoforms obliquely. Shoreline trajectories from such oblique sections are not likely to be the same as shoreline trajectories interpreted from sections through the main axis of delta progradation. Consequently, information extracted from these different shoreline trajectories (i.e axis parallel versus oblique) regarding RSL and supply history is likely to contrast.

9.6 Consequences of modelled stratal geometries for sequence stratigraphy

9.6.1 Identification of systems tracts

The siliciclastic systems tract concept aims to provide a linkage between contemporaneous depositional systems (*Catuneanu*, 2006), because systems tracts correspond to 'genetic stratigraphic units that incorporate strata deposited within a synchronous sediment dispersal system' (*Galloway*, 2004). Like many aspects of sequence stratigraphy, the systems tract approach assumes a dominant control by accommodation (*Catuneanu et al.*, 2009), and that sediment distribution within a basin (sediment dispersal systems, *Galloway*, 2004) is constant during the deposition of each systems tract. There are several ways in which the results from this thesis complicate the system tract concept and make distinguishing between the systems tracts difficult.

Contemporaneous system tract deposition?

Sequence boundaries (SB) and maximum transgressive surfaces (MTS) are significant indicators of falling-stage and transgressive systems tracts, respectively. In seismic data, SBs are identified by truncation of underlying stratal terminations, and MTSs are recognised by downlapping stratal terminations. However, non-uniqueness of these two important surfaces (Chapter 6) has implications for the systems tract methodology.

Non-unique MTSs complicate the systems tract concept by leading to different system tract formation contemporaneously along a single basin margin. Consider a basin margin experiencing RSL rise, with two rivers separated along strike by several kilometres to several tens of kilometres. River one has a high volume of constant sediment supply while river two experiences a shut-down in sediment supply. At the locality of river one, high volumes of sediment supply lead to normal regression and delivery of sand to the marine slope. Meanwhile the second river generates a supply-driven MTS. These two stratal geometries would lead to different system tract labels for contemporaneous strata at different locations in the same sedimentary basin margin.

Complications of non-uniqueness for system tract definition

The falling-stage systems tract (FSST) is assumed to be distinctive and easily identifiable from lowstand (LST), highstand (HST) and transgressive (TST) systems tracts because

it is the only systems tract to lack aggradational topset strata and be capped above by a subaerial unconformity (*Catuneanu*, 2002, *Hunt and Tucker*, 1992). However, modelling results in Chapter 4 add to the growing evidence from model- and field-based studies that disagree with the systems tract definitions (Chapter 4 and references therein), because topset aggradation occurs across a wide range of amplitudes and durations of RSL fall. This means that not only is topset aggradation present in strata deposited during falling RSL, but also that a subaerial unconformity is absent in modelled FSSTs. This directly contradicts the FSST definition described above (*Catuneanu*, 2002, 2006, *Catuneanu et al.*, 2009, *Hunt and Tucker*, 1992, *Posamentier et al.*, 1992). Consequently, distinguishing the FSST from other systems tracts is likely to be difficult because FSST, HST, LST and TST will all contain topset aggradation strata. Non-unique subaerial unconformities demonstrated in Chapter 5 also complicate the systems tract definitions. Identifying a subaerial unconformity would not be uniquely indicative of a FSST, because it could occur at any point during a RSL cycle due to increased fluvial discharge and therefore be present in any systems tract. If this is the case, other features are required to identify those systems tracts.

Shoreline trajectories

One key feature that may help alleviate the systems tract identification issue described above is the shoreline trajectory. However, as discussed in chapters 4,5, and 7 shoreline trajectories can be easily modified during burial, and their interpretation is not straightforward.

System tract identification & implications for petroleum system elements

If systems tracts are difficult to distinguish then this may have important implications for prediction of petroleum system elements. For example, sequence stratigraphic models predict that deposition of reservoir sands occurs primarily during the FSST. Clearly this is an over simplification (e.g., *Burgess and Hovius*, 1998, *Burgess and Steel*, 2008, *Covault and Graham*, 2010, *Porbski and Steel*, 2006, *Posamentier et al.*, 1991), but if we assume for the moment the model prediction is correct, indistinguishable systems tracts would make this predictive element of the model difficult to apply.

9.7 Implications for predicting petroleum system elements

Sequence stratigraphy is widely used as a predictive tool for determining the likely presence of source rocks, and the distribution of reservoirs and seals. However, if stacking patterns and stratigraphic surfaces of sequence stratigraphic significance are non-unique, and identification of systems tracts may be more difficult than often assumed, an important question is how these issues impact our ability to predict petroleum system elements. Some key issues are discussed below, and summarised in Table 9.1.

Prediction of favourable source rock environment

Non-unique MTSs (i.e. both supply driven and accommodation driven examples that are difficult to distinguish) are problematic for predicting favourable source rock environments. Source rocks are likely to occur in condensed sections formed during generation of MTSs because dilution of organic material is minimised during these low-sedimentation rate events (*Catuneanu*, 2006). Having identified a MTS and source rock interval at a particular location, assuming MTSs are uniquely accommodation-driven and hence isochronous would suggest that a source rock will be present at an alternative location at the same chronostratigraphic interval. However, if diachronous MTSs can form by a shut down in sediment supply locally, and independently of regional changes in accommodation, the basis for this source rock prediction becomes less tenable. For example, MTSs seen in different locations along a basin margin may differ in age to the extent that global or regional ocean anoxic events present during one flooding event may not still be occurring during another.

Regional seals

During periods of regional maximum flooding (i.e. accommodation-dominated MTSs) high sea-level precipitates deposition of fine-grained lithologies (and hence candidate seals) in more proximal areas. However, if supply-driven MTSs are not distinguishable from accommodation-driven MTSs, than what are local seals could be misinterpreted as regional seals assumed to have resulted from basin wide flooding.

Predicting sand partitioning to marine slope and deepwater settings

The assumption that significant bypass and deposition of sand to deepwater depositional systems is most common during periods of RSL lowstand (e.g., *Catuneanu et al.*, 2009, *Posamentier et al.*, 1992) has been called into question by previous studies. This is due

Non-unique stratal geometries		Interpretation of petroleum system elements		
Name	***Mode of formation***	***Seal***	***Reservoir***	***Source***
Maximum transgressive surface	**Accommodation-driven** - increase in rate of RSL rise during constant sediment supply (conventional model)	Regional contemporaneous seal occurrence due to regional RSL rise	Reduced chance of deep-water sand deposition at time of flooding event. High sediment supply volumes and discharge rates required	Regional source rock conditions
	Supply-driven - shut-down in sediment supply during constant RSL rise	Perhaps only local sealing potential.	Reduction in sediment supply during RSL rise suggests a period of low reservoir potential	Local source rock conditions not definitely regional for that MTS interval
Sequence bounding subaerial unconformity	**Accommodation driven** - falling RSL drives fluvial erosion and incision (conventional mode)	(Conventional interpretation) Period of RSL fall provides potential for fluvial incision regionally, providing sand fills (reservoir) sealed by valley walls & capped by transgressive shales	Conventional lowstand model-suggests deepwater reservoirs developed regionally or even globally	Moderate source potential (pelagic deepwater)
	Climate-driven - erosion and incision during steady RSL due to increased *k*	Above interpretation is not tenable for a local sequence boundary.	High percent sand partitioning to deepwater locally	Improved when compared to the accommodation-driven case
Topset aggradation	Aggradation during steady to rising RSL (conventional systems tract model)	Good at highstand (e.g., overbank facies). Otherwise poor	Good reservoir potential within topset at HST, LST & TSST. Assumed bad at FSST	Low potential
	Aggradation during falling RSL due to low *k*	Generally poor due to high sand/mud ratio	Good at all systems tracts, due to low *k*	Low potential
Shoreline trajectory	Combinations of parameter values of accommodation, supply and *k*	Multiple possible interpretations of sediment supply and accommodation history. Conflicting information for predicting petroleum system elements		

FIGURE 9.1: Implications of non-unique stratal geometries demonstrated in Chapter 6 for the interpretation of petroleum system elements.

to the fact that shelf-edge delta formation and associated deepwater sand deposition is also likely to occur during RSL highstands, particularly in basin settings with narrow shelves, as a result of high rates of fluvial sediment supply, fluvial discharge and shelf transport (e.g., *Burgess and Steel*, 2008, *Burgess et al.*, *Covault and Graham*, 2010, *Porbski and Steel*, 2006, *Posamentier et al.*, 1991).

Formation of aggradational topset strata during RSL lowstands as demonstrated in Chapter 4 is an additional complication in the conventional sequence stratigraphic model. This is because, as well as regular sand deposition to deepwater systems during highstands of RSL, falling-stage topset aggradation due to low sediment transport rates suggests reduced volumes of sand deposition to deepwater systems during RSL lowstands. So, not only might sand bypass be common at highstands, bypass volumes may be less than commonly assumed at lowstands.

Model One and Model Two in Figure 9.2 illustrate two examples of sediment partitioning during falling RSL. The two model runs have been selected from the multiple model runs presented in Chapter 4, however, here the sand distribution is also considered, and plotted to show the proportion of the strata composed of sand in each case. Model One, generated with a 50 m amplitude RSL fall, constant sediment supply and relatively high sediment transport rates leads to a stratal geometry with a subaerial unconformity and no topset strata, reflected by the t/f ratio of zero. Sand distribution for Model One consists of high net:gross delta foresets with up to 30 to 40% sand, and net:gross of 25% in the toeset basin floor strata. Model One is similar to the conventional sequence stratigraphic model in the sense that a subaerial unconformity has formed along with high volumes of sediment bypass as a result of RSL fall. In contrast to Model One, Model Two shows different sand distribution despite an identical accommodation and supply history to Model One. This is a result of topset aggradation during RSL fall, which has reduced the volumes of sand partitioned to the delta foresets and toesets.

If topset aggradation is common in forced regressive strata and volumes of sand deposited to deepwater environments during periods of RSL lowstand are lower than assumed, this could lead to prediction errors during exploration for deepwater reservoir sands. For example, by following a sequence stratigraphic framework, identification of a stratal geometry represented by model one (subaerial unconformity, no topset strata) suggests high volumes of sand deposition to deepwater depositional systems on a regional scale

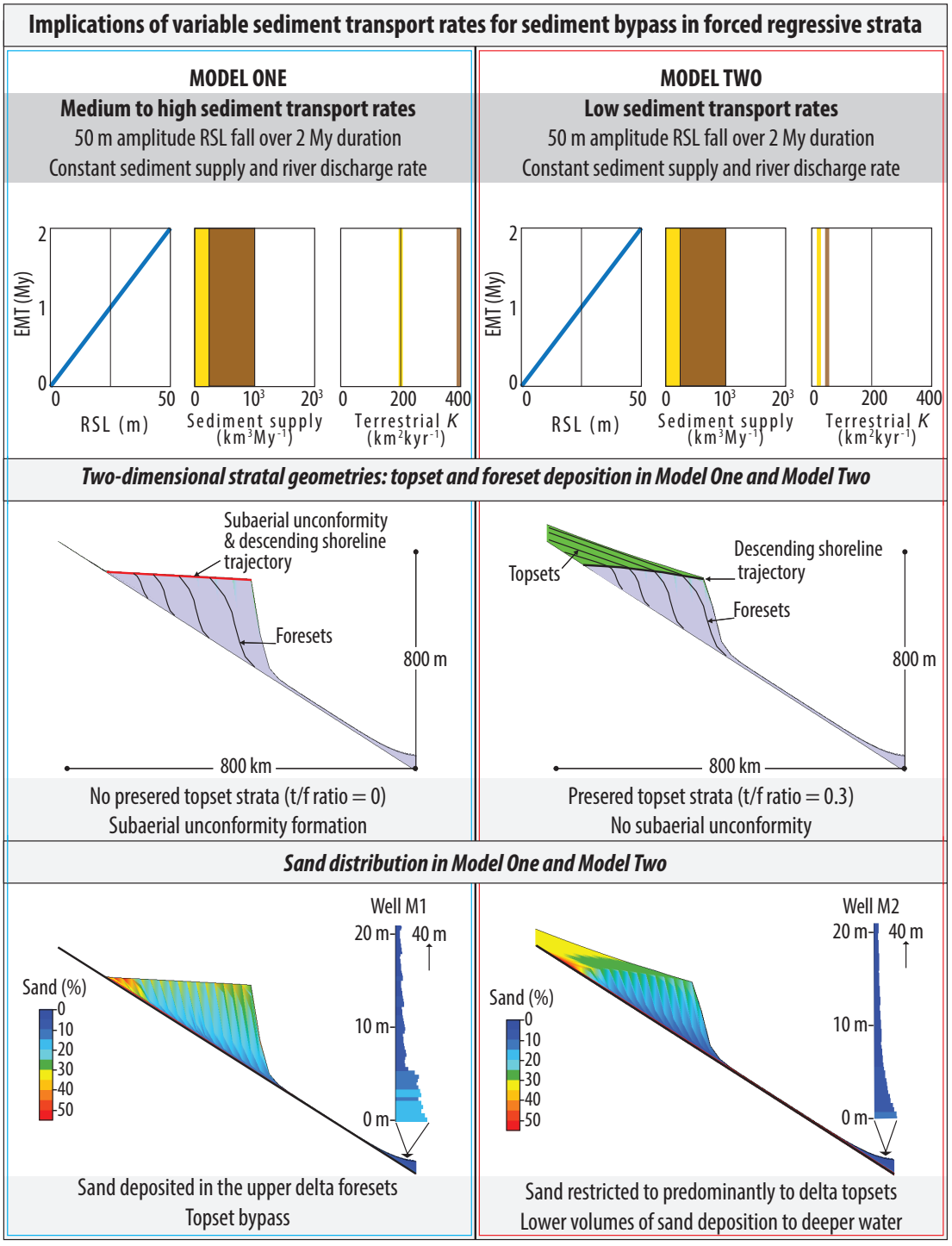

FIGURE 9.2: Summary diagram using results from Chapter 4 to illustrate the consequences of falling-stage topset aggradation for predicting sediment partitioning in forced regressive strata. Model One, generated with high terrestrial diffusion coefficients representing high sediment transport rates in the terrestrial topset environment, has no topset strata preserved and relatively high proportions of sand grade sediment is deposited to the delta foresets and deep marine environment (Well M1). In contrast, Model Two generated with low terrestrial diffusion coefficients shows low amounts of sand deposition to delta foresets and deeper water due to topset aggradation during falling RSL. Scale is the same of all model cross sections. Model One and Model Two have the same parameter values for sediment supply and amplitude and duration of RSL fall.

due to a RSL lowstand. However, the situation for that RSL lowstand interval may be quite different. For example, rivers along a basin margin may be aggrading due to relatively high sediment supply volumes and/or relatively low river discharge rates (leading to low rates of sediment transport). In this case there will be less regional sediment bypass and lower potential for development of contemporaneous deepwater sand reservoirs.

9.8 Final conclusions

- Several hundred numerical simulations of forced and unforced regressive strata demonstrate that topset aggradation can occur across a wide range of terrestrial diffusion coefficients and amplitudes and durations of RSL fall. The results suggest that falling-stage topset aggradation is likely to be common in ancient strata.

- Shoreline trajectories interpreted from strata generated in numerical models with a range of terrestrial and marine diffusion coefficients for different RSL histories suggest that sediment transport rates may be an important control on shoreline trajectories. This is because strata with quite different shoreline trajectories are generated in models with identical RSL and supply histories, but differing terrestrial or marine diffusion coefficients.

- Differential compaction of shoreline trajectories generated in the numerical model demonstrates that individual shoreline transits, such as horizontal or ascending shoreline trajectories, can be geometrically modified to the extent that the original horiztonal or ascending shoreline trajectories appear descending. Results suggest that more complicated shoreline trajectories (i.e. repeated regressive and transgressive transits) subjected to differential compaction will still exhibit the same general shoreline trajectory trend, but interpreting likely amplitudes of RSL variations may be unreliable.

- Results from this thesis also show how a maximum transgressive surface (MTS), a sequence bounding unconformity (SB), topset aggradation and shoreline trajectories can be non-unique stratal geometries. MTSs are generated due to an increase in rate of RSL rise during constant sediment supply and an increase in rate of sediment supply during steady rise in RSL. SBs are generated due to falling RSL

with relatively low rates of sediment transport and steady RSL with relatively high rates of sediment transport. Similar volumes of topset strata are generated in model runs with a range of amplitudes of rising and falling RSL, depending on the sediment transport rate, and similar shoreline trajectories are generated in models with different sediment supply and accommodation histories. Non-uniqueness presents a serious problem for sequence stratigraphy because it challenges our ability to extract a single, unique solution from the stratigraphic record. Extracting information from the stratigraphic record using these non-unique stratal geometries, for example to better understand sediment bypass and RSL histories, is not likely to be reliable. Non-uniqueness also makes it difficult to assign chronostratigraphic significance to stratigraphic surfaces which has implications for our ability to correlate strata.

- Three modelled scenarios of delta progradation demonstrate how shoreline trajectories interpreted from different dip orientated cross sections in a delta system can show significant variability. This variability exists because delta progradation is a three-dimensional process that can lead to complicated spatial and temporal sediment deposition and erosion (e.g., lobe switching). If shoreline trajectories from a single delta system can look different, then interpreting accommodation and supply histories from shoreline trajectories is not a reliable method for understanding clinoform development in three dimensions.

9.9 Future considerations

This thesis has investigated controls on stratal geometries using a numerical stratigraphic forward model based on a modified diffusion equation of sediment transport. As discussed in relevant chapters through the thesis, an important consideration for the realism of the results presented here is how plausible the diffusion approach is for representing various process of basin margin sediment transport. A useful test for any numerical modelling work is to repeat experiments in an alternative model formulation. This was done in Chapter 4 with a simple geometric model. Given the implications of issues highlighted in this work for sequence stratigraphy, it would be valuable to further test results presented here with other numerical stratigraphic forward models that are not based on simple predefined geometries or modified diffusion formulations (examples

listed in Table 3.1, Chapter 3). In addition to further numerical experiments, it would be interesting to investigate to what extent flume tanks generate non-unique stratal geometries.

Parameter values tested through the thesis have represented geological examples of passive margins. Going forward, it would be useful to run similar numerical experiments with parameter values representative of present day continental margins, particularly given that few ramp margins exist today. For example, similar experiments presented here could be run with values for dip of shelf and slope from modern margins. The fastest RSL fall or rise modelled in this thesis has been around 100 m/400 Kyr^{-1}. However, some recent icehouse period RSL changes are on the sub-400 Kyr^{-1} time scale with strongly asymmetric profiles, so it would be interesting to re-run models in this thesis with these parameter values. Finally, validation of the modelled falling-stage topset aggradation with real world examples would be a useful realisation.

The suggestion from many of the points raised in this work is the requirement for modification of the sequence stratigraphic methods so that the full range of possibilities presented by issues of non-uniqueness are incorporated. Factors such as sediment supply variations through time and variable sediment transport rates are often mentioned in the mainstream sequence stratigraphic literature, yet few attempts (e.g., *Burgess et al.*, 2006, *Falivene et al.*, 2014) have been made to constructively address the limitations of sequence stratigraphy.

Bibliography

Allen, P. A., and J. R. Allen (2005), *Basin analysis: principles and applications*, 451 pp., Blackwell Scientific, Oxford.

Ames, W. F. (1977), *Numerical Methods for Partial Differential Equations*, second ed., 365 pp., Academic Press, Florida.

Barrell, J. (1917), Rhythms and the measurement of geologic time, *Geological Society of America Bulletin*, pp. 745–904.

Best, J. L., and P. J. Ashworth (1997), Scour in large braided rivers and the recognition of sequence stratigraphic boundaires, *Nature*, *387*, 275–277.

Blum, M. D. (1994), Genesis and architecture of incised valley fill sequences: a Late Quaternary example from the Colorado River, Gulf Coastal Plain of Texas, in *Siliciclastic sequence stratigraphy: recent developments and applications*, edited by P. Weimer and H. Posamentier, 58 ed., pp. 259–283, American Association of Petroleum Geologists Memoir.

Blum, M. D., and T. E. Törnqvist (2000), Fluvial responses to climate and sea-level change: a review and look forward, *Sedimentology*, *47*, 2–48.

Boldrin, A., L. Langone, S. Miserocchi, M. Turchetto, and F. Acri (2005), Po River plume on the Adriatic continental shelf: Dispersion and sedimentation of dissolved and suspended matter during different river discharge rates, *Mediterranean Prodelta Systems*, *222-223*(0), 135–158.

Bradshaw, M., A. Yeates, R. Beynon, A. Brakel, R. Langford, J. Totterdel, and M. Yeung (1988), Paleogeographic evolution of the North West Shelf region, in *The North West Shelf Australia, Proceedings North West Shelf Symposium*, edited by P. Purcell and R. Purcell, pp. 29–54, Perth.

Brown, L. F., and W. L. Fisher (1977), Seismic-stratigraphic interpretation of depositional systems: examples from Brazilian rift and pull-apart basins, in *Seismic stratigraphy: applications to hydrocarbon exploration*, edited by C. Payton, american a ed., pp. 213–248, American Association of Petroleum Geologists.

Burgess, P. M., and P. a. Allen (1996), A forward-modelling analysis of the controls on sequence stratigraphical geometries, *Geological Society, London, Special Publications*, *103*(1), 9–24.

Burgess, P. M., and N. Hovius (1998), Rates of delta progradation during highstands: consequences for timing of deposition in deep-marine systems, *Journal of the Geological Society, London*, *155*(2), 217–222.

Burgess, P. M., and R. Steel (2008), Stratigraphic forward modeling of basin margin clinoform systems: Implications for controls on topset and shelf width and timing of formation of shelf-edge, *Society of Economic Paleontologists and*, *90*, 1–12.

Burgess, P. M., M. Gurnis, and L. Moresi (), Formation of sequences in the cratonic interior of North America by interaction between mantle, eustatic, and stratigraphic processes, *Geological Society of America Bulletin*, *109*(12), 1515–1535.

Burgess, P. M., H. Lammers, C. van Oosterhout, and D. Granjeon (2006), Multivariate sequence stratigraphy: Tackling complexity and uncertainty with stratigraphic forward modeling, multiple scenarios, and conditional frequency maps, *AAPG Bulletin*, *90*(12), 1883–1901.

Burton, R., C. Kendall, and I. Lerche (1987), Out of our depth: on the impossibility of fathoming eustasy from the stratigraphic record, *Earth Science Review*, *24*, 237–277.

Cant, D. J. (1991), Geometric modelling of facies migration: theoretical development of facies successions and local unconformities, *Basin Research*, pp. 51–62.

Carvajal, C., and R. Steel (2009), Shelf-Edge Architecture and Bypass of Sand to Deep Water: Influence of Shelf-Edge Processes, Sea Level, and Sediment Supply, *Journal of Sedimentary Research*, *79*(9), 652–672.

Carvajal, C., R. Steel, and A. Petter (2009), Sediment supply: The main driver of shelf-margin growth, *Earth-Science Reviews*, *96*(4), 221–248.

Carvajal, C. R., and R. J. Steel (2006), Thick turbidite successions from supply-dominated shelves during sea-level highstand, *Geology*, *34*, 665.

Cathro, D. L., and J. A. Austin (2001), An early mid-Miocene , strike-parallel shelfal trough and possible karstifcation in the Northern Carnarvon Basin , northwest Australia, *Marine Geologyne*, *178*, 157–169.

Cathro, D. L., and G. D. Karner (2006), CretaceousTertiary inversion history of the Dampier Sub-basin, northwest Australia: Insights from quantitative basin modelling, *Marine and Petroleum Geology*, *23*(4), 503–526.

Cathro, D. L., J. a. Austin, and G. D. Moss (2003), Progradation along a deeply submerged OligoceneMiocene heterozoan carbonate shelf: How sensitive are clinoforms to sea level variations?, *AAPG Bulletin*, *87*(10), 1547–1574.

Cattaneo, A., and R. J. Steel (2003), Transgressive deposits: a review of their variability, *Earth-Science Reviews*, *62*(3-4), 187–228.

Catuneanu, O. (2002), Sequence stratigraphy of clastic systems: concepts, merits and pitfalls, *Journal of African Earth Sciences*, *35*, 1.

Catuneanu, O. (2006), *Principles of Sequence Stratigraphy*, 1st ed., Elsevier B.V, AMSTERDAM.

Catuneanu, O., et al. (2009), Towards the standardization of sequence stratigraphy, *Earth-Science Reviews*, *92*(1-2), 1–33.

Catuneanu, O., et al. (2010), Sequence stratigraphy: common ground after three decades of development, *First Break*, *28*(January), 21–34.

Catuneanu, O., W. E. Galloway, C. G. S. C. Kendall, A. D. Miall, H. W. Posamentier, A. Strasser, and M. E. Tucker (2011), Sequence Stratigraphy: Methodology and Nomenclature, *Newsletters on Stratigraphy*, *44*(3), 173–245.

Covault, J. a., and S. a. Graham (2010), Submarine fans at all sea-level stands: Tectono-morphologic and climatic controls on terrigenous sediment delivery to the deep sea, *Geology*, *38*(10), 939–942.

Cross, T. A., and M. A. Lessenger (1999), Construction and application of a stratigraphic inverse model, in *Numerical Experiments in Stratigraphy Recent Advances in*

Stratigraphic and Sedimentologic Computer Simulations, edited by J. W. Harbaugh, W. L. Watney, E. C. Rankey, R. Slingerland, R. H. Goldstein, and K. E. Franseen, 62, special pu ed., pp. 69–83, SEPM.

Curray, J. (1964), Transgressions and regressions, in *Papers in Marine Geology*, edited by R. Miller, pp. 175–205, Macmillan, New York.

Curtis, D. (1970), Miocene deltaic sedimentation, Louisiana Gulf Coast, in *Deltaic sedimentation modern and ancient*, edited by J. P. Morgan, special pu ed., pp. 293–308, Society of Economic Paleontologists and Mineralogists.

Day, J. W. J., et al. (2007), Restoration of the Mississippi Delta: Lessons from Hurricanes Katrina and Rita, *Science*, *315*(5819), 1679–1684.

Driscoll, N. W., and G. D. Karner (1998), Lower crustal extension across the Northern Carnarvon basin, Australia: Evidence for an eastward dipping deatchment, *Journal of Geophysical Research*, *103*, 4975–4991.

Driscoll, N. W., and G. D. Karner (1999), Three-dimensional quantitative modeling of clinoform development, *Marine Geology*, *154*(1-4), 383–398.

Edmonds, D. a., J. B. Shaw, and D. Mohrig (2011), Topset-dominated deltas: A new model for river delta stratigraphy, *Geology*, *39*(12), 1175–1178, doi:10.1130/G32358.1.

Emery, D., and K. J. Myers (1996), *Sequence Stratigraphy*, 297 pp., Blackwell, Oxford, UK.

Falivene, O., A. Frascati, S. Gesbert, J. Pickens, Y. Hsu, and A. Rovira (2014), Automatic calibration of stratigraphic forward models for predicting reservoir presence in exploration, *AAPG Bulletin*, *20*.

Flemings, P., and J. Grotzinger (1996), STRATA: Freeware for analyzing classic stratigraphic problems, *GSA TODAY*, *6*(12).

Flemings, P. B., and T. E. Jordan (1989), A synthetic stratigraphic model of foreland basin development, *Journal of Geophysical Research*, *94*(B4), 3851–3866.

Frazier, D. E. (1974), Depositional episodes: their relationship to the Quaternary stratigraphic framework in the northwestern portion of the Gulf Basin, *University of Texas at Austin, Bureau of Economic Geology, Geological Circular*, *4*(1), 28.

Galloway, W. E. (1989), Genetic stratigraphic sequences in basin analysis, I. Architecture and genesis of flooding-surface bounded depositional units, *American Association of Petroleum Geologists Bulletin*, *73*, 125–142.

Galloway, W. E. (2004), Accommodation and the sequence stratigraphic paradigm, *Reservoir, Canadian Society of Petroleum Geologists*, *31*(5), 9–10.

Grabau, A. W. (1913), *Principles of stratigraphy*, 1185 pp., A. G. Seiler, New York.

Granjeon, D. (2002), 3D Stratigraphic of deep-water settings: comparison of ancient and modern case studies, in *American Association of Petroleum Geologists, International Conference, Houston (U.S.A.)*.

Granjeon, D., and P. Joseph (1999), Concepts and applications of a 3D multiple lithology, diffusive model in stratigraphic modeling, in *Numerical Experiments in Stratigraphy: Recent Advances in Stratigraphic and Sedimentologic Computer Simulations*, vol. 62, edited by J. Harbough, W. Watney, E. Rankey, R. Slingerland, R. Goldstein, and E. Franseen, 62 ed., pp. 197–210, SEPM (Society for Sedimentary Geology).

Griffiths, C. M., C. Dyt, E. Paraschivoiu, and K. Liu (2001), Sedsim in Hydrocarbon Exploration, in *Geological Modeling and Simulation*, edited by D. Merriam and J. C. Davies, pp. 71–97, Kluwer Academic Publishers, New York.

Griffths, C. M., and E. Paraschivoiu (1998), Three-dimensional forward stratigraphic modelling of Early Cretaceous sedimentation on the Leveque and Yampi Shelves, Browse Basin, *The Australian Petroleum Production and Exploration Association Journal*, *38*, 47–158.

Hampson, G. J., P. J. Sixsmith, R. L. Kieft, C. a. L. Jackson, and H. D. Johnson (2009), Quantitative analysis of net-transgressive shoreline trajectories and stratigraphic architectures: mid-to-late Jurassic of the North Sea rift basin, *Basin Research*, *21*(5), 528–558.

Haq, B., J. Hardenbol, and P. Vail (1987), Chronology of fluctuating sea levels since the Triassic (250 million years ago to present), *Science*, *235*, 1156–1166.

Harbaugh, J. W., and G. Bonham-Carter (1981), *Computer Simulation in Geology*, 575 pp., Wiley and Sons.

Heath, R., and M. Apthorpe (1984), New formation names for the late Cretaceous and Tertiary sequence of the Southern North West Shelf, *Australian Geological Survey Record*, *1984/7*.

Helland-Hansen, W. (2009), Towards the standardization of sequence stratigraphy, *Earth-Science Reviews*, *94*(1-4), 95–97.

Helland-Hansen, W., and J. G. Gjelberg (1994), Conceptual basis and variability in sequence stratigraphy: a different perspective, *Sedimentary Geology*, *92*(1-2), 31–52.

Helland-Hansen, W., and G. J. Hampson (2009), Trajectory analysis: concepts and applications, *Basin Research*, *21*(5), 454–483.

Helland-Hansen, W., and O. J. Martinsen (1996), Shoreline trajectories and sequences; description of variable depositional-dip scenarios, *Journal of Sedimentary Research*, *66*(4), 670–688.

Heller, P., B. A. Burns, and M. Marzo (1993), Stratigraphic solution sets for determining the roles of sediment supply, subsidenc and sea level on transgressions and regressions, *Geology*, *21*, 747–750.

Heller, P. L., C. Paola, I.-g. Hwang, B. John, and R. Steel (2001), Geomorphology and sequence stratigraphy due to slow and rapid base-level changes in an experimental subsiding basin (XES 961), *American Association of Petroleum Geologists Bulletin*, *5*(5), 817–838.

Hocking, R., H. Moors, and W. Van De Graff (1987), Geology of the Carnarvon Basin, Western Australia, *Geological Survey of Western Australia Bulletin*, *123*.

Hubscher, C. ., and V. Spieß(2005), Forced regression systems tracts on the Bengal Shelf.

Hughes, B. D. (1995), *Random Walks and Random Environments, Vol 1: Random Walks*, 654 pp., Oxford University Press, New York.

Hunt, D., and M. E. Tucker (1992), Stranded parasequences and the forced regressive wedge systems tract: deposition during 'base-level' fall, *Sedimentary Geology*, *81*, 1–9.

Hunt, D., and M. E. Tucker (1995), Stranded parasequences and the forced regressive wedge systems tract: deposition during base-level fall reply, *Sedimentary Geology*, *95*, 147–160.

Hutton, E. W., and J. P. Syvitski (2008), Sedflux 2.0: An advanced process-response model that generates three-dimensional stratigraphy, *Computers & Geosciences*, *34*(10), 1319–1337.

Jervey, M. T. (1988), Quantitative Geological Modeling of Siliciclastic Rock Sequences and their Seismic Expression, in *Sea-Level Changes: An Integrated Approach*, pp. 7–69, Society of Economic Paleontologists and Mineralogists.

Johannessen, E. P., and R. J. Steel (2005), Clinoforms and their exploration significance for deepwater sands, *Basin Research*, *17*, 521–550.

Kendall, C., J. Strobel, P. Harris, P. Moore, R. Cannon, J. Bezdek, and G. Biswas (1989), Simulation of Capitan shelf margin (Late Permian, Guadalupian) of West Texas/New Mexico-a response to eustatic change and an example of the use of SEDPAK, in *28th International Geological Congress*, p. 175.

Kenyon, P. M., and D. L. Turcotte (1985), Morphology of a delta prograding by bulk sediment transport, *Geological Society of America Bulletin*, *96*(11), 1457–1465.

Kertznus, V., and B. Kneller (2009), Clinoform quantification for assessing the effects of external forcing on continental margin development, *Basin Research*, *21*(5), 738–758.

Koss, J. E., F. G. Ethridge, and S. A. Schumm (1994), An experimental study of the effects of base-level change on fluvial, coastal plain and shelf systems, *Journal of Sedimentary Research*, *B64*(2), 90–98.

Kundzewicz, Z. W., D. Nohara, J. Tong, T. Oki, S. Buda, and K. Takeuchi (2009), Discharge of large Asian rivers Observations and projections, *Larger Asian Rivers: Climate Change, River Flow and Sediment Flux*, *208*(1-2), 4–10.

Leeder, M. R., and M. D. Stewart (1996), Fluvial incision and sequence stratigraphy: alluvial responses to relative sea-level fall and their detection in the geological record, *Geological Society of London Special Publication*.

Lesser, G., J. Roelvink, J. van Kester, and G. Stelling (2004), Development and validation of a three-dimensional morphological model, *Coastal Engneering*, *51*, 883–915.

Loseth, T. M., R. J. Steel, J. P. Crabaugh, and M. Schellpeper (2006), Interplay between shoreline migration paths, architecture and pinchout distance for siliciclastic shoreline tongues: evidence from the rock record, *Sedimentology*, *53*(4), 735–767.

Mackin, H. (1948), Concept of the graded river, *Geological Society of America*, *59*, 463–512.

Marion, C., F. Dufois, M. Arnaud, and C. Vella (2010), In situ record of sedimentary processes near the Rhône River mouth during winter events (Gulf of Lions, Mediterranean Sea), *Continental Shelf Research*, *30*(9), 1095–1107.

Marr, J. G., J. B. Swenson, C. Paola, and V. R. Voller (2000), A two-diffusion model of fluvial stratigraphy in closed depositional basins, *Basin Research*, *12*(3-4), 381–398.

Martin, J., C. Paola, V. Abreu, J. Neal, and B. Sheets (2009), Sequence stratigraphy of experimental strata under known conditions of differential subsidence and variable base level, *AAPG Bulletin*, *93*(4), 503–533.

Martin, J., A. Cantelli, C. Paola, M. D. Blum, and M. A. Wolinsky (2011), Quantitative Modeling of the Evolution and Geometry of Incised Valleys, *Journal of Sedimentary Research*, *81*(1), 64–79.

Martinez, P., and J. W. Harbaugh (1993), *Simulating nearshore environments*, 265 pp., Pergamon Press, New York.

Martinsen, O. J., and W. Helland-Hansen (1995), Strike variability of clastic depositional systems: Does it matter for sequence-stratigraphic analysis?, *Geology*, *23*(5), 439.

Meijer, X. D. (2002), Modelling the drainage evolution of a river-shelf system forced by Quaternary glacio-eustasy Stream transport, *Basin Research*, *14*, 361–377.

Miall, A. D. (2010), *The Geology of Stratigraphic Sequences*, second ed., 526 pp., Springer, Berlin.

Miller, K. G., et al. (2005), The Phanerozoic Record of Global Sea-Level Change, *Science*, *310*(5752), 1293–1298, doi:5.

Mitchum, R. M., P. R. Vail, and S. Thompson, III. (1977), Seismic stratigraphy and global changes of sea-level, part 2: the depositional sequence as a basic unit for stratigraphic analysis, in *Seismic Stratigraphy Applications to Hydrocarbon Exploration*, vol. 26, edited by C. Payton, 26 ed., pp. 53–62, American Association of Petroleum Geologists Memoir.

Mø ller, L. K., E. S. Rasmussen, and O. R. Clausen (2009), Clinoform migration patterns of a Late Miocene delta complex in the Danish Central Graben; implications for relative sea-level changes, *Basin Research*, *21*(5), 704–720.

Moss, G. D., D. L. Cathro, and J. a. Austin (2004), Sequence Biostratigraphy of Prograding Clinoforms, Northern Carnarvon Basin, Western Australia: A Proxy for Variations in Oligocene to Pliocene Global Sea Level?, *Palaios*, *19*(3), 206–226.

Muto, T., and R. Steel (1992), Retreat of the front in a prograding delta, *Geology*, *20*, 967–970.

Muto, T., and R. Steel (1997), Principles of regression and transgression: the nature of the interplay between accommodation and sediment supply, *Journal of Sedimentary Research*, *67*(6), 994–1000.

Muto, T., and R. J. Steel (2001), Autostepping during the transgressive growth of deltas: Results from flume experiments, *Geology*, *29*, 771–774.

Muto, T., and R. J. Steel (2004), Autogenic response of fluvial deltas to steady sea-level fall: Implications from flume-tank experiments, *Geology*, *32*, 401.

Muto, T., and J. B. Swenson (2005), Large-scale fluvial grade as a nonequilibrium state in linked depositional systems: Theory and experiment, *Journal of Geophysical Research*, *110*, 1–15.

Muto, T., and J. B. Swenson (2006), Autogenic attainment of large-scale alluvial grade with steady sea-level fall: An analog tank-flume experiment, *Geology*, *34*(3), 161.

Muto, T., R. J. Steel, and J. B. Swenson (2007), Autostratigraphy: a framework norm for genetic stratigraphy, *Journal of Sedimentary Research*, *77*, 2.

Neal, J., and V. Abreu (2009), Sequence stratigraphy hierarchy and the accommodation succession method, *Geology*, *37*, 779–782.

Paola, C. (2000), Quantitative models of sedimentary basin filling, *Sedimentology*, *47*, 121–178.

Paola, C., P. Hellert, and C. Angevinet (1992), The large-scale dynamics of grain-size variation in alluvial basins 1: Theory, *Basin Research*, *4*, 73–90.

Paola, C., G. Parker, D. Mohrig, and K. Whipple (1999), The influence of transport fluctuations on the spatially averaged topography on a sandy, braided fluvial fan, in *Numerical Experiments in Stratigraphy: Recent Advances in Stratigraphic and Sedimentological Computer Simulations*, vol. 62, edited by J. Harbaugh, L. Watney, G. Rankey, R. Slingerland, R. Goldstein, and E. Franseen, 62 ed., pp. 211–218, SEPM (Society for Sedimentary Geology).

Parker, G., C. Paola, L. X. Whipple, and D. Mohrig (1998), Alluvial fans formed by channelized fluvial and sheet flow. 1: Theory, *Journal of Hydraulical Engineering*, *985*(October), 985–995.

Petter, A. L., and T. Muto (2008), Sustained alluvial aggradation and autogenic detachment of the alluvial river from the shoreline in response to steady fall of relative sea level, *Journal of Sedimentary Research*, *78*, 98.

Pigram, C. J., and H. L. Davies (1987), Terranes and the accretion history of the New Guinea orogen, *Bureau of Mineral Resources (BMR), Journal of Australian Geology and Geophysics*, *10*(1982), 193–212.

Plint, A. G., and D. Nummedal (2000), The falling stage systems tract: recognition and importance in sequence stratigraphic analysis, in *Sedimentary Response to Forced Regression*, edited by D. Hunt and R. L. Gawthorpe, October 2010, special pu ed., pp. 1–17, Geological Society of London, London.

Porbski, S. J., and R. J. Steel (2003), Shelf-margin deltas their stratigraphic significance and relation to deepwater sands, *Earth Science Review*, *62*, 283.

Porbski, S. J., and R. J. Steel (2006), Deltas and Sea-Level Change, *Journal of Sedimentary Research*, *76*(3), 390–403.

Posamentier, H., R. Erskine, and R. Mitchum (1991), Submarine fan deposition within a sequence stratigraphic framework, in *Seismic facies and sedimentary processes of subma- rine fans and turbidite systems*, edited by P. Weimer and M. Link, pp. 127–136, Springer-Verlag, New York.

Posamentier, H. W., and G. P. Allen (1999), Siliciclastic sequence stratigraphy: concepts and applications, *SEPM Concepts in Sedimentology and Paleontology*, *9*(210).

Posamentier, H. W., and W. R. Morris (2000), Aspects of the stratal architecture of forced regressive deposits, *Geological Society, London, Special Publications*, *172*(1), 19–46.

Posamentier, H. W., and P. R. Vail (1988), Eustatic controls on clastic deposition IIsequence and systems tract models, in *Sea Level ChangesAn Integrated Approach*, vol. 42, edited by C. K. Wilgus, B. S. Hastings, C. G. S. Kendall, H. W. Posamentier, C. A. Ross, and J. C. V. Wagoner, 42 ed., pp. 125–154, SEPM (Society for Sedimentary Geology).

Posamentier, H. W., M. T. Jervey, and P. R. Vail (1988), Eustatic controls on clastic deposition I conceptual framework, in *Sea Level ChangesAn Integrated Approach*, edited by C. K. Wilgus, B. S. Hastings, C. G. S. C. Kendall, H. W. Posamentier, Ross C. A., and J. C. W. Van, 42 ed., pp. 110–124, SEPM.

Posamentier, H. W., G. P. Allen, D. P. James, and M. Tesson (1992), Forced regressions in a sequence stratigraphic framework: concepts, examples, and exploration significance, *American Association of Petroleum Geologists Bulletin*, *76*, 1687.

Press, W. H., S. A. Teukolsky, W. T. Vetterling, and F. B. P (2007), *Numerical Recipes: The Art of Scientific Computing*, third edit ed., 1194 pp., Cambridge University Press.

Prince, G. D., and P. M. Burgess (2013), Numerical Modeling of falling-stage topset aggradation: implications for distinuishing between forced and unforced regressions in the geological record, *Journal of Sedimentary Research*, *83*, 767–781.

Reading, H. G., and J. D. Collinson (1996), Clastic Coasts, in *Sedimentary Environments: Processes, Facies and Stratigraphy*, edited by H. G. Reading, 3rd ed., chap. 6, Wiley-Blackwell.

Rittenour, T., M. D. Blum, and R. J. Goble (2007), Fluvial evolution of the lower Mississippi River valley during the last 100 k.y. glacial cycle: response to glaciation and sea-level change, *Geological Society of America Bulletin*, *119*, 586–608.

Rivenæ s, J. (1992), Application of a dual-lithology, depth-dependent diffusion equation in stratigraphic simulation, *Basin Research*, *4*(2), 133–146.

Rivenæ s, J. C. (1997), Impact of sediment transport efficiency on large-scale sequence architecture: results from stratigraphic computer simulation, *Basin Research*, *9*(2), 91–105.

Sanchez, C. M., C. S. Fulthorpe, and R. J. Steel (2012a), Middle Miocene-Pliocene siliciclastic influx across a carbonate shelf and influence of deltaic sedimentation on shelf construction, Northern Carnarvon Basin, Northwest Shelf of Australia, *Basin Research*, pp. 1–19.

Sanchez, C. M., C. S. Fulthorpe, and R. J. Steel (2012b), Miocene shelf-edge deltas and their impact on deepwater slope progradation and morphology, Northwest Shelf of Australia, *Basin Research*, pp. 1–16.

Schlager, W. (1993), Accommodation and supply - a dual control on stratigraphic sequences, *Sedimentary Geology*, *86*, 111–136.

Schumm, S. A. (1993), River Response to Baselevel Change: Implications for Sequence Stratigraphy, *The Journal of geology*, *101*(2, 100th Anniversary Symposium: Evolution of the Earth's Surface), pp. 279–294.

Schumm, S. A., M. P. Mosley, and W. E. Weaver (1987), *Experimental Fluvial Geomorphology*, John Wiley, New York.

Simmons, M. D., P. R. Sharland, D. M. Casey, R. B. Davies, and O. E. Sutcliffe (2007), Arabian Plate sequence stratigraphy: Potential implications for global chronostratigraphy, *GeoArabia*, *12*(4), 101–130.

Sinclair, H. D., B. J. Coakly, P. A. Allen, and A. B. Watts (1991), Simulation of Foreland Basin Stratigraphy using a Diffusion-Model of Mountain Belt Uplift and Erosion - an Example from the Central Alps, Switzerland, *Tectonics*, *10*(3), 599–620.

Sloss, L. L. (1962), Stratigraphic models in exploration, *Journal of Sedimentary Petrology*, *32*, 415–422.

Sloss, L. L., W. C. Krumbein, and E. C. Dapples (1949), Integrated facies analysis, in *Sedimentary facies in geologic history*, vol. 39, edited by C. R. Longwell, pp. 91–124, Geological Society of America Memoir.

Steckler, M. S., D. J. Reynolds, B. J. Coakley, B. A. Swift, and R. Jarrard (1993), Modelling passive margin sequence stratigraphy, in *Sequence stratigraphy and Facies*

Assocations, edited by H. W. Posamentier, C. P. Summerhayes, B. U. Haq, and G. P. Allen, special pu ed., pp. 19–41, International Association of Sedimentologists.

Strong, N., and C. Paola (2008), Valleys That Never Were: Time Surfaces Versus Stratigraphic Surfaces, *Journal of Sedimentary Research*, *78*(8), 579–593.

Swenson, J. B. (2005), Fluviodeltaic response to sea level perturbations: Amplitude and timing of shoreline translation and coastal onlap, *Journal of Geophysical Research*, *110*(F3), 1–19.

Swenson, J. B., and T. Muto (2005), Controls on alluvial aggradation and degradation during steady fall of relative sea level: theory, in *Proceedings of the 4th International Association of Hydraulic Engineering and Research Symposium: River, Coastal and Estuarine Morphodynamics*, vol. 2, edited by G. Parker and M. H. Garcia, volume 2 ed., pp. 675–684, International Association of Hydraulic Engineering and Research Symposium.

Swenson, J. B., and T. Muto (2007), Response of coastal plain rivers to falling relative sea-level: allogenic controls on the aggradational phase, *Sedimentology*, *54*(1), 207–221.

Swenson, J. B., C. Paola, L. Pratson, V. R. Voller, and A. B. Murray (2005), Fluvial and marine controls on combined subaerial and subaqueous delta progradation: Morphodynamic modeling of compound- clinoform development, *Journal of Geophysical Research*, *110*, 1–16.

Sydow, J., and H. H. Roberts (1994), Stratigraphic framework of a Late Pleistocene shelf-edge delta, northeast Gulf of Mexico, *American Association of Petroleum Geologists Bulletin*, *78*, 1276.

Tetzlaff, D., and J. Harbaugh (1989), *Simulating clastic sedimentation*, 202 pp., Van Nostrand Reinhold, 1989.

Thorne, J. A. (1992), An analysis of the implicit assumptions of the methodology of seismic sequence stratigraphy, *AAPG Memoir*, *53*, 375–394.

Vail, P. (1987), Seismic stratigraphy interpretation procedure, in *Atlas of Seismic Stratigraphy*, edited by A. W. Bally, 27 ed., pp. 1–10, American Association of Petroleum Geologists Studies in Geology.

Vail, P., R. Mitchum, and S. Thompson (1977), Seismic stratigraphy and global changes of sea-level. Part 3. Relative changes of sea-level from coastal onlap, in *Seismic Stratigraphy Applications to Hydrocarbon Exploration*, vol. 26, edited by C. E. Payton, 26 ed., pp. 83–97, American Association of Petroleum Geologists Memoir.

Vail, P. R. (1975), Eustatic cycles from seismic data for global stratigraphic analysis (abstract), *American Association of Petroleum Geologists Bulletin*, *59*, 2198–2199.

van Heijst, M. W. I. M., and G. Postma (2001), Fluvial response to sea-level changes: a quantitative analogue, experimental approach, *Basin Research*, *13*(3), 269–292.

Van Wagoner, J., H. Posamentier, R. Mitchum, P. Vail, J. Sarg, T. Loutit, and J. Hardenbol (1988), An overview of sequence stratigraphy and key definitions, in *Sea Level ChangesAn Integrated Approach*, edited by C. Wilgus, B. Hastings, C. Kendall, H. Posamentier, and J. Ross, C.A., Van Wagoner, special pu ed., pp. 39–45, Society of Economic Paleontologists and Mineralogists (SEPM).

Van Wagoner, J., R. Mitchum Jr., K. Campion, and V. Rahmanian (1990), Siliciclastic sequence stratigraphy in well logs, core, and outcrops: concepts for high-resolution correlation of time and facies., *American Association of Petroleum Geologists Methods in Exploration Series*, *7*, 55.

Wallace, M. W., E. Condilis, A. Powell, J. Redfearn, K. Auld, M. Wiltshire, G. Holdgate, and S. Gallagher (2003), Geological controls on the sonic velocity in the Cenozoic carbonates of the Northern Carnarvon Basin, Northwest Shelf, Western Australia, *APPEA Journal*, *43*, 385–399.

Wehr, F. (1993), Effects of variations in subsidence and sediment supply on parasequence stacking patterns, in *Siliciclastic sequence stratigraphy: recent developments and applications*, edited by P. Weimer and H. Posamentier, aapg memoi ed., pp. 369–379, American Association of Petroleum Geologists.

Weiss, G. H. (1994), *Aspects and Applications of the Random Walk*, 378 pp., North Holland Press, Amsterdam.

Wheeler, H. E. (1959), Unconformity bounded units in stratigraphy, *American Association of Petroleum Geologists Bulletin*, *43*, 1975–1977.

Wheeler, H. E. (1964), Baselevel, lithosphere surface, and timestratigraphy, *Geological Society of America Bulletin*, *75*, 599–610.

Wheeler, H. E., and H. H. Murray (1957), Baselevel control patterns in cyclothemic sedimentation, *American Association of Petroleum Geologists Bulletin*, *41*, 1985–2011.

Williams, H. D., P. M. Burgess, V. P. Wright, G. Della Porta, and D. Granjeon (2011), Investigating Carbonate Platform Types: Multiple Controls and a Continuum of Geometries, *Journal of Sedimentary Research*, *81*(1), 18–37.

Wood, L. J., F. G. Ethridge, and S. Schumm (1993a), An experimental study of the influence of subaqueous shelf angles on coastal plain and shelf deposits, in *Siliciclastic Sequence Stratigraphy: Recent Developments and Applications*, edited by P. Weimer and H. Posamentier, memoir 58 ed., pp. 381–391, American Association of Petroleum Geologists.

Wood, L. J., F. G. Ethridge, and S. A. Schuum (1993b), The effects of rate of base-level fluctuation on coastal-plain, shelf and slope depositional systems; an experimental approach, in *Sequence stratigraphy and Facies Assocations*, edited by H. W. Posamentier, C. P. Summerhayes, B. U. Haq, and G. P. Allen, special pu ed., pp. 43–53, International Association of Sedimentologists.

Woolfe, K. J., P. Larcombe, T. Naish, and R. G. Purdon (1998), Lowstand rivers need not incise the shelf: An example from the Great Barrier Reef, Australia, with implications for sequence stratigraphic models, *Geology*, *26*(1), 75–78.